Development of semiconductor metal oxide gas sensors for the detection of NO_2 and H_2S gases

Thesis submitted to

Cochin University of Science and Technology

in partial fulfilment of the requirements

for the award of the degree of

Doctor of Philosophy

Nisha R.

Department of Instrumentation

Cochin University of Science and Technology

Cochin - 682 022, Kerala, India

March 2013

Development of semiconductor metal oxide gas sensors for the detection of NO_2 and H_2S gases

Author

Nisha R.
Department of Instrumentation
Cochin University of Science and Technology
Cochin – 682 022, Kerala, India
email: @gmail.com

Supervising Guide

DR. K. N Madhusoodanan
Associate Professor
Department of Instrumentation
Cochin University of Science and Technology
Cochin - 682 022, India
email: madhu@cusat.ac.in

March 2013

Cover page: Integrated Gas Sensor

DR. K. N Madhusoodanan
Associate Professor
Department of Instrumentation
Cochin University of Science and Technology
Cochin – 682 022

Mob: 9349406334
Phone: +91 4842575008
Email: madhu@cusat.ac.in

Certificate

Certified that the thesis entitled **"Development of semiconductor metal oxide gas sensors for the detection of NO_2 and H_2S gases"** submitted by **Ms. Nisha R.** is an authentic record of research work carried out by her under my supervision at the Department of Instrumentation in partial fulfilment of the requirements for the award of degree of Doctor of Philosophy of Cochin University of Science and Technology and the work embodied in this thesis has not been included in any other thesis submitted previously for the award of any other degree.

Cochin – 22
Date:

DR. K. N Madhusoodanan
Supervising guide

Declaration

I hereby declare that the thesis entitled **"Development of semiconductor metal oxide gas sensors for the detection of NO_2 and H_2S gases"** submitted for the award of degree of Doctor of Philosophy of Cochin University of Science and Technology is based on the original work done by me under the guidance of **DR. K. N Madhusoodanan**, Associate Professor, Department of Instrumentation, Cochin University of Science and Technology, Cochin - 682 022 and this work has not been included in any other thesis submitted previously for the award of any other degree.

Cochin – 22 **Nisha R.**
Date:

Dedicated to my Parents..

"No matter what conditions you encounter in life, your right is only to the works - not to the fruits thereof. You should not be impelled to act for selfish reasons, nor should you be attached to inaction.

- Bhagavad Gita 2.47"

Acknowledgements

Apart from the efforts of myself, the success of this work depends largely on the encouragement and support of many others. I take this opportunity to express my gratitude to the people who have been instrumental in the successful completion of this project. First and foremost, I would like to thank Almighty for his guidance and spiritual comfort in making this quest of knowledge possible.

I would like to acknowledge and extend my heartfelt gratitude to my supervising guide DR. K. N. Madhusoodanan. His willingness to motivate me contributed tremendously to my research work. Without his insightful guidance and persistent help, this thesis would never have been accomplished. I am thankful for his patient guidance, enthusiastic encouragement, valuable suggestions and useful critiques during the course of this research work.

I express my sincere thanks to DR. K. Rajeev Kumar for his valuable help, fruitful discussions and suggestions throughout the work. My grateful thanks are also extended to DR. Jhoney Issac. I extend my sincere thanks to DR. Stephen Rodriguez, Head of the department for allowing me to use the department facilities.

I would like to offer my thanks to Prof. Jacob Philip and all the staff of STIC and SAIF for their help during my research work.

I am particularly grateful for the valuable suggestions from DR S.K.Gupta and DR Shashwati Sen Technical Physics and Prototype Engineering Division, BARC, Mumbai during the initial stage of my work.

My earnest thanks to Mr. Murali and Mr. Joshy for their timely assistance through out my work. I am grateful to the help and cooperation of all the staff of our department. Ms. Allikutty, Mr. Antony, Mr. Mathew, Mr. Gopi

Menon, Mr. Jose, Mr. Jose Jacob, and Mr. Casmir are gratefully acknowledged for all their timely help. I extend my sincere thanks for the timely help from the office staff of the department

I would like to extend my special thanks to Ms.Anu for her constant support and comfort during all my tough times. I extend my sincere thanks to Ms. Pramitha, Mr. Subin, Mr. Maju , Mr. Shyam, Ms. Smitha and Mr. Jolly for their timely help. I thank Mr. Sreejith and Mr. Vimal for helping me with their samples during research work. I thank Ms. Hasna for the Raman measurements.

I acknowledge KCSTE and Cochin University of Science and Technology for providing fellowships to pursue my research.

I am indebted to many colleagues who supported me. I thank Ms. Uma for her timely console during the course of my research work. I will always remember the affection and support of my lab mates Ms. Viji, Ms. Benjamin, Ms. Nisha M R, Mr. Ginson, Ms. Simitha , Ms. Jayalakshmi, Ms. Rehana, Ms. Savitha, Ms. Rakhi and Ms. Lidiya. I thank Mr. Nissam for the productive scientific discussions. I thank Mr. Rahman and Ms. Soumya for the editorial work. I remember Mr. Satish , Who chose the abode of God. My heartfelt thanks to my seniors Mr. Alex, Mr. Alex mathew , Mr. Reghu, Ms. Preethy, Mr.Rajesh and Ms. Manjusha.

I express my sincere thanks to all my friends at CUSAT, especially, Ms. Jitha, Ms. Aami, Ms. Bybi, Ms. Remya, Ms. Gini, Ms. Prabha, Ms. Angel, Ms. Misha, Ms.Vijutha, Ms. Geetha and Ms. Manju for their encouragement and loving support throughout my days at CUSAT. I express my sincere thanks to all my friends at CUSAT for their encouragement and loving support throughout my days at CUSAT.

I am thankful to Ms. Rakhi, Ms. Leena, Ms. Shiji, Ms. Preethi and Ms. Shajira for making my days at Athulya hostel memorable. I can't forget my room-mates Ms. Diya, Ms. Radhika and Ms. Kavitha who didn't allow me to feel that I am away from home. I rejoice the wonderful time with my friends in

Athulya hostel. I am so grateful to all my friends from college days for their everlasting love and encouragement. Especially Ms. Divya, Ms. Helen, Ms. Rani, Ms. Vinitha, Ms. Vijayalekshmi, Ms. Shilpa, Mr. Aravind, Mr.Anoop, Mr. Arun, Mr.Ajith, Mr. Anumod, Mr. Jessy, Mr.Prem, Ms. Susmitha, my B.Sc and M.Sc classmates.

I owe a lot to my parents especially to my father who encouraged, supported and helped me at every stage of my personal and academic life, and longed to see this achievement come true. I thank my brother, Mr. Pradeep, for his timely advice and support. He has been instrumental in instilling confidence throughout my research work. I extend my thanks to my sis-in-law also for her support and help. Words are not enough to thank the most special person in my life, my husband, Mr. Sreekumar, whose love, patience and support helped me in completing the work. I'd like to thank my mother-in law and sister- in- law for their support to finish this piece of work. I remember the pleasant and wonderful moments I had with my niece, Vaishnavi. I would like to cherish the moments with the sunshine of my life my baby, Hrishikesh, whose innocent smile at the end of the day makes all the stress vanish and make me to look forward for the bright future.

Finally I convey my sincere thanks to my entire well - wishers and friends who have directly or indirectly helped me.

Nisha R.

Preface

As the atmospheric pollution has considerably increased in the recent years, the detection of harmful and flammable gases is a subject of growing importance in both domestic and industrial environments. The atmospheric pollutants like: SO_2, NO_2, O_3, NO, CO, CO_2 and particulates matter (PM) have negative effects on human and animal health. If these pollutants remain in the same place the problem of the pollution would be easier to solve, but unfortunately, they move hundreds or thousands kilometres from their transmission source resulting in the formation of acid rains, eutrophication, photochemical pollution and global warming.

Detection of pollutant, toxic, refining, combustive and process gases is important for system and process control, safety monitoring and environmental protection. Various methods can be used to accomplish gas sensing including gas chromatography, fourier-transform, infrared spectroscopy, chemiluminescence detectors, mass spectrometry, semiconductor gas sensors and others. Gas sensors based on solid state semiconductor materials offer considerable advantages in comparison to other gas sensing methods. Semiconductor sensors are inexpensive to produce, easy to miniaturize, rugged, reliable, and can be designed to operate over a range of conditions including high temperatures. Semiconductor sensors can be produced in arrays to allow sensing of multiple species simultaneously.

Gas sensors using metal oxide semiconductors have been the subject of extensive investigations for more than three decades, primarily focusing on SnO_2 .In more recent research, the interest shifted to some other promising metal oxides, with interesting properties as gas sensing materials. Use of metal oxides has several advantageous, features such as simplicity in device structure, low cost for fabrication, robustness in practical applications and adaptability to a wide variety of reducing or oxidising gases. The gas detection technique is primarily based on a change in the electrical resistance of the semiconducting metal oxide films. The principal detection process is the change of the oxygen concentration at the surface of these metal oxides, caused by the adsorption and heterogeneous catalytic reaction of oxidizing and reducing gaseous species. The

electrical conductivity depends on the gas atmosphere and on the temperature of the sensing material exposed to the test gas. The signal generated from the sensing element strongly depends on the temperature of the element.

One of the main challenges in the development of metal-oxide gas sensors is enhancement of selectivity to a particular gas. Currently, two general approaches exist for enhancing the selective properties of sensors. The first one is aimed at preparing a material that is specifically sensitive to one compound and has low or zero cross-sensitivity to other compounds that may be present in the working atmosphere. To do this, the optimal temperature, doping elements, and their concentrations are investigated. Nonetheless, it is usually very difficult to achieve an absolutely selective metal oxide gas sensor in practice. Another approach is based on the preparation of materials for discrimination between several analyte in a mixture. It is impossible to do this by using one sensor signal. Therefore, it is usually done either by modulation of sensor temperature or by using sensor arrays.

The present work focus on the characterization of n-type semiconducting metal oxides like Tungsten oxide (WO_3), Zinc Oxide (ZnO) and Indium oxide (In_2O_3) for the gas sensing purpose. For the purpose of gas sensing thick as well as thin films were fabricated. Two different gases, NO_2 and H_2S gases were selected in order to study the gas sensing behaviour of these metal oxides. To study the problem associated with selectivity the metal oxides were doped with metals and the gas sensing characteristics were investigated.

The present thesis is entitled “Development of semiconductor metal oxide gas sensors for the detection of NO_2 and H_2S gases” and consists of six chapters.

Chapter 1 deals with a brief description of the chemical sensors and their classification. General aspects concerning the gas sensors based on metal oxide semiconductors are presented. A short review about the various semiconducting metal oxides used as gas sensors are discussed. The basic characteristics of a gas sensor along with the conduction mechanism and the principal factors which affect the metal oxide semiconductor performances are discussed. The influence of catalytic additives and a review of different metal additives are also presented. The effect of nanoparticle on the sensing mechanism is also discussed.

Chapter 2 deals with the gas sensing measurement facility that we have fabricated. The different gas sensing method, electrical characterization and different methods for active layer preparation are discussed. The effective volume of the fabricated gas sensing measurement chamber is 280ml. An inlet is provided for inserting the desired concentration of the gas to the chamber. Sensor characteristics is monitored in terms of variation in electrical resistance of sensor in the absence and presence of gas. Details of the measurement, data acquisition, temperature controller are presented in this chapter. The different analytical characterisation tools used to characterise the gas sensing materials were XRD, SEM, EDS and Raman spectroscopy. A short discussion about the characterization tools are also given in this chapter.

Chapter 3 is devoted to the preparation, characterisation and temperature dependent gas sensing behaviour of pure and copper doped tungsten oxide thick films. The nanopowders of tungsten oxide were synthesized by precipitation technique from aqueous solutions of ammonium tungstate para penta hydrate and nitric acid. For copper doping, copper acetate monohydrate dissolved in water was added to the solution containing ammonium tungstate para pentahydrate and nitric acid. Hence pure, 0.5wt% 1.5wt% and 3wt% copper doped tungsten oxide powder were prepared. Thick film sensors were fabricated by dispersing the powder in methanol and drop coating on glass substrate and annealing at 600^0C overnight. The structural properties, surface morphology, compositional analysis of the prepared samples were characterized by XRD, SEM, EDS and Raman spectroscopy. Gas sensing performance in the detection of NO_2 and H_2S gases are presented as a function of the operating temperature and the gas concentration. Optimum operating temperature of the pure and copper doped sensors was studied. Response and recovery time of the sensors at various temperatures were also calculated. With the incorporation of copper we were able to enhance the performance of the tungsten oxide towards NO_2 gas. A detailed discussion on the results obtained is included in this chapter.

Chapter 4 presents the preparation, characterization and temperature dependent gas sensing behaviour of pure and indium doped zinc oxide thin films. Zinc oxide thin films were prepared on soda lime glass substrate using Chemical Spray Pyrolysis technique (CSP). Zinc acetate solution (0.3 M) was

prepared in a mixture of propanol and water, taken in the volume ratio 1:1. Compressed air was used as the carrier gas and temperature of substrate was kept at 450 $\pm 5^0$C. Indium was doped by adding the required quantity of indium nitrate in the spray solution itself. Doping percentage of indium was varied from 0.5 to 3 volume%. Sprayed ZnO and indium doped thin film samples were of thickness 550 nm. As prepared pure and indium doped ZnO films were annealed at 600^0C overnight before conducting the gas sensing measurements. Structural properties, surface morphology, compositional analysis of the prepared samples were characterized by XRD, SEM, EDS and Raman spectroscopy. Sensor response of pure and indium doped zinc oxide films to NO_2 and H_2S gases as a function of the operating temperature and the gas concentration is evaluated in this chapter. Optimum operating temperature of the pure and indium doped sensors were studied. Response and recovery time of the sensors at various temperatures were also calculated. Results obtained from the indium doping studies proved that pure zinc oxide thin films itself acted as a very good sensor when compared with doped one. The reduced sensor performance due to the incorporation of indium is discussed in detail.

Chapter 5 presents the preparation, characterization and temperature dependent gas sensing behaviour of pure and copper doped indium oxide thick films. Analytically pure indium oxide powder was purchased and copper doping was done by powder impregnation method. The doping percentage was varied from 0.5 to 3wt% .Thick films of the pure and copper doped indium oxide sensors were fabricated by dispersing the powder in methanol and drop coating on glass substrate and annealing at 600^0C overnight. Sensor response of pure and copper doped indium oxide thick films to NO_2 and H_2S gases as a function of the operating temperature and the gas concentration is evaluated in this chapter. Optimum operating temperature of the pure and copper doped indium oxide sensors was studied. Response and recovery time of the sensors at various temperatures were also calculated. With copper doping NO_2 and H_2S gas sensing properties of Indium oxide sensors were enhanced. A much less response and recovery time was obtained for the H_2S gas sensing properties of copper doped indium oxide when compared with pure indium oxide. For NO_2 gas sensing properties, the 3wt% copper doped sensors showed a maximum sensitivity when

compared to the pure sensor. A detailed discussion concerning the enhancement in sensitivity for NO_2 and H_2S gases with copper doping as well as the reduced dynamic properties obtained for the gases are also included in this chapter.

The summary of research work and the salient features of the above discussed sensors are outlined in **chapter 6.** The scope of future is also presented.

Part of the thesis has been published in the following Journal

- NO_2 Gas Sensing Properties of Copper Doped Tungsten Oxide, Nisha.R and K.N. Madhusoodanan, Journal of Instrument Society of India, 204-207 2011.
- Effect of Indium doping on the Gas sensing behavior of Zinc oxide films obtained by Chemical spray pyrolysis method, Nisha.R, K.N.Madhusoodanan, T.V.Vimalkumar and K.P.Vijayakumar, IEEE Xplore digital library, 232, 2012. Digital Object Identifier: 10.1109/ISPTS.2012.6260923
- A Comparative study of thin and thick film indium oxide gas sensors to a lower concentration of NO_2 gas, Nisha.R, K.N.Madhusoodanan, Sreejith K., Arthur E Hill, Richard D Pilkington . Journal of Instrument Society of India (accepted).
- Enhanced NO_2 gas sensing properties of copper doped tungsten oxide thick films, Nisha.R and K.N. Madhusoodanan, (to be communicated)

Other publication to which author has contributed

- The deposition and NO_2 gas sensitivity of low temperature sputtered In_2O_3 films using pulsed d.c magnetron sputtering from a powder target, Sreejith Karthikeyan, Nisha.R, Arthur E Hill, Richard D Pilkington, Kottarathil Naduvil Madhusoodanan (to be communicated)

Conference papers

- PC Based Temperature Controller, Nisha.R and K.N. Madhusoodanan, Proceedings of the Second Control Instrumentation System Conference (CISCON 2005) ,52-53, 2005.
- AC Conductivity Measurement Setup for Sensor Material Characterizations, Nisha.R and K.N. Madhusoodanan, Proceedings of the National Symposium on Instrumentation (NSI-30), 99, 2005.
- NO_2 gas sensing properties of In_2O_3 thin films prepared by pulsed d.c magnetron sputtering technique, Nisha.R,K.N.Madhusoodanan, Sreejith K., Arthur E Hill, Richard D Pilkington. National Seminar on Sensors (NSPTS-17).

Contents

…..ꕥ…..

Chapter 1

An Introduction to Gas Sensors

A brief introduction about gas sensors and their different type of classification is included in this chapter. The advantage of using semiconductor metal oxide as chemiresistive gas sensor, various metal oxides used for gas sensing, the basic characteristics of gas sensor, the detection principle for metal oxide gas sensing, the role of additives in gas sensing and the effect of nanoparticle in gas sensing are reviewed.

1.1 Sensors

Sensor is a device that produces a measurable response to a change in a physical condition, such as temperature, pressure etc.. Sensors are particularly useful for making in-situ measurements such as in industrial process control. They are the critical components in all measurement and control application, responsible for converting some type of physical phenomenon into a quantity measurable by a data acquisition (DAQ) system. A sensor does not function by itself; it is always a part of larger system that may incorporate many other detectors, signal conditioners, signal processors, memory devices, data recorders and actuators.

'Sensor', the term started to gain currency during the 1970s [1]. This development was caused by technological developments which are part of a technical revolution that continues to this day. Rapid advances in microelectronics made available technical intelligence. Machines became more intelligent and more autonomous. There arose a demand for artificial sensing organs that would enable machines to orient themselves independently

in the environment. A generation ago, the word sensor was not widely used. Today, however, sensors are becoming ubiquitous in our daily lives. Our world is changing rapidly and sensors play an important role in this process. Broad agreements about attributes of sensors are:

- Be in direct contact with the investigated subject
- Transform non-electric information into electric signals
- Respond quickly
- Operate continuously or at least in repeated cycles
- Be small

The most important characteristics of a sensor are

- Sensitivity
- Stability
- Repeatability

Normally, a sensor is only useful if all the three components are tightly specified for a given range of measurand values and time of operation. A highly sensitive device is not useful if its output drifts greatly during the measurement time and the data obtained may not be reliable if the measurement is not repeatable. Other sensor characteristics, such as selectivity and linearity can often be compensated for by using additional, independent sensors or by signal conditioning circuits.

Sensor classification schemes range from very simple to the complex. One good way to look at a sensor is to consider all of its properties, such as stimulus, specifications, physical phenomenon, conversion mechanism, material and application field. Generally sensors can be classified based on stimulus applied as acoustic electric, magnetic, optical and thermal.

1.2 Chemical Sensor

Chemical sensors, as a special variety of sensors analyze our environment, i.e. they detect which substances are present and in what concentration. With our senses we can not only see, hear and feel but also smell and taste. The latter sensations are the results of some kind of chemical analysis of our environment, either of the surrounding air or of liquids and solids in contact with us. Consequently, chemical sensors can be considered as artificial noses or artificial tongues.

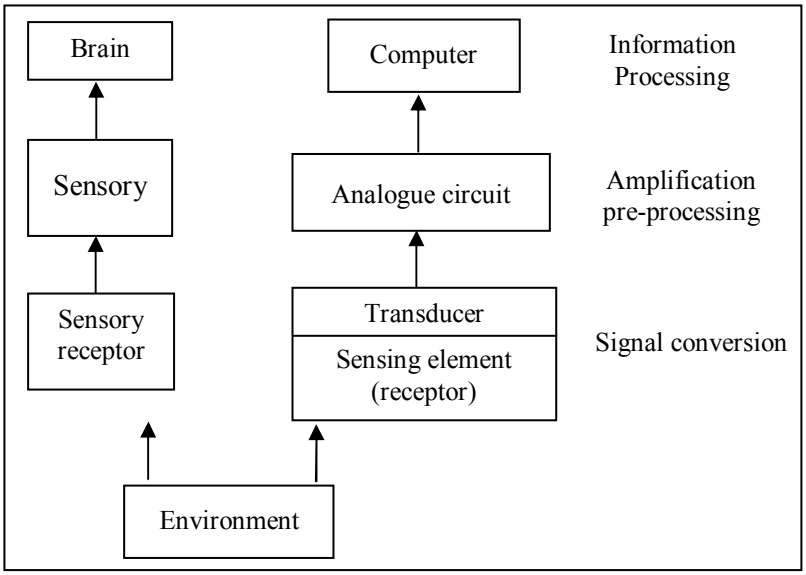

Fig. 1.1 Similarities between biological and technical systems

Figure 1.1 illustrates the similarities between biological and technical systems. As in a living organism, we find a receptor which is a part of the technical system. The receptor responds to environmental parameters by changing some of its inherent properties. In the adjacent transducer, primary information is transformed into electrical signals. Modern sensor systems

contain additional parts for signal amplification or conditioning. At the end of the chain is a microcomputer, working like the central nervous system in a living organism.

The definition of chemical sensor as given by IUPAC in 1991 is: A chemical sensor is a device that transforms chemical information, ranging from concentration of a specific sample component to total composition analysis, into an analytically useful signal [2]. The chemical information, mentioned above, may originate from a chemical reaction of the analyte or from a physical property of the system investigated. Many authors have provided more general or specific definitions for this sort of sensors. According to Wolfbeis: chemical sensors are small-sized devices comprising a recognition element, and a signal processor capable of continuously and reversibly reporting a chemical concentration [3]. Reversibility means that the sensor signals should not 'freeze' but respond dynamically to changes in sample concentration in the course of measurement. According to Göpel and Schierbaum [4] chemical Sensors are devices which convert a chemical state into a electric signal. Chemical sensors are just the primary link of the measuring chain, in other words, an interface between the chemical world and the electronics.

Some typical properties associated with chemical sensors, according to Stetter and Penrose [5] is:

- Sensitive layer is in chemical contact with the analyte
- A change in the chemistry of the sensitive layer (a reaction) is produced after the exposure to the analyte.
- The sensitive layer is on a platform that allows transduction of the change to electric signals.
- They are physically small

- They operate in real time.
- They do not necessarily measure a signal or simple physical or chemical property
- They are typically less expensive and more convenient than an equivalent instrument for the same chemical measurements.

A chemical sensor is an essential component of an analyzer**.** In addition to the sensor, the analyzer may contain devices that perform the following functions: sampling, sample transport, signal processing, data processing. An analyzer may be an essential part of an automated system. The analyzer, working according to a sampling plan as a function of time, acts as a monitor. Chemical sensors contain two basic functional units: a receptor part and a transducer part. Some sensors may include a separator which is, for example, a membrane. In the receptor part of a sensor which is a chemical interface, the analyte interacts chemically with a surface, producing a change in physical /chemical properties. The chemical information is transformed into a form of energy which may be measured by the transducer. The transducer part is a device capable of transforming the energy carrying the chemical information about the sample into a useful analytical signal. The transducer as such does not show selectivity.

The receptor part of chemical sensors may be based upon various principles:

- Physical, where no chemical reaction takes place. Typical examples are those based upon measurement of absorbance, refractive index, conductivity, temperature or mass change.
- Chemical, in which a chemical reaction with participation of the analyte gives rise to the analytical signal.

- Biochemical, in which a biochemical process is the source of the analytical signal. Typical examples are microbial potentiometric sensors or immuno sensors. They may be regarded as a subgroup of the chemical ones. Such sensors are called biosensors.

In some cases it is not possible to decide unequivocally whether a sensor operates on a chemical or on a physical principle. This is, for example, the case when the signal is due to an adsorption process.

Classification of chemical sensors is accomplished in different ways. As per IUPAC [2] chemical sensors may be classified according to the operating principle of the transducer. The table 1.1 shows the various sensor classification based on the transduction principle.

This classification represents one of the possible alternatives. Sensors have, for example, been classified not according to the primary effect but to the method used for measuring the effect. As an example the so-called catalytic devices in which the heat effect evolved in the primary process are measured by the change in the resistance of a thermistor. Also, the electrical devices are often put into one category together with the electrochemical devices.

Sensors have also been classified according to the application to detect or determine given analyte. Examples are sensors for pH, for metal ions or for determining oxygen or other gases. Another basis for the classification of chemical sensors may be according to the mode of application, for example sensors intended for use in vivo, or sensors for process monitoring and so on. It is, of course, possible to use various classifications as long as they are based on clearly defined and logically arranged principles.

The biosensors are not presented as a special class because the process on which they are based is, in general, common to chemical sensors. They may be also differentiated according to the biological elements used in the receptor. Those may be: organisms, tissues, cells, organelles, membranes, enzymes, antibodies, etc. The biosensors may have several enzymatic systems coupled which serve for amplification of the signal.

Table 1.1 Classification of Sensors based on Transduction Principles

Sensor Classification	*Transduction Principle*
Optical	Absorbance, reflectance, luminescence, fluorescence, refractive index, optothermal effect and light scattering.
Electrochemical	Voltammetric and potentiometric devices, chemically sensitized field effect transistor (CHEMFET) and potentiometric solid electrolyte gas sensors.
Electrical	Metal oxide and organic semiconductors, electrolytic conductivity and electric permittivity.
Mass sensitive	Piezoelectric and surface acoustic waves.
Magnetic	Paramagnetic gas properties
Thermometric	The measurement of the heat effect of a specific chemical reaction or adsorption which involves the analyte.
Others	Emission or absorption of radiation

1.3 Gas Sensors

The problems related to air quality monitoring are important issues of the current research activity. The living standards of human race in the past few decades have grown at a remarkable pace owing to industrial revolution. Technological developments in the recent decades have brought along with it several environmental problems and human safety issues. Growing industrialization and ever increasing pollutants from vehicular exhaust has resulted into increased air pollution. Industrialization demands the specific

gas detection and monitoring for the benefit of the society. Detection of pollutant, toxic, refining, combustible and process gases is important for system and process control, safety monitoring and environmental protection. A key component in many process controls, product development, environmental monitoring etc. is the measurement of concentration of one or the other gaseous component of the ambient. In such situations suitable sensors can provide the necessary interface between the ambient and the back up electronic instrumentation to detect the target gas. Hence, sensors which detect toxic and inflammable chemicals quickly are necessary.

Gas sensors which from a sub-class of chemical sensors have found extensive applications in process control industries and environmental monitoring. In recent years, the number of gaseous species to be covered with gas sensors has increased dramatically. Toxic or bad smelling gases frequently encountered in living circumstances such as H_2S and NH_3 as well as hazardous gases used for industrial processes have long been the targets of gas sensors. The detection of the various volatile gases or smells generated from foods or food materials has become increasingly important in food industries. These gaseous components are often present at very low levels and mixed with several disturbing gases. The recent global issues of energy and environment are increasing the necessity of those sensors which can detect air-pollutants in environments such as SO_X, CO_X and NO_X or can be applied for the control systems of combustion exhausts from stationary facilities and automobiles. Various gas sensors should be developed for such new target gases. In addition, different sensors may be needed even for the same gas depending on the conditions of sensor operation. Thus there is a need of gas sensors to measure the pollution level in the atmosphere so that appropriate steps can be followed to control the pollution. In addition, the flammable gases also need to be monitored to protect against the unwanted

incidence of fire or explosion. Thus there is huge demand for the monitoring of useful as well as flammable / hazardous gases. It may be seen most of these gases must be detected at parts per million (ppm) levels in the ambient. While other gases (for example H_2) are not toxic at ppm levels but they are combustible and form explosive mixtures when their concentration in air exceeds a threshold value. Table 1.2 shows threshold limit value (TLV) data for some of the common toxic gases and table 1.3 shows the lower explosive limit (LEL) and ignition temperature of some typical combustible gases/vapors [6-8].

Table 1.2 Long and short term exposure limits of some typical toxic gases/ vapors

Gas/vapor	Long term exposure limit, 8hr (ppm)	Long term exposure limit, 10min (ppm)
H_2S	10	15
CO	50	300
NO_x	3	5
SO_2	2	5
CH_3OH	200	250
Cl_2	0.5	1
NH_3	25	35

Table 1.3 Lower explosive limit and ignition temperature of some typical combustible gases/vapors

Gas/vapor	Long term explosive limit (%v/v)	Ignition Temp (^{0}C)
H_2	4	560
CO	12.5	605
CH_4	5	595
CS_2	1	102
C_4H_{10}	1.5	365
CH_3OH	6.7	455
Kerosine	0.7	210
C_2H_6	3	515
C_2H_2	1.5	305

In order to meet such a need for various gas sensors, one has to have a concept of gas sensor design. Generally speaking, a gas sensor should posses two basic functions, a function to recognize a particular gas species (receptor function) and another to transduce the gas recognition into a sensing signal (transducer function). In many cases, the gas recognition is carried out through gas solid interactions such as adsorption, chemical reactions and electrochemical reactions. On the other hand, the way of transduction is heavily dependent on the materials utilized for the gas recognition. The gas recognition by semi conducting oxides is conventionally transduced into a sensing signal through the electrical resistance changes of the sensor elements, while capacitance can be used for the elements using dielectric materials. Electromotive force, resonant frequency, optical absorption or emission etc can also be utilized as sensing signals for other types of sensor material.

1.4 Various Technologies in Gas sensing application

The most commonly used gas sensors can be divided into three major groups depending on the technology applied in their development.

- Optic
- Spectroscopic
- Solid

Optical sensors measure absorption spectra after the target gas has been stimulated by light. They require a complex measurement system: a monochromatic excitation source and an optical sensor to analyse the absorbed spectra. Expensive analytical techniques (such as infrared spectroscopy, ultraviolet fluorescence, chromatography, etc.) are used to analyse gases.

Spectroscopic systems make a direct analysis of the molecular mass or vibrational spectrum of the target gas. They can quantitatively measure the composition of the different gases with good precision. Gas chromatography and mass spectrometry are the most important spectroscopic gas sensor systems. The gas chromatograph (GC) is very often combined with a mass spectrometer (GC - MS) for separating and identifying compounds. Through mass spectroscopy, the molecular mass and typical fragmentation of an unknown volatile can be obtained and compared with reference libraries. Infrared spectroscopy using fourier transform methods can also be combined with a gas chromatograph (GC-FTIR). Due to its ability to differentiate between isomers, it can complement GC-MS [9]. To detect odours, the gas chromatographic separation of volatiles can be combined with sensory analysis of individual peaks, using a split gas-stream GC-technique [10]. All these techniques are very precise, sophisticated and require a technician with a lot of experience to work with the equipment in order to obtain better result.

While spectroscopic and optic systems are too expensive for domestic use and sometimes difficult to implement in reduced spaces such as car engines, the so-called solid state sensors have great advantages due to their fast sensing response, simple implementation and low prices [11-13]. They are small, so they can be portable, they are low-power consuming, they are inexpensive because of the considerable production of semiconductor materials and they can be used in complex systems such as sensor arrays. Furthermore, these sensors are capable to work on-line without need of specially trained operators.

1.5 Solid State Gas Sensors

Solid state gas sensors, based on a variety of principles and materials, are the best candidates to the development of commercial gas sensors for a

wide range of such applications [14-18]. The great interest of industrial and scientific world on solid state gas sensors comes from their numerous advantages, like small sizes, high sensitivities in detecting very low concentrations (at level of ppm or even ppb) of a wide range of gaseous chemical compounds, possibility of on-line operation and, due to possible batch production and low cost. On the contrary, traditional analytical instruments such as mass spectrometer, NMR and chromatography are expensive, complex and large in size. In addition, most analysis requires sample preparation, so that real-time analysis is difficult. Solid-state chemical sensors have been widely used, but they also suffer from limited measurement accuracy and problems of long-time stability. However, recent advances in nanotechnology, i.e. in the cluster of technologies related to the synthesis of materials with new properties by means of the controlled manipulation of their microstructure on a nanometer scale, produce novel classes of nanostructured materials with enhanced gas sensing properties.

Several physical effects are used to achieve the detection of gases in solid state gas sensors. This is tabulated in table 1.4. In contrast to optical processes, which employ infra-red absorption of gases, chemical processes, which detect the gas by means of a selective chemical reaction with a reagent, mainly utilize solid-state chemical detection principles. A characteristic of solid state gas sensors is the reversible interaction of the gas with the surface of a solid-state material. In addition to the conductivity change of gas-sensing material, the detection of this reaction can be performed by measuring the change of capacitance, work function, mass, optical characteristics or reaction energy released by the gas/solid interaction.

Table 1.4 Classification of Solid-state gas sensors

Type of sensor	Gas sensor	Detection Principle
Solid State Sensors	Chemiresistive	A change in conductivity of semiconductor is measured when it interacts with the analyzing gas
	Chemical field effect transistors(ChemFET)	Current-Voltage (I-V) curves of a field effect transistor(FET) are sensitive to a gas when it interacts with gate
	Calorimetric	The concentration of combustible gas is measured by detecting the temperature rise resulting from the oxidation process on a catalytic element.
	Potentiometric	The signal is measured as the potential difference (voltage) between the working electrode and the reference electrode. The working electrode's potential must depend on the concentration of the analyte in the gas phase.
	Amperometric	Diffusion limited current of an ionic conductor is proportional to the gas concentration

Organic or inorganic (as semiconducting metal oxides) materials, deposited in the form of thick or thin films, are used as active layers in such gas sensing devices. The read-out of the measured value is performed via electrodes, diode arrangements, transistors, surface wave components, thickness-mode transducers or optical arrangements. Indeed, although the

basic principles behind solid state gas sensors are similar for all the devices, a multitude of different technologies have been developed. Hence, nowadays the number of different solid state based gas sensors is really very large. Due to the large variety of sensors, a rich fabric of interdisciplinary science ranging from solid state physics, chemistry, electronics, biology, etc., governs the modern gas-sensing devices. Solid state sensors depend strongly on the development of technologies with applications in other areas. A steering technology is that of micromachining which for chemical sensors has led to the development of gas sensor devices with small power consumption and short time constants, greater portability and easy integration with electronics.

Semiconductor based chemiresistor sensors are most investigated and widely used for detection of combustible and toxic gases owing to their low cost and relative simplicity. Chemiresistors or conductometric gas sensors mainly operate on the base of surface reactions. The chemiresistive gas sensors work on the principle of a change in electrical resistance due to an interaction between the semiconductor and the gas [19-23].These sensors have excellent sensitivity, very short response time, low cost, and very good suitability for design of portable instruments, which compensate their disadvantages and open great possibilities for those sensors application in alarm systems, portable instruments and electronic nose.

1.6 Chemiresistive Gas Sensors

Semiconductor gas sensors (SGS), known also as chemiresistive gas sensors, are typically based on metal oxides. Atoms and molecules interact with semiconductor metal oxide surfaces, and influence such surface properties as conductivity and surface potential. The effect of the ambient atmosphere upon the electrical conductance of semiconductors was

described earlier [24, 25]. Later on in 1962, Seiyama et al demonstrated for the first time that the conductivity of ZnO films, heated to 300^0C, was sensitive to the presence of traces of reactive gases present in air [26]. In the year 1970 Taguchi reported similar properties for SnO_2, with an additional advantage of a greater stability [27]. Since then, semiconductor gas sensors have been widely used as domestic and industrial gas detectors for gas-leak alarm, process control, pollution control, etc. Compared to the organic (such as phenenthrene, polybenzimidole) and elemental (such as Si, Ge, GaAs,GaP) semiconductors, semiconductor oxides have been more successfully employed as sensing materials for the detection of different gases, such as CO, CO_2, H_2, alcohol, H_2O, NH_3, O_2, NO_x, etc. Both n-type and p-type semiconductor oxides can be used as gas sensor materials. There is a vast amount of literature devoted to the development and study of solid state gas sensor [28-31]. Various semi conducting metal oxides (SnO_2, ZnO, WO_3, In_2O_3) [32-35], catalytic oxides (V_2O_5, MoO_3, CuO, NiO) [36-39] and mixed oxides ($LaFeO_3$, $ZnFe_2O_4$, $BaTiO_3$ and $Cd_2Sb_2O_{6.8}$) [40-44] have been studied for gas sensing properties and many more new oxides are currently being explored. However, most of the gas-sensing studies are based on empirical methods, though there have been some good scientific publications dedicated to the understanding of the gas sensing mechanisms [45, 46]. Nevertheless, metal oxides based gas sensors are a commercial success and, for a host of gases, are easily available in the market for last 25 years. Nowadays, there are many companies offering metal oxide based gas sensors, such as Figaro, FIS, MICS, UST, CityTech, Applied-sensors, NewCosmos, etc… A summary of literature survey of chemiresistive gas sensors using different oxides and analysed gases are tabulated in table 1.5.

Table 1.5 Various Chemiresistive materials, additives and the analyzing gas

Chemiresistive material	Base Material	Additives	Analysing gas	Ref.
Metal-Oxides	Al_2O_3	Al, SiO_2/Si	Humidity, Methane, Ammonia	47-50
	Bi_2O_3	Sb_2O_3	Smoke, Carbon monoxide, Nitric Oxide	51-53
	CdO	$ZnFe_2O_4$	Ethanol	54
	CeO_2	SnO_2	Oxygen, Hydrogen Sulphide	55-57
	Cr_2O_3	TiO_2	Nitrogen dioxide, Oxygen, Ammonia, Humidity	58-60
	Co_3O_4	SiO_2	Ammonia, Carbon monoxide, Methane, Propane, Hydrogen, Nitrogen dioxide, Chlorine	61-63
	CuO	SnO_2	Carbon monoxide, Ethanol, Hydrogen Sulphide	64-67
	Fe_2O_3	Au, Zn (Pt, Pd, RuO_2)	Methane, Propane, Benzene, Toluene, Carbon monoxide, Nitrogen dioxide, Methanol, Acetone.	68-72
	Ga_2O_3	SnO_2, Pd, Ta_2O_5, WO_3, NiO	Oxygen, Carbon monoxide , Methane, Nitric Oxide, Ammonia.	73-77
	In_2O_3	MoO_3, Au, Al, SnO_2	Ozone, Nitrogen dioxide, Hydrogen, Carbon monoxide, Propane, Hydrogen Sulphide, Chlorine, Carbon dioxide, Sulphur dioxide, Ammonia, Ethanol, Acetone	78-87
	MoO_3	Ti	Ammonia, Carbon monoxide, Nitrogen dioxide	88-91
	Nb_2O_5	SnO_2	Ammonia, Carbon monoxide, Ethanol, Hydrogen	92-94
	NiO	Li, TiO_2	Hydrogen, Formaldehyde, Methane, Acetic acid, Carbon monoxide, Nitrogen dioxide.	95-98
	Ta_2O_5	-	Humidity	99
	SnO_2	Pt, Ag, Pd, Os, Fe, Au, In, Ru, Bi_2O_3, CeO_2, CuO	Carbon monoxide, Methane, Sulphur dioxide, Nitrous Oxide, Carbon dioxide, Nitrogen dioxide, Propane, Methanol, Ethanol, Hydrogen, LPG, Hydrogen Sulphide, Ammonia, C_nH_{2n+2}, Toluene	6, 100-121
	TiO_2	La, Pt, Cr_2O_3, WO_3	Methanol, Ethanol, Propyl Alcohol, Nitrogen dioxide, Oxygen, Hydrogen, Ammonia	122-133
	WO_3	Mg, Zn, Mo,Re, Au, Pd	Nitrogen dioxide, Ammonia, Hydrogen Sulphide, Ozone	134-147
	V_2O_5	Fe_2O_3, SnO_2, TiO_2	Nitrogen dioxide, Ammonia, Ethanol, Butyl amines, Propanol, Toluene	148-150
	ZnO	Al, Sn, Cu, Pd,Fe_2O_5	Ammonia, Hydrogen, LPG, Methane, Carbon monoxide, Hydrogen Sulphide, Nitrogen dioxide, Methanol, Propyl Alcohol, Ethanol	151-160

An oxide semiconductor gas sensor detects an inflammable gas from a change in electric resistance of a polycrystalline element. It is unanimously agreed that the resistance change on exposure to the gas arises through a surface phenomenon of the oxide semiconductor used [161-163], but this is only a part of the whole gas-sensing processes taking place in the element. Generally speaking, a chemical sensor consists of two functions, i.e., receptor function which recognizes or identifies a chemical substance, and transducer function which transduces the chemical signal into an output signal. For the basic understanding of the semiconductor gas sensor, therefore, one needs to differentiate these two functions. Figure 1.2 shows schematically how a semiconductor sensor element generates sensing signals upon contact with an inflammable gas. Apparently, the receptor function is provided with the surface of each semiconductor particle. The obtained chemical signal is then transduced through the microstructure of coagulating particles into the resistance of the polycrystalline element.

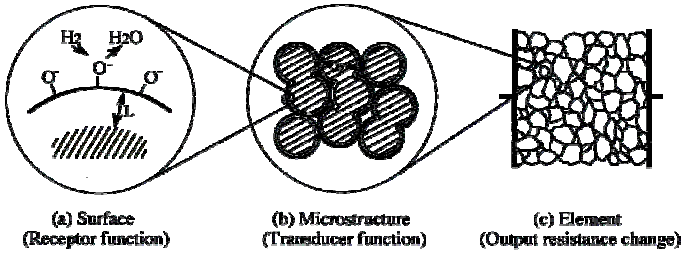

Fig. 1.2 Receptor and transducer functions of the semiconductor gas sensor

The gas/semiconductor surface interaction is based on the gas-sensing mechanism of SGS occuring at the grain boundaries of the polycrystalline oxide film. They generally include reduction/oxidation processes of the semiconductor, adsorption of the chemical species directly on the semiconductor and/or adsorption by reaction with surface states associated with pre-adsorbed ambient oxygen, electronic transfer of delocalized conduction-band electrons to

localized surface states and vice versa, catalytic effects and in general complex surface chemical reactions between the different adsorbed chemical species. The effect of these surface phenomena is a reversible and significant change in electrical resistance. This resistance variation can be easily observed and used to detect chemical species in the ambient.

The working temperature, at which these devices work, varies depending on the specific target gas in the ambient and on the selected sensor material in conjunction with its properties in every case. As this working temperature ranges usually from 200 to 400 °C, it is necessary to implement a heating element in sensor device. A simple SGS is thus basically composed of a substrate in alumina, glass, quartz or silicon (on which the sensing layer is deposited), the electrodes (to measure the resistance changes of the sensing film) and the heater (commonly a Pt resistive type heater) to reach the optimum sensing temperature. Semiconductor gas sensors offer low cost, high sensitivity and a real simplicity in function, advantages that should work in their favour as new applications emerge. Moreover, the possibility of easily combining in the same device the functions of a sensitive element and signal converter and control electronics markedly simplifies the design of a sensor and constitutes the main advantage of chemiresistive-type sensors over biochemical, optical, acoustic, and other gas sensing devices. In spite of the numerous advantages of resistive-type gas sensors, they show different disadvantages as poor reproducibility, long-time instability due to aging, cross sensitivity to other gases, selectivity, sensitivity to water vapour etc...

1.7 Basic Characteristics

The electrical resistance of a chemiresistive sensor changes drastically (increase or decrease) when exposed to the molecules of analyzing gas.

Increase or decrease in resistance depends on the nature of sensor material (n-type or p-type) and the gas (reducing or oxidizing). A typical response curve, that is, variation of resistance of sensor with time on exposure and withdrawal of analyzing gas, is schematically depicted in Figure 1.3.

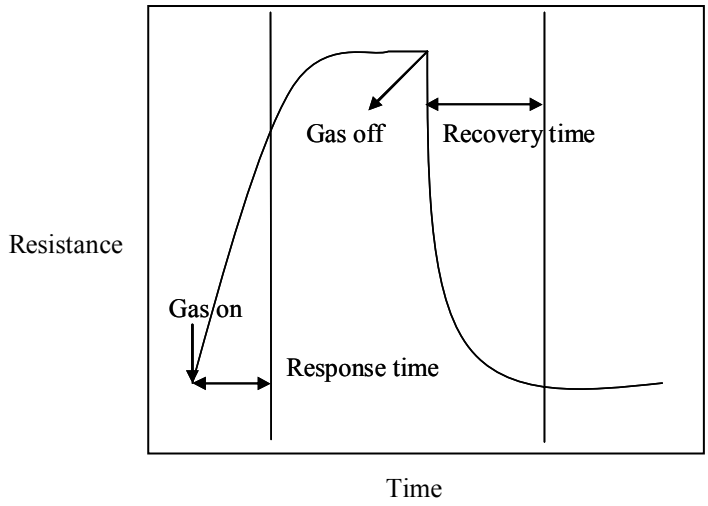

Fig. 1.3 Schematic response-curve of a chemiresistive gas sensor

The response curve of a sensor is characterised by following five parameters:

a) Sensitivity
b) Selectivity
c) Stability
d) Response time
e) Recovery time

These parameters are discussed below.

1.7.1 Sensitivity

This is the device characteristic to percept a variation in physical and /or chemical properties of the sensing material under gas exposure. The sensitivity is generally defined as the ratio of the resistance of the sensing element in the target gas to that in air. The sensitivity is highly dependent on film porosity, film thickness, operating temperature, presence of additives and crystallite size. In order to improve it, it will be of great interest to work with the most appropriate sensing material in every case and reach its optimum detecting temperature. As suggested by several authors [164-165] working with nanostructure materials will give a higher surface area in front of gas. Taking into account that sensing reactions take place mainly on sensor layer surface, the control of semiconductor particle size will be one of the first requirements for enhancing the sensitivity of the sensor.

1.7.2 Selectivity

This characteristic is related to the discrimination capacity of a sensor towards a mixture of gases. Selectivity plays a major role in gas identification. Generally, a 'fingerprinting' method relies on a unique signature of the target gas signal. However, gases often produce very similar sensor responses (except when comparing reducing to oxidizing gases). For example, gases such as ethanol, carbonmonoxide, and methane have appreciable cross-sensitivity that hinders the development of a domestic gas sensor that can distinguish these species [166]. Common techniques of improving the selectivity of gas sensors include controlling the sensor operating temperature, selective gas filters used in series with gas sampling, and using additives. Different operating temperatures allow the control of the sensitivity toward a particular gas when there is a unique T_{crit} (critical temperature / optimum temperature with maximum sensor response) for each

gas; thus allowing the sensor to produce distinguishable signals for two gases at a selected temperature. The film morphology and sensor architecture can also play a key role in selectivity [167]. Distinguishing poorly reactive gases from reactive gases can be facilitated by placing electrodes further inside the bulk of the sensing material to allow reactive materials to be filtered by the sensing material near the surface of the sensor. Another technique uses catalysts, which generally reduce the operating temperature of a gas sensor for a particular gas species and thus allow the target gas to be distinguished from other gases due to the differences in sensitivity. In other words, addition of catalysts can maximize the sensitivity of target gases to produce a distinct signal

1.7.3 Stability

It is a characteristic that takes into account the repeatability of device measurements after a long use. The success of the sensor will be limited if the sensor performance is not demonstrated as repeatable and stable over long-term testing. Problems of stability, as outlined by Park and Akbar [167] may be attributed to three primary areas of concern. The first is that a surface conductive sensor can suffer from surface contamination. Second, changes in the sensor characteristics (such as intergranular connectivity) can occur due to thermal expansion coefficient mismatch and / or interfacial reactions at the metal electrode / ceramic interface. Last the film morphology may change over time due to the relatively high operating temperatures of the sensor, which may change over time due to the relatively high operating temperatures of the sensor, which may also cause migration of additives.

To avoid the effects of non-repeatability after repeated use, the sensor materials are submitted to a thermal pre- treatment, which would decrease posterior material instabilities. During these treatments samples are

submitted to high calcinations temperatures (from 400 to 1000^0C during 1 to 8 hours) to avoid instabilities during their working life, continuously heated at 200-400^0C. Most often the sensor element gets covered with decomposition products like carbon, CO_2, and H_2O causing a gradual decrease in the sensitivity at the operating temperature. A periodic change in sensor temperature removes all the adsorbed species and unburnt organic contaminants from the surface.

1.7.4 Response Time

The response time is the time interval over which resistance attains a fixed percentage (usually 90%) of final value when the sensor is exposed to full scale concentration of the gas. Time response is especially dependent on the sensor characteristics such as crystallite size, additives, electrode geometry, electrode position, diffusion rates, etc... A small value of response time is indicative of a good sensor.

1.7.5 Recovery Time

This is the time interval over which the sensor resistance reduces to 10% of the saturation value when the sensor is exposed to full scale concentration of the gas and then placed in clean air. A good sensor should have a small recovery time so that sensor can be used over and over again.

1.8 Detection Principle

Unlike other semiconductors which, under long-term or cycled heating in air, undergo irreversible chemical transformations by forming stable oxide layers, metal oxides bind oxygen on their surface in a reversible way. The principle detection process is the change of oxygen concentration at the surface of these metal oxides, caused by adsorption and heterogeneous

catalytic reaction of oxidizing and reducing gaseous species. The electrical conductivity depends on the gas atmosphere and on the temperature of the sensing material exposed to the test gas.

According to Williams and Moseley [168], most target gases are detected due to their influence on the oxygen stoichiometry of the surface. Studies have revealed that the key reaction involves modulation of the concentration of surface oxygen ions. The conductivity changes are caused by the formation of a space charge region induced by either gas adsorption or by the formation of oxygen vacancies on the surface.

Many studies have been devoted to identify the surface oxygen species. The form of adsorbed oxygen (either molecular or atomic) depends on the temperature of the sensor where O_2^- species have been observed at lower temperatures (below 175^0C) and O^- and O^{2-} species have been observed at higher temperatures (above 175^0C) occurs [169-171].

In an n-type semiconductor the sensor conductivity increases in the presence of a reducing gas (such as CO) and decreases in the presence of an oxidizing gas (such as O_2). In most of the metal oxide based gas sensor the sensor response is due to the surface interactions between the sensor and the surrounding gases. The general steps involved in sensor response upon exposure to air and to a reducing gas, R, are shown in figure 1.4. As shown in the left of column in figure 1.4, oxygen from the air is adsorbed on to the surface of the metal oxide. Electrons from the surface region of the sensor are transferred to the adsorbed oxygen, leading to the formation of an electron depleted region near the surface of the sensor. The electron depleted region, also called the space-charge layer, is an area of high resistance and the core region of the particle, where electron densities are high, is an area of relatively low resistance.

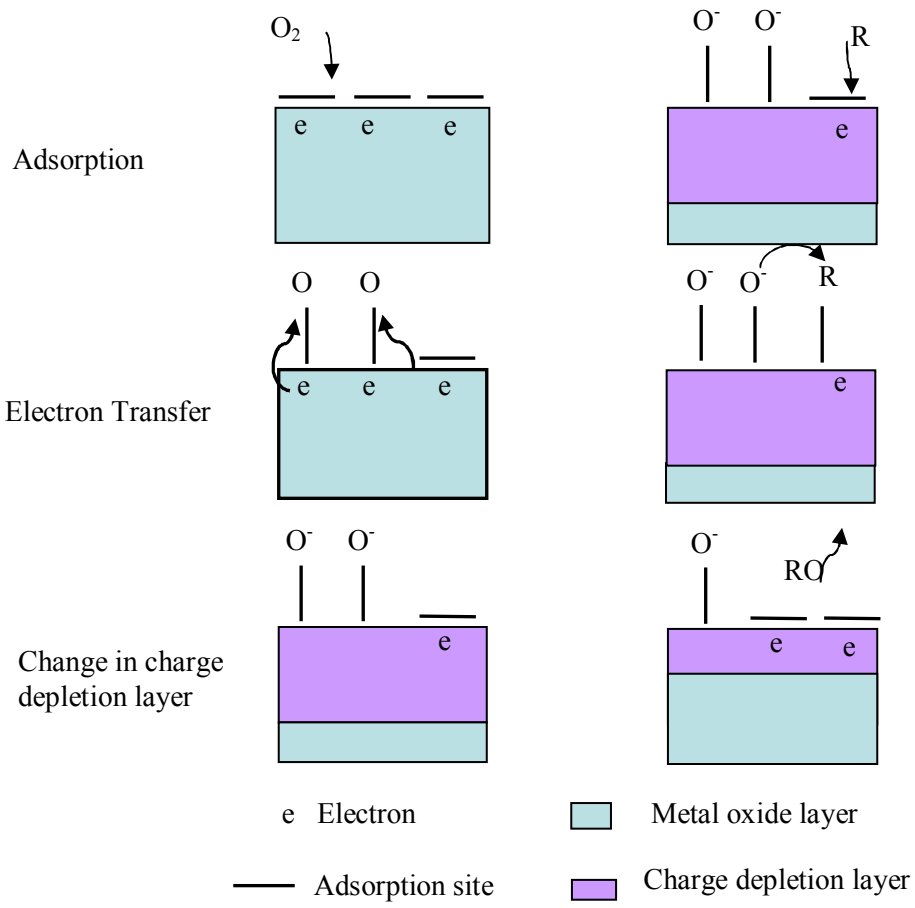

Fig 1.4. Schematics indicating the mechanisms leading to n-type semiconducting metal oxide sensor response to oxidizing and reducing gases

As shown in right hand column of figure 1.4, when exposed to a reducing gas like CO, surface reactions such as,

$$CO + O^{-}{}_{ads} \rightarrow CO_2 + e^{-} \quad \text{and}$$
$$2CO + O^{-}{}_{2\,ads} \rightarrow 2CO_2 + e^{-}$$

release electrons back to the metal oxide and lead to a decrease in the resistance of the space charge layer hence an increase in conductivity. The n-

type metal oxide semiconductor materials have relatively few adsorption sites available due to the development of potential barriers on the particle surface [172]. In addition the fraction of surface sites occupied is low in comparison with the sites available on the surface of metal oxide [167].

Consequently incorporating species that have a comparably high number of adsorption sites with high fractional occupancy in the metal oxide sensing material can have significant impact on the sensor performance. Improved efficiency and sensing selectivity of these devices require detailed understanding of the surface and interfacial processes at the atomic level, and their relationship with materials properties and device performance.

1.9 Catalytic Additives on Metal Oxide Semiconductor Sensors

Almost all metal oxides suffer from the problem of poor selectivity. Attempts have been made in literature to improve the selectivity of metal oxides using different means. The addition of an appropriate amount of metal additives has been shown to improve the detection of various kinds of gases via the enhancement of the sensor response and a decrease of the temperature of maximum sensor response. A decrease in response time and a better selectivity are also claimed to be achievable by using these additives. Table 1.4 shows the various metal additivies used in metal oxide semiconductor gas sensor for achieving selectivity.

The addition of metal additives can lead to two different sensitisation mechanisms: Chemical sensitisation (spill over mechanism) and electronic sensitisation (Fermi level mechanism) [173]. Figure 1.5 shows the schematic representation of mechanism of sensitization by metal or metal oxide additive. In the first case, the promoting effect is due to the ability of noble metals to activate inflammable gases by enhancing their spill-over, so that

they react with oxygen adsorbates more easily. The promoter in this case activates a test gas to facilitate its catalytic oxidation on the semiconductor surface. In other words, the promoter does not affect the resistance of the element directly, leaving the gas-sensing mechanism essentially the same as in the case without it. In this type of sensitization, an inflammable gas eg. , H_2 is activated by the metal additive and the activated fragments (H) of the gas are spilt-over to the semiconductor surface to react with the adsorbed oxygen. The metal additive thus facilitates chemical reaction of the gas on the semiconductor [16]. The promoter increases the gas sensitivity as it increases the rate of the chemical processes leading to a decrease in concentration of the negatively charged adsorbed oxygen. This is why the effect is called chemical sensitization [172]. In this way, the additives exert a sort of remote control on the catalytic and sensing properties of the metal oxide.

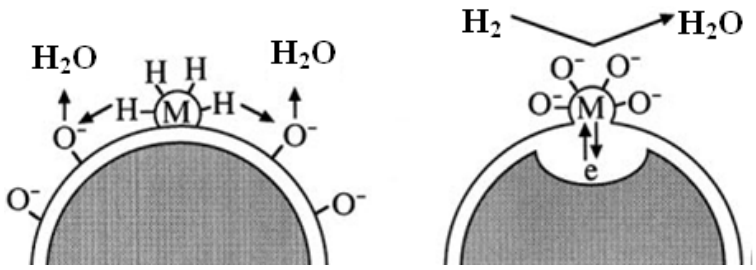

(a) Chemical sensitization (a) Electronic sensitization

Fig. 1.5 Mechanism of sensitization by metal or metal oxide additive

On the other hand, the electronic sensitisation is associated with oxidised metal additives. Electronic sensitization comes out through a direct electronic interaction between the promoter and the semiconductor surface. When the oxidation state of the promoter changes with the surrounding atmosphere, the electronic state of the semiconductor will also change accordingly. The addition of fine particles of some metals to n-type metal

oxides usually results in a rise of the base resistance of semiconductor metal oxide in air. There is a decrease in the electron concentration in the oxide surface layer, which corresponds to an increase of the space charge depth as a result of the electron transfer from the metal oxide to the metal loaded on to its surface. When the metal surface is covered with oxygen adsorbates at elevated temperatures in air (i.e. the metal is oxidised), the oxygen adsorbates extract electrons from the metal, which in turn extracts electrons from the metal oxide, leading to a further increase in the space-charge depth. More specifically these oxidised metal additives will be easily reduced to metals in presence of an inflammable gas. Consumption of oxygen adsorbates on the metal, in addition to those on the metal oxide surface, by reaction with flammable gases, causes the enhanced sensitivity. In this case therefore the promoting effect arises mainly from the change in the oxidation state of the loaded material.

1.10 Metal Oxide Semiconductor Nanoparticles for Chemical Gas Sensors

Gas adsorption is mainly a surface related process. The grain size and area of active surface layers are the main parameters, controlling gas sensing effects in semiconducting gas sensors. Hence decreasing the particle size has a dramatic effect in gas sensing related topics. Due to a high specific surface area, semiconductor nanoparticles are very well suited to the fabrication of chemical gas sensors. Their surface to bulk ratio is much larger than that of coarse micro-grained materials, which yields a large interface between the oxide and the gaseous medium. Therefore, for the same chemical composition, the smaller the nanomaterials are, the more sensitive the sensor is. The interaction taking place between a gas and a solid mainly takes place on the surface and interfaces are critical for controlling the properties of the

gas sensor. In a nanocrystalline material the portion of the surface atoms is very high [174-177]. Indeed the large density of molecules which can possibly adsorb on the semiconductor nanoparticles, results into large variations of the electrical conductivity. Hence decreasing the crystallite size can dramatically improve the sensor sensitivity. The gas sensing principles are same as that of standard metal oxide sensors [178].

Crystallite size effects on sensor performance are generally explained in terms of the relative values of the characteristic dimensions of the connection between adjacent particles (the neck width) and thickness of the space charge layer. The thickness of the space charge layer is typically indicated by the Debye length, L_D, of the electrons in the oxide sensor. The change in conductivity of a sensing layer is often explained by 'grain boundary models' [179]. In this context, the term grain is used as a synonym for a single crystalline particle, regardless of whether or not the grain is agglomerated or sintered to form larger entities (polycrystalline). It has been shown, that the particle size as well as the connection of adjacent metal oxide grains, either agglomerated or sintered, affects substantially the conductivity and thus the sensitivity of a sensor. The gas response increases abruptly when the particle size D becomes comparable or smaller than the depletion layer thickness L, which for example, is determined to be 5-15 nm for SnO_2 grains. Furthermore, a proportional relation between the sensitivity to 1/D was obtained by theoretical simulation, confirming the experimental results [164,180]. In this regard, a semi quantitative model was proposed by Xu et al. [179], which concerns the relationship between grain size D and L of sintered and agglomerated grains, whereas three different cases can be distinguished, illustrated in figure 1.6.

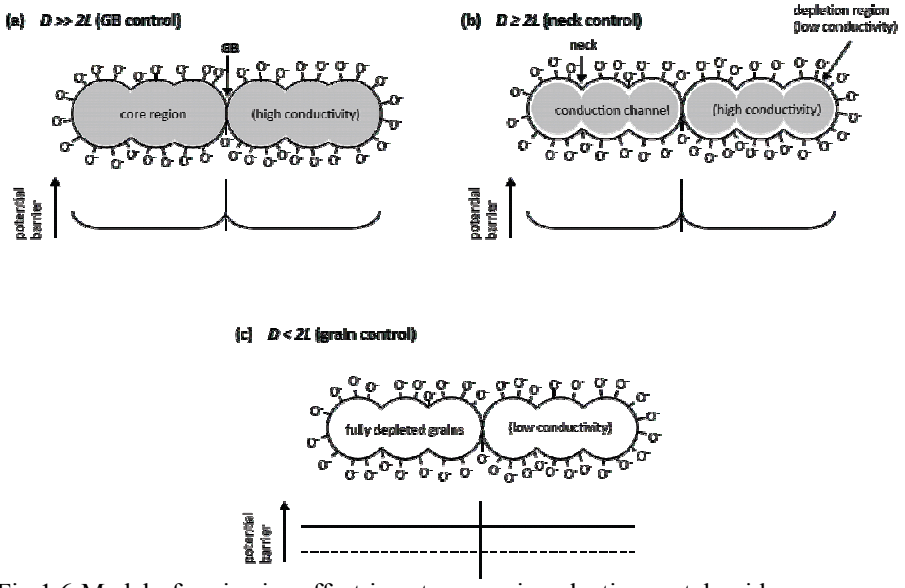

Fig.1.6 Model of grain size effect in n-type semiconducting metal oxide gas sensor. (a)D >> 2L, conductivity is grain boundary controlled, (b) D ≥ 2L, the conductivity is neck controlled, (c) D < 2L, the conductivity is grain controlled.

In case of large grains with a small surface-to-volume ratio, *L* is significantly smaller than the single crystallite size *(D >> 2L)*. Most of the volume of the crystallites is unaffected by the surface interactions with the gas phase. The electron conducting channels through necks are too wide to be influenced by the surface effect. Basically, the conductivity depends on the grain boundary barrier height (GB) for inter crystallite charge transport from one grain to another (see Figure 1.6, a) and is therefore independent of the grain size (grain boundary controlled). In case of higher surface-to-volume ratio, *i.e.* smaller grains but still larger than twice the depletion layer *(D ≥ 2L)*, that region extends into the grains forming constrictions, so called necks (see Figure 1.6, b). As a consequence, the conductivity is affected by the cross section area of these necks which is dependent on the ambient gas composition (neck controlled). Compared to the former case (*D >> 2L*) the

mentioned constriction effect adds up to the effect of GB barriers resulting in an improvement of the gas sensitivity. Again, oxidizing gases increase the depletion layer thickness leading to smaller necks, whereas reducing gases cause a decrease, resulting in larger necks. When $D < 2L$, the depletion layer extends throughout the whole grain and the crystallites are almost entirely depleted (see Figure 1.6, c). Under this situation, grains share a major part of the resistance and control the gas sensitivity. Thus the conductivity decreases steeply since the conduction channels between the grains are not present. The energy bands are nearly flat throughout the whole structure of the interconnected grains, and since there are no significant barriers for intercrystallite charge transport the conductivity is primarily controlled by the intracrystallite conductivity (grain controlled). It was found empirically as well as theoretically, that the highest gas sensitivity towards reducing gases (CO and H_2) is obtained in this case. Already very small variations in the trapped charge density lead to a significant change in the effective carrier concentration and finally in the electrical conductivity. Moreover, a proportional relation between the sensitivity to 1/D was found theoretically by Rothschild [181], approving the results previously obtained experimentally by Xu et al [179]. The considerations reveal that high surface-to-volume ratios, present in nanocrystalline metal oxides, are desired for gas sensing purposes. A more extensive discussion about the complex processes of the gas detection is given in some reviews [179, 182, 183]. Superior gas sensing properties have been reported for semiconductor metal oxide materials for sizes in 5-50 nm range [7, 8, 14, 15, 172]. Due to this enhanced sensitivity metal oxide semiconductor nanoparticles present a new trend in the area of gas sensing.

1.11 Objective of Present Study

The essentially positive outlook for the gas sensors industry stems from the undeniable fact that gas sensors are indispensable to numerous, key

industries, since they provide vital information about the gaseous composition of the ambient. Moreover, driven by the continued proliferation of more advanced electronic control systems to increase efficiencies, users of gas sensors require ongoing advances in sensor accuracy, reliability, response time, robustness, miniaturization, and/or communications capability. Such requirements drive the trends of R&D in gas sensors industry, which in turn fuels opportunities for technology advancements that can open up new applications of gas sensors. While many different approaches to gas detection are available, the R&D of solid state gas sensors has enormously advanced in recent years. Gas sensors operate on the principle of conversion of gas concentration into a measurable signal. Among the solid-state gas sensors, semiconductor metal oxide gas sensors have received the most attention as they show good potential for continuous monitoring of gases.

Gas sensors using oxide semiconductors have been subjected to extensive research and development and have now grown to be important devices for detecting the leakage of several inflammable gases and toxic gases, since the pioneering works reported in 1962 by Seiyama et al. and Taguchi [26,27]. These sensors offer a wide variety of advantages over the traditional analytical instruments which include lower cost, easier manufacturing, smaller size, short response and faster recovery. The basic part of efforts made nowadays by scientific research community in semiconductor gas sensor field is devoted both to optimize the performances of gas sensors by improving their sensitivity, selectivity and stability for the detection of single gases and the development of electronic noses for application mainly in environmental control and in food industry. In the field of this type of gas sensors, recent applied studies and products releases have shown some significant trends on nanotechnologies. Several theoretical and applied articles have shown the advantage of reducing the metal oxide grain size down to nanometer scale in

order to improve the sensing properties (mainly sensitivity and selectivity) as well as stability over time of the oxide layer. Nanocrystalline semiconducting metal oxides as gas sensors constitute a new and exciting subject of research.

The aim of present work is development of nanocrystalline oxide semiconductor gas sensors based on tungsten oxide (WO_3), zinc oxide (ZnO) and indium oxide (In_2O_3) for the detection of environmental polluting gas like nitrogen dioxide (NO_2) and hydrogen sulphide (H_2S). Nitrogen dioxide is produced from combustion processes, which is a typical air pollutant. It can react with water in the atmosphere to form nitrous acid and nitric acid, which are one of the factors that cause the acid rain. Hence, detection and emission control of toxic NO_2 gases is of great importance. H_2S is a colourless gas with odour of rotten eggs at very low concentrations. It occurs naturally in crude petroleum, natural gas, in volcanic gases, lake and marine sediments. It is formed also from bacterial breakdown of organic matter containing sulphur, or produced by human and animal wastes. The fabrication of gas sensor and different structural characterisation techniques adopted for the sensor are presented in the thesis. The sensor response is different at different working temperatures depending upon the oxide sensor and the analyte gases. Hence the response of the sensor at different operating temperatures is studied in this work and the sensitivity at different temperature for all the oxides for both gases is obtained. The major problem associated with metal oxide gas sensors is poor selectivity. Better selectivity to the gases studied can be obtained by suitable addition of dopants. The additives added can enhance the sensor response, decrease the optimum operating temperature for maximum sensor response, decrease the response and recovery time in addition to better selectivity. In our studies we have used dopants like copper and indium to study the effect of presence of additives in the gas sensing properties of the fabricated sensor. Thick as well

as thin film sensors of the oxides are studied for the purpose of gas sensing. The optimum operating temperature, response time, recovery time, minimum and maximum detectable limits of the fabricated sensors are also presented. A detailed discussion of the sensing mechanism associated with the test gas for each sensor is also included in the thesis.

References

[1] PeterGründler Chemical Sensors: An Introduction for Scientist and Engineers, Springer, (2007) New York.

[2] A. Hulanicki, S. Geab and F. Ingman Pure and Appl. Chem. (1991) 63, 1247.

[3] O. S. Wolfbeis Fresenius J. Anal Chem. (1990) 337, 522.

[4] W. Göpel and K. Schierbaum Sensors (1991) 2, 2.

[5] J. Stetter and W. Penrose Sensors update (2002) 10, 189.

[6] G. C. Franco, A. T. Silver, J. M. Domínguez and A. S. Juárez Thin Solid Films (2000) 373, 141.

[7] S. C. Gadkari, K. Manmeet, V. R. Katti, V. B. Bhandarkar, K.P. Muthe, S. K. Gupta Encyclopedia of sensors, American Scientific Publishers (2006).

[8] D. S. Lee, H. Y. Jung, J. W. Lim, M. Lee, S. W. Ban, J. S. Huh, D. D. Lee Sensors and Actuators (2000) 71, 90 .

[9] L. Dori, S. Nicoletti and I. Elmi Sensors and Materials (2000) 12, 163.

[10] T. Aishima Anal. Chim. Acta (1991) 243, 293.

[11] H. Meixner, J. Gerblinger, U. Lampe and M. Fleischer Sensors and Actuators B (1995) 23, 119.

[12] T. Takeuchi Sensors and Actuators (1988) 14, 109.

[13] J. T. Woetsman and E. M. Logothetis The Industrial Physicst Maz. (1995) 20.

[14] P. T. Moseley and B. C. Tofield (eds.) Solid State Gas Sensors Adam Hilger Bristol and Philadelphia (1987).

[15] M. J. Madou and S. R. Morrison (eds.) Chemical Sensing with Solid State Devices Academic Press New York (1989).

[16] A. Mandelis and C. Christofides (eds.) Physics, Chemistry and Technology of Solid State Gas Sensor Devices Wiley (1993).

[17] P. T. Moseley Meas. Sci. and Technol. (1997) 8, 223.

[18] I. Lundström Sensors and Actuators B (1996) 35, 11.

[19] G. Sberveglieri, R. Murri and P. Nicola Sensors and Actuators B (1995) 23, 177.

[20] M. Andersson, M. Holmberg, I. Lundström, A. Lloyd-Spetz, P. Mårtensson, R. Paolesse, C. Falconi, E. Proietti, C. Di Natale and A. D'Amico Sensors and Actuators B (2001) 77, 567.

[21] S. J. Jung and H. Yanagida Sensors and Actuators B (1996) 37, 55.

[22] S. Nakagomi, K. Okuda and Y. Kokubun Sensors and Actuators B (2003) 96, 364.

[23] S. Jonda, M. Fleischer and H. Meixner Sensors and Actuators B (1996) 34, 396.

[24] N. Barsan, D. Koziej and U. Weimar Sensors and Actuators B (2007) 121, 18.

[25] A. Bielanski, J. Deren and J. Haber Nature (1957) 179, 668.

[26] T. Seiyama, A. Kato, K. Fujisishi and M. Nagatoni Analytical Chemistry (1962) 34, 1052.

[27] K. Ihokura and J. Watson The Stannic Oxide Gas Sensor, (1993) CRC Press.

[28] G. Eranna, B. C. Joshi, D. P. Runthala and R. P. Gupta Critical Reviews in Solid State and Materials Sciences (2004) 29, 111.

[29] A. Basudam and M. Sarmishtha Prog. Ploym. Sci (2004) 29, 699.

[30] G. S. Korotchenkov, S. V. Dmitriev and V. I. Brynzari Sensors and Actuators B (1999) 54, 202.

[31] S. Middelhoek, A. A. Bellekom, U. Dauderstadt, P. J. French, S.R. Hout, W. Kindt, F. Riedijk and M. J. Vellekoop Meas. Sci. and Technol. (1995) 6, 1641.

[32] B. Panchapakesan, D. L. Devoe, M. R. Widmaer, R. Cavicchi and S. Semancik Nanotechnology (2001) 12, 336.

[33] J. L. Solis, S. Saukko, L. B. Kish, C. G. Granqvist and V. Lantto Sensors and Actuators B (2001) 77, 316.

[34] G. Korotcenkov Sensors and Actuators B (2005) 107, 209.

[35] H. Nanto, T. Minami and S. Takata J. Appl. Phys. (1986) 60, 482.

[36] J. Liu, X. Wang, Q. Peng and Y. Li Sensors and Actuators B (2006) 115, 481.

[37] D. Mutschall, K. Holzner and E. Obermeier Sensors and Actuators B (1996) 35, 320.

[38] M. Frietsch, F. Zudock, J. Goschnick and M. Bruns Sensors and Actuators B (2000) 65, 379.

[39] I. Hotovy, V. Rehacek, P. Siciliano, S. Capone and L. Spiess Thin Solid Films (2002) 418, 9.

[40] S. Zhao, J. K. O. Sin, B. Xu, M. Zhao, Z. Peng and H. Cai Sensors and Actuators B (2000) 64, 83.

[41] C. Xiangfeng, L. Xingqin and M. Guangyao Sensors and Actuators B (1999) 55, 19.

[42] J. Holc, M. Hrovat and J. Sluneko Sensors and Actuators B (1995) 26, 99.

[43] Z. G. Zhou, Z. L. Tang and Z. T. Zhang Sensors and Actuators B (2003) 93, 356.

[44] F. Gao, Y. Liu and X. Liu Sensors and Actuators B (2001) 77, 653.

[45] J. Watson, K. Ihokuras and G. S. V. Colest Mea. Sci. Technol. (1993) 7, 711.

[46] N. Bârsan and U. Weimar J. Phys. Cond. Mat. (2003) 15, R813.

[47] G. Sberveglieri, R. Anchisini, R. Murri, C. Ercoli and N. Pinto Sensors and Actuators B (1996) 32, 1.

[48] R. K. Nahar Sensors and Actuators B (2000) 63, 49.

[49] R. Andrey, L. Michel and G. Alexandre Sensors and Actuators B (2005) 109, 91.

[50] E. C. Dickey, O. K. Varghese, K. G. Ong, D. Gong, M. Paulose and C. A. Grimes Sensors (2002) 2, 91.

[51] G. Sarala Devi, S. V. Manorama, and V. J. Rao J. Electrochem. Soc. (1998) 145, 1039.

[52] Z. N. Adamian, H. V. Abovian and V. M. Aroutiounian Sensors and Actuators B (1996) 35, 241.

[53] A. Cabot, A. Marsal, J. Arbiol and J. R. Morante Sensors and Actuators B (2004) 99, 74.

[54] C. Xiangfeng, L. Xingqin, and M. Guangyao Sensors and Actuators B (2000) 65, 64.

[55] J. Beie and A. Gnörich Sensors and Actuators B (1991) 4, 393.

[56] P. Jasinski, T. Suzuki and H. U. Anderson Sensors and Actuators B (2003) 95, 73.

[57] G. Fang, Z. Liu, C. Liu and K. Yao Sensors and Actuators B (2000) 66, 46.

[58] Y. Li, W. Wlodarski, K. Galatsis, S. H. Moslih, J. Cole, S. Russo and N. Rockelmann Sensors and Actuators B (2002) 83, 160.

[59] G. Neri, A. Bonavita, G. Rizzo and S. Galvagno J. Euro. Cer. Soc. (2004) 24, 1435.

[60] J. Du, Y. Wu and K. L. Choy Thin Solid Films (2006) 497, 42.

[61] D. P. Runthala, R. P. Gupta, P. D. Vyas, G. Eranna, R. Paris and D. Schipanski Ind. J. Engg. Mats. Sci. (2000) 7, 336.

[62] M. Ivanovskaya, D. Kotsikau, G. Faglia, P. Nelli and S. Irkaev Sensors and Actuators B (2003) 93, 422.

[63] C. Cantalini, M. Post, D. Buso, M. Guglielmi and A. Martucci Sensors and Actuators B (2005) 108, 184.

[64] A. Cruccolini, R. Narducci and R. Palombari Sensors and Actuators B (2004) 98, 227.

[65] J. Liu, X. Huang, G. Ye, W. Liu, Z. Jiao, W. Chao, Z. Zhou and Z. Yu Sensors (2003) 3, 110.

[66] M. Frietsch, F. Zudock, J. Goschnick and M. Bruns Sensors and Actuators B (2000) 65, 379.

[67] V. R. Katti, A. K. Debnath, K. P. Muthe, Manmeet Kaur, A. K. Dua, S. C. Gadkari, S. K. Gupta and V. C. Sahni Sensors and Actuators B (2003) 96, 245.

[68] P. Althainz, L. Schuy, J. Goschnick and H. J. Ache Sensors and Actuators B (1995) 24, 448

[69] G. Neri, A. Bonavita, G. Rizzo, S. Galvagno, S. Capone and P. Siciliano Sensors and Actuators B (2006) 114, 687

[70] S. V. Ryabtsev, A. V. Shaposhnick, A. N. Lukin and E. P. Domashevskaya Sensors and Actuators B (1999) 59, 26.

[71] H. Tang, H. Zhang, S. Li, X. Ma, M. Wang and D. Yang Sensors and Actuators B (2006) 114, 910.

[72] G. Neri, A. Bonavita, S. Galvagno, P. Siciliano and S. Capone Sensors and Actuators B (2002) 82, 40.

[73] M. Ogita, K. Higo, Y. Nakanshi and Y. Hatanaka Applied Surf. Sci. (2001) 175, 721.

[74] M. Ogita, S. Yuasa, K. Kobayashi, Y. Yamada and Y. Nakanshi, Y. Hatanaka Applied Surf. Sci. (2003) 212, 397.

[75] J. Frank, M. Fleischer, H. Meixner and A. Feltz Sensors and Actuators B (1998) 49, 110.

[76] U. Lampe, E. Simon, R. Pohle, M. Fleischer, H. Meixner and H.-P. Frerichs, M. Lehmann and G. Kiss Sensors and Actuators B (2005) 111, 106.

[77] M. Fleischer, M. Seth, C. D. Kohl and H. Meixner Sensors and Actuators B (1996) 36, 290.

[78] T. Doll, A. Fuchs, I. Eisele, G. Faglia, S. Groppelli and G. Sberveglieri Sensors and Actuators B (1998) 49, 63.

[79] G. Faglia, B. Allieri, E. Comini, L. E. Depero, L. Sangaletti and G. Sberveglieri Sensors and Actuators B(1999) 57, 188.

[80] Z. Jiao, M. Wu, J. Gu and X. Sun Sensors and Actuators B (2003) 94, 216.

[81] A. Forleo, L. Francioso, M. Epifani, S. Capone, A. M. Taurino and P. Siciliano Thin Solid Films (2005) 490, 68.

[82] W. Y. Chung, G. Sakai, K. Shimanoe, N. Miura, D. D. Lee and N. Yamazoe Sensors and Actuators B (1998) 46, 139.

[83] J. Xu, X. Wang and S. Jianian Sensors and Actuators B (2006) 115, 642.

[84] J. Tamaki, J. Niimi, S. Ogura and S. Konishi Sensors and Actuators B (2005) 117, 353.

[85] R. Winter, K. Scharnagl, A. Fuchs, T. Doll and I. Eisele Sensors and Actuators B (2000) 66, 85.

[86] H. Mbarek, M. Saadoun and B. Bessais Material Science and Engineering: C (2006) 26, 500.

[87] A. Gurlo, N. Bârsan, M. Ivanovskaya, U. Weimar and W. Göpel Sensors and Actuators B (1998) 47, 92.

[88] D. Mutschall, K. Holzner and E. Obermeier Sensors and Actuators B (1996) 36, 320.

[89] E. Comini, G. Faglia, G. Sberveglieri, C. Cantalini, M. Passacantando, S. Santucci, Y. Li, W. Wlodarski and W. Qu Sensors and Actuators B (2000) 68, 168.

[90] M. Ferroni, V. Guidi, G. Martinelli, M. Sacerdoti, P. Nelli and G. Sberveglieri Sensors and Actuators B (1998) 48, 285.

[91] C. Imawan, F. Solzbacher, H. Steffes and E. Obermeier Sensors and Actuators B (2000) 64, 193.

[92] L. Chambon, J. P. Germain, A. Pauly, V. Demarne and A. Grisel Sensors and Actuators B (1999) 60, 138.

[93] T. Weber, R. Andrade, E. R. Leite and E. Longo Sensors and Actuators B (2001) 72, 180.

[94] T. Hyodo, J. Ohoka, Y. Shimizu and M. Egashira Sensors and Actuators B (2006) 117, 359.

[95] M. Matsumiya, F. Qiu, W. Shin, N. Izu, N. Murayama and S. Kanzaki Thin Solid Films (2002) 419, 213.

[96] J. A. Dirksen, K. Duval and T. A. Ring Sensors and Actuators B (2001) 80, 106.

[97] I. Hotovy, J. Huran, P. Siciliano, S. Capone, L. Spiess and V. Rehacek Sensors and Actuators B (2001) 78, 126.

[98] I. Hotovy, V. Rehacek, P. Siciliano, S. Capone and L. Spiess Thin Solid Films (2002) 418, 9.

[99] M. Kimura Sensors and Actuators A (1996) 33, 156.

[100] J. Lančok, A. Santoni, M. Penza, S. Loreti, I. Menicucci, C. Minarini and M. Jelinek Surf Coatings Technology (2005) 200, 1057.

[101] S. K. Song, J. S. Cho, W. K. Choi, H. J. Jung, D. Choi, J.Y. Lee, H. K Baik and S. K. Koh Sensors and Actuators B (1998) 46, 42.

[102] S. S. Park and J. D. Mackenzie Thin Solid Films (1996) 274, 154.

[103] J. Santos, P. Serrini, B. O'Beirn and L. Manes Sensors and Actuators B (1997) 43, 154.

[104] R. K. Sharma, Z. Tang, P.C. H. Chan, J. K. O. Sin and I. M. Hsing Sensors and Actuators B (2000) 64, 49.

[105] T. Oyabu J. Appl. Phys (1982) 53, 2785.

[106] M. Gaidi, B. Chenevier and M. Labeau Sensors and Actuators B (2000) 62, 43.

[107] R. Rella, P.Siciliano, L.Vasanelli, C. Geradi and A. Licciulli. J. Appl. Phys. (1998) 83, 2369.

[108] S. Sharma, K. Nomura and Y. Ujihira J. Appl. Phys. (1992) 71, 2000.

[109] E. Comini, A. Vomiero, G. Faglia, G. D. Mea and G. Sberveglieri Sensors and Actuators B (2005) 115, 561.

[110] H. E. Endres, W. Göttler, R. Hartinger, S. Drost, W. Hellmich, G. Müller, C. B. Braunmühl, A. Krenkow, C. Perego and G. Sberveglieri, Sensors and Actuators B (1996) 36, 353.

[111] A. Salehi and M. Gholizade Sensors and Actuators B (2003) 89, 173.

[112] H. Liu, L. Zhang and Y. J. He Thin Solid Films (1997) 304, 13.

[113] R. S. Niranjan, S. R. Sainkar, K. Vijayamohanan and I. S. Mulla Sensors and Actuators B (2002) 82, 82.

[114] Q. Qi, T. Zhang, L. Liu and X. Zheng Sensors and Actuators B (2009) 137, 471.

[115] J. M. Lee, B. U. Moon, C. H. Shim, B. C. Kim, M. B. Lee, D. D. Lee and J.H. Lee Sensors and Actuators B (2005) 108, 84.

[116] A. Khanna, R. Kumar and S. S. Bhatti Appl. Phys. Letts. (2003) 82, 4388.

[117] A. Chowdhuri, P. Sharma, V. Gupta, K. Sreenivas and K. V. Rao J. Appl. Phys. (2002) 92, 2172.

[118] B. Esfandyarpour, S. Mohajerzadeh and A. Khodadadi, IEEE Sensors Journal (2004) 4, 449.

[119] E. Comini, G. Faglia, G. Sberveglieri, D. Calestani, L. Zanotti and M. Zha Sensors and Actuators B (2005) 111, 2.

[120] E. Comini, G. Faglia, G. Sberveglieri, Z. Pan and Z. Wang Appl. Phys. lett. (2002) 81, 1869.

[121] M. Law, H. Kind, B. Messer. F. Kim and P. Yang Angew. Chem. Int. Ed. (2002) 41, 2405.

[122] R. K. Sharma, M. C. Bhatnagar and G. L. Sharma Sensors and Actuators B (1997) 45, 209.

[123] L. Zheng, M. Xu and T. Xu Sensors and Actuators B (2000) 66, 28.

[124] F. H. Babaei, M. Keshmiri, M. Kakavand and T. Troczynski Sensors and Actuators B (2005) 110, 28.

[125] M. Taurino, S. Capone, P. Siciliano, T. Toccoli, A. Boschetti, L. Guerini and S. Iannotta Sensors and Actuators B (2003) 92, 292.

[126] D. Manno, G. Micocci, R. Rella, A. Serra, A. Taurino and A. Tepore J. Appl. Phys. (1997) 82, 54.

[127] Y. K. Jun, H. S. Kim, J. H. Lee and S. H. Hong Sensors and Actuators B (2005) 107, 264.

[128] K. D. Benkstein and S. Semancik Sensors and Actuators B (2006) 113, 445.

[129] M. Ruiz, A. Cornet and J. R. Morante Sensors and Actuators B (2005) 111, 7.

[130] I. Hayakawa, Y. Iwamoto, K. Kikuta, S. Hirano Sensors and Actuators B (2000) 62, 55.

[131] Y. Li, W. Wlodarski, K. Galatsis, S. H. Moslih, J. Cole, S. Russo and N. Rockelmann Sensors and Actuators B (2002) 83, 160.

[132] L. E. Depero, M. Ferroni, V. Guidi, G. Marca, G. Martinelli, P. Nelli, L. Sangaletti and G. Sberveglieri Sensors and Actuators B (1996) 36, 381.

[133] G. N. Chaudhari, A. M. Bende, A. B. Bodade, S. S. Patil and V. S. Sapkal Sensors and Actuators B (2005) 115, 297.

[134] N. Xu, N. Miura, Y. Ishida, K. Matsuda and N. Yamazoe Sensors and Actuators B (2000) 65, 163.

[135] B. T. Marquis and J. F. Vetelino Sensors and Actuators B (2001) 77, 100.

[136] X. Wang, N. Miura and N. Yamazoe Sensors and Actuators B (2000) 66, 74.

[137] P. Ivanov, J. Hubalek, K. Malysz, J. Prášek, X. Vilanova, E. Llobet and X. Correig Sensors and Actuators B (2004) 100, 221.

[138] V. R. Katti, M. Kaur, K. P. Muthu, V. B. Bhandarkar, S. C. Gadkari and S. K. Gupta DAE Solid Stae Physics Symposium (2003) 46, 441.

[139] N. Yamazoe, J. Tamaki and N. Miura Materials Sci. Engg. (1996) 41, 178.

[140] V. B. Bhandarkar, V. R. Katti, M. Kaur, S. C. Gadkari and S. K. Gupta Asian J. Phys. (2005) 9, 1.

[141] M. Stankova, X. Vilanova, E. Llobet, J. Calderer, C. Bittencourt, J. J. Pireaux and X. Correig Sensors and Actuators B (2005) 105, 271.

[142] L. Tommie. Jr. Royster, D. Chatterjee, G. R. Paz-Pujalt and C. A. Marrese Sensors and Actuators B (1998) 53, 155.

[143] W. Qu and W. Wlodarski Sensors and Actuators B (2000) 64, 42.

[144] Y. S. Kim, S. C. Ha, K. Kim, H. Yang, S. Y. Choi, Y. T. Kim, J. T. Park, C. H. Lee, J. Choi, J. Paek and K. Lee Appl. Phys. Lett. (2005) 86, 213105.

[145] L. G. Teoh, I. M. Hung, J. Shieh, W. H. Lai and M. H. Hon Electrochem. Solid State Lett. (2003) 6, G108.

[146] M. Bendahan, R. Boulmani, J. L. Seguin and K. Aguir Sensors and Actuators B (2004) 100, 320.

[147] J. Tamaki, A. Hayashi, Y. Yamamoto and M. Matsuoka Sensors and Actuators B (2003) 95, 111.

[148] J. Liu, X. Wang, Q. Peng and Y. Li, Sensors and Actuators B (2006) 115, 481.

[149] I. Raible, M. Burghard, U. Schlecht, A. Yasuda and T. Vossmeyer Sensors and Actuators B (2005) 106, 730.

[150] S. Capone, R. Rella, P. Siciliano and L. Vasanelli Thin Solid Films (1999) 350, 264.

[151] H. Nanto, T. Minami, and S. Takata J. Appl. Phys. (1986) 60, 482.

[152] P. Mitra, A. P. Chatterjee and H. S. Maiti Materials Letters (1998) 35, 33.

[153] P. Nunes, E. Fortunato, A. Lopes and R. Martins Int. J. Inorganic mat. (2001) 3, 1129.

[154] K. Hazra and S. Basu Sensors and Actuators B (2006) 117, 177.

[155] X. L. Cheng, H. Zhao, L. H. Huo, S. Gao and J. G. Zhao Sensors and Actuators B (2004) 102, 248.

[156] T. Shishiyanu, T. S. Shishiyanu and O. I. Lupan Sensors and Actuators B (2005) 107, 379.

[157] T. Mazingue, L. Escobaus, L. Spalluto, F. Flory, G. Socol, C. Ristoscu, E. Axente, S. Grigorescu, I.N. Mihailesu and N.A. Vainos J. Appl. Phys. (2005) 98, 074312.

[158] H. Gong, J. Q. Hu, J. H. Wang, C. H. Ong and F. R. Zhu Sensors and Actuators B (2006) 115, 247.

[159] H. T. Wang, B. S. Kang, F. Ren, L. C. Tien, P. W. Sadik, D. P. Norton, S. J. Pearton and J. Lin Appl. Phys. Lett. (2005) 86, 243503.

[160] C. Wang, X. Chu and M. Wu Sensors and Actuators B (2006) 113, 320.

[161] S. R. Morrison Sensors and Actuators (1982) 2, 329.

[162] G. Heiland Sensors and Actuators (1982) 2, 343.

[163] N. Yamazoe and T. Seiyama Proc. 3rd Int. Co@ Solid-State Sensors and Actuators (Transducers'85), philadelphia (1985), 376.

[164] Y. Shimizu and M. Egashira MRS Bulletin (1999) 24, 18.

[165] C. Xu, T. Jun, N. Miura and N. Yamazoe Chemical Letters (1990) 3, 441.

[166] G. G. Mandyo, E. Castaño, F. J. Gracia, A. Cirera, A. Cornet and J. R. Morante Sensors and Actuators B (2003) 95, 90.

[167] C. O. Park and S. A. Akbar, J. Mater.Sci (2003) 38, 4611.

[168] P. Moseley, J. Norris and D. Williams Techniques and mechanisms in gas sensing, Adam Hilger, (1991) Bristol.

[169] W. Göpel Surf.Sci. (1977) 62, 165.

[170] N. Yamazoe, J. Fuchigami, M. Kishikawa and T. Seiyama Surf.Sci. (1979) 86, 335.

[171] S. C. Chang J. Vac. Sci. Technol. (1980) 17, 366.

[172] S. R. Morrison Sensors and Actuators (1987) 12, 425.

[173] N. Yamazoe, G. Sakai and K. Shimanoe Catalysis Surveys from Asia (2003) 7, 63.

[174] H. Gleiter Prog. Mater. Sci. (1989) 33, 223.

[175] H. Gleiter Mater. Sci. Forum (1995) 189, 67.

[176] R. W. Siegel Ann. Rev. Mater. Sci. (1991) 21,559.

[177] R. W. Siegel Mater. Sci. Forum (1997) 235, 851.

[178] G. J. Cadena, J. Riu and F. X. Rius Analyst (2007) 132, 1083.

[179] C. Xu, J. Tamaki, N. Miura and N. Yamazoe Sensors and Actuators B (1991) 3, 147.

[180] N. Yamozoe Sensors and Actuators (1991) 5, 7.

[181] A. Rothschild and Y. Komem J. Appl. Phys. (2004) 95, 6374.

[182] R. Ionescu, A. Hoel, C. G. Granqvist, E. Llobet and P. Heszler Sensors and Actuators (2005) 104, 132.

[183] C. S. Rout, M. Hegde and C. N. R. Rao Sensors and Actuators (2008) 128, 488.

Chapter 2

Experimental Methods

This chapter gives an account of gas sensing test facility that we have fabricated. The methods of preparation of sensor material are discussed. A short description of the test gas used for the gas sensing analysis is given. The different characterisation techniques used are also discussed in this chapter.

2.1 Sensor Testing Setup

Sensor characterisation is an important feature to identify the various aspects of performance, of the gas sensor in order to optimise its use. Because of the varied and complex mechanisms involved, the device operating conditions and the performance characteristics are highly interdependent. Testing at the development stage must also determine the parameters, which need to be included in the performance tests essential for any sensors produced on commercial basis.

2.1.1 Methods of Measurement

The response of a gas sensor is tested by measuring the resistance or conductance of the sensor element in air and in the presence of a known amount of the analyte gas. There are two ways in which the response of the sensor can be investigated [1].

2.1.1.1 Flow Through Method

In this method the response curve is recorded under a continuous flow of a known amount of analyte gas. The concentration of analyte gas is

controlled by mixing it with a carrier gas using mass flow controllers (MFC). For recovery measurements, the MFC of analyte gas is switched off.

2.1.1.2 Static Environment Method

In this method the sensor element is mounted in an enclosed chamber of known volume. In order to measure the sensor resistance in a desired concentration of the analyte gas, a known amount of gas is injected into the housing using a syringe. The resistance of the sensor as a function of time is measured till the steady state is achieved. The recovery of the sensor is studied by removing the sensor from housing and exposing to air.

2.2 Test System Fabrication

We have indigenously fabricated a test chamber for purpose of gas sensing measurements. In the test system fabricated we have incorporated the facilities for both static and dynamic measurements. Figure 2.1 and 2.2 illustrates schematic and photograph of the gas sensing setup.

In our measurements we have employed the static method where the gas concentration was determined by the volume ratio. The sensor is brought to the desired temperature with the help of the temperature controller. Once the temperature is reached the desired concentration of the gas is taken from pre calibrated gas cylinders with the help of a syringe and injected into the test chamber. The variation of the sensor resistance in presence of test gas is monitored via keithley 195A digital multimeter. All the measurements are carried out at atmospheric pressure.

The test system that we have fabricated consists of a stainless steel chamber of diameter 7.5cm and 6.35cm height. The effective volume of the chamber is 280ml. An inlet is provided for inserting the desired concentration

of the test gas to the chamber with a syringe. A septum is provided at the inlet for the purpose of injection of gas. A valve is connected at the outlet of the chamber for exhaust purpose. For dynamic measurement this valve can be connected to the inlet of a vacuum pump. Electrical connections from the sensor are done with the help of two thin copper wires, bonded to the sensor with silver paint. The sensing capabilities of the sensor is characterised at different operating temperatures to find out the optimum temperature. A heater is incorporated in the chamber in order to heat the sample to the desired temperature. The heater consists of a nichrome wire wounded over a mica sheet and inserted between two copper pieces.

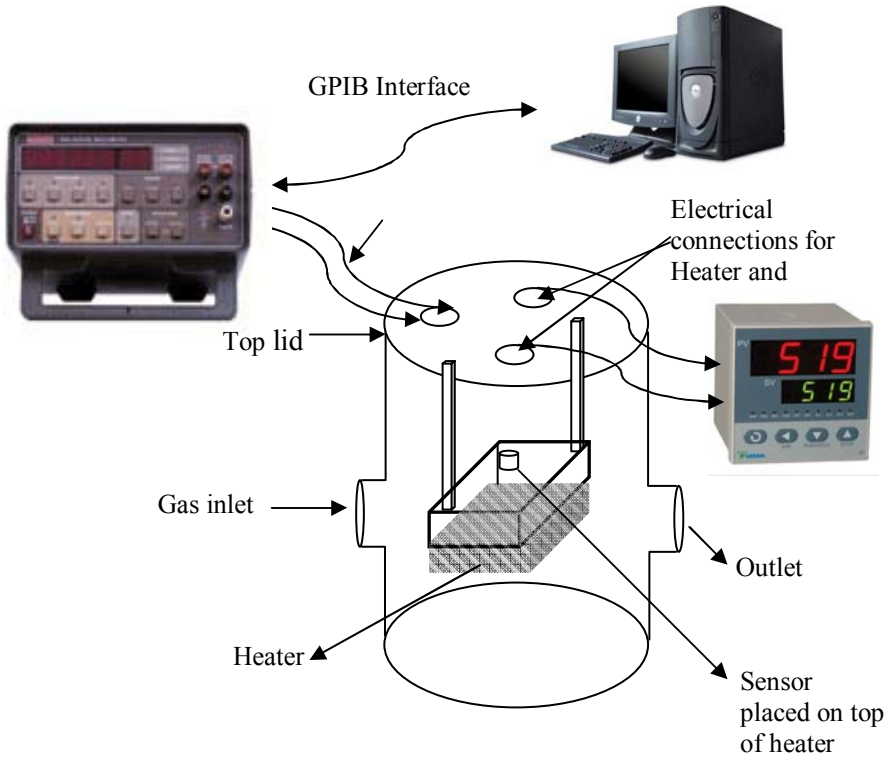

Fig. 2.1 Sensor testing set up

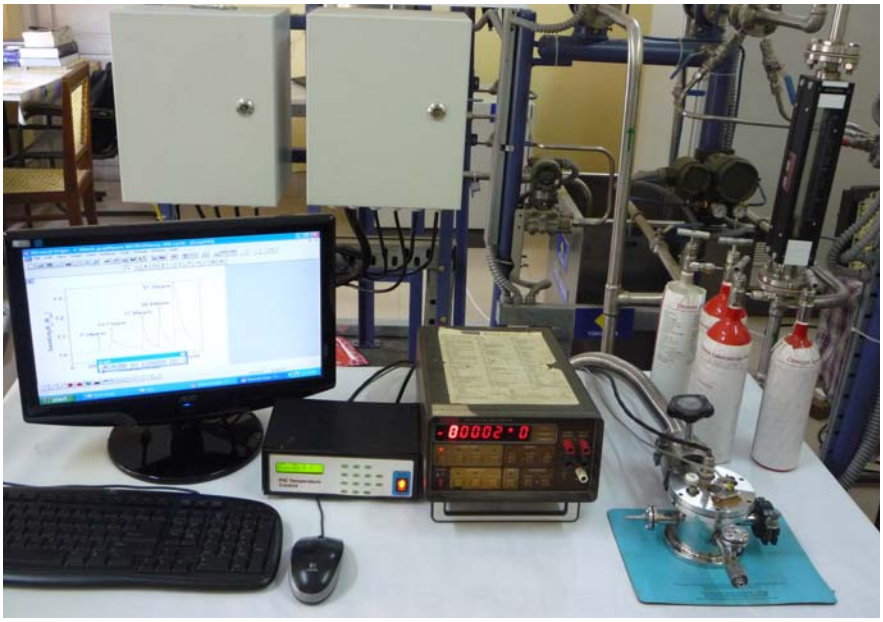

Fig. 2.2 Photograph of gas sensing setup

2.3 Electrical Characterisation

The electrical characteristics of the metal oxide sensors were obtained by directly measuring the D.C. resistance of the sample before and after introducing gas using a keithely 195A digital mutimeter. Sensor response (sensitivity) is presented as R_{gas} / R_{air} in case of oxidising gas and R_{air} / R_{gas} for reducing gas. The response and recovery time is defined as the time taken by the sensor to reach 90% of its maximum value (after introduction of gas) and 10% of its base value (before introduction of gas).

The sensor resistance can also be calculated by connecting a load resistance (R_L) in series with the sensor resistance (R_S) as shown in figure 2.3 [2-4]. A voltage source (V_C) is applied to the combination to provide the current I_S which drops voltages V_S and V_L across the sensor and load

respectively. The output voltage across the load is measured and the sensor resistance is calculated as

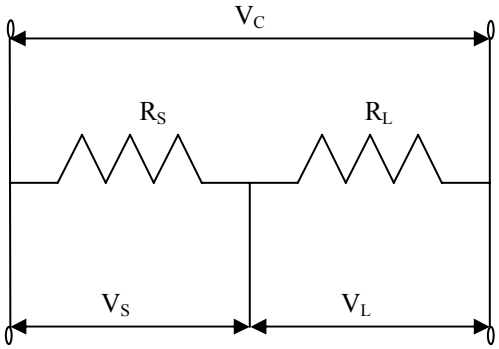

Fig. 2.3 Circuit for the determination of sensor resistance

$$R_S = R_L\left(\frac{V_C}{V_L} - 1\right)$$

The sensor resistance can also be calculated by measuring the current along the sensor when a constant dc voltage is applied [5-6].

Capacitive type gas sensors measure the change in dielectric constant of the films between the electrodes as a function of gas concentration. Capacitance changes are typically in the range of pF and are dependent on the operating frequency and surrounding conditions, like humidity and temperature. The capacitive sensor relies on inter-digitated electrode structures, which correspond to the two plates of as standard capacitor, to monitor changes of the dielectric coefficient of the film.

2.4 Active Layer Deposition Technology

Various processing schemes have been tested effectively, even though only on a laboratory scale. Processing techniques should be able to afford the

desired oxide composition with specific doping and the minimum number of processing steps. Film processing techniques are grouped in two main categories: thin-film deposition processes such as sputtering, evaporation (i.e. physical vapour deposition – PVD) and chemical vapour deposition (CVD), for thicknesses in the range 0.005-2μm, and thick-film deposition processes such as screen printing, drop coating and tape casting for thicknesses greater than 10μm. Thermal spraying can be used to deposit coatings of metals, ceramics and cermets that are thicker than ~50μm. Below are summarised the different processing methods used for synthesising gas sensor films [8].

2.4.1 Thin Film Technology

Many chemical and physical methods of thin-film deposition are available. Chemical vapour deposition (CVD) involves the flow of a gas with diffused reactants over a hot surface [9] . The gas that carries the reactants is called the carrier gas. While the gas flows over the hot solid surface, the energy supplied by the surface temperature provokes chemical reactions of the reactants that form films during and after the reactions. The by-products of the chemical reactions are then vented. Thin films of desired composition can thus be created over the surface of the substrate. CVD methods provide excellent film-coating conformity over uneven surfaces. Variations of CVD techniques, such as plasma-enhanced CVD (PECVD) and atmospheric-pressure CVD (APCVD), have been used to produce both nanopowders and nanostructured thin films.

Physical vapour deposition (PVD) involves the direct impingement of particles on the substrate surfaces. The most important feature of PVD techniques is that the transport of vapours from the source to the substrate takes place by physical means. There are different methods of PVD [10]. In

vacuum evaporation [11] the technique consists of vaporization of the solid material by heating it to sufficiently high temperatures and condensing it onto a cooler substrate to form a film. Sputtering occurs as a result of momentum transfer between the impinging ions and the atoms of the target being bombarded. The sputtered species can be condensed on a substrate to form a thin film. There are a variety of sputtering techniques like Diode sputtering, Bias sputtering, Magnetron sputtering, RF sputtering. The process, called low-pressure flame deposition (LPFD), is based on the combustion flame-chemical-vapour condensation process used to produce oxide nano-particles with minimal aggregation. Pulsed laser deposition (PLD) is a thin film deposition, specifically a physical vapor deposition, technique where a high power pulsed laser beam is focused inside a vacuum chamber to strike a target of the material that is to be deposited. This material is vaporized from the target (in a plasma plume) which deposits it as a thin film on a substrate (such as a silicon wafer facing the target).

Considerable emphasis is given to developing solution-based thin-film deposition techniques as an economical alternative to the more expensive chemical vapour deposition and reactive sputtering processes. However, the quality of the film produced by vapour deposition processes remains superior.

The sol-gel technique consists of a system going from a liquid sol (colloidal suspension of miniature solid particles in a liquid) to a viscous gel in which the suspended particles are organised in a loose, but definite three-dimensional arrangement [12, 13]. Gel layers can be formed by spin-coating (the solution is poured onto the substrate surface, which is then spun to expel fluid and create a uniform thickness), by dip-coating (the substrate surface is dipped into the solution) and by spray-coating (the solution is sprayed onto the sensor surface).

In Spray pyrolysis, the atomization of the chemical solution into as pray of fine droplets is effected by the spray nozzle with the help of a filtered carrier gas which may (as in the case of SnO_X films) or may not (as in the case of CdS films) be involved in the pyrolytic reaction. The carrier gas and the solution are fed into the spray nozzle at predetermined and constant pressure and flow rates.

2.4.2 Thick Film Technology

In most applications one of the greatest justifications for the existence of thick-film technology is the need to combine different electronic technologies, but in advanced sensor applications it is dominant. The single chip solution is often treated as a holy grail by designers, but so far it has rarely made sense, though demand is always driving developers of technologies towards providing such solutions, and it is an active area of research. Thick-film technology was first introduced more than 30 years ago. Nowadays there is a big amount of companies which are using this technology: Envin Scientific, Zellweger Analitics, Trafag and Oliver IGD, (gas sensors) GfG, OLDHAM, Industrial Scientific Corporation, GMI, BW technologies, Draeger Industrie and KANE (gas detectors), B+B Thermo-Technic and M&C Products (gas sampling probes).

One of the most important thick-film deposition methods is screen-printing, which is similar to that used for ceramics, textiles, etc. Thick-film paste can be formulated to paint or print an active layer onto a substrate [14]. To formulate the paste, finely milled metal oxides or other sensing materials are combined with small amounts of glass frit of a similar size (for adhesion to the substrate), catalysts (if desired), and an organic vehicle to form a printable paste. The particle size of the constituents varies, although for screen printing powders it should be 0.5 μ m or less in diameter. The paste is

spread on the substrate by means of a screen made from non-rusting steel mesh, polyester or nylon, mounted on a metallic frame. The screen is coated with an ultraviolet-sensitive emulsion. These regions were drawn by photographic methods. The screen is maintained at 0.5 mm from the substrate surface in the screen-printing machine. The paste is pushed through the defined regions by pressure from a spatula. The paste is printed onto a ceramic substrate, typically alumina, dried, and fired at temperatures between 500 and 1000° C for one or more hours. Standard printable thick-film materials for resistive heaters and conductor lines may be applied to the substrate before or after the sensor layer (normally pastes of noble metals like Pt and Au).

Tape casting is a forming technique for producing thin, flat ceramics. The method was originally developed for producing electronic ceramics (insulating substrates and packages and multilayer capacitors). Ceramic slurry is spread evenly onto a flat horizontal surface by means of a 'doctor blade'. Once dry, the flexible 'green tape' is cut, laminated or shaped and sintered. The thickness of the tape is generally in the range 25 μm to 1 mm, but tapes as narrow as 5 μm can be produced.

Another thick film method is drop-coating. A particular thickness can be obtained by varying the number of drops that are deposited. This method is highly dependent on solution viscosity and density. Once the solution is deposited, the solvent evaporates by itself or with the help of gentle firing. Another method is by dispersing the powders in a suitable medium and then coating on the substrate with a brush. The sample thus coated can be annealed at higher temperatures and can be used. In dip coating the substrate is dipped into a solution, taken out, and dried by allowing the solvent to evaporate, leaving behind a solid film on the substrate.

The effectiveness of gas sensors prepared from thick films of semi conducting oxides depends on such factors as the nature of the reaction taking place at the oxide surface, the temperature, the catalytic properties of the surface, the electronic properties of the bulk oxide and the microstructure. Good control over thickness and microstructure is possible and the lifetime is expected to be longer.

2.5 Sensor Fabrication

In this work, thick film sensors were obtained by dispersing the nanopowder in suitable medium. Nano crystalline powder obtained was thoroughly powdered in a mortar. The finely powdered sample is then dispersed in methanol. For uniform dispersion the solution was kept under constant stirring for two to four hours in a magnetic stirrer. It is then coated on the glass substrate with a painting brush to obtain a thick film of the sensor. Thin film based sensor for gas sensing measurements were fabricated by spray pyrolysis method. Thin and thick film sensors thus prepared is annealed at 600^0C overnight, prior to sensing measurements. The actual temperature at the sample surface was within a range of 5% of this set temperature. An average of 20-25 gas sensors of each type (pure and doped) was deposited. Among the deposited samples 5 sensors of each type were selected for the gas sensing measurements Figure 2.4 represents the schematic representation of the sensor fabricated. The distance between the two electrodes is adjusted to 5mm.

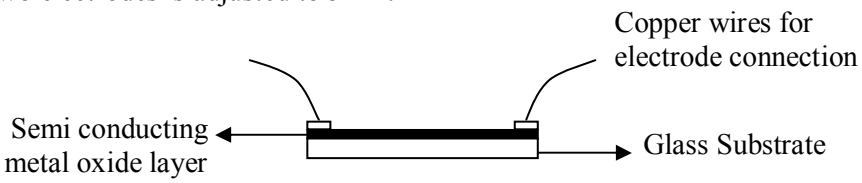

Fig. 2.4 Schematic representation of sensor fabricated

2.6 Gases Employed for Sensor Characterisation

2.6.1 Nitrogen Dioxide

Two of the most toxicologically significant nitrogen oxides are nitric oxide (NO) and nitrogen dioxide (NO_2); both are non-flammable and colourless to brown at room temperature. Nitric oxide is a sharp sweet-smelling gas at room temperature, whereas nitrogen dioxide is a strong and harsh odour gas. Nitrogen oxides are released to the air from the exhaust of motor vehicles, the burning of coal, oil, or natural gas, and during processes such as arc welding, electroplating, engraving, and dynamite blasting. They are also produced commercially by reacting nitric acid with metals or cellulose. The threshold limit value for short-term exposure is 5ppm for 10minutes and long term exposure is 3ppm for 8hr [1].

Nitrogen oxides are used in the production of nitric acid, lacquers, dyes, and other chemicals. Nitrogen oxides are also used in rocket fuels, nitration of organic chemicals, and the manufacture of explosives. Nitrogen oxides are broken down rapidly in the atmosphere by reacting with other substances commonly found in the air. The reaction of nitrogen dioxide with chemicals produced by sunlight leads to the formation of nitric acid, which is a major constituent of acid rain. Nitrogen dioxide also reacts with sunlight, which leads to the formation of ozone and smog conditions in the air we breathe. Ground level ozone is a severe irritant, responsible for the burning eyes, choking and coughing associated with smog. Ozone often damages lungs, aggravates infections and is particularly harmful to children. Elevated ozone levels can also inhibit plant growth and cause widespread damage to trees and crops. Nitrogen dioxide when inhaled by human beings cause severe damage to human respiratory organs and nerves. Therefore, exceeding critical nitrogen oxide levels poses immediate health and

environmental problems. Small amounts of nitrogen oxides may evaporate from water, but most of it will react with water and form nitric acid. When released to soil, small amounts of nitrogen oxides may evaporate into air. However, most of it will be converted to nitric acid or other compounds.

The general population is primarily exposed to nitrogen oxides by breathing in air. People who live near combustion sources such as coal burning power plants or areas with heavy motor vehicle use may be exposed to higher levels of nitrogen oxides. Households that burn a lot of wood or use kerosene heaters and gas stoves tend to have higher levels of nitrogen oxides in them when compared to houses without these appliances. Nitric oxide and nitrogen dioxide are found in tobacco smoke, so people who smoke or breathe in second-hand smoke may be exposed to nitrogen oxides. Workers employed in facilities that produce nitric acid or certain explosives like dynamite and trinitrotoluene (TNT), as well as workers involved in the welding of metals may breathe in nitrogen oxides during their work.

2.6.2 Hydrogen Sulphide

Hydrogen sulphide occurs naturally in crude petroleum, natural gas, volcanic gases, and hot springs. It can also result from bacterial breakdown of organic matter or produced by human and animal wastes. Other sources are industrial activities, such as food processing, coke ovens, craft paper mills, tanneries, and petroleum refineries. Hydrogen sulphide is a colorless, flammable gas under normal conditions. It is commonly known as hydrosulphuric acid, stink damp and sewer gas. It smells like rotten eggs and people can smell it at low levels (less than 1 ppb).The threshold limit value for short term exposure is 15ppm for 10minutes and long term exposure limit is 10ppm for 8hour [1].

Hydrogen sulphide is released primarily as a gas and can spread in the air. When released as a gas, it will form sulphur dioxide and sulphuric acid in the atmosphere. Hydrogen sulphide remains in the atmosphere for about 18 hours. In some instances, it may be released as a liquid waste from an industrial facility. Hydrogen sulphide is evolved by crude petroleum, natural gas, volcanic gases and hot springs. People working in the petroleum refining, petrochemical, or natural gas industry; food processing; wastewater treatment; coke oven plants; tanneries; or pulp and paper mills are also exposed to this gas. A small amount of hydrogen sulphide is produced by bacteria in our mouth and gastrointestinal tract and by enzymes in our brain and muscle.

2.7 Analytical Characterisation Techniques

Pure and doped samples for sensing purpose are obtained in the form of thick and thin films. Samples prepared for sensing purpose are characterised by different analytical techniques. Various techniques such as chemical composition and structure analysis are employed. The analytical techniques used for solid characterisation are based on the interaction between electromagnetic radiation, electrons or ions, and the solid, followed by the examination of the emitted secondary particles or radiation. The various characterisation techniques used in the present work are XRD, SEM, EDS and Raman spectroscopy.

2.7.1 X-ray Diffraction

X-ray diffraction (XRD) is a very important experimental technique that has been used to address all issues related to crystal structure of bulk solids and thin films including lattice constants and geometry, identification of unknown materials, orientation of single crystals and preferred orientation of polycrystalline films, defects, stress etc [15]. X-ray methods are

advantageous because they are non-destructive and do not require elaborate sample preparation. The other advantages that this analytical technique brings are an easy quantification of crystalline phases that compose the samples and the possibility of evaluating the mean grain size of the polycrystalline films.

This technique allows identifying and studying crystalline materials by using the phenomenon of diffraction. When the X-rays are incident on a crystal, they get diffracted from different planes of the crystal. They follow the Bragg's Law

$$n\lambda = 2d\sin(\theta)$$

Where, d is the interplanar separation

λ is the X-ray wavelength.

n is the order of diffraction

Briefly, diffraction occurs when penetrating radiation, such as X-rays, enters a crystalline substance and is scattered. The direction and intensity of the scattered (diffracted) beams depends on the orientation of the crystal lattice with respect to the incident beam. Any face of a crystal lattice consists of parallel rows of atoms separated by a unique distance (d-spacing), which are capable of diffracting X-rays. In order for a beam to be 100% diffracted, the distance it travels between rows of atoms at the angle of incidence must be equal to an integral multiple of the wavelength of the incident beam. D-spacings that are greater or lesser than the wavelength of the directed X-ray beam at the angle of incidence will produce a diffracted beam of less than 100% intensity. The resulting analysis is described graphically as a set of peaks with intensity on the Y-axis and goniometer angle on the X-axis.

If the sample is powdered, it provides, theoretically, all possible orientations of the crystal lattice, the goniometer provides a variety of angles of incidence, and the detector measures the intensity of the diffracted beam. The exact angle and intensity of a set of peaks is unique to the crystal structure being examined. A comparison with standard tables, such as JCPDS spectra published by the American Society for Testing and Materials, provides valuable information about the composition of the powder. By comparing the peak position with the standard JCPDS card values of the material the orientation of the crystallites can be determined.

Besides, XRD can be used to determine the crystallite size of the sample, which is a key point in the field of gas sensors based on nanostructured metal oxides. An X-ray scan of a sample occurs automatically, taking a few minutes to a few hours and the resulting XRD peaks average diffraction effects from billions of individual nano sized crystals. The simplest approach is to use the peak breadth at half maximum (FWHM) and the Scherer equation.

The crystallite size is given by the Scherrer's formula.

$$D = \frac{0.9\lambda}{B\cos\theta} \tag{2.1}$$

where D is crystallite size.

λ is the wavelength of X-rays.

B is the full width half maxima in radians.

θ is the angle in degrees at which the intensity peak appears.

The size that is measured by XRD may be related to the size of the individual crystals in the sample, rather than the size of particles formed from the agglomeration of these crystals

In this investigation, information about the crystallite structure of the powder and their crystallite size has been obtained from XRD data. The XRD patterns of the nanopowders were obtained with a Bruker AXS D8 advance X-ray diffractometer using Cu-kα radiation.

2.7.2 Scanning Electron Microscopy (SEM)

Accelerated electrons in a scanning electron microscope (SEM) carry significant amounts of kinetic energy, and this energy is dissipated as a variety of signals produced by electron-sample interactions when the incident electrons are decelerated in the solid sample. These signals include secondary electrons (that produce SEM images), backscattered electrons (BSE), diffracted backscattered electrons (EBSD that are used to determine crystal structures and orientations of minerals), photons (characteristic X-rays that are used for elemental analysis and continuum X-rays), visible light (cathodoluminescence--CL), and heat. Secondary electrons and backscattered electrons are commonly used for imaging samples. Secondary electrons are most valuable for showing morphology and topography on samples and backscattered electrons are most valuable for illustrating contrasts in composition in multiphase samples (i.e. for rapid phase discrimination). X-ray generation is produced by inelastic collisions of the incident electrons with electrons in discrete orbital (shells) of atoms in the sample. As the excited electrons return to lower energy states, they yield X-rays that are of a fixed wavelength (that is related to the difference in energy levels of electrons in different shells for a given element). Thus, characteristic X-rays are produced for each element in a mineral that is "excited" by the electron beam. SEM analysis is considered to be "non-destructive"; that is, x-rays generated by electron interactions do not lead to volume loss of the sample, so it is possible to analyze the same materials repeatedly.

The SEM uses a focused beam of high-energy electrons, ranging from a few KeV to 50KeV, to generate a variety of signals at the surface of solid specimens. The signals that derive from electron-sample interactions reveal information about the sample including external morphology (texture), chemical composition, and crystalline structure and orientation of materials making up the sample. In most applications, data are collected over a selected area of the surface of the sample, and a 2-dimensional image is generated that displays spatial variations in these properties. Areas ranging from approximately 1 cm to 5 microns in width can be imaged in a scanning mode using conventional SEM techniques (magnification ranging from 20X to approximately 30,000X, spatial resolution of 50 to 100 nm). The SEM is also capable of performing analyses of selected point locations on the sample; this approach is especially useful in qualitatively or semi-quantitatively determining chemical compositions (using EDS), crystalline structure, and crystal orientations (using EBSD).

In this study SEM analysis has been done with a JEOL Model JSM - 6390LV. The images obtained were used to analysis the particle morphology, film surface topography and grain size.

2.7.3 Energy Dispersive X-ray analysis (EDAX)

EDX Analysis stands for Energy Dispersive X-ray analysis. It is sometimes referred to also as EDS or EDAX analysis. It is a technique used for identifying the elemental composition of the specimen, or an area of interest thereof. The EDX analysis system works as an integrated feature of scanning electron microscope [16, 17].

During EDX analysis, the specimen is bombarded with an electron beam inside the scanning electron microscope. The bombarding electrons collide with the specimen atoms electrons, knocking some of them off in the

process. A position vacated by an ejected inner shell electron is eventually occupied by a higher-energy electron from an outer shell. To be able to do so, however, the transferring outer electron must give up some of its energy by emitting an X-ray.

The amount of energy released by the transferring electron depends on which shell its is transferring to. Furthermore the atom of every element releases X-rays with unique amounts of energy during the transferring process. Thus by measuring the amounts of energy present in the X-rays being released by a specimen during the electron beam bombardment, the identity of the atom from which the X-rays was emitted can be established.

The EDX spectrum is just a plot of how frequently an X-ray is received for each energy level. An EDX spectrum normally displays peaks corresponding to the energy levels for which the most x-rays had been received. Each of these peaks is unique to an atom, and therefore corresponds to a single element. The higher a peak in a spectrum, the more concentrated the element is in the specimen.

An EDX spectrum plot not only identifies the element corresponding to each of its peaks, but the type of X-ray to which it corresponds as well. For example, a peak corresponding to the amount of energy possessed by X-rays emitted by an electron in the L-shell going down to the K-shell is identified as a K-Alpha peak. The peak corresponding to X-rays emitted by M-shell electrons going to the K-shell is identified as a K-Beta peak [7]. Figure 2.5 illustrates this.

In this investigation EDS data has been obtained using a JEOL Model JED – 2300 used for elemental speciation of the sample.

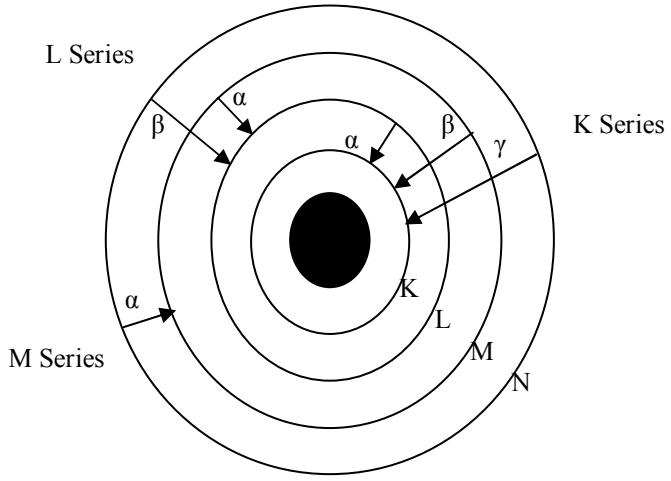

Fig. 2.5 Elements in an EDX spectrum are identified based on the energy content of the X-rays emitted by their electrons as these electrons transfer from a higher energy shell to a lower energy one.

2.7.4 Raman Spectroscopy

The scattering mechanisms between an incident radiation and a certain substance can be classified on the basis of the difference between the energies of the incident and scattered photons. Briefly, if the energy of the incident photon is equal to that of the scattered one, the process is called Rayleigh scattering. If the energy of the incident photon is different to that of the scattered one, the process is called Raman scattering.

In crystalline solids, the Raman effect deals with phonons. A phonon is Raman-active only if the first derivative of the polarizability with respect the vibrational normal co-ordinate has a non-zero value, and this in turns depends by the crystal symmetry. A phonon can be either IR or Raman active only in crystals without centre of inversion. For every crystal symmetry class, is possible to calculate which phonons are Raman active. Performing measurements in controlled polarisation configurations is

possible to obtain information about the symmetry of the crystalline lattice. The Raman signal is very weak: only 1 photon in 10^7 gives rise to the Raman effect. The Raman spectra are usually plotted in intensity vs. the difference in wave number between the incident beam and the scattered light, and so peaks are in correspondence to the phonon frequency. In nanocrystalline materials, Raman features are broadened and shifted by the phonon confinement. By using an adequate model, it is possible to estimate the size of the nanocrystals. From the band-shifts and the presence of "forbidden" peaks, using the Raman spectroscopy is also possible to obtain information on the disorder and the strains present in the crystalline lattice. In this investigation, information on the structural properties of sensor materials and of additives in some cases, have been obtained by Raman spectroscopy. General references about Raman spectroscopy can be found in [18, 19]. Raman scattering measurements were obtained using Horiba Jobin Yvon LabRam HR system at a spatial resolution of 2 mm in a backscattering configuration. The 514.5 nm line of argon ion laser was used for excitation.

References

[1] D. K. Aswal and S. K. Gupta Science and Technology of Chemiresistor Gas sensors Nova Science Publishers (2007) India.

[2] Y. K. Chung. M. H. Kim, W. S. Um, H. S. Lee, J. K. Song, S. C. Choi, K. M. Yi, M. J. Lee and K. W. Chung Sensors and Actuators B (1999) 60, 49.

[3] G. S. D. Evi, S. Manorama, V. J. Rao Sensors and Actuators B (1995) 28, 31.

[4] H. Liu, S. P. Gong, Y. X. Hu, J. Q. Liu, D. X. Zhou Sensors and Actuators B (2009) 140, 190.

[5] Y. Yamada and M. Ogita Sensors and Actuators B (2003) 93, 546.

[6] S. H. Wang, T. C. Chou and C. C. Liu Sensors and Actuators B (2003) 94, 343.

[7] J. Gratt and D. C. Bell, Energy Dispersive X-ray analysis in the electron microscope, Bios Scientific Publishers Ltd (2003) Oxford U.K.

[8] F. Cosandey, G. Skandan, A. Singhal, JOM-e (2000) 52, 10.

[9] T. Minami, Y. Kuroi, S. Dakata J. Vac. Sci. Technol. A (1996) 14, 1736.

[10] N. Honda, T. Suzuki, T. Yunogami, H. Suematsu, W. Jiang and K. Yatsui Jpn. J. Appl. Phys. (2005) 44, 695.

[11] L. I. Maissel and R. Glang Handbook of Thin film Technology McGraw-Hill New York (1970), 22.

[12] T. Sei, Y. Nomura and T. Tsuchiya J. Non- Cryst. Solids (1997) 218, 135.

[13] Z. Ji, L. Kun, S. Yongliang and Y. Zhizhen J. Cryst. Growth (2003) 255, 353.

[14] N. M. White and J. D. Turner Meas. Sci. and Technol. (1997) 8, 1.

[15] B. D. Cullity and S. R. Stock Elements of X-ray diffraction Prentice Hall New Jersey (2001), 170.

[16] P. E. J. Flewit and R. K. Wild Physical methods for material characterisation IOP publishing Ltd. London (2003), 501.

[17] D. K. Schroder Semiconductor material and device fabrication John Wiley and Sons (1998), 700.

[18] N. B. Colthup, L. H. Daly and S. E. Wiberly Introduction to Infrared and Raman spectroscopy, Academic Press Inc., (1990) New York and London, 3rd ed. 18.

[19] J. G. Graselli and B. J. Bulkin Analytical Raman spectroscopy, John Wiley and Sons Inc., (1991) New York 19.

Chapter 3

Gas Sensors Based on Pure and Copper Doped Tungsten Oxide

Thick film gas sensors based on pure and copper doped tungsten oxide were fabricated on glass substrates. The copper doping concentration was varied in the range 0.5, 1.5 and 3wt%. The structural, chemical and compositional characterizations of the prepared pure and doped sensors were done. The temperature dependent gas sensing property of the fabricated gas sensors to NO_2 and H_2S were investigated. The optimum operating temperature, response time and recovery time of pure and doped sensors to both test gases were obtained. The concentration dependent studies were performed on pure and doped sensors for both test gases. The gas sensing detection mechanisms for both gases are also presented.

3.1 Introduction

Tungsten oxide (WO_3) is an n-type semiconductor with a reported band gap of about 2.6-2.8eV [1]. The intrinsic conductivity arises from its non-stoichiometric composition giving rise to a donor level formed by oxygen vacancy defect in the lattice. Tungsten has many oxidation states i.e 2,3,4,5 and 6. The typical forms of tungsten oxides are tungsten (VI) oxide (WO_3, lemon yellow appearance) and tungsten (IV) oxide (WO_2, brown and blue appearance). Such electronic properties make the tungsten oxides suitable for various applications such as electrochromic [2], photochromic [3], photocatalyst [4] etc.

Tungsten trioxide exhibits a cubic perovskite like structure based on the corner sharing of WO_6 regular octahedra, with the O atoms (W atoms) at the corner (centre) of each octahedron [5]. The crystal network can also be viewed as the results of alternating disposition of O and WO_2 planes, placed normally to each crystallographic direction. This structure is also found in rhenium trioxide structure (ReO_3), from which takes its common name (ReO_3-structure). Actually, the symmetry of WO_3 is lowered from the ideal ReO_3 structure by two distortions: tilting of WO_6 octahedra and displacement of tungsten from the centre of its octahedron [6]. Variations in the details of these distortions give rise to several phase transitions. In fact tungsten trioxide adopts at least five distinct crystallographic modifications between absolute zero and its melting point at 1700K. When the temperature is decreased from melting point, crystallographic symmetry for WO_3 changes in the sequence: tetragonal–orthorhombic-monoclinic- triclinic-monoclinic. Most of transitions appear to be first order and they often display large hysteresis in transition temperature. A summary of these transitions is given in table 3.1. The identification of these phases, mainly by X-ray diffraction and Raman spectroscopy has been reported in literature [7, 8, 9]. Figure 3.1 represents the schematic model of crystalline WO_3. It is interesting to notice that, as suggested by the table 3.2 the coexistence of triclinic and monoclinic in WO_3 at room temperature is common and is confirmed experimentally by Filho et al. [8].

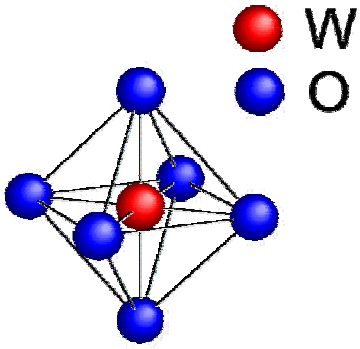

Fig. 3.1 Schematic model of crystalline WO_3 in the undistorted cubic phase. The unit octahedron presents the tungsten atom at the centre and 6 equivalent oxygen atoms at the corners.

Table 3.1 Known polymorphs of WO_3

Phase	Symmetry	Temperature range(K)	Reference
α- WO_3	Tetragonal	1010-1170	10
β- WO_3	Orthorombic	600-1170	11
γ- WO_3	Monoclinic	290-600	12-13
δ- WO_3	Triclinic	230-290	7,14
ε - WO_3	Monoclinic	0-230	15

Electrical and optical characteristics of tungsten trioxide are dependent on the crystalline structure. Saljie and Viswanathan found the resistivity to decrease from approximately 2.0 to 0.2 Ωcm upon heating from 293 to 1123K [16]. The optical band gap (2.58eV at room temperature) is found gradually decrease and become increasingly diffuse as the temperature is raised to 773K [17].

Another point worth noting is that tungsten trioxide structure is likely to host several kinds of defects. One of the most elementary defects, as in most metal oxides, is the lattice oxygen vacancy, where an

oxygen atom is absent from a normal lattice site. From an electronic point of view, an oxygen vacancy causes the increase of the electronic density on the metallic (W) adjacent cations, leading to the formation of donor-like states slightly below the edge of the conduction band of the oxide [18].

In particular pure or doped WO_3 is a promising material for the detection of various gases. These films are particularly attractive because they show a high catalytic behavior both in oxidation and reduction reactions on their surface. Being an n-type semiconductor the resistance of the WO_3 increases in the presence of oxidizing gases and decreases in the presence of reducing gases. Pure WO_3 and metal tungstate thick films have outstanding sensitive properties toward nitrogen oxides at low and also at elevated temperatures. Both thin and thick films are sensitive to NO_x (NO_2, NO) at elevated temperatures.

3.2 Review of WO_3 for Gas Sensing

The first report on WO_3 for gas sensing was published by Shaver in 1967 [19]. He showed that conductivity of Pt-activated WO_3 increased by one order of magnitude on exposure to H_2. In the following years, several reports on WO_3 based sensors have been published. It has been found that WO_3 can be used for detecting a variety of gases such as hydrogen (H_2), methane (CH_4), ammonia (NH_3), carbon monoxide (CO), nitric oxide (NO), oxygen (O_2), hydrogen sulphide (H_2S), nitrogen dioxide (NO_2), ethanol (C_2H_5OH), ozone (O_3), trimethylamine ($(CH_3)_3N$), sulphur dioxide (SO_2), and chlorine (Cl_2). A summary of selected publications related to NH_3, H_2S, NO_2, H_2, NO, CO is presented in table 3.2 to 3.7.

Table 3.2 Summary of published results on NH_3 gas sensing characteristics of WO_3

Material	Concentration (ppm)	Temperature (^{0}C)	*Sensitivity	Year (reference)	Method of Preparation
NH_3					
WO_3:Au	50	450	40	1992 [20]	Powder dip coating
WO_3	10	300	1.1	1995 [21]	Sputtering
WO_3:Pt	500	150	0.65	1998 [22]	RF sputtering
WO_3	1000	300	6	2000 [23]	Drop coating
WO_3:Mo	30	350	10.1	2000 [24]	Powder dip coating
WO_3:Au:MoO_3	5	450	10	2000 [25]	Painted thin layer
WO_3 :Mo	30	350	10.1	2000 [24]	Thick film paste
WO_3:Au	10	350	1	2001 [26]	Sputtering
WO_3	100	400	7	2003 [27]	Sputtering
WO_3:Bi_2O_3:CuO	1000	350	17	2004 [28]	Screen printing
WO_3	10	200	18.2	2005 [29]	Modified thermal evaporation
WO_3	100	350	2	2005 [30]	RF sputtering
WO_3:In	500	300	2.75	2005 [31]	Screen printed
WO_3: Pt	1000	260	1000	2006 [32]	RF sputtering
WO_3:Cr	100	350	10	2006 [33]	Drop coating
WO_3: MWCNTs	10	150	4	2006 [34]	Drop coating
WO_3	55	200	22	2006 [35]	Painted thick layer
WO_3	500	200	1.22	2007 [36]	RF sputtering
WO_3	200	400	4	2007 [37]	Drop coating
WO_3	100	220	7	2008 [38]	Thermal oxidation
WO_3: Pt	400	350	1.6	2008 [39]	Screen printing
$W_{18}O_{49}$ nanowires	0.01	Room temperature	1.1	2009 [40]	Drop casting
WO_3	0.002	400	1.25	2009 [41]	RF sputtering
WO_3:Pt	4000	350	130	2010 [42]	Screen printed
WO_3:Cr	500	250	40	2010 [43]	Drop coating
WO_3 nanofiber	100	300	1.7	2011 [44]	Electrospinning
WO_3:Pd	2.5	225	2	2011 [45]	RF sputtering
WO_3	20	200	1	2012 [46]	Electron beam evaporation

* The sensitivity values presented in this table are taken directly from the respective literature. Their magnitude cannot be compared as different authors have used different formula to calculate sensitivity. The main intent of this table is to highlight the published results on WO_3 based gas sensors.

Table 3.3 Summary of published results on H_2S gas sensing characteristics of WO_3

Material	Concentration (ppm)	Temperature (^{0}C)	*Sensitivity	Year (reference)	Method of preparation
H_2S					
WO_3	200	200	2	1990 [47]	Powder dip coating
WO_3:Au	100	200	30	1993 [48]	Sputtering
WO_3	3	200	2	1994 [49]	Sputtering
WO_3:Pt	100	220	9.9	1994 [50]	Thermal evaporation
WO_3	10	200	12	1996 [51]	RF sputtering
WO_3	0.05	200	2	1998 [52]	Metal organic deposition
WO_3:Au	10	200	1.5	1998 [22]	RF sputtering
WO_3:Au	100	250	50	2000 [50]	Sputtering
WO_3: Bi	1	180	1.44	2001 [53]	RF sputtering
WO_3:Au:Pt	1	220	5.5	2002 [54]	RF sputtering
WO_3	5	200	1.15	2003 [55]	Thick film
WO_3	0.1	200	8	2004 [56]	RF sputtering
WO_3	0.02	200	1.1	2005 [57]	Thermal evaporation
WO_3	40	250	355	2005 [58]	Thermal Evaporation
WO_3:Pd	10	Room temperature	5000	2005 [59]	Thermal evaporation
WO_3:Au	3.5	250	46	2006[32]	RF sputtering
WO_3:Al	10	125	3500	2006 [60]	Thermal evaporation
$WO_{2.72}$ nanowires	1000	250	3313	2008 [61]	Thick film paste
WO_3	150	300	40	2012 [62]	Drop casting
WO_3	100	200	300	2012 [63]	Thick film paste

Table 3.4 Summary of published results on NO_2 gas sensing characteristics of WO_3

Material	Concentration (ppm)	Temperature (^{0}C)	*Sensitivity	Year (reference)	Method of Preparation
NO_2					
WO_3	80	300	97	1991 [64]	Powder dip coating
WO_3	10	300	90	1994 [65]	Printed paste
WO_3	2	350	20	1995 [66]	Screen printing
WO_3	100	350	20	1996 [67]	Powder evaporation
WO_3:TiO_2	20	340	10	1996 [68]	RF Sputtering
WO_3	1.7	250	45	1996 [69]	Thermal evaporation
WO_3:SiO_2	0.4	350	11.2	1997 [70]	Spin coating
WO_3	100	250	130	1998 [71]	RF sputtering
WO_3:Pd	10	200	6.51	1998 [22]	RF sputtering
WO_3: TiO_2	30	350	200	1999 [72]	Powder printing
WO_3	100	100	200	1999 [73]	Screen printing
WO_3	5	200	210	2000 [74]	DC sputtering
WO_3	1	200	11.6	2000 [75]	Sol-gel thin film
WO_3:TiO_2	30	340	100	2000 [76]	Screen printing
WO_3	10	300	3.3	2000 [77]	Thermal evaporation
WO_3:MO_3	1	300	2.3	2002 [78]	Thin film evaporation
WO_3	5	200	60	2002 [79]	Pulverization coating
WO_3	200	400	170	2002 [80]	Pulsed laser deposition
WO_3	100	200	2170	2003 [81]	Suspension dropping

WO_3	0.55	300	4	2003 [82]	Spin coating
WO_3	2	250	22.5	2003 [83]	DC magnetron sputtering
WO_3	100	100	226	2003 [84]	Sol-gel thin film
WO_3:Bi_2O_3	10	350	10	2004 [85]	Screen Printing
WO_3	500	200	90	2004 [86]	Spin coating
WO_3:Au	200	300	70	2004 [87]	Laser deposition
$WO_{2.72}$nanorods	3	Room temperature	1.12	2005 [88]	MEMS
WO_3	10	350	75	2005 [30]	RF sputtering
WO_3	0.2	100	20	2005 [29]	Thermal evaporation
WO_3:Ag	100	260	10	2006 [32]	RF sputtering
WO_3	10	200	40	2007 [89]	Thermal evaporation
WO_3:Cu	1	230	10	2007 [90]	Screen printing
WO_3	100	250	33	2008 [38]	Thermal oxidation
WO_3:Au	10	150	430	2008 [91]	Colloidal chemical method
WO_3 nanorods	20	350	525	2009 [92]	Drop casting
WO_3	0.45	130	28.5	2010 [93]	Plasma spray
$W_{18}O_{49}$ nanowires	5	200	123.6	2010 [94]	Spin coating
WO_3	0.2	150	168	2011 [95]	Hydrothermal treatment
WO_3:Ti nanowires	4	Room temperature	20	2012 [96]	Spin coating
WO_3 nanowires	1	250	1.25	2012 [97]	Spin coating
WO_3:Fe	5	250	375	2012 [49]	Drop casting
WO_3nanowires	3	100	38	2012 [98]	Electron beam evaporation

Table 3.5 Summary of published results on H_2 gas sensing characteristics of WO_3

Material	Concentration (ppm)	Temperature (^{0}C)	*Sensitivity	Year (reference)	Method of preparation
H_2					
WO_3	100	Room temperature	0.3	2000 [99]	Thermal evaporation
WO_3	1000	300	13.6	2009 [100]	DC magnetron sputtering
WO_3	1000	250	15	2010 [101]	Electrochemical anodizing
WO_3:Pt	200	200	8.5	2011 [102]	RF sputtering
WO_3:Pd	200	200	10	2011 [103]	Chemical synthesis
WO_3	10000	450	1.4	2011 [104]	Thermal oxidation
WO_3:Pd	200	200	21	2012 [105]	Screen printing
WO_3:Pt	100	150	3.3	2012 [106]	Reactive magnetron sputtering

Table 3.6 Summary of published results on NO gas sensing characteristics of WO_3

Material	Concentration (ppm)	Temperature (^{0}C)	*Sensitivity	Year (reference)	Method of preparation
NO					
WO_3	4000	250	130	1998 [71]	RF sputtering
WO_3:Pd	440	200	100.3	1998 [22]	RF sputtering
WO_3	27	200	25	2000 [75]	WO_3
WO_3:Zn	40	350	8.33	2000 [24]	WO_3:Zn

Table 3.7 Summary of published results on CO gas sensing characteristics of WO_3

Material	Concentration (ppm)	Temperature (^{0}C)	*Sensitivity	Year (reference)	Method of preparation
CO					
WO_3:Pd	200	100	1.6	2011 [103]	Chemical route
WO_3:Fe	1000	150	20	2011 [107]	Thermal evaporation
WO_3	400	200	20	2005 [32]	Thermal evaporation
WO_3:Co	800	250	1.2	2010 [108]	Pulsed laser deposition

Iron-doped nanostructured WO_3 thin films prepared by Electron Beam Evaporation (EBE) technique were investigated towards acetaldehyde by Tesfamichael et al. [109]. Addition of 10 at.% Fe slightly decreased the band gap energy and subsequent annealing at 300ºC for 1 hour in air further decreased the band gap energy. The annealed Fe-doped WO_3 sensor produced gas selectivity but a reduced gas sensitivity towards acetaldehyde as compared to WO_3 sensor. Iron addition lower than 10 at.% to WO_3 films prepared by reactive RF sputtering produced an enhancement in sensor response when exposed to NO_2 [110]. Additionally, iron addition was found to be advantageous in sensing ozone, CO and ethanol. The H_2S, nitrous oxide (N_2O) and CO sensing performance of Al-doped WO_3 nanoparticle films prepared by advanced gas deposition was investigated by Hoel et al. [111]. A maximum sensitivity towards H_2S, N_2O and CO was observed at temperatures 130ºC, 250ºC and 430ºC respectively.

Khatko et al. [36] investigated the NO_2, NH_3 and ethanol sensing performance of WO_3 thin films deposited by reactive RF sputtering with interruptions during the deposition process. Sensitivity was found to increase with increase in number of interruptions and interruption time, which was attributed to observed grain size reduction during interruption. In another study, the authors observed that the response of these sensors to ozone is up to four times higher than that of the sensors prepared using RF sputtering [112]. A high sensitivity to NO_2 at a temperature of 50ºC for a sensor made of WO_3 particles of size ~36 nm was reported by Meng et al [113]. In this study, WO_3 nanoparticles were prepared by evaporating tungsten filament under a low pressure of oxygen gas, namely, by gas evaporation method. The deposition was carried out under various oxygen pressures and samples were annealed at different temperatures. The sensitivity was found to increase with decreasing particle size, irrespective of oxygen partial pressure during deposition and annealing temperature.

The electrical response of WO_3 based sensors for ozone detection was reported by Boulmani et al. [114]. Thin films (40 nm thick) of WO_3 were deposited by RF reactive magnetron sputtering on SiO_2/Si substrate with Pt interdigitated micro electrodes. The response towards ozone was found to strongly depend on film morphology which depends on the oxygen concentration during the deposition process. The sensor response was also affected by bias voltage, sputtering time and oxygen concentration during deposition.

The hydrogen response of WO_3 nanotextured thin films coated with a 2.5 nm Pt layer was investigated by Yaacob et al. [115]. The films exhibited gas chromic characteristics when tested in visible-NIR (400-900 nm) range. The total absorbance in this range increased by 15% upon exposure to 600 ppm H_2 in dry air and 60% upon exposure to 10,000 ppm H_2 in dry air.

The films were found to be highly sensitive with stable and repeatable responses towards low concentrations of H_2 at 100ºC. However, the recovery time was found to be slow at room temperature.

The effect of cerium oxide additive on WO_3 nanoparticles prepared by sol-gel method towards volatile organic compound (VOC) gases was investigated by Luo et al. [116]. The highest gas response of Ce-added WO_3 samples was found to shift to lower temperatures compared to pure WO_3 samples. Grain boundaries were pinned due to CeO_2 which resulted in reduction in grain size and increase in surface area. Complex impedence spectroscopy analysis indicated that grain boundary resistance increased and grain boundary capacitance decreased with increasing concentration of CeO_2 which indicates that Ce ions mainly exist at WO_3 grain boundaries and help to improve the microstructure.

WO_3 films have also shown a good sensing performance towards ethanol [117-121]. The sensitivity towards ethanol has been attributed to the desorption of oxygen at the surface of grains [121]. Azad et al [122] investigated the sensing performance of WO_3 towards 100 ppm CO. The authors achieved sensitivity towards CO by modulating ambient oxygen partial pressure to create oxygen deprivation on the metal oxide surface. However, WO_3 responded to CO only at 450^0C.

From the preceding section, it is clear that WO_3 based gas sensors are of high interest at the moment because of their good sensing properties to many gases. Various methods have been used to improve gas sensitivity of WO_3, including modification of morphology and microstructure (i.e., grain size, film thickness, phase) by using different deposition techniques, or by doping with different metals.

3.3 Motivation of the Work

The present study evaluates sensing properties of thick-film gas sensors based on pure and copper activated WO_3. The first objective of this study was to synthesize pure and catalyzed WO_3 nanocrystalline powders. The gas sensors were fabricated from the prepared nanopowder. The additive chosen to improve sensor response was copper. The structural properties, surface morphology and compositional analysis of obtained materials were characterized with XRD, Raman Spectroscopy, SEM, EDS and XPS. The target gases are nitrogen dioxide and hydrogen sulphide. Typically, sensors were evaluated at different working temperatures under a chosen concentration of the target gas in air. Once optimum working temperature is found, sensor responses to different concentrations of target gas are studied. The mechanism involved in the detection properties of pure and copper doped WO_3 to both NO_2 and H_2S gas is also discussed.

3.4 Gas Sensor Fabrication

The nanocrystalline powders were synthesized by precipitation technique from aqueous solutions of ammonium tungstate para penta hydrate {$(NH_4)_{10}W_{12}O_{41}.5H_2O$, Otto Chemi} and nitric acid {HNO_3, Sd-fine Chem Limited} [123]. A pre-determined amount of tungstate salt is dissolved in de-ionised water. With vigorous stirring, a warm, concentrated nitric acid was added dropwise. With continuous stirring the mixed solution was kept at 80^0C, after which the precipitates were allowed to settle for one day at room temperature. The precipitate was washed by addition of a large amount of de-ionized water into the precipitate followed by stirring for about 10 minutes and allowing the precipitates to settle down before decanting the liquid. The washing procedure was carried out for five to six times. Finally the precipitates were separated by filtration. The obtained precipitate was

dried at 100^0C overnight. The precipitate was thoroughly powdered in a mortar and calcined at 400^0C for six hour. The powder obtained was again powdered in mortar. The thick film sensors were prepared by dispersing the nanocrystalline powder in methanol. The solution was stirred in a magnetic stirrer thoroughly and coated on glass substrate with a painting brush and annealed at an approximate temperature of 600^0C overnight. The films thus prepared had an approximate thickness of 20µm. Copper doped WO_3 was prepared by adding stoichiometric amount of copper acetate monohydrate, dissolved in de-ionised water, to the solution containing ammonium tungstate-nitric acid solution before heating at 80^0C. The remaining washing, filtration, drying and calcinations steps were followed as explained above. The copper doping was performed in the range 0.5wt%, 1wt% and 3wt%.

3.5 Structural and Spectroscopic Characterization

3.5.1 XRD Characterization

The crystalline structure and particle size of the 600^0C annealed pure and copper doped WO_3 thick film sensor were examined by X-ray diffraction measurement (XRD, Bruker AXS D8 Advance). Fig. 3.2 shows the XRD spectra of pure and copper doped WO_3 annealed at 600^0C overnight. The 0.5wt%, 1.5wt% and 3wt% copper doped WO_3 films were represented as WO_3 + 0.5wt% Cu, WO_3 + 1.5wt% Cu and WO_3 + 3wt% Cu respectively. Main peaks were found at $2\theta = 23.0^0$, 23.6^0 and 24.3^0, which were identified as corresponding to Miller index (002), (020) and (200) respectively, in triclinic WO_3 (JCPDS# 20-1323). Therefore the thick film sensor of pure and doped WO_3 obtained after annealing at 600^0C was crystalline in nature.

The crystallite size (D) was calculated from peak broadening using the Scherrer approximation, which is defined as

$$D = \frac{0.9\lambda}{B\cos\theta} \qquad (3.1)$$

Where λ is the wavelength of the X-ray (1.5418 A^0), B is the full width at half maximum (FWHM, radian) and θ is the Bragg angle (degree). The average particle size of the pure WO_3, 0.5wt%, 1.5wt%, 3wt% copper doped thick film sensor were found to be 30nm, 32nm, 30nm and 33nm respectively.Particle size was estimated individually from the FWHM of each plane and the average of all the planes was taken to obtain the average particle size. Hence annealed sensor was identified by XRD as nanocrystalline in nature.

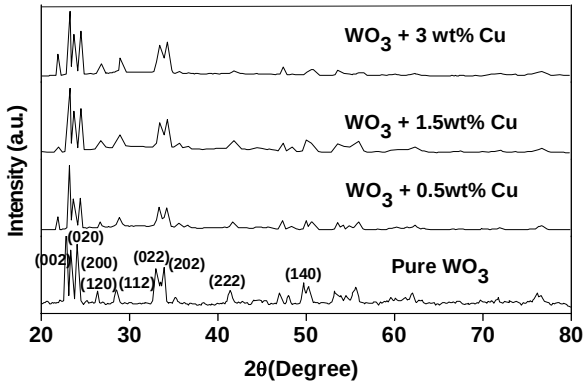

Fig. 3.2 XRD patterns of pure and copper doped WO_3 thick film sensor annealed at 600^0C

3.5.2 Scanning Electron Microscopy

Fig. 3.3 shows the SEM (JEOL Model JSM - 6390LV) micrographs of pure and copper doped WO_3 thick film sensor. The most important factors that influence the sensor characteristics are probably microstructure and surface area. The films exhibiting a porous structure have a large fraction of atoms residing at surfaces and interfaces between the pores, which suggests that the microstructure of the films is suitable for gas-sensing purposes. In the other

words, it can be said that the high sensitivity of a sensor can be attributed to the full exposure of surface adsorption sites to chemical environments. From the SEM images it is clear that our thick film sensor surfaces are highly porous and this makes it highly suitable for sensing application. Compared to the estimated particle size by XRD measurements small variations in particle size are seen in SEM images, since from XRD measurements we have estimated the average particle size. Particle agglomeration which can be seen in SEM images may also result in this size variation.

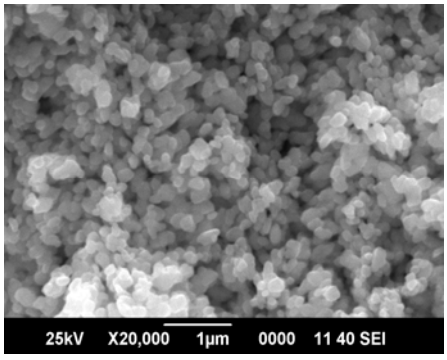

(a) SEM image of pure WO_3 sensor

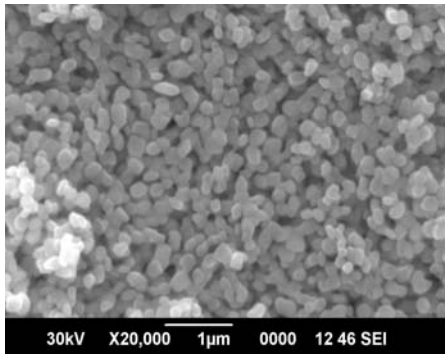

(b) SEM image of 0.5wt% copper doped WO_3 sensor

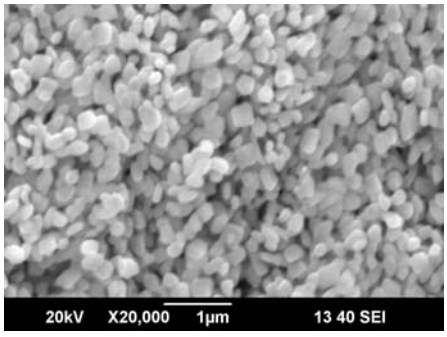

(c) SEM image of 1.5wt% copper doped WO_3 sensor

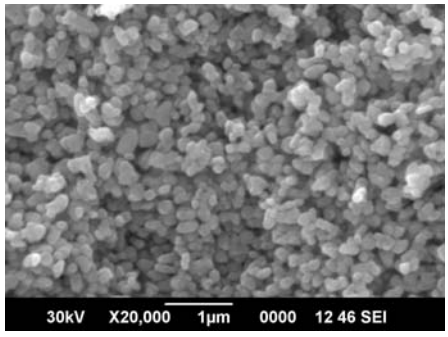

(d) SEM image of 3wt% copper doped WO_3 sensor

Fig. 3.3 SEM images of pure and copper doped WO_3 thick film sensor

3.5.3 EDS

The EDS spectrum of 600^0C annealed pure WO_3 thick film sensor obtained is shown in fig. 3.4. Spectrum reveals presence of tungsten and oxygen elements only. The O/W ratio obtained was 2.98. Fig. 3.5 shows the EDS spectrum of 1.5wt% copper doped WO_3 thick film sensor. Spectrum gives clear evidence for presence of copper in the doped samples.

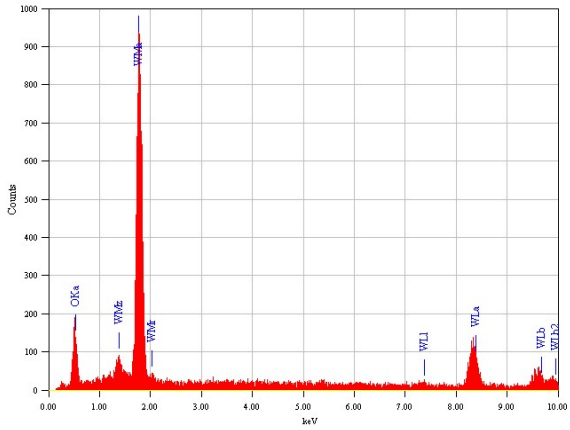

Fig. 3.4 EDS spectrum of 600^0C annealed pure WO_3 thick film sensor.

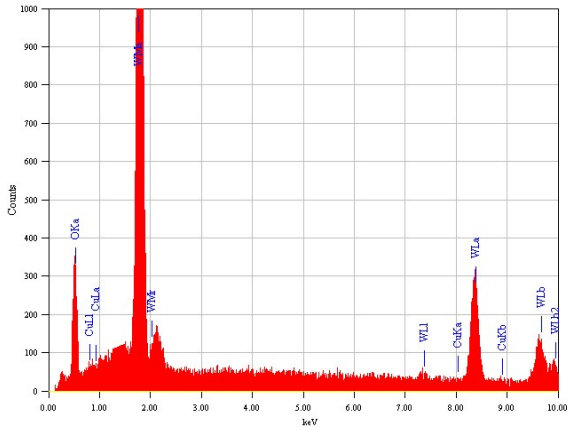

Fig. 3.5 EDS spectrum of 600^0C annealed 1.5wt% copper doped WO_3 thick film sensor.

3.5.4 Raman Spectroscopy

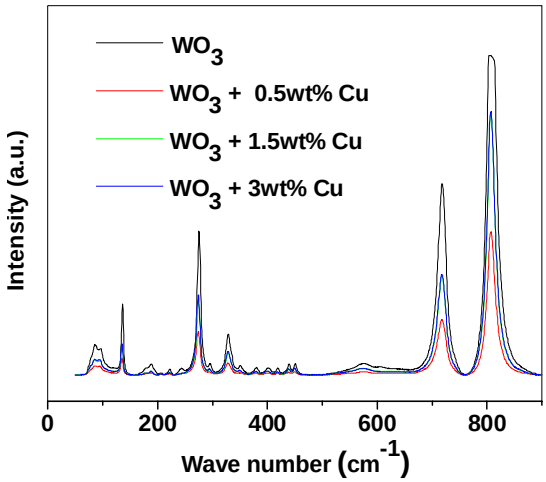

Fig. 3.6 Raman spectra of 600^0C annealed pure and copper doped WO_3 thick film sensor

The Raman spectra were obtained using Horiba Jobin Yvon LabRam HR system at a spatial resolution of 2 mm in a backscattering configuration. The 514.5 nm line of argon ion laser was used for excitation. The Raman spectra of 600^0C annealed pure and copper activated WO_3 thick film sensors are shown in fig. 3.6. The 0.5wt%, 1.5wt% and 3wt% copper doped WO_3 films were represented as WO_3 + 0.5wt% Cu, WO_3 + 1.5wt% Cu and WO_3 + 3wt% Cu respectively. The spectra can be divided into three main regions at 600-900, 200-400 and below 200cm^{-1}. Peaks below 200cm^{-1} are associated with lattice modes, the intermediate frequencies (200–400 cm^{-1}) showing O–W–O bending mode features, and the higher frequencies (600–900 cm^{-1}) with the peaks related to W–O stretching modes [124]. The copper doped spectra indicated a decrease in intensity of the peaks in the three main regions. The decrease in intensity is probably because of formation of Cu-O-W bonds [125,126].

3.5.5 X-ray Photoelectron Spectroscopy

In order to understand the chemical composition of pure and copper doped WO_3 thick film sensor, we carried out XPS measurement. Fig 3.7 (a) and (b) represents XPS spectrum of W4f and O1s peaks of 600^0C annealed pure and 3wt% copper doped sample. The W4f core level spectrum recorded on 600^0C annealed pure WO_3 sensor shows the two components associated with $W4f_{5/2}$ and $W4f_{7/2}$ spin orbit doublet at 36.8 and 34.9 eV. Binding energy values obtained for spin orbits shows a small shift towards the lower binding energy for 600^0C pure sample. This shift may be caused by the contribution from W^{5+} or W^{4+} states, resulting in oxygen vacancies in thick film sensor [127]. These results indicate that film prepared is non – stoichiometric WO_3. The O1s peak is located at 529.7 eV, which is ascribed to the W-O peak. In copper doped sensors there is shift to higher energy side for W4f peaks. The peaks for $W4f_{5/2}$ and $W4f_{7/2}$ are located at 37.391eV and 35.391eV which agree well with the +6 oxidation sate of tungsten [101,128].

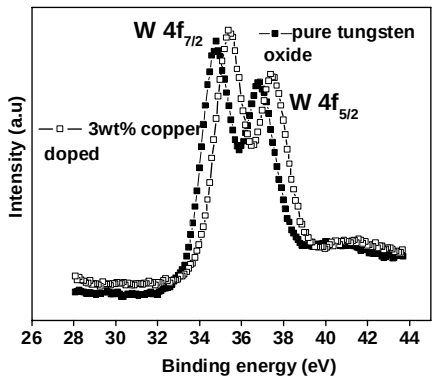

Fig. 3.7(a) XPS spectra of W4f

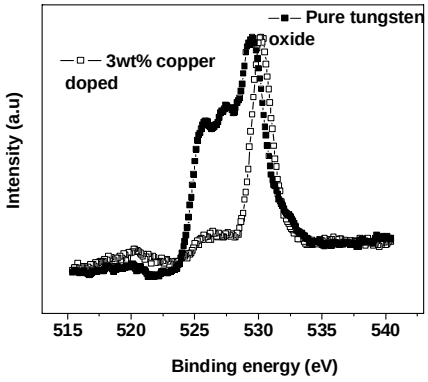

Fig. 3.7(b) XPS spectra of O1s

The O1s spectrum is also shifted to 530.2eV. The XPS data did not revealed any copper centers. This may be due to the nominal concentration of copper present in the doped sample. Another reason may be that copper has been able to diffuse inside the structure of WO_3 and thus it cannot be detected by XPS [129].

3.6 Gas Sensors Based on Pristine WO_3

3.6.1 Nitrogen Dioxide Detection

Response of WO_3 thick film sensor towards a low concentration of 7 ppm was studied in the temperature range of 100^0C to 225^0C. The response of sensor was measured as ratio of resistance R_{gas}/R_{air}, here R_{gas} is resistance of the sensor in presence of gas and R_{air} is the resistance of the sensor before the introduction of gas. Fig. 3.8 (a) to (f) shows the response of WO_3 sensor at different temperature towards a concentration of 7 ppm. The response time is taken as the time taken by the sensor to reach 90% of maximum value and recovery time is taken as the time taken by the sensor to reach 10% of base value (value before the introduction of gas) in all the measurements.

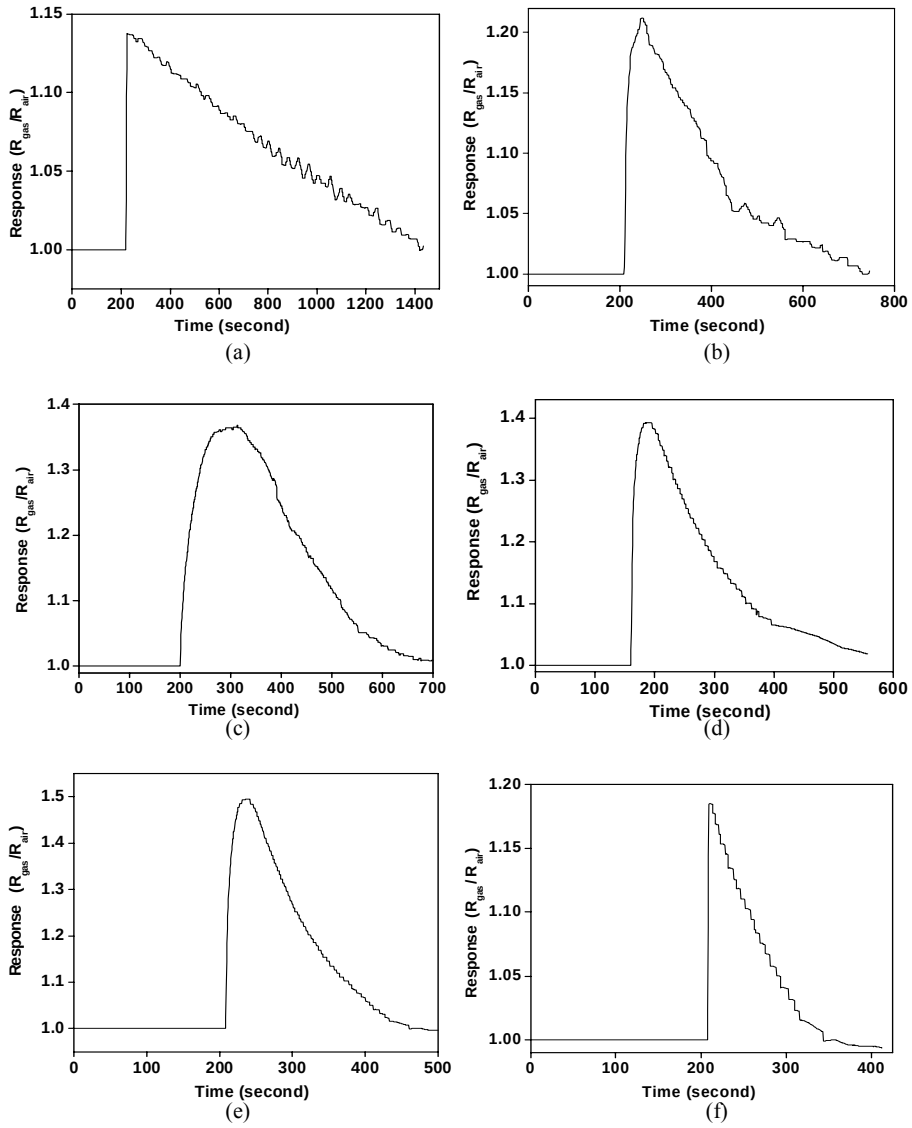

Fig. 3.8 Response of WO_3 thick film sensor towards 7 ppm of NO_2 gas at (a) 100 ^{0}C (b) 125^{0}C (c) 150 ^{0}C (d) 175^{0}C (e) 200^{0}C (f) 225^{0}C

Fig. 3.9 (a) shows sensitivity of WO_3 sensor at different temperatures towards a concentration of 7 ppm. Maximum response value in figures 3.8 (a) to (f) is taken as the representative sensitivity value in fig. 3.9 (a). It is found that at a temperature of 200^0C the sensitivity was maximum. Beyond this temperature the sensitivity of sensor decreases. The response time and recovery time of sensor at different temperatures towards 7 ppm concentration of gas is shown in fig 3.9 (b) and 3.9 (c) respectively. At 200^0C response time and recovery time were relatively small and has a value of 14 seconds and 2.9 minutes respectively.

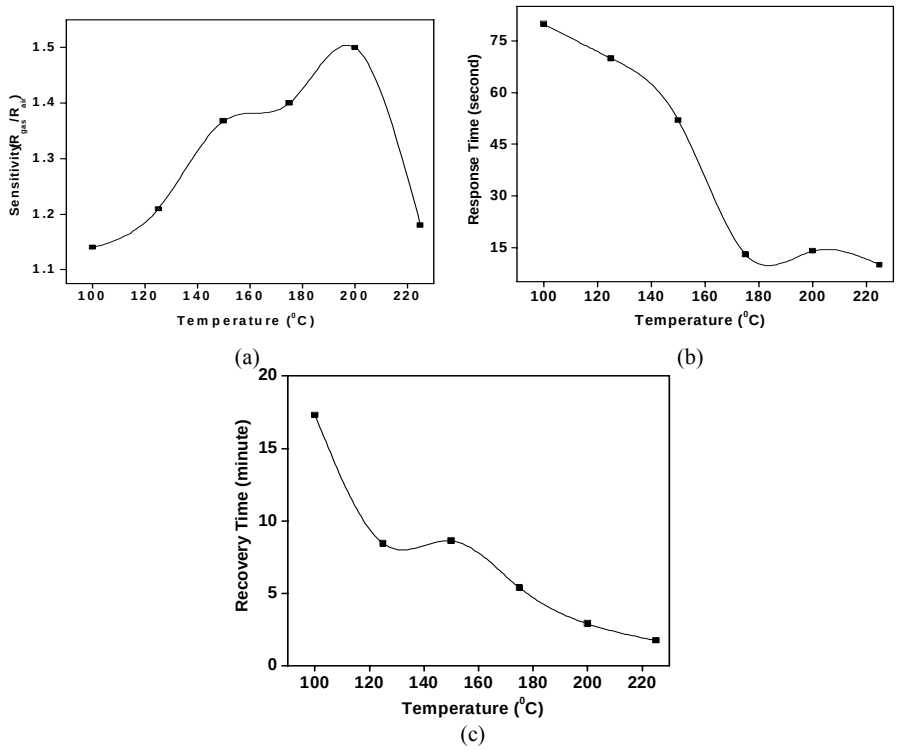

Fig. 3.9 (a) Sensitivity (b) Response time (c) Recovery time of WO_3 thick film sensor towards 7 ppm of NO_2 gas at different temperatures

Selecting optimum temperature is a critical factor in the operation of gas sensors. Considering sensitivity, response time and recovery time at different temperatures, 200^0C was considered as optimum operating temperature for the working of WO_3 sensor. At this temperature a maximum sensitivity of 1.5 was achieved for 7 ppm NO_2 with lower response and recovery time. Hence further studies depending on various concentrations were carried out at this optimum temperature of 200^0C. Response of sensor to different concentrations at optimum operating temperature is shown in fig. 3.10 (a) and (b). From concentration dependent studies it was found that sensor was able to determine concentration as low as 1.8 ppm with a sensitivity of 1.01. The highest concentration measured with the set up was 86 ppm with a sensitivity of 58.4. Fig. 3.11 shows sensitivity of sensor at 200^0C towards different gas concentration.

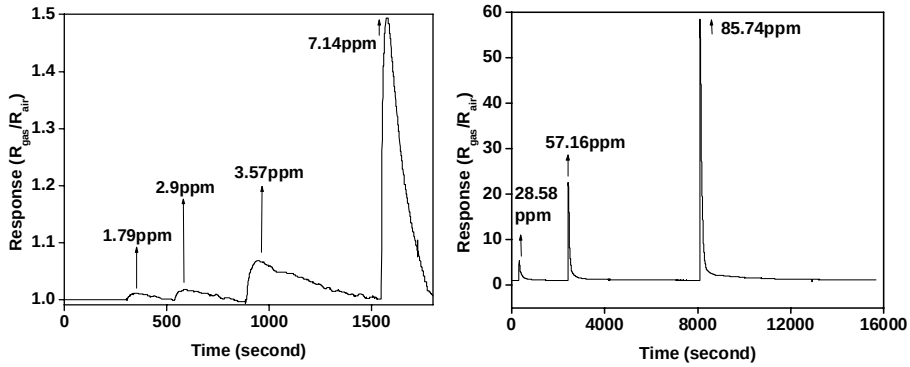

Fig. 3.10 Response of WO_3 thick film sensor towards different concentrations of NO_2 at 200^0C

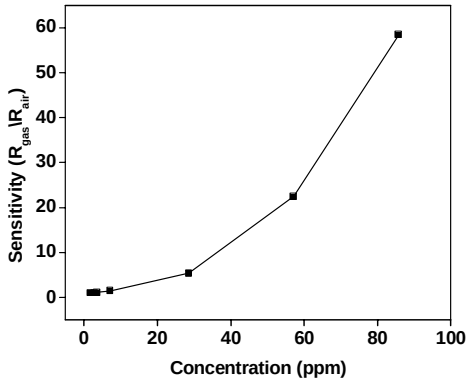

Fig. 3.11 Sensitivity of WO_3 thick film sensor towards different concentrations of NO_2 at 200^0C

3.6.2 Hydrogen Sulphide Detection

WO_3 based thick film sensor response towards 17.85 ppm of H_2S gas concentration was measured in temperature range 100 to 225^0C. The sensor response in case of H_2S gas was calculated as ratio of R_{air}/R_{gas}, here R_{air} is resistance of thick film sensor before introduction of gas and R_{gas} is resistance of sensor in presence of gas. Fig. 3.12 (a) to (f) shows response of sensor towards a concentration of 17.85 ppm of H_2S at various temperatures. The response time and recovery time is taken as the time taken by the sensor to reach 90% of maximum value and 10% of base value (value before the introduction of gas) respectively in all the measurements. The temperature dependent gas sensing response at 100 and 125^0C show a fluctuation which is due to 0.5^0C accuracy of the temperature controller. Since the variation of resistance upon induction of H_2S gas is small at these temperatures the accuracy of controller affects the measurements.

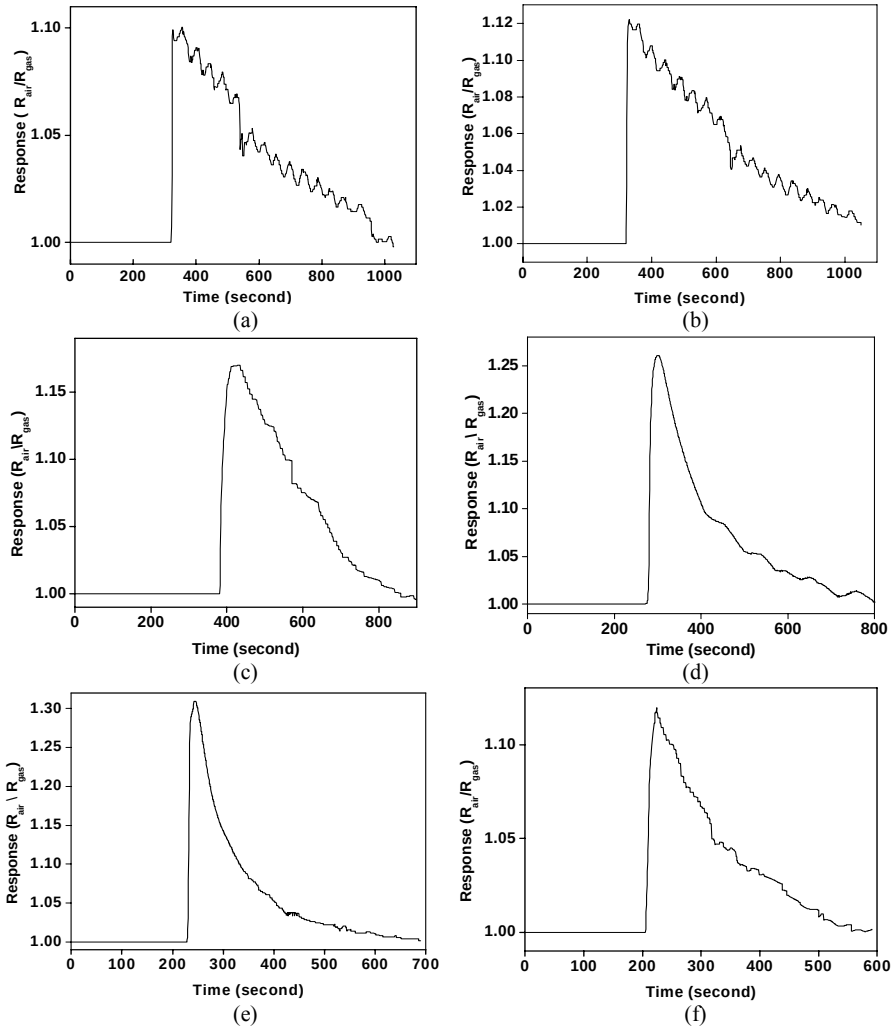

Fig. 3.12 Response of WO_3 thick film sensor towards 17.85 ppm of H_2S gas at (a) 100 ^{0}C (b) 125^{0}C (c) 150 ^{0}C (d) 175^{0}C (e) 200^{0}C (f) 225 ^{0}C

Sensitivity of sensor at different temperatures towards a concentration of 17.85 ppm is shown in fig. 3.13 (a). At a temperature of 200^{0}C thick film sensor showed a maximum response of 1.3 towards 17.85 ppm beyond which sensitivity of sensor decreases. Fig. 3.13 (b) and (c) shows response

and recovery time of sensor towards a concentration of 17.85 ppm at different temperatures. At 200^0C response time and recovery time were relatively small with values 22 seconds and 4.1 minutes respectively.

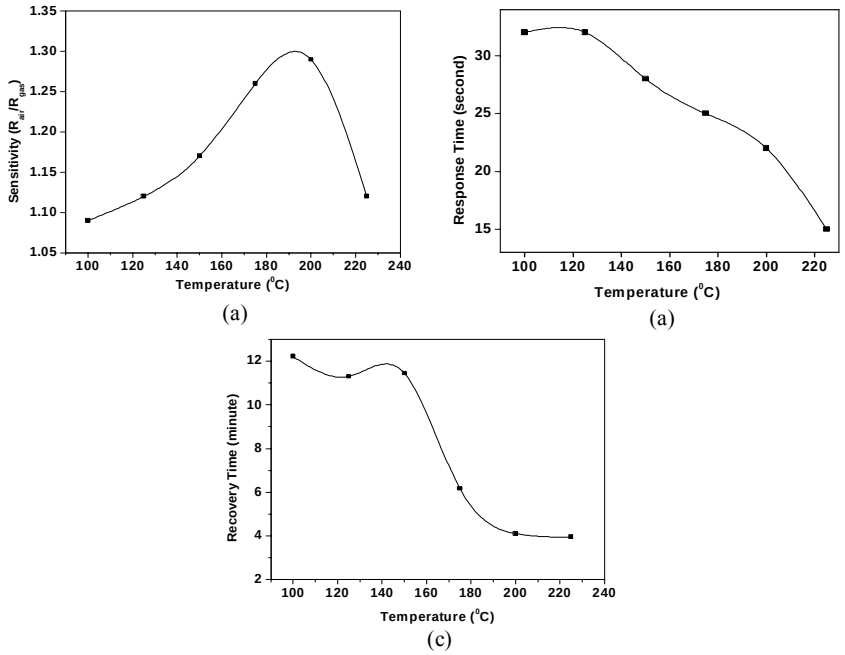

Fig. 3.13 (a) Sensitivity (b) Response time (c) Recovery time of WO_3 thick film sensor towards 17.85 ppm of H_2S gas at different temperatures

Considering the sensitivity, response time and recovery time at different temperatures 200^0C was considered as optimal working temperature for sensor. Hence concentration dependent studies of sensor were conducted at this optimum temperature of 200^0C. Concentration dependent studies showed that lowest measured concentration was 7.14 ppm with a sensitivity of 1.01. Highest measured concentration was 200 ppm with a sensitivity of 3. Fig. 3.14 (a) and (b) shows response of sensor towards different concentrations at an optimal temperature of 200^0C. Fig. 3.15 shows the sensitivity towards different concentrations at 200^0C

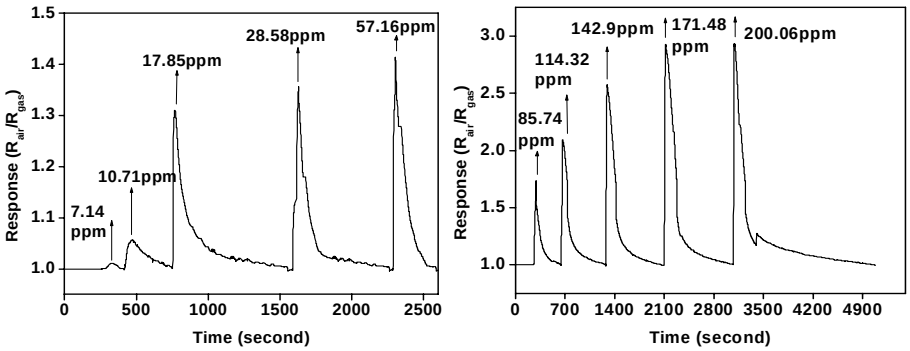

(a) (b)

Fig. 3.14 Response of the WO_3 thick film sensor towards different concentrations of H_2S at 200^0C

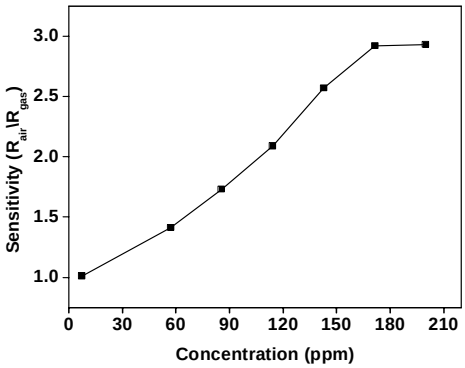

Fig. 3.15 Sensitivity of the WO_3 thick film sensor towards different concentrations of H_2S at optimal temperature of 200^0C

3.7 Gas Sensors Based on 0.5wt% Copper Doped WO_3

3.7.1 Nitrogen Dioxide Detection

Response of the 0.5wt% copper doped WO_3 sensor towards a relatively low concentration of 7 ppm of NO_2 gas was studied in the temperature range of 100 to 225^0C. Fig. 3.16 (a) to (f) shows response of sensor at different temperatures towards this concentration.

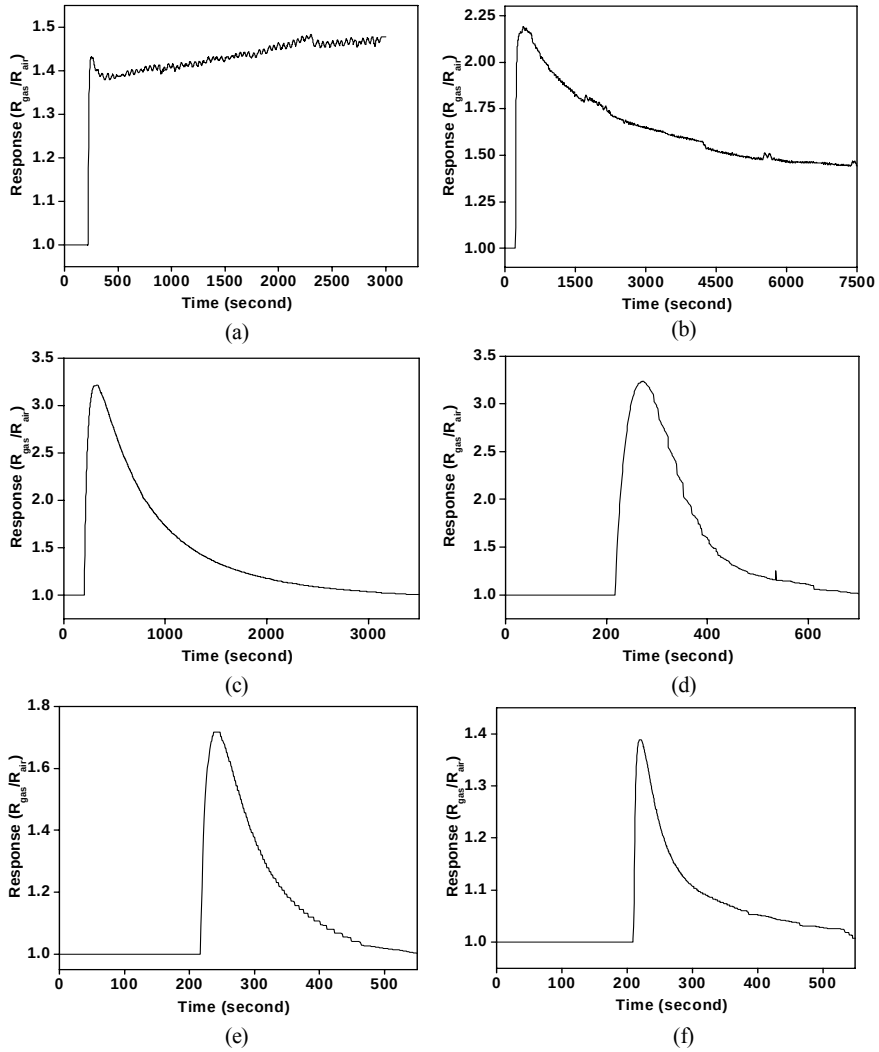

Fig. 3.16 Response of 0.5 wt% copper doped WO_3 thick film sensor towards 7 ppm of NO_2 gas at (a) 100 ^{0}C (b) 125^{0}C (c) 150 ^{0}C (d) 175^{0}C (e) 200^{0}C (f) 225 ^{0}C

The sensitivity of sensor at different temperatures towards of 7 ppm concentration is shown in fig. 3.17 (a). At 100 and 125^{0}C the recovery time of the sensor was very large hence measurements were discontinued. From

sensitivity graph at various temperatures it is found that at 175^0C sensor has a maximum response of 3.23 after which response decreases. The response and recovery time of sensor at different temperatures towards the concentration of 7 ppm is shown in fig. 3.17 (b) and (c). At 175^0C sensor showed a response time of 33 seconds and recovery time of 3.56 minutes. The concentration dependent studies on the sensor were conducted at 175^0C.

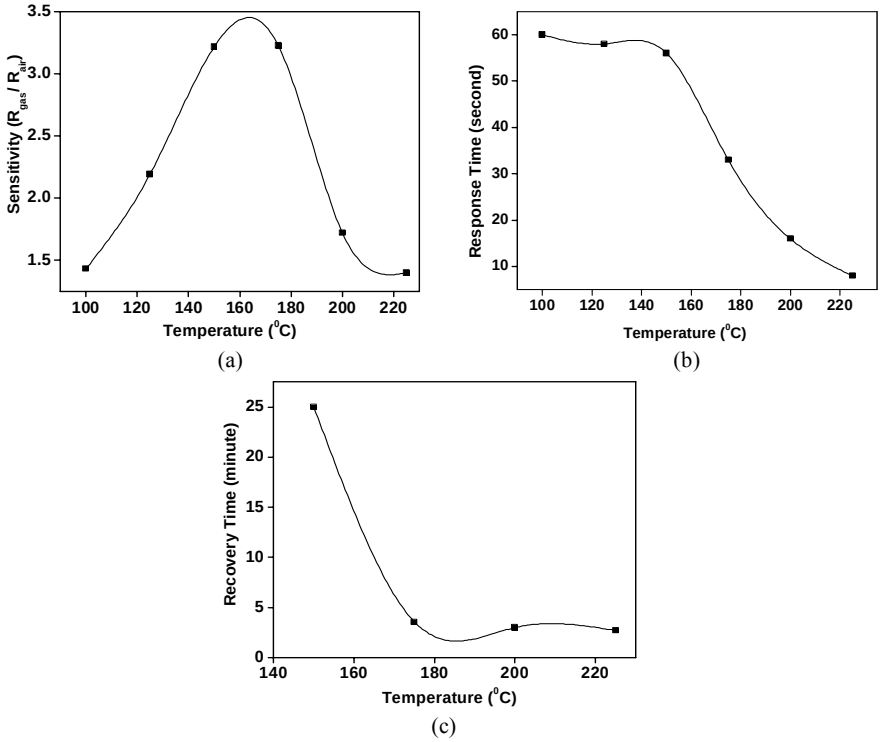

Fig. 3.17 (a) Sensitivity (b) Response time (c) Recovery time of 0.5 wt% copper doped WO_3 thick film sensor towards 7 ppm of NO_2 gas at different temperature

Concentration dependent studies performed at optimum temperature of 175^0C showed that lowest measurable concentration was 1.79 ppm with a sensitivity of 1.03. Highest concentration measured with the setup was 57.16 ppm with a sensitivity of 26.67. Fig. 3.18 (a) and (b) shows response of sensor

towards different concentrations at optimal temperature of 175^0C. Fig. 3.19 shows sensitivity towards different concentrations at 175^0C.

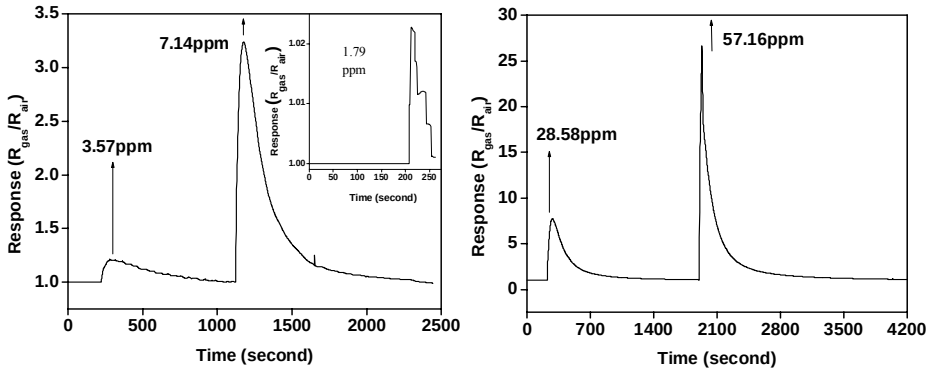

(a) (b)

Fig. 3.18 Response of 0.5wt% copper doped WO_3 thick film sensor towards different concentrations of NO_2 at 175^0C

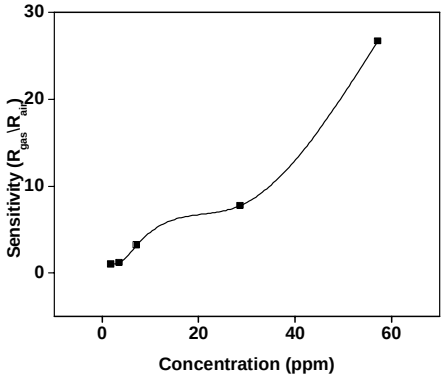

Fig. 3.19 Sensitivity of 0.5wt% copper doped WO_3 thick film sensor towards different concentrations of NO_2 at optimal temperature of 175^0C

3.7.2. Hydrogen Sulphide Detection

Response of the 0.5 wt% copper doped WO_3 sensor towards a concentration of 17.85 ppm was recorded at temperatures ranging from 125 to 250^0C. At 100^0C sensor did not show any response towards this concentration. Hence measurements were carried out at temperatures from

125 to 250^{0}C. Fig. 3.20 (a) to (f) shows response of sensor towards17.85 ppm H_2S concentration at various temperatures.

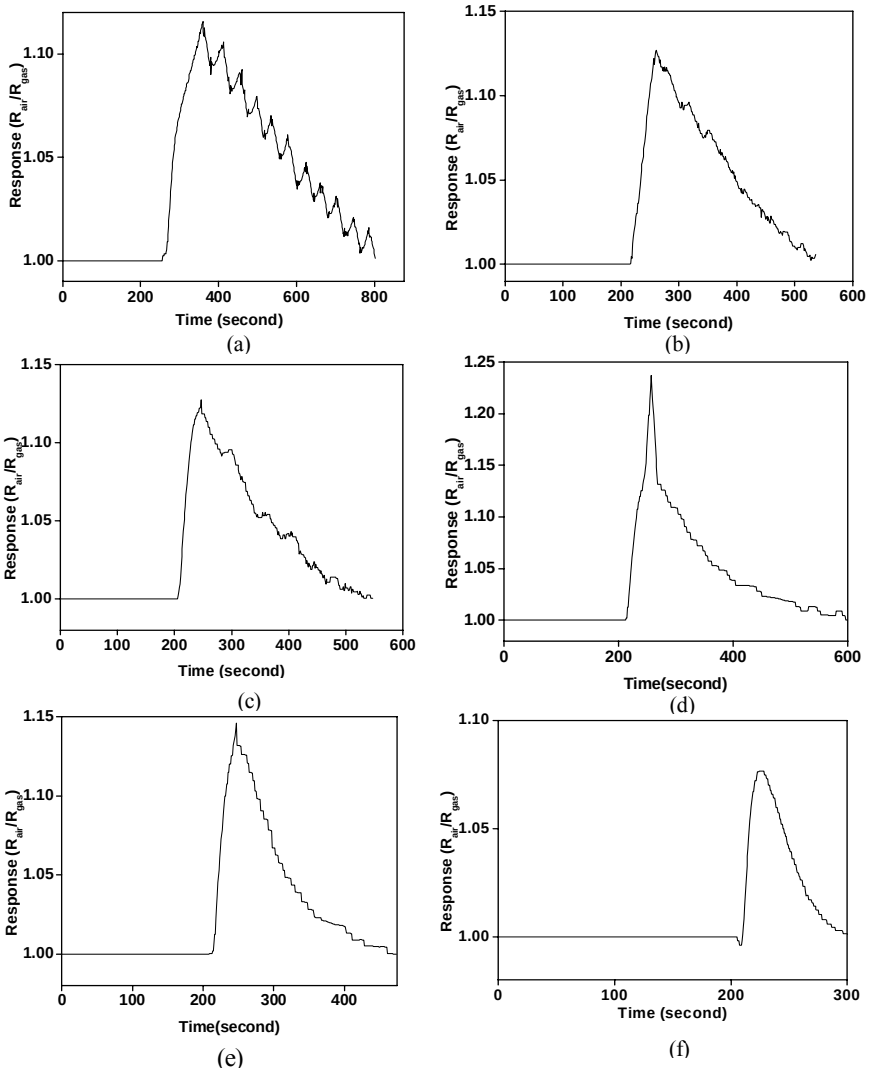

Fig. 3.20 Response of 0.5 wt % copper doped WO_3 thick film sensor towards 17.85 ppm of H_2S gas at (a) 125 ^{0}C (b) 150^{0}C (c) 175 ^{0}C (d) 200^{0}C (e) 225^{0}C (f) 250 ^{0}C

The sensitivity of 0.5 wt% copper doped WO_3 sensor towards the concentration of 17.85 ppm H_2S gas at temperatures from 125 to 250^0C is shown in fig. 3.21 (a). Response and recovery time of sensor to this concentration at various temperatures is shown in fig. 3.21 (b) and (c). The plot representing sensitivity of sensor at different temperatures for the concentration of 17.85 ppm shows that maximum sensitivity is attained at 200^0C with a response value of 1.24. At this temperature sensor had a response and recovery time of 33 seconds and 4.18 minutes respectively. Considering these factors operating temperature of sensor could be fixed as 200^0C.

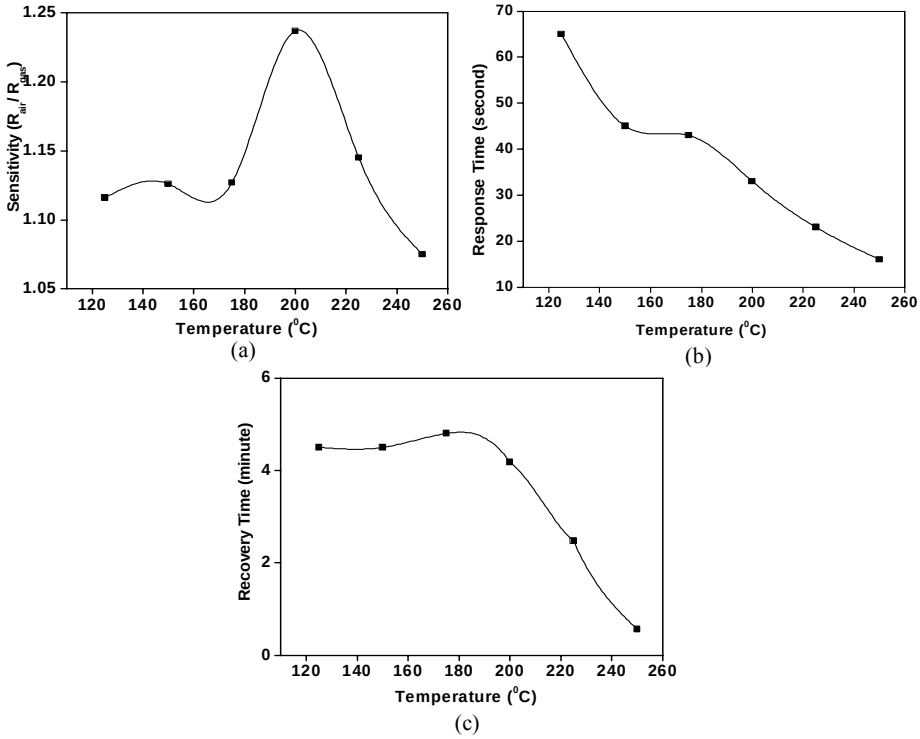

Fig. 3.21 (a) Sensitivity (b) Response time (c) Recovery time of 0.5 wt % copper doped WO_3 thick film sensor towards 17.85 ppm of H_2S gas at different temperatures

Further, concentration dependent studies on sensor were conducted at this operating temperature of 200^0C. Fig. 3.22 (a) and (b) shows response of 0.5 wt% copper doped WO_3 sensor towards different concentration at optimal temperature of 200^0C. The concentration dependent studies show that lowest detection concentration of sensor was 17.85 ppm with a response value of 1.15 and highest measured concentration was 286 ppm with a response value of 4.47. Sensitivity of sensor at different concentrations is shown in fig. 3.23.

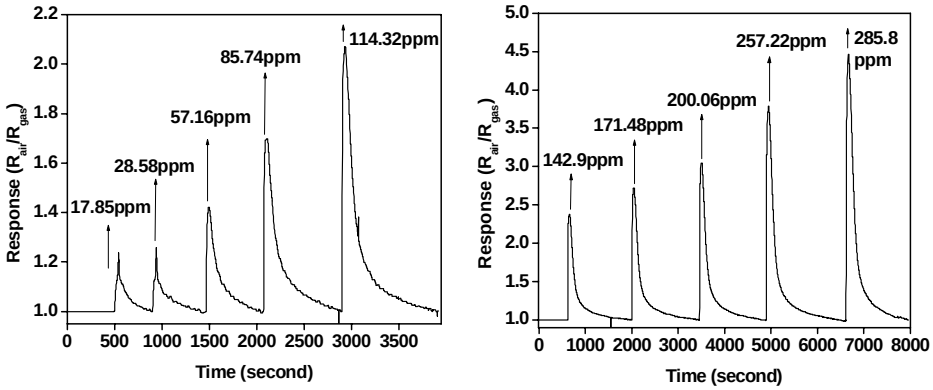

(a) (b)

Fig.3.22 Response of 0.5wt% copper doped WO_3 thick film sensor towards different concentrations of H_2S at 200^0C

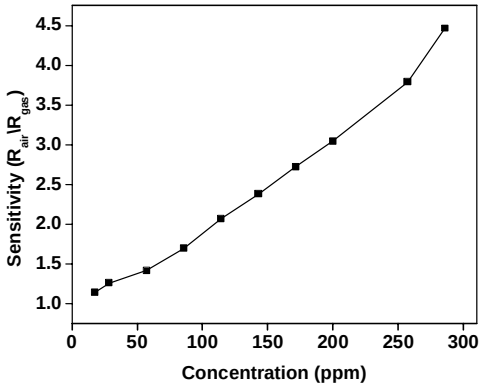

Fig. 3.23 Sensitivity of 0.5wt% copper doped WO_3 thick film sensor towards different concentrations of H_2S at optimal temperature of 200^0C

3.8 Gas Sensors Based on 1.5wt% Copper Doped WO_3

3.8.1 Nitrogen Dioxide Detection

Response of sensor 1.5 wt% copper doped WO_3 sensor towards a concentration of 7 ppm of NO_2 gas was studied in temperature range of 100 to 225^{0}C. Fig. 3.24 (a) to (f) shows response of sensor at different temperatures towards the 7 ppm concentration.

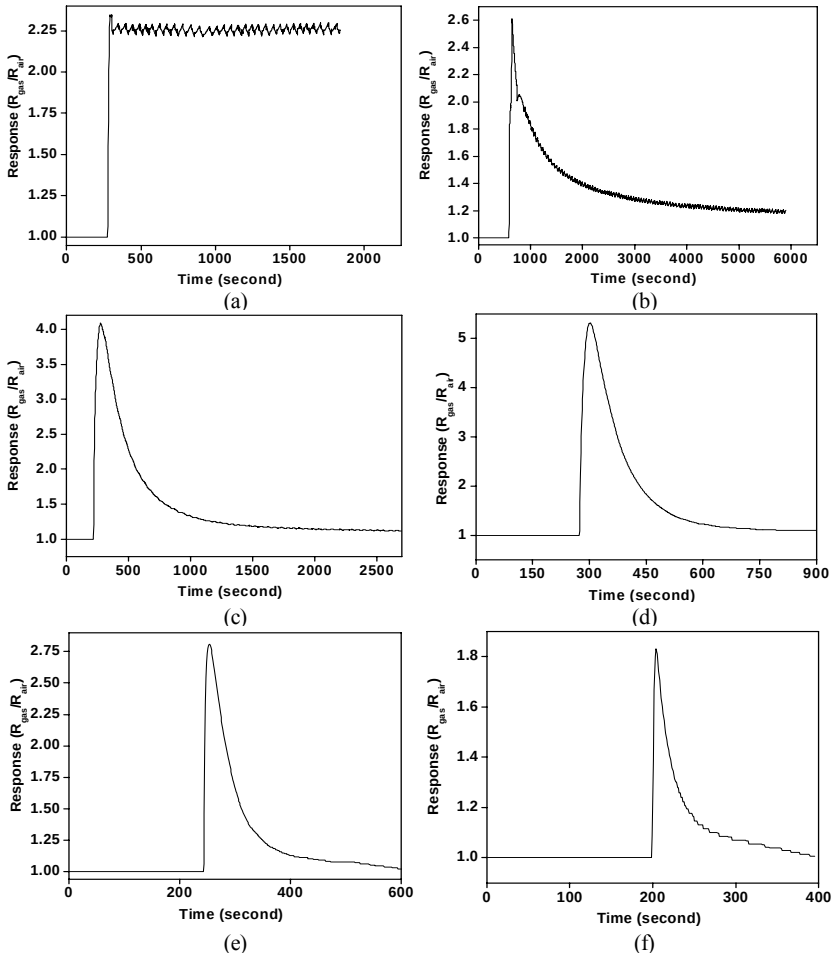

Fig. 3.24 Response of 1.5 wt% copper doped WO_3 thick film sensor towards 7 ppm of NO_2 gas at (a) 100 ^{0}C (b) 125^{0}C (c) 150 ^{0}C (d) 175^{0}C (e) 200^{0}C (f) 225 ^{0}C

Sensitivity of sensor at different temperatures towards a concentration of 7 ppm is shown in fig. 3.25 (a). Temperature dependent gas sensing behaviour shows that optimum operating temperature for 1.5wt% copper doped WO_3 sensor is 175^0C with a sensitivity, response and recovery time of 5.31, 18 seconds and 3.53 minutes respectively. Response and recovery time of sensor at different temperature towards a concentration of 7 ppm is shown in fig. 3.25 (b) and (c)

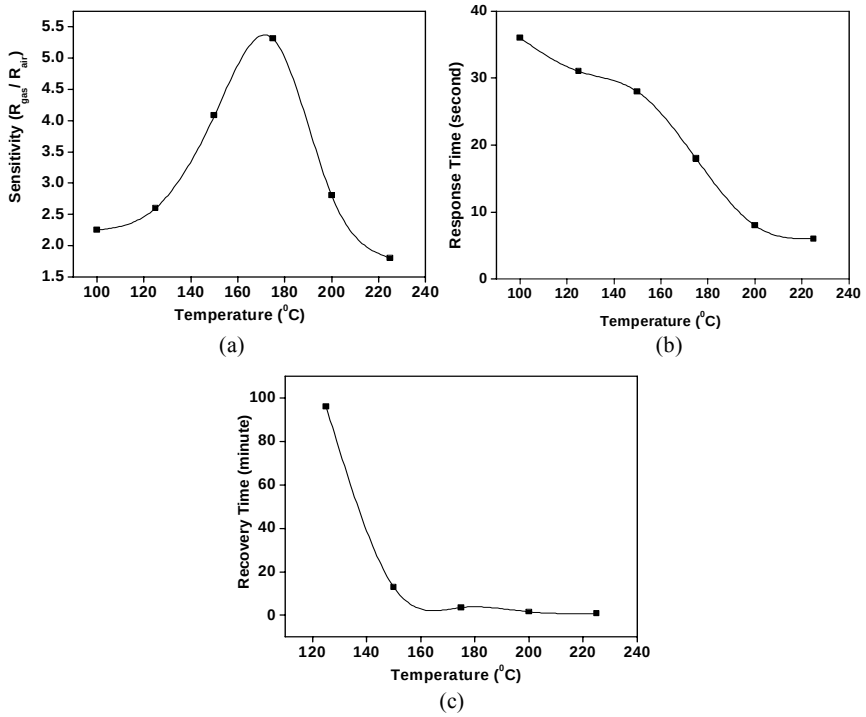

Fig. 3.25 (a) Sensitivity (b) Response time (c) Recovery time of 1.5 wt% copper doped WO_3 thick film sensor towards 7 ppm of NO_2 gas at different temperatures

The concentration dependent studies conducted at his optimum temperature of 175^0C shows that lowest measurable concentration was 1.79 ppm with a sensitivity of 1.03. The highest measured concentration here was

57.16 ppm with a sensitivity of 32.88. Fig. 3.26 (a) and (b) shows response of sensor towards different concentration at the optimal temperature of 175^0C. Fig. 3.27 shows sensitivity towards different concentration at 175^0C.

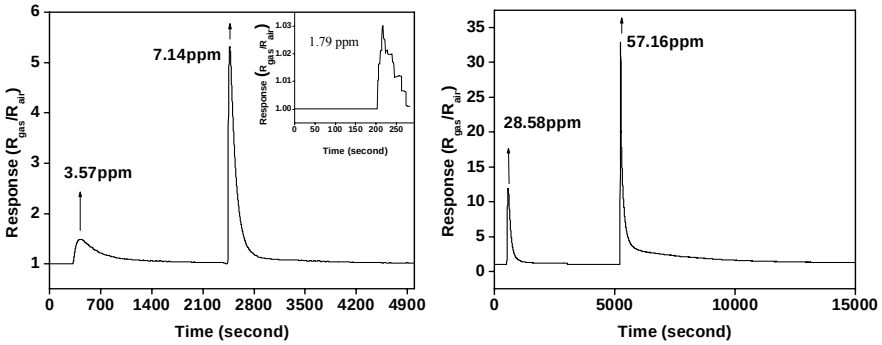

Fig. 3.26 Response of 1.5wt% copper doped WO_3 thick film sensor towards different concentrations of NO_2 at 175^0C

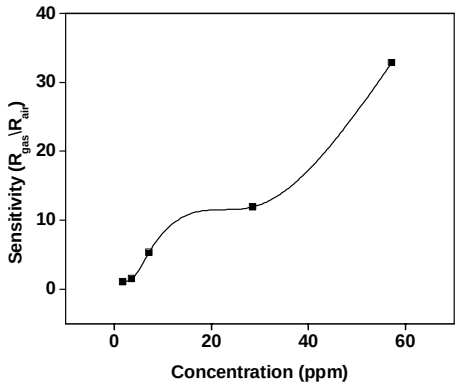

Fig. 3.27 Sensitivity of the 1.5wt% copper doped WO_3 thick film sensor towards different concentrations of NO_2 at optimal temperature of 175^0C

3.8.2 Hydrogen Sulphide Detection

Response of the 1.5wt% copper doped WO_3 sensor towards a concentration of 17.85 ppm was measured at temperatures ranging from 100 to 250^0C. Fig. 3.28 (a) to (g) shows response of sensor towards this concentration at various temperatures.

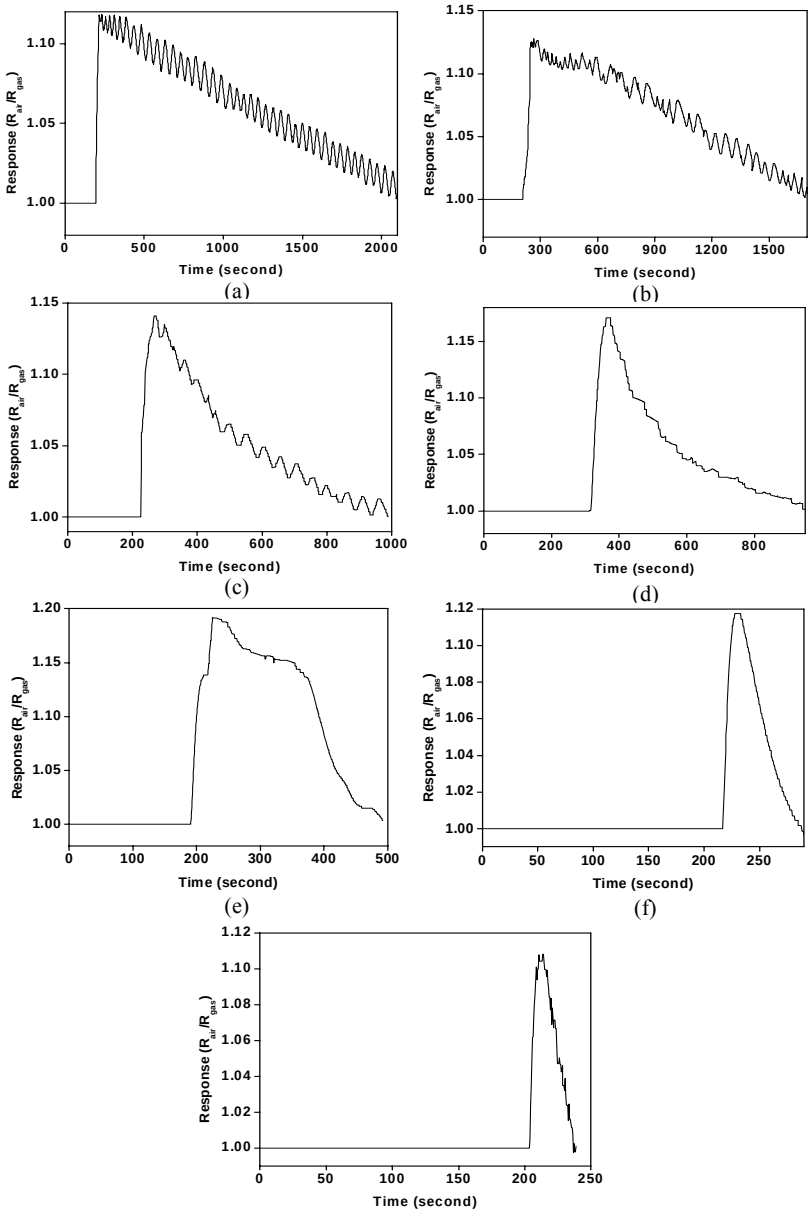

Fig. 3.28 Response of 1.5 wt % copper doped WO_3 thick film sensor towards 17.85 ppm of H_2S gas at (a) 100 ^{0}C (b) 125^{0}C (c) 150 ^{0}C (d) 175^{0}C (e) 200^{0}C (f) 225 ^{0}C (g) 250^{0}C

Sensitivity of sensor at different temperatures towards the concentration of 17.85 ppm is shown in fig. 3.29 (a). Temperature dependent studies shows that optimum operating temperature is 200^0C with a response of 1.19 for the 17.85 ppm concentration studied. Response and recovery time were 39 seconds and 4 minutes for this concentration at 200^0C. The temperature dependence of response time and recovery time are shown in figures 3.29 (b) and (c) for 17.85 ppm concentration.

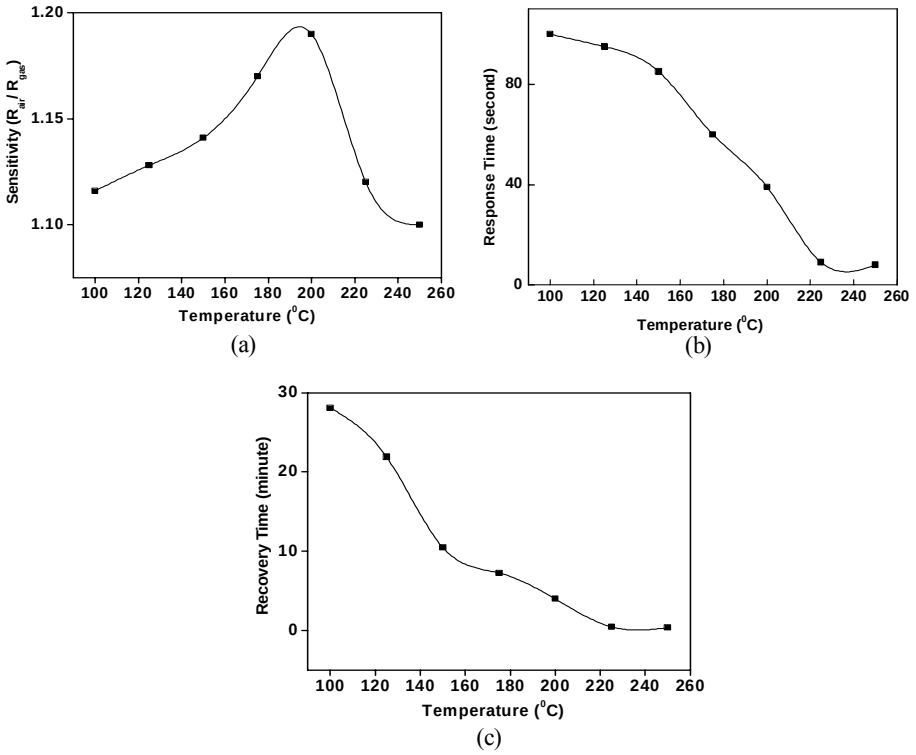

Fig. 3.29 (a) Sensitivity (b) Response time (c) Recovery time of 1.5 wt% copper doped WO_3 thick film sensor towards 17.85 ppm of H_2S gas at different temperature

Concentration dependence of the sensitivity was investigated at the identified optimum temperature of 200^0C. Minimum detectable concentration

was 17.85 ppm with a response of 1.19 and maximum measured concentration was 286 ppm with a response of 3.4. Fig. 3.30 (a) and (b) shows response of sensor towards different concentrations at optimal temperature of 200^0C. Sensitivity of sensor towards different concentrations at this temperature is shown in fig. 3.31.

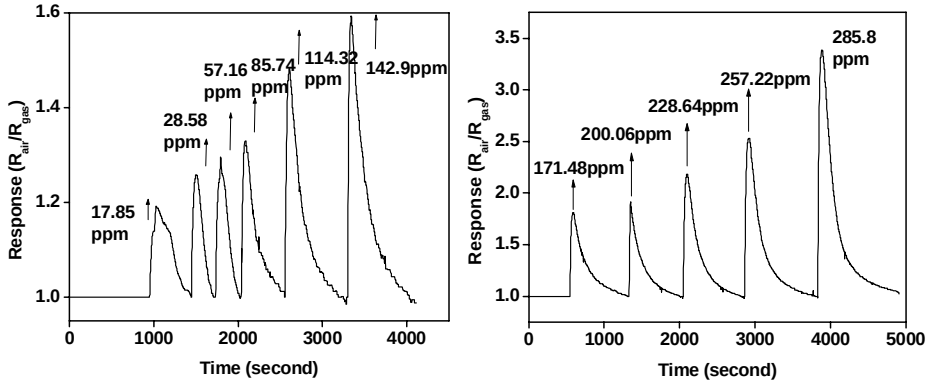

Fig. 3.30 Response of 1.5wt% copper doped WO_3 thick film sensor towards different concentrations of H_2S at 200^0C

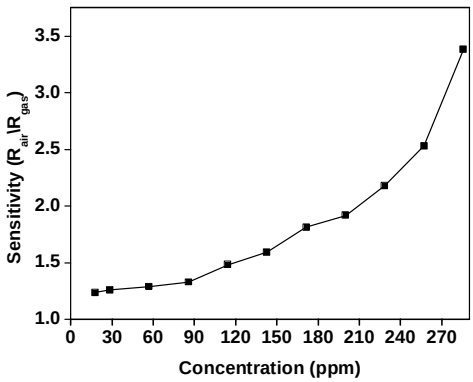

Fig. 3.31 Sensitivity of 1.5wt% copper doped WO_3 thick film sensor towards different concentrations of H_2S at optimal temperature of 200^0C

3.9 Gas Sensors Based on 3wt% Copper Doped WO_3

3.9.1 Nitrogen Dioxide Detection

Response of the 3wt% copper doped WO_3 sensor towards a concentration of 7 ppm of NO_2 gas studied in temperature range of 100 to 225^0C is presented in the figures 3.32 (a) to (f).

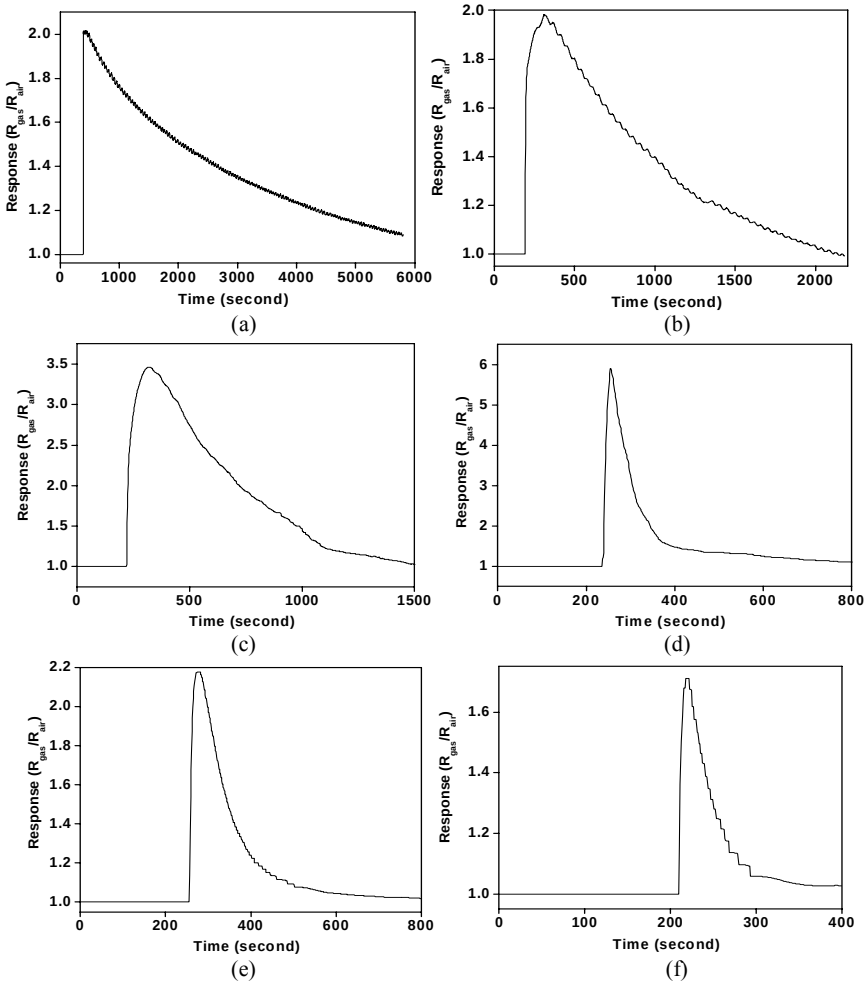

Fig. 3.32 Response of 3wt% copper doped WO_3 thick film sensor towards 7 ppm of NO_2 gas at (a) 100 ^{0}C (b) 125^{0}C (c) 150 ^{0}C (d) 175^{0}C (e) 200^{0}C (f) 225 ^{0}C

Sensitivity of sensor at different temperatures towards this concentration is shown in fig. 3.33 (a). Maximum sensitivity was achieved at an operating temperature of 175^0C with a response of 6. The response and recovery times at this optimum temperature was found to be 15 seconds and 3 minutes respectively. The response time and recovery time at different temperature for the concentrations studied is shown in figures 3.33 (b) and (c).

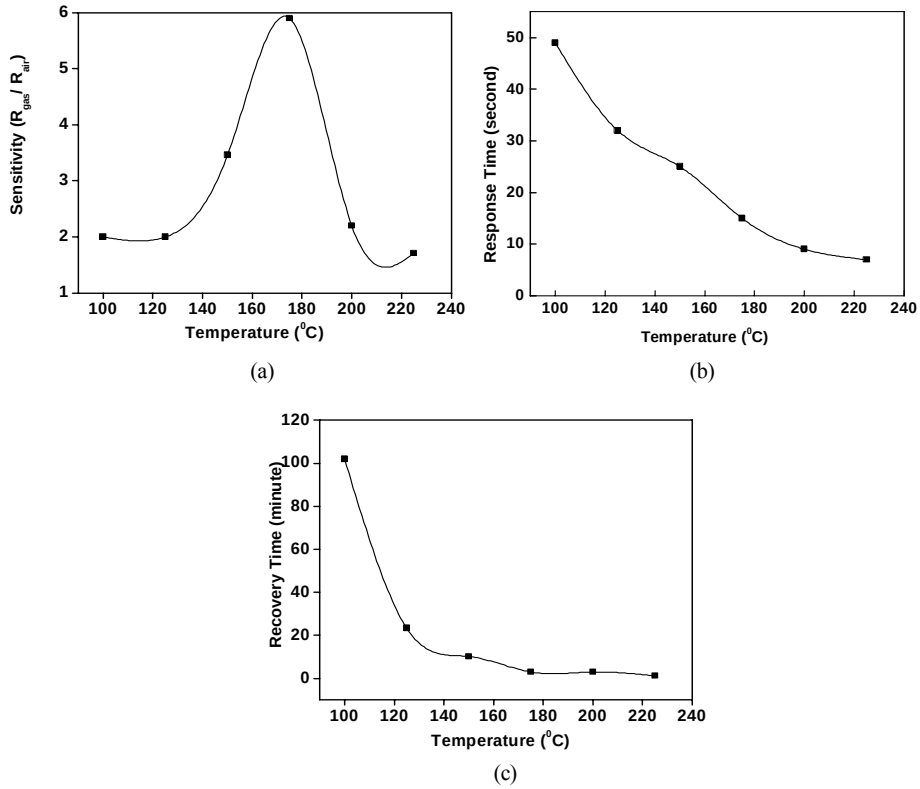

Fig. 3.33 (a) Sensitivity (b) Response time (c) Recovery time of 3wt% copper doped WO_3 thick film sensor towards 7 ppm of NO_2 gas at different temperatures

The concentration dependent studies at the optimum temperature of 175^0C are shown in fig. 3.34 (a) and (b). The lowest detectable concentration

was found to be 1.79 ppm with a response of 1.04 and maximum concentration measured with the method was 57.16 ppm with a response of 42.83. Fig. 3.35 shows the sensitivity towards different concentrations at 175^{0}C.

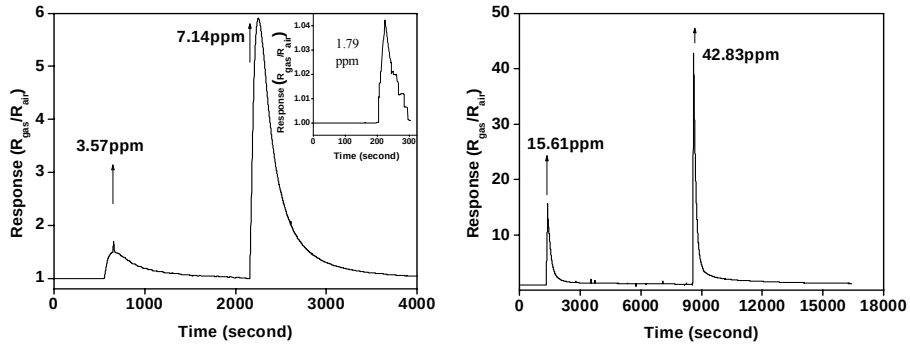

(a) (b)

Fig. 3.34 Sensitivity of the 3wt% copper doped WO_3 thick film sensor towards different concentrations of NO_2 at optimal temperature of 175^{0}C

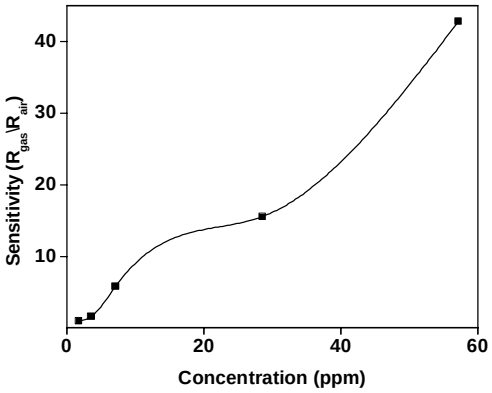

Fig. 3.35 Sensitivity of the 3wt% copper doped WO_3 thick film sensor towards different concentrations of NO_2 at optimal temperature of 175^{0}C

3.9.2 Hydrogen Sulphide Detection

Response of the 3wt% copper doped WO_3 sensor towards a concentration of 17.85 ppm was measured at temperatures ranging from 125

to 250^{0}C. Fig. 3.36 (a) to (f) show response of sensor towards this concentration at various temperatures.

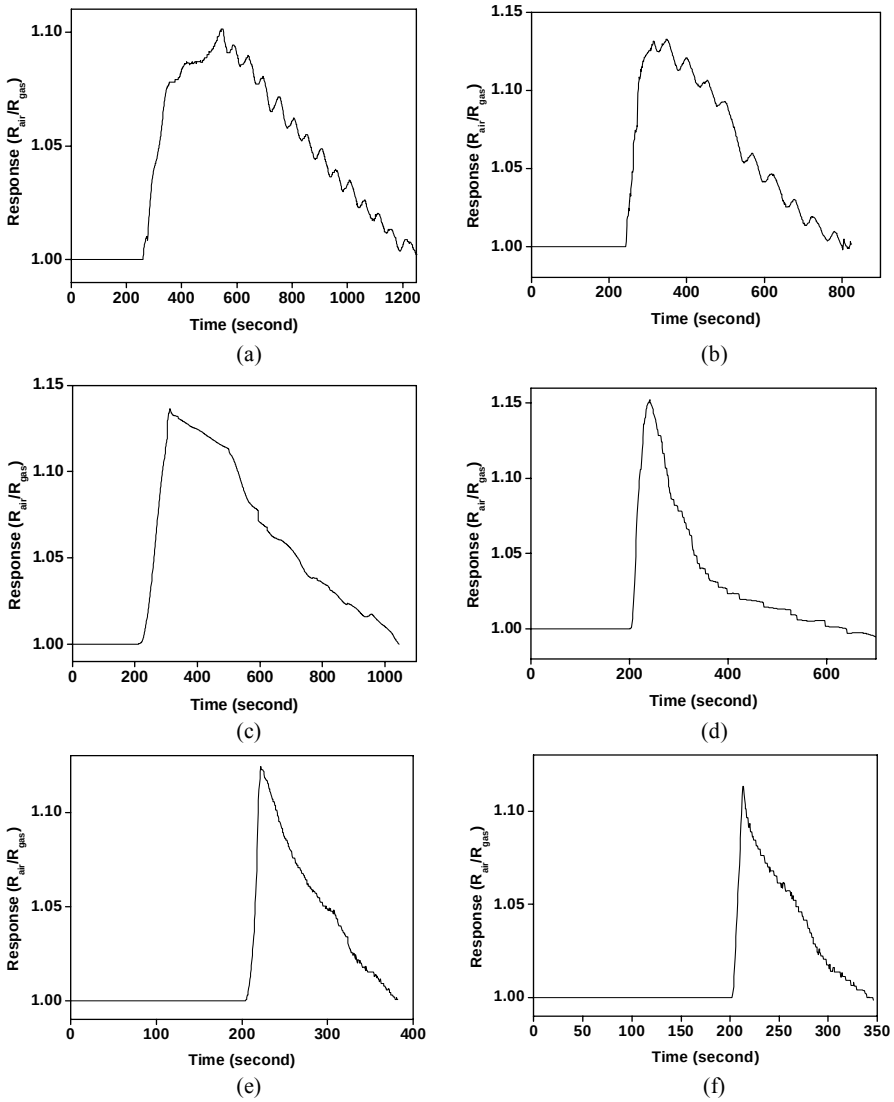

Fig. 3.36 Response of 3wt % copper doped WO_3 thick film sensor towards 17.85 ppm of H_2S gas at (a) 125 ^{0}C (b) 150^{0}C (c) 175 ^{0}C (d) 200^{0}C (e) 225^{0}C (f) 250 ^{0}C

Sensitivity of the sensor at different temperatures towards this concentration is shown in fig. 3.37 (a). It can be observed from the figure that the maximum response is achieved at a temperature of 200^0C with a response of 1.15. Response and recovery time were 26 seconds and 4.35 minutes respectively. Response and recovery times at different temperatures for 17.85 ppm concentration studied are shown in figures 3.37 (b) and (c).

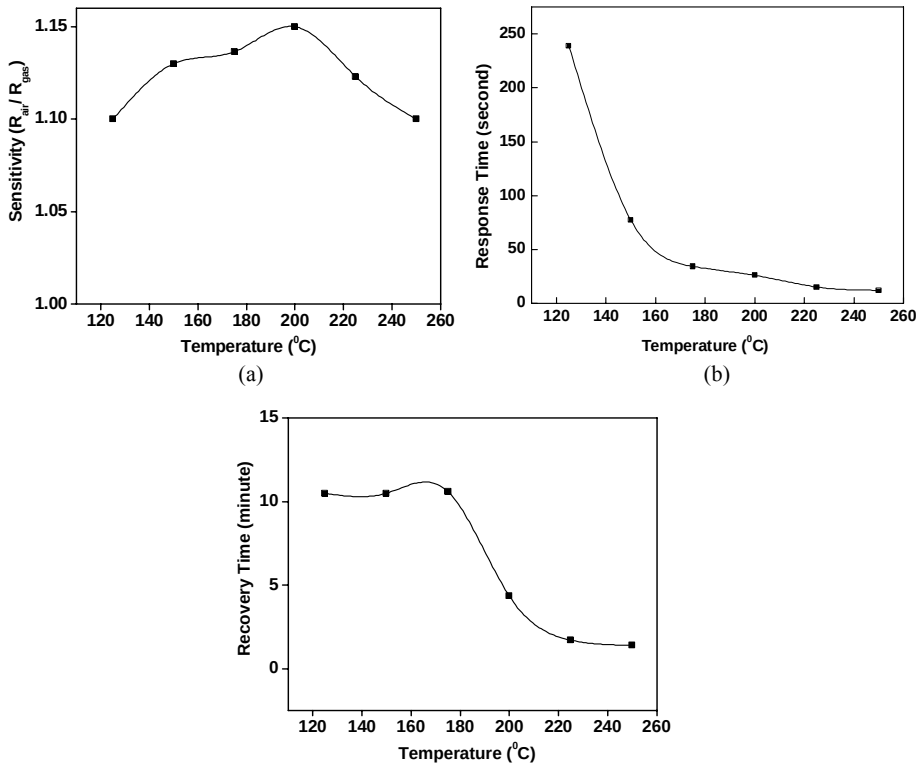

Fig. 3.37 (a) Sensitivity (b) Response time (c) Recovery time 3wt% copper doped WO_3 thick film sensor towards 17.85 ppm of H_2S gas at different temperatures

Concentration dependent studies at this optimum temperature of 200^0C are carried out as shown in fig. 3.38 (a) and (b). The lowest

concentration studied was found to be 7.14 ppm with a response of 1.10 and maximum measured concentration was 228.64 ppm with a response of 2.25. Fig. 3.39 shows sensitivity towards different concentrations at 200^0C.

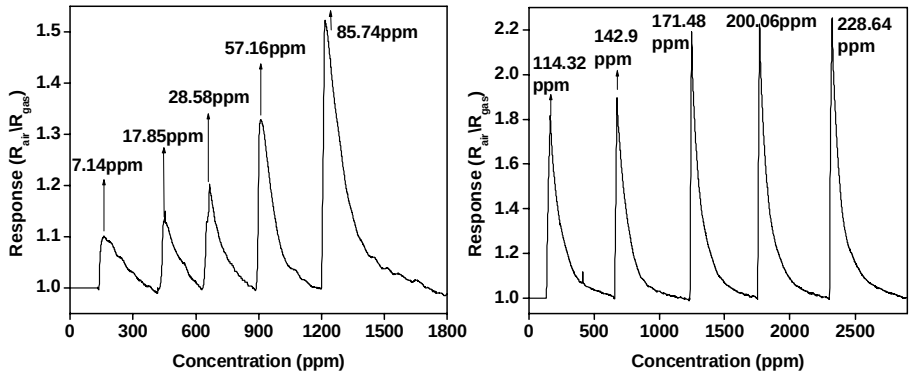

(a) (b)

Fig. 3.38 Response of 3wt% copper doped WO_3 thick film sensor towards different concentrations of H_2S at 200^0C

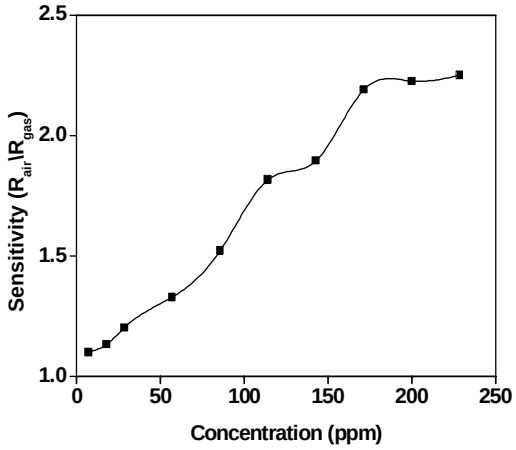

Fig. 3.39 Sensitivity of 3wt% copper doped WO_3 thick film sensor towards different concentrations of H_2S at optimal temperature of 200^0C

3.10 Discussion of the Results

The sensitivity of metal oxide gas sensors greatly depends on temperature. It is known that the reaction between metal oxide and adsorbed gas is dynamic and reversible process and both kinetics and equilibrium depend on the temperature. Oxygen is one of the most active components in air and the amount of oxygen in air is approximately 20.9% by volume. Metal oxides are often naturally self-passivated against oxygen as there is always oxygen adsorbed to the metal oxide surface when the surface is exposed to air. The oxygen molecule can bind to vacancy sites on the metal oxide surface, trap electrons from the surface of the metal oxide and remains tightly bound as a charged oxygen anion. The trapped electron is no longer available for conductivity in the solid, thus increasing the resistance of the oxide surface. These processes can be represented by the following reactions.

$$O_{2\,(gas)} \rightarrow O_{2\,(ads)} \tag{3.2}$$

$$O_{2\,(ads)} + e^- \rightarrow O_2{}^-{}_{(ads)} \tag{3.3}$$

$$O_{2\,(ads)} + e^- \rightarrow 2O^-{}_{(ads)} \tag{3.4}$$

$$O^-{}_{(ads)} + e^- \rightarrow O^{2-}{}_{(ads)} \tag{3.5}$$

In these surface reactions, (gas) and (ads) stands for free gas and species adsorbed on the surface respectively, e^- stands for electrons contributed by metal oxide. $O_2{}^-{}_{(ads)}$, $O^-{}_{(ads)}$ and

$O^{2-}{}_{(ads)}$ stand for the different chemisorbed surface oxygen species. At low temperatures (under 150°C), oxygen will trap electrons on the surface to

produce O_2^- surface species, while O^- and O^{2-} are the predominant oxygen species at higher temperatures (150 – 450°C) [130].

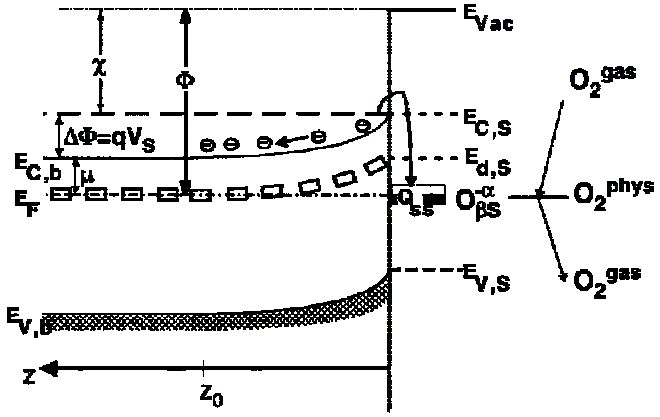

Fig. 3.40 Band bending on an n-type semiconductor (after ionosorption of oxygen on Qss levels).

The effect of oxygen ionosorption as O_2^- or O^- is a negative charge at the surface and an increase in the band bending ($q\Delta V_S>0$) and work function ($\Delta\Phi>0$) is shown in fig. 3.40. For semiconducting metal oxides the relative changes in work function ($\Delta\Phi$) accompanying adsorption processes contain qualitative and quantitative information [131], i.e., $\Delta\Phi = \Delta\mu + q\Delta V_S + \Delta\chi$ [where$\mu = (E_C - E_F)_b$ is the energy difference between the conduction band and the Fermi level in the bulk, $qV_S = E_{C,S} - E_{C,B}$ →band bending, χ→ electron affinity]. In principle, gas exposure and the resultant adsorption processes may change all three of them. Due to the assumption that the difference between Fermi level and conduction band in the bulk is unaffected by gas adsorption at the surface, changes in work function consist of changes in band bending and/or electron affinity ($\Delta\Phi = q\Delta V_S + \Delta\chi$). z_0 denotes the depth of the depletion region; q - elementary charge, $E_{V,b}$ and $E_{C,b}$,$E_{V,S}$ and $E_{C,S}$ are the valence and the conductance band edges in the bulk

and at the surface, respectively; E_F -the Fermi level; $E_{d,S}$ - the donor level at the surface; O_2^{gas},O_2^{phys}, and $O_{\beta S}^{\alpha-}$- an oxygen molecule in the ambient atmosphere, a physisorbed, and a chemisorbed oxygen species (O^-,O_2^-, or O_2^{2-}), respectively.

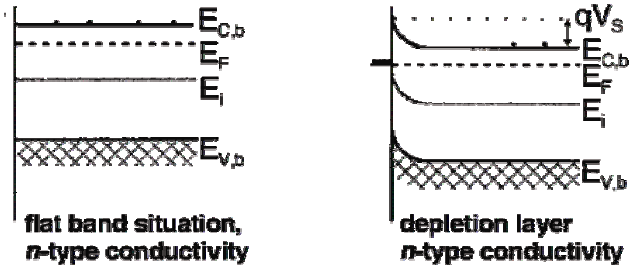

(a) (b)

Fig. 3.41 Flat band situation and depletion layer formation on an n-type semiconductor

Figure 3.41 (a) shows the flat band situation in the beginning (before oxygen adsorption) and 3.41 (b) shows adsorption of oxidizing species (oxygen and then nitrogen dioxide) at the surface leads to an increase in band bending and formation of a depletion layer. For an *n*-type semiconductor the creation of a depletion layer leads to decrease in surface conductance [132]. The electron depleted region also called the space charge layer, is an area of high resistance and the core region of the particle where electron densities are high, is an area of relatively low resistance. The thickness of the surface charge layer (L) as well as height of the surface potential barrier is determined by: (a) the surface charge, which depends on the amount of adsorbed oxygen; and (b) the Debye length, which is a characteristic of the semiconductor used with its donor concentration. Reducing gases react with ionosorbed oxygen at the surface freeing electrons that can return to the bands. Thus, the effect is a decrease in the band bending ($q\Delta V_S$<0 and $\Delta\Phi$<0) and , for an *n*-type semiconductor, an increase

of the surface conductance. The oxidizing gas in turn will remove electrons causing a further increase in band bending and for an *n*-type semiconductor, a decrease of the surface conductance. The best way to describe the conduction process is to consider that the free charge carriers must overcome the intergranular barriers of height qV_S formed by band bending at the adjoining surfaces of neighboring grains. Barrier heights and occupancies of surface states can be altered by the adsorption of molecules from the gas phase. Therefore, at constant temperature the variation of conductance *G* can be attributed to changes of surface conductance G_S [133].

The sensor element consists of semiconductor nanoparticle. The microstructure and morphology of these aggregates are considered to be very important for the transducer function. Each particle is connected with its neighbors either by grain-boundary contacts or by necks. In the case of grain-boundary contacts, electrons should move across the surface potential barrier at each boundary. The change of the barrier height makes the electric resistance of the element dependent on the gaseous atmosphere, as first pointed out by Ihokura [134]. The resistance, and hence the gas sensitivity, in this case are not basically dependent on the particle size. In the case of necks, electron transfer between particles takes place through a channel which is formed inside the space-charge layer at each neck. The width of the channel is determined by the neck size and thickness of the surface charge layer (L) and its change with gases gives rise to the gas-dependent resistance of the element, as first pointed out by Mitsudo [135]. Obviously the gas sensitivity in this case is dependent on the particle size. These two models, although rather conceptual, indicate the importance of the microstructure for the transducer function of the element. Tamaki et al. [65] studied the grain size effects in WO_3 for nitrogen oxide detection. The results indicate that for a crystallite size greater than 30nm the conduction is under grain boundary

control. The average crystallite size of pure and copper doped WO_3 is in the range of 30-33nm. Hence we deduce that in our sensors the conduction is through grain boundary contacts.

Initial gas sensing experiments were performed at room temperature to measure the response of pure and copper doped WO_3 films to test gases. However, as almost no response was observed for measurements at room temperature. Hence electrical conductance measurements were performed at various temperatures in order to determine the temperature at which the WO_3 sensors are most sensitive to analyzed gases. The temperature at which sensors are most sensitive to analyzed gases is defined as optimum working temperature of the sensor. In general, it is known that the sensitivity of the sensors is affected by the working temperature. The higher temperature enhances surface reaction of sensors and gives higher sensitivity in that temperature range. The interaction between metal oxide and adsorbed gas is a dynamic process. When the film is exposed to a test gas in air, the adsorption and desorption processes occur simultaneously. In the response process the adsorption dominates on desorption process until stationary conditions are attained. In this situation the number of adsorbed gas molecules will be equal to the number of the desorbed ones, and the electrical conductivity attains a constant value. After the test gas is cut off, the desorption prevails on the re-adsorption process and the conductivity will return to its original value.

3.10.1 NO_2 Detection Mechanism

Pure and copper doped WO_3 sensors responded to turning on and off NO_2 flow by the reversible changes of electrical resistance. When WO_3 based sensor material is exposed to atmosphere of NO_2, resistance of the sensor increases. The potential theory suggested that a potential barrier is

formed between the surface of semiconductor film and the ambient environment [136]. NO_2 gets adsorbed onto WO_3 surface, and the oxygen of NO_2 served as the accepter, extracting electrons from the conduction band of WO_3. Therefore, the barrier of WO_3 was increased and resistance of the WO_3 film was also increased whenever NO_2 was adsorbed on WO_3 surface. NO_2 can not only capture the electrons of the semiconductor due to its higher electrophilic property, but also react with the adsorbed oxygen ion leading to the formation of adsorbed NO_2^-, the process of the reaction can be described as follows [137].

$$NO_{2(g)} + e^- \rightarrow NO_2^-{}_{(ads)} \quad (3.6)$$

$$NO_{2(g)} + O_2^-{}_{(ads)} + 2e^- \rightarrow NO_2^-{}_{(ads)} + 2O^-{}_{(ads)} \quad (3.7)$$

The above reactions decreased the concentration of electron on the surface of material, thus resulting in an increase of the material resistance. In addition, the reaction occurs between $NO_2^-{}_{(ads)}$ and $O_2^-{}_{(ads)}$:

$$NO_2^-{}_{(ads)} + O_2^-{}_{(ads)} \rightarrow 2O^-{}_{(ads)} + NO_2 \quad (3.8)$$

Thus the cyclic reaction continues. These series of reactions resulted in the concentration of electron on the surface of the material to further decrease, which led to the decrease in conductivity of the material (increase of the resistance) and hence the detection of NO_2 is achieved.

The temperature dependent NO_2 gas sensing results (Sensitivity Vs Temperature graphs in fig. 3.9 (a), 3.17(a), 3.25(a), 3.33(a)) indicate that the sensitivity of pure and copper doped sensors increases with increasing temperature up to the optimum operating temperature. In all cases a further increase of the temperature reduces the response value. At lower temperature a low interaction happens between adsorbed oxygen species and detected

NO_2 gas. Thus the response of the WO_3 thick film sensor is low at lower temperature. At higher temperature some of the adsorbed oxygen species may be desorbed from the film which contributes to low response value. When the operating temperature is very high the charge carrier concentration is also very high in a semiconductor. The electrons received by adsorbed NO_2 gas is much less than the number of charge carriers in sensitive material, which hardly causes the conductivity change of the sensitive film. As a result, there is an optimal operating temperature to balance the above two effects in order to achieve maximum gas response. In pure WO_3 based sensors the optimal operating temperature was found to be 200^0C beyond which the sensitivity of the sensor decreases. All copper doped WO_3 sensors presented a lower optimum operating temperature of 175^0C above which the sensitivity decreased significantly. Lowering of optimum operating temperature due to metal doping is reported in literature [22, 138]. The temperature dependent recovery time data (fig. 3.9 (c), 3.17(c), 3.25(c), 3.33(c)) shows that at temperature of 100 and 125^0C the sensor had a very large recovery time or the sensor does not retain its base value. At low working temperature the adsorbed reaction products are not able to completely desorb from the surface of the sensor and this causes prolonged recovery time. At optimum temperature the response and recovery time was found to be relatively small.

Semiconductor sensors sensed gas using its non-stoichiometric structure and the free electrons originated from the oxygen vacancy. The sensing properties of pure WO_3 were controlled by the surface defect and structure rather than the native properties according to Bringans et al. [139]. There was more oxygen vacancies on the surface of pure WO_3 calcined at higher temperature [140]. The amount of chemisorbed oxygen on surface and surface species available for adsorption highly influences the change in

conductivity [141]. In pure WO_3 the chemisorptions sites are owing to the various oxidation states of tungsten arising because of the oxygen deficiency created at the annealing temperature. The XPS studies on pure WO_3 also reveal that there is a shift in oxidation state of tungsten from +6, the oxidation state of tungsten in stoichiometric WO_3. This shift may be caused by the contribution from W^{5+} or W^{4+} states, resulting in oxygen vacancies in thick film sensor. Accordingly, a possible interaction mechanism between nitrogen dioxide and WO_3 may be as follows.

$$NO_2 + W^{5+} \leftrightarrow W^{6+} + NO_2^- \qquad (3.9)$$

It has been reported earlier that when annealing temperature increases over 400^0C [62], reactive sites for the adsorption of NO_2 and oxygen molecules are created owing to the drifting of oxygen deficiencies to surface [137,142]. The presence of unsaturated bonds on the material surface may lead to the formation of chemical bonds between gaseous species and metal oxides. Hence the amount of chemisorbed species increases with surface defect concentration [143].

Additives are used for sensitizing and increasing the gas response to particular gases. Generally it is assumed that metal or metal-oxide additives reside on the surface of the semiconducting, gas sensing oxide in the form of dispersed clusters. The diffusion of these additives into grains is dependent on the preparation conditions. In our study with copper doping we were able to achieve an enhanced sensitivity for NO_2 gas. The sensitivity for undoped, 0.5wt%, 1.5wt%, and 3wt% was found to be 1.5, 3.23, 5.31 and 6 respectively for 7 ppm concentration at the optimum temperature. Fig. 3.42 show the sensitivity of the sensor due to different copper doping concentration for 7 ppm NO_2 gas at respective optimum temperature.

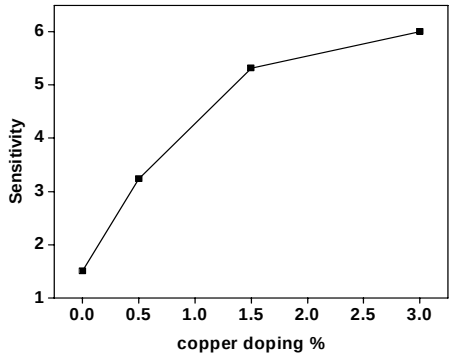

Fig. 3.42 Sensitivity at different copper doping % to 7 ppm NO_2 gas at respective optimum temperature

With increase in doping concentration the sensitivity also enhanced. It is interesting to find that among the copper doped concentrations studied, a maximum sensitivity 4 times, higher than undoped WO_3 was achieved for 3wt% doped copper. The incorporation of metal additives creates more adsorption sites that are believed to be crucial for the enhanced sensitivity obtained in the case of doped WO_3. The incorporation of copper may lead to the formation of Cu-O-W bonds that creates adsorption sites of copper and tungsten due to their change in oxidation states. Hence the target gas molecules have more adsoption sites to react with the sensor. The XPS data indicates that oxidation state of tungsten in copper doped material is +6 whereas in pure WO_3 sensor the oxidation state is estimated to be +5 or +4. This change in oxidation state may be due to presence of copper. Copper can exist in +1 oxidation state [144] or +2 [145,146] oxidation state. Earlier works has presented the coexistence of both the oxidation states in the doped metal oxide ie copper can exist as CuO or Cu_2O [147]. The local oxygen deficiency, when annealing, may trigger the occurrence of the following reaction:

$$2CuO \rightarrow Cu_2O + 1/2\ O_2\uparrow \qquad (3.10)$$

which reduces some Cu^{2+} to Cu^{+} and thus, Cu^{2+} and Cu^{+} coexist.

The detection mechanism is proposed as follows. Cu^{+} ions are located on the surface of the sensing element. When NO_2 gas molecules are brought in contact with the sensing element, NO_2 is adsorbed on active centers, Cu^{+}. Hence NO_2 gets reduced to NO_2^{-} radicals mean while Cu^{+} gets oxidized to Cu^{2+}. The highly active NO_2^{-} combines with preadsorbed O^{-} or O_2^{-}. The activation of NO_2 gas molecules to NO_2^{-} is an important step. It seems that more energy is needed for the NO_2 to grab adsorbed oxygen from the surface of WO_3 in the absence of copper oxide. Apparently, the copper ions play an important role in the interaction of NO_2 with sensing materials greatly influencing the sensitivity. The concentration dependent studies performed on the pure and doped tungsten oxide thick film sensors also proves the enhancement in sensitivity obtained due to copper doping.

3.10.2 H_2S Detection Mechanism

As discussed earlier the adsorbed oxygen from the atmosphere influence the carrier concentration in the conduction band of WO_3 layer by capturing electrons from the WO_3 film surface. The capturing of charge carriers from the surface of WO_3 by adsorbed oxygen is expected to reduce the concentration of charge carriers in the conduction band thereby reduces the conductivity of depletion layer in comparison to the WO_3 bulk conductivity. The interaction of the reducing sensing gas species with the chemisorbed oxygen results in a release of trapped electrons thereby increasing the electron carrier concentration in the sensor material. In the presence of reducing gas molecules the concentration of charge carriers in WO_3 starts increasing due to the removal of adsorbed oxygen from the sensor surface and by releasing the trapped electrons. The adsorbed oxygen species play a crucial role in H_2S sensing. At lower temperature reaction for H_2S sensing is given by [61]

$$2H_2S + 3O_2^{-}(ads) \leftrightarrow 2SO_2 + 2H_2O + 3e^{-} \qquad (3.11)$$

For higher temperature operation, the reaction taking place is given by

$$H_2S + O^-(ads) \leftrightarrow H_2O + S + e^- \quad (3.12)$$

According to eqs. (2), (3) and (4), oxygen adsorption reaction occurs prior to H_2S sensing, creating a thin electron-depleted layer at the surface of WO_3. As H_2S is adsorbed, electrons are released into conduction band according to Eq. (3.11) and (3.12). Hence resistance of WO_3 sensor decreases and hence conductivity increases on interaction with H_2S gas. Another reaction that can play a role in gas sensing is formation of additional surface oxygen vacancies, created due to interaction with test gas [148].

$$WO_3 + 7H_2S \rightarrow 3WS_2 + SO_2 + 7H_2O \quad (3.13)$$

The above reaction takes place on surface and involves a reduction of W^{6+} to W^{4+}. Oxygen leaves surface thereby releasing electrons into the grains so that conductivity of film is increased. Further, reoxidation of vacancies by O_2 results in a competition with formation of oxygen vacancies by H_2S.

From the temperature dependent sensitivity graphs for 17.85 ppm in fig. 3.13 (a), 3.21 (a), 3. 29 (a), 3.37 (a) the pure and copper doped sensors show low sensitivity at lower temperature. The recovery characteristics (fig. 3.13 (c), 3.21(c), 3. 29(c), 3.37(c) of these sensors were also very poor at lower temperatures. At optimum temperature the response and recovery time was found to be relatively small. Low sensitivity of sensor at lower operating temperature is due to slow reaction kinetics between H_2S and adsorbed oxygen ions. Long recovery time is due to incomplete desorption of adsorbed reaction products and H_2S after exposure to test gas. As the temperature is increased reactions described by equation (3.3), (3.4), (3.11) and (3.12) as well as desorption of products are faster,

which explains the increase of sensitivity and decrease in recovery time. At temperatures above 200^0C sensor exhibits reduced sensitivity. This is due to higher desorption rate than adsorption process that occur on surface of thick film sensor. The optimum operating temperature for both pure and copper doped sensor was found to be 200^0C.

Our XPS results ascertain that in pure WO_3 the oxidation sate of tungsten was +5. Hence W^{5+} states (oxygen vacancies) act as donors in the semiconducting state of pure WO_3 and the presence of these donors has significant impact on conductivity of the film. Earlier reports with the help of XPS studies established that presence of H_2S in the gas phase reduces oxidized donor centers in the oxide film which liberates electrons near the conduction band of the film. XPS was able to identify directly the nature of these donor centers as W^{5+} sites (oxygen vacancies) [149]. The addition of copper to WO_3 showed no enhancement in sensor response to H_2S. Fig. 3.43 shows the sensitivity of the sensor due to different copper doping concentrations for 17.85 ppm H_2S gas at respective optimum temperature.

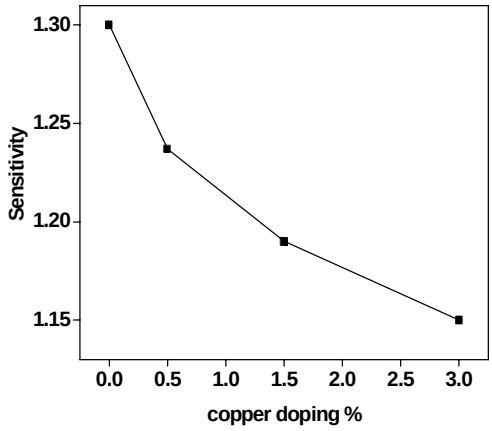

Fig. 3.43 Sensitivity at different copper doping % to 17.85 ppm H_2S gas at respective optimum temperature

Copper doped WO_3 H_2S gas sensing studies performed by I. J. Gallardo [129] also obtained similar reduced sensitivity. This is a different result, especially considering the high number of publications reporting that CuO-SnO_2 sensors exhibit a high sensor response to hydrogen sulphide [150-152]. Briefly, these papers claim that copper oxide is transformed into copper sulphide, which has a higher conductivity, and thus sensor responses increases dramatically. In our case, this effect was not found since sensor response of copper catalyzed WO_3 was slightly lower than that of pure WO_3. This suggests that either this sulphurisation is not happening or its electrical effect is not as effective as in the case of tin oxide. I. J. Gallardo [129] suggested that lower sensitivity due to copper doping could be the different disposition of copper, since in those papers CuO is really forming islands between SnO_2 grains and this may not be happening in our case.

3.11 Conclusion

Nanocrystalline pure and copper doped WO_3 powders were prepared. The copper doping was done in the range of 0.5wt%, 1.5wt% and 3wt%. Sensitive layers of pure and copper doped WO_3 were prepared by dispersing the prepared pure and copper doped WO_3 powder in methanol and drop casting on glass substrates followed by overnight annealing at 600^0C. Thus the pure and doped sensors for gas detection were fabricated. The main conclusions drawn from the above presented experimental data on pure and copper doped WO_3 sensors are discussed below.

Crystalline structure of pure and copper doped WO_3 sensor was mainly triclinic in nature. Average crystallite size is not considerably affected by the addition of copper. The crystallite size for pure WO_3, 0.5wt%, 1.5wt%, and 3wt% copper doped thick film sensor was found to be 30nm, 32nm, 30nm and 33nm respectively.

According with XRD data, additives form neither a separate crystalline phase, nor cause noticeable distortions to the WO_3 bulk crystalline phase. On the other hand, main Raman WO_3 vibration was affected by additive addition. The intensity was found to decrease with copper addition. This may indicate that additives do diffuse to the bulk.

The surface morphology and elemental composition were characterized by scanning electron microscopy and energy dispersive X-ray analysis. It was found that pure and doped WO_3 thick film sensor consisted of crystalline aggregates and surface is highly porous. The addition of copper did not alter the surface morphology of the sensor. The presence of copper was established from the EDS analysis.

The surface composition and elemental state of the elements existed in pure and copper doped WO_3 thick film sensor was studied by XPS measurements. In pure samples the tungsten existed in +5 or +4 oxidation state .There is a shift to +6 oxidation state for tungsten due to copper doping. No trace of copper was found in the XPS analysis. This may be due to nominal concentration of copper present in the doped sample. It may also due to that the impregnation method used is not efficient enough and most of the copper is lost in the evaporation of the precursors or the annealing process. Another possibility is that copper may have diffused inside the bulk of the material.

The temperature dependent gas sensing property of pure and copper doped WO_3 thick film sensor was investigated in order to find the optimal sensor operating temperature and sensor response to NO_2 test gas. Copper addition was found to enhance the NO_2 gas sensing capability of copper doped WO_3. This is attributed due to the additional adsorption site available

due to copper incorporation. A decrease in optimum operating temperature was obtained due to copper addition.

The table 3.8 below presents the sensitivity of the sensors obtained, along with their optimal operating temperature, response and recovery time for the studied concentration of 7 ppm.

Table 3.8 Summary of NO_2 gas sensing results of pure and copper doped WO_3 thick film sensor

Sensor	Sensitivity	Optimum temperature	Response time (sec)	Recovery time (min)
Pure WO_3	1.5	200^0C	14	2.90
WO_3 + 0.5wt% Copper	3.23	175^0C	33	3.56
WO_3 + 1 .5wt% Copper	5.31	175^0C	18	3.53
WO_3 + 3wt% Copper	6	175^0C	15	3.00

Similarly gas sensing behavior of pure and copper doped WO_3 thick film sensor to 17.85 ppm is tabulated in the table 3.9 below. Copper addition was found to slightly lower sensitivity of pure WO_3 sensor while operating temperature remained same.

Table3.9 Summary of H_2S gas sensing results of pure and copper doped WO_3 thick film sensor

Sensor	Sensitivity	Optimum temperature	Response time (sec)	Recovery time (min)
Pure WO_3	1.3	200^0C	22	4.10
WO_3 + 0.5wt % Copper	1.24	200^0C	33	4.18
WO_3 + 1 .5wt % Copper	1.19	200^0C	39	4.00
WO_3 + 3wt % Copper	1.15	200^0C	26	4.35

Concentration dependent studies for both test gases were done at optimum operating temperature.

References

[1] M. A. Butler J. Appl. Phys. (1977) 48, 1914.

[2] C. G. Ganqvist Solar Ener. Mater. Solar Cell (2000) 60, 201.

[3] M. Sun, N. Xu, Y. W. Yao and E. G. Wang J. Mater. Res. (2000) 15, 927.

[4] G. R. Bamwenda and H. Arakawa Appl. Catal. A (2001) 210, 181.

[5] P. A. Cox Transition Metal Oxides Clarendon Press, Oxford (1995).

[6] P. Woodward and A. Sleight J. Sol. State. Chem. (1997) 131, 9.

[7] P. Woodward, A. Sleight and T. Vogt J. Phys. Chem. Solids (1995) 56, 1035.

[8] S. Filho, V. Freire, J. Sasaki, J. M. Filho, J. Juliao and U. Gomes J. Raman Spect. (2000) 31, 451.

[9] E. Cazzanelli, C. Vinegoni, G. Mariotto, A. Kuzmin and J. Purans J. Sol. State. Chem. (1999) 143, 24.

[10] W. Kehl, R. Hay and D. Wahl J. Appl. Phys. (1952) 23, 212.

[11] E. Salije Acta crystallogr. B (1977) 33, 547.

[12] S. Tanisaki J. Phys. Soc. Jpn. (1960) 15, 573.

[13] B. O. Loopstra and H. Rietveld Acta crystallogr. B (1969) 25, 1420.

[14] R. Diehl, G. Brandt and E. Salije Acta crystallogr. B (1974) 34, 1105.

[15] E. Salije, Ferroelectrics (1976) 12, 215.

[16] E Saljie and K. Viswanathan Acta crystallogr. A (1975) 31, 356.

[17] E. Salije J. Appl. Crystallogr. (1974) 7, 615.

[18] J. Nowotny and L. Dufour Surface and near surfaces chemistry of oxides materials (1988) Elsevier Amsterdam.

[19] J. Shaver, Appl. Phys. Lett. (1967) 11, 255.

[20] T. Mearkawa, J. Tamaki, N. Miura and N. Yamazoe Chemistry Letters (1992) 4, 639.

[21] G. Sberveglieri, L. Depero, S. Groppelli, and P. Nelli Sensors and Actuators B (1995) 26, 89.

[22] M. Penza, C. Martucci, and G. Cassano Sensors and Actuators B (1998) 50, 52.

[23] E. Llobet, G. Molas, P. Molinas, J. Calderer, X.Vilanova, J. Brezmes, J. E. Sueiras and X. Correig Journal of the Electrochemical Society (2000) 147, 776.

[24] X. Wang, N. Miura and N. Yamazoe Sensors and Actuators B (2000) 66, 74.

[25] C. N. Xu, N. Miura, Y. Ishida, K. Matsuda and N. Yamazoe Sensors and Actuators B (2000) 65, 163.

[26] B. T. Marquis and J. F. Vetelino Sensors and Actuators B (2001) 77, 100.

[27] J. Wöllenstein, J. A. Plaza, C. Cané, Y. Min, H. Böttner and H. L. Tuller *Sensors and Actuators B* (2003) **93**, 350.

[28] P. Ivanov , J. Hubalek , K. Malysz , J. Prášek , X. Vilanova , E. Llobet and X. Correig Sensors and Actuators B (2004) 100, 221.

[29] A. Ponzoni, E. Comini, M. Ferroni, and G. Sberveglieri Thin Solid Films (2005) 490, 81.

[30] M. Stankova , X. Vilanova, E. Llobet, J. Calderer, C. Bittencourt, J. J. Pireaux and X. Correig Sensors and Actuators B (2005) 105, 271.

[31] V. Khatko, E. Llobet, X.Vilanova, J. Brezmes, J. Hubalek, K. Malysz and X. Correig Sensors and Actuators B (2005) 111, 45.

[32] M. Stankova, X.Vilanova, J. Calderer, E. Llobet, J. Brezmes, I. Gràcia, C. Cané, and X.Correig Sensors and Actuators B (2006) 113, 241.

[33] M. Ruiz, X. Illa , R. D´ıaz , A. R. Rodr´ıguez and J. R. Morante Sensors and Actuators B (2006) 118, 318.

[34] C. Bittencourt, A. Felten , H. B. Espinosa, R. Ionescu , E. Llobet , X. Correig and J. J Pireaux Sensors and Actuators B (2006) 115, 33.

[35] M. Sriyudthsak and S. Supothina Sensors and Actuators B (2006) 113, 265.

[36] V. Khatko , S. Vallejos , J. Calderer , E. Llobet , X. Vilanova, X. Correig Sensors and Actuators B (2007) 126, 400.

[37] L. Wang, J. Pfeifer, C. Balázsi and P. I. Gouma Materials and Manufacturing Processes, (2007) 22, 773.

[38] T. Siciliano, A. Tepore, G. Micocci, A. Serra, D. Manno and E. Filippo Sensors and Actuators B (2008) 133, 321.

[39] V. Srivastava and K. Jain Sensors and Actuators B (2008) 133, 46.

[40] M. Zhao and Y.Q. Zhu Sensors and Actuators B (2009) 137, 27.

[41] V. Khatko, S. Vallejos, J. Calderer, I. Gracia, C. Cané, E. Llobet and X. Correig Sensors and Actuators B (2009) 140, 356.

[42] T. D. Senguttuvan, V. Srivastava, J. S. Tawal, M. Mishra, S. Srivastava and K. Jain Sensors and Actuators B (2010) 150, 384.

[43] M. Epifani, T. Andreu, C. R. Maga˜na, R. Díaz, J. Arbiol, P. Siciliano and J. R. Morante. Sensors and Actuators B (2010) 148, 200.

[44] T. A. Nguyen, S.I Park, J. B. Kim, T. K. Kim, G. H. S.,J. Choo and Y. S. Kim, Sensors and Actuators B (2011) 160, 549.

[45] C. Zhang, A. Boudib, M.G. Olivier, R. Snyders and M. Debliquy, Sensors and Actuators B (2012) 175, 53.

[46] T. Tesfamichael, A. Ponzoni, M. Ahsan and G. Faglia Sensors and Actuators B (2012) 168, 345.

[47] E. P. S Barrett, G. C. Georgiades and P. A. Sermon Sensors and Actuators B (1990) 1, 116.

[48] D. J. Smith, J.F.Vatelino, R.S.Falconer, and E.LWittman Sensors and Actuators B (1993) 13, 264.

[49] R. Ruokamo, T. Karkkainen, J. Huusko, T. Ruokanen, M. Blomberg, H. Torvela, and V. Lantto Sensors and Actuators B, (1994) 18, 486.

[50] M. Lin, C. M. Hsu, H. Y. Yang, P. Y. Lee and C. C. Yang Sensors and Actuators B (1994) 22, 63

[51] J. L. Gore, K. Snow, J. D. Galipeau and J. F. Vetelino Sensors and Actuators B (1996) 35, 164.

[52] T. L. Royster, D. Chatterjee, G. R. P.Pujalt and C. A. Marrese Sensors and Actuators B (1998) 53,155.

[53] M. Penza, G. Cassano and F.Tortorella Sensors and Actuators B (2001) 81, 115.

[54] W. H.Tao and C. H. Tsai Sensors and Actuators B (2002) 81, 237.

[55] I. Jime´nez, J. Arbiol, G. Dezanneau, A. Cornet and J. R .Morante Sensors and Actuators B (2003) 93, 475.

[56] M. Stankova , X. Vilanova, J. Calderer, E. Llobet, P.Ivanov , I. Gràcia , C. Canéc and X. Correig Sensors and Actuators B (2004) 102, 219.

[57] R. Ionescu, A. Hoel, C. G. Granqvist, E. Llobet and P. Heszler Sensors and Actuators B (2005) 104, 132.

[58] R. Ionescu, A. Hoel, C.G. Granqvist, E. Llobet and P. Heszler Sensors and Actuators B (2005) 104, 124.

[59] A. Hoel , L.F. Reyes , S. Saukko, P. Heszler , V. Lantto and C. G. Granqvist Sensors and Actuators B (2005) 105,283.

[60] L. F. Reyes, A. Hoel, S. Saukko , P. Heszler, V. Lantto and C. G. Granqvist Sensors and Actuators B (2006) 117, 128.

[61] C. S. Rout, M. Hegde and C.N.R. Rao Sensors and Actuators B (2008) 128,488.

[62] W. Mickelson, A. Sussman and A. Zett Applied Physics Letters (2012) 100, 173110.

[63] X. Niu, T. Cui, X. Lu and J. Zhou Micro & Nano Letters (2012) 7, 41.

[64] M. Akiyama, J. Tamaki, N. Miura and N.Yamazoe Chemistry Letters (1991) 20, 1611.

[65] J. Tamaki, Z. Zhang, K. Fujimori, M. Akiyama, T. Harada, N. Miura and N.Yamazoe Journal of the electrochemical society, (1994) 141, 8.

[66] T. Inoue, K. Ohtsuka, Y. Yoshida, Y. Matsuura and Y. Kajiyama Sensors and Actuators B (1995) 24, 368.

[67] H.T Sun, C.Cantalini, L.Lozzi, M.Passacantando, S. Santucci, and M. Pelino Thin Solid Films (1996) 287, 258.

[68] L. E. Depero, M. Ferroni , V. Guidi, G. Marca , G. Martinelli , P. Nelli , L. Sangaletti and G. Sberveglieri Sensors and Actuators B (1996) 35, 381.

[69] C. Cantalini, M. Pelino, H.T. Sun, M. Faccio, S. Santucci, L. Lozzi and M. Passacantando Sensors and Actuators B (1996) 35, 112.

[70] X. Wang, G. Sakai, K. Shimanoe, N. Miura, and N. Yamazoe Sensors and Actuators B (1997) 45, 141.

[71] M. Penza , M.A. Tagliente, L. Mirenghi, C. Gerardi, C. Martucci, G. Cassano Sensors and Actuators B (1998) 50, 9.

[72] D. S. Lee, S.D Han, J. S. Huh, and D.D Lee Sensors and Actuators B (1999) 60, 57.

[73] K. Chung, M. H. Kim, W. S. Um, H. S. Lee, J. K. Song, S. C. Choi, K. M. Yi, M. J. Lee and K.W. Chung Sensors and Actuators B (1999) 60, 49.

[74] S. Kim, Y. B. Kim, K. S. Yoo, G. S. Sung and H. J. Jung Sensors and Actuators B (2000) 62,102.

[75] C. Cantalini, W. Wlodarski, Y. Li , M. Passacantando, S. Santucci, E. Comini, G. Faglia and G. Sberveglieri Sensors and Actuators B (2000) 64,182.

[76] D. S. Lee, S. D. Han, S. M. Lee, J. S. Huh and D. D. Lee Sensors and Actuators B (2000) 65, 331.

[77] D. S. Lee, J.W. Lim, S. M. Lee, J. S. Huh and D.D. Lee Sensors and Actuators B (2000) 64, 31.

[78] K. Galatis, Y. X. Li, W. Wlodarski, E. Comini, G. Sberveglieri, C. Cantalini, S. Santucci and M. Passacantando Sensors and Actuators B (2002) 15, 276.

[79] I. Jiménez, J. Arbiol, A. Cornet, and J. R. Morante, IEEE sensors journal (2002) 2, 329.

[80] H. Kawasakia, J. Namba, K. Iwatsuji, Y. Suda, K. Wada, K. Ebihara and T. Ohshima Applied Surface Science (2002) 197,547.

[81] J. Tamaki, A. Hayashi, Y. Yamamoto and M. Matsuoka Sensors and Actuators B (2003) 95, 111.

[82] S. H. Wang, T. C. Chou and C. C. Liu Sensors and Actuators B (2003) 94, 343.

[83] X. He, J. Li, X. Gao and L. Wang Sensors and Actuators B (2003) 93, 463.

[84] L.G. Teoh, Y.M. Hon, J. Shieh, W.H. Lai and M.H. Hon Sensors and Actuators B (2003) 96, 219.

[85] P. Ivanov , J. Hubalek , K. Malysz , J. Prášek , X. Vilanova , E. Llobet and X. Correig Sensors and Actuators B (2004) 100, 221.

[86] Y. G. Choi, G. Sakai, K. Shimanoe and N. Yamazoe Sensors and Actuators B (2004) 101,107.

[87] H. Kawasaki, T. Ueda, Y. Suda and T. Ohshima Sensors and Actuators B (2004) 100,266.

[88] S. Kim, S.C. Ha, K. Kim, H. Yang and S.Y. Choi Applied physics letters (2005) 86, 213105

[89] G. Xie, J. Yu, X. Chen and Y. Jiang Sensors and Actuators B (2007) 123, 909.

[90] E. Rossinyol, A.Prim, E. Pellicer, J. Rodr´ıguez, F. Peir´o, A. Cornet, J. R. Morante, B. Tian, T. Bob and D. Zhao Sensors and Actuators B (2007) 126,18

[91] H. Xia, Y. Wang, F. Kong, S.Wang, B. Zhu, X. Guo, J. Zhang, Y. Wang, and S.Wu Sensors and Actuators B, 2008 134, 133.

[92] Z. Liu, M. Miyauchi, T. Yamazaki and Y. Shen Sensors and Actuators B (2009) 140, 514.

[93] C. Zhang, M. Debliquy, A. Boudiba, H. Liao and C. Coddet Sensors and Actuators B, (2010) 144, 280.

[94] Y. Qin, M. Hu and J. Zhang Sensors and Actuators B (2010) 150, 339.

[95] L. You, Y. F Sun, J.Ma, Y.Guan, J. M. Sun, Y. Duand and G.Y.Lu, Sensors and Actuators B (2011) 157, 401.

[96] Y. Qin, X. Sun, X. Li and M. Hu Sensors and Actuators B (2012) 162, 244.

[97] V. Hieu, H. V. Vuong, N. V. Duy and N. D. Ho Sensors and Actuators B (2012) 171, 760.

[98] D. Meng, N. M. Shaalan, T. Yamazaki and T. Kikuta Sensors and Actuators B (2012) 169, 113.

[99] K. H. Lee , Y. K. Fang, W. J. Lee , J. J. Ho , K. H. Chen and K. C. Liao Sensors and Actuators B (2000) 69, 96.

[100] Y. Shen, T. Yamazaki, Z. Liu, D. Meng, T. Kikuta and N. Nakatani Thin Solid Films (2009) 517, 2069.

[101] R. Calavia, A. Mozalev, R. Vazquez, I. Gracia, C.Can, R. Ionescu and E. Llobet Sensors and Actuators B (2010) 149, 352.

[102] C. Zhang, A. Boudiba, C. Navio, C. Bittencourt, M.G.Olivier, R. Snyders, and M.Debliquy International Journal of Hydrogen Energy (2011) 36, 1107.

[103] A. Boudiba, C. Zhang, C. Navio, C. Bittencourt, R. Snyders and M. Debliquy Procedia Engineering (2010) 5, 180.

[104] G. Papadimitropoulos, M. Vasilopoulou and D. Davazoglou Procedia Engineering (2011) 25, 300.

[105] A. Boudiba, P. Rousse, C. Zhang, M. G. Olivier, R. Snyders and M. Debliquy Sensors and Actuators B (2012) (accepted for publication).

[106] C. Zhang, A. Boudiba, M. G. Olivier, R. Snyders and M. Debliquy Thin Solid Films (2012) 520, 3679.

[107] M. Ahsan, T. Tesfamichael, M.Ionescu, J. Bell and N.Motta Sensors and Actuators B (2011) 162, 14.

[108] I. Karkkanen, M. Kodu, T. Avarmaa, J. Kozlova, L. Matisen, H. Mandar, A. Saar, V. Sammelselg and R.Jaaniso Procedia Engineering, (2010) 5, 160.

[109] T. Tesfamichael, M. Arita, T. Bostrom, and J. Bell, Thin Solid Films (2010) 518. 4791.

[110] E. Comini, L. Pandolfi, S. Kaciulis, G. Faglia and G. Sberveglieri Sensors and Actuators B (2007) 127, 22.

[111] A. Hoel, L. F. Reyes, P. Heszler, V. Lantto and C. G. Granqvist Current Applied Physics (2004) 4, 547.

[112] S.Vallejos, V. Khatko, J. Calderer, I. Gracia, C. Cané, E. Llobet and X. Correig Sensors and Actuators B (2008) 132, 209.

[113] D. Meng, T. Yamazaki, Y. Shen, Z. Liu and T. Kikuta Applied Surface Science (2009) 256, 1050.

[114] R. Boulmani, M. Bendahan, C. L. Mauriat, M. Gillet and K. Aguir Sensors and Actuators B (2007) 125,622.

[115] M. H.Yaacob, M. Breedon, K. Kalantar-zadeh and W. Wlodarski Sensors and Actuators B (2009) 137, 115.

[116] S. Luo, G. Fu, H. Chen, Z. Liu and Q. Hong Solid-State Electronics (2007) 51, 913.

[117] V. Khatko, G. Gorokh, A. Mozalev, D. Solovei, E. Llobet, X. Vilanova and X. Correig Sensors and Actuators B (2006) 118, 255.

[118] A. Labidi, E. Gillet, R. Delamare, M. Maaref and K. Agui Sensors and Actuators B (2006) 120, 338.

[119] A. Labidi, C. Lambert-Mauriat, C. Jacolin, M. Bendahan, M. Maaref and K. Aguir Sensors and Actuators B (2006) 119, 374.

[120] M. Sriyudthsak and S.Supothina Sensors and Actuators B (2006) 113, 265.

[121] Y. Lyashkov, A. S. Tonkoshkur and V.O. Makarov Sensors and Actuators B (2010) 148, 1.

[122] M. Azad and M.Hammoud Sensors and Actuators B (2006) 119, 384.

[123] S. Supothina, P. Seeharaj, S.Yoriya and M. Sriyudthsak Ceramics International (2007) 33, 931.

[124] A. Baserga, V. Russo, F. Di Fonzo, A. Bailini, D. Cattaneo, C. S. Casari, A. Li Bassi and C. E. Bottani, Thin Solid Films (2007) 515, 6465.

[125] S. Zhu, X. Liu, Z. Chen, C. Liu, C. Feng, J. Gu, Q. Liu and D. Zhang Journal of Materials Chemistry (2010) 20, 9126.

[126] J. Koo, B. S. Bae and H. K. Na J. Non-Cryst. Solids (1997) 212, 173.

[127] S. C. Moulzolf, S. Ding and R. J. Lad (2001) Sensors and actuators B (2001) 77, 375.

[128] J. C. Dupin, D. Gonbeau, P. Vinatier and A. Levasseur Phys. Chem. (2000) 2, 1319.

[129] J. Gallardo Tungsten oxide nanocrystalline powders for gas sensing applications Doctoral Thesis University of Barcelona, 2003.

[130] K. D. Schierbaum, U. Weimar, W. Göpel, R. Kowalkowski Sensors and Actuators B (1991) 3, 205.

[131] H. Lüth Surfaces and Interfaces of Solids Springer, Berlin (1993).

[132] G. Heiland Sensors and Actuators (1982) 2, 343.

[133] N. Bârsan and U. Weimar J. Phys. Condens. Matter (2003) 15, R813.

[134] H. Ihokura SnO based inflammable gas sensors, Doctoral Thesis, Kyushu University, 1983, 52.

[135] H. Mitsudo Ceramics, (1980) 15, 339.

[136] J. Ding, T. J. Mc. Avoy, R. E. Cavicch and semancik Sensors and Actuators B (2001) 77, 597.

[137] M. Ivanovskaga, A. Gurlo and P. Bogdanov Sensors and Actuators B (2001) 77, 264.

[138] H.Y. Lai and C.H. Chen J. Mater. Chem. (2012) 22, 13204.

[139] R. D. Bringans, H. Hochst and H.R. Shanks Phys. Rev. B (1981) 24, 3481.

[140] H. T. Sun, C. Cantalini, L. Lozzi, M. Passacantando, S. Santucci and M. Pelino Thin Solid Films (1996) 287, 258.

[141] J. Mizsei Sensors and Actuators B (1995) 23, 173.

[142] S. R. Aliwell, J. F. Halsall, K. F. E. Pratt, J. O. Sullivan, R. L. Jones, R. A. Cox, S. R. Utembe, G. M. Hansford and D. E. Williams Meas. Sci. and Technol. (2001) 12, 684.

[143] E. Henrich and P. A. Cox The surface Science of Metal Oxides Cambridge University Press Cambridge (1994), 257.

[144] D. J. Liu and H. J. Robota Appl. Catal. (1994) B4, 155.

[145] R. Pirone, P. Ciambell, G. Moretti, and G. Russo Appl. Catal. (1996) B8,197

[146] M. F. Garcia, C. M. Alvarez, I. R. Ramos, A. G. Ruiz and G.L. Haller J. Phys. Chem. (1995) 99, 16380.

[147] G. Zhang and M. Liu Sensors and Actuators B (2000) 69, 144.

[148] B. Fruhberger, M. Grunze and D. J. Dwyer Sensors and actuators B (1996) 31, 167

[149] J. Dwyer Sensors and Actuators B (1991) 5, 155

[150] J. Tamaki, K. Shimanoe, Y. Yamada, Y. Yamamoto, N. Miura and N. Yamazoe Sensors and Actuators B (1998) 49, 121.

[151] S. Manorama, G. Devi and V. Rao Applied physics letters (1994) 64, 3163.

[152] R. S. Niranjan, K. R. Patil, S. R. Sainkar and I. S. Mulla Mat. Chem. Physics (2003) 80, 250.

Chapter 4

Gas Sensors Based on Pure and Indium Doped Zinc Oxide

Thin film gas sensors based on pure and indium doped ZnO were fabricated by spray pyrolysis on glass substrates. The doping concentration was varied in the range 0.5, 1 and 3vol%. The structural, chemical and compositional characterizations of the prepared pure and doped sensors were done. The temperature dependent gas sensing property of the fabricated gas sensors to NO_2 and H_2S were studied. The optimum operating temperature, response and recovery times were obtained. The concentration dependent studies were performed on pure and doped sensors for both test gases. The gas sensing detection mechanisms for both gases are also discussed.

4.1 Introduction

Zinc oxide (ZnO) has long been a research material of interest, with investigations going back to the 1930's. Its non-toxicity and the abundant availability in the earth's crust make it a good candidate as electrical transparent contact for thin-film amorphous and/or microcrystalline silicon solar cells. Today, ZnO is widely studied because of its many promising properties for the semiconductor industry such as electrical characteristics, processing properties, and inherent advantages for some applications. ZnO has a unique position among semiconducting oxides due to its piezoelectric and transparent conducting properties. It has a high electrical conductivity and optical transmittance in the visible region. These properties make it an ideal candidate for applications like transparent conducting electrodes in flat

panel displays and window layers in solar cells [1, 2, 3]. ZnO has a wide band gap (3.37 eV) [4] and a large exciton binding energy (60 meV) [10] and exhibits many potential applications in areas such as laser diodes, solar cells, gas sensors, optoelectronic devices. It is a widely used material in various applications such as UV resistive coatings, piezoelectric devices, short-wavelength nano-lasers, spin electronics, field-effect transistors, varistors and surface acoustic wave (SAW) devices [5, 6]. Recently, ZnO has also attracted attention for its possible application in short-wavelength light emitting diodes (LEDs) and laser diodes (LDs) because the optical properties of ZnO are similar to those of gallium nitride (GaN) [7-9].

Most of the group II–VI binary compound semiconductors crystallize in either cubic zinc blende (ZB) or hexagonal wurtzite (WZ) structure where each anion is surrounded by four cations at the corners of a tetrahedron and vice versa. This tetrahedral coordination is typical of sp^3 covalent bonding nature, but these materials also have a substantial ionic character that tends to increase the bandgap beyond the one expected from the covalent bonding [10]. The ionicity of ZnO resides at the borderline between the covalent and ionic semiconductors. ZnO has three crystal forms: the hexagonal wurtzite (B4), the cubic zinc blende (B3) and the cubic rock salt (B1) which is rarely observed. The wurtzite structure is most commonly used as it has the highest stability under normal working conditions [10] with a = 0.325 nm and c = 0.521 nm [2]. The wurtzite structure has an ABAB hexagonal close packing (HCP) structure. The structure of ZnO consists of alternating planes composed of O^{2-} and Zn^{2+} ions which are tetrahedrally co-ordinated and stacked along the c-axis on an alternate basis (Fig. 4.1). The Zn^{2+} and O^{2-} ions create a normal dipole moment and instant polarization which results in a diversification of surface energy.

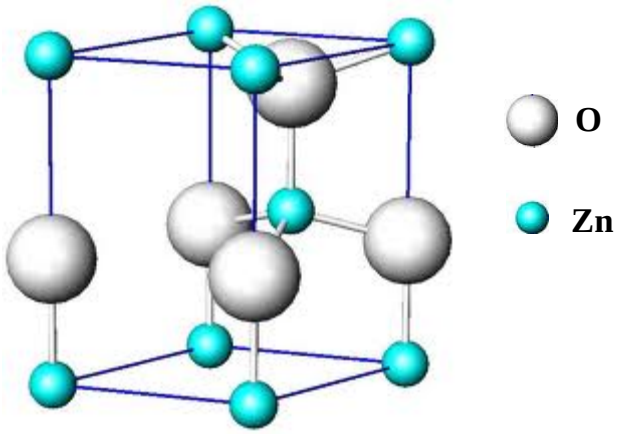

Fig. 4.1 Wurtzite structure of ZnO

The zinc blende structure is only stable when grown on cubic substrates. The rock salt structure is formed only at high pressure (~10 GPa) [10]. The wurtzite phase can be converted to the rock salt phase by applying high pressure (~10-15 GPa), which causes the bonds to change from covalent in nature to ionic in nature. The shifting from wurtzite to rock salt structure also causes a reduction in volume by about 17%. The transition is reversible at room temperature.

ZnO is naturally an n-type semiconductor due to oxygen vacancies and zinc interstitial defects. Oxygen vacancies have lower formation energy than zinc interstitials and are therefore more abundant in a Zn-rich environment. Conversely, in an oxygen rich environment, zinc defects are more abundant. The electron density in intrinsic, undoped ZnO has been measured to be about 10^{21} cm^{-3}[11].

ZnO is one of the popular materials for gas-sensing application next to the tin oxides. Their use as a gas sensor, in which the surface conductivity changes in response to adsorbed gases, made them an ideal candidate in the

early days of surface science. Point defects on ZnO surfaces are extremely important in gas sensing as they produce very large changes in the surface conductivity. The changes occur at the surface of the grains as a result of charge transfer and band bending caused by the adsorbates. The dominant defects identified in these films are oxygen vacancies. Heating the films to high temperatures generally creates these vacancies. These surface defects do not produce any new filled electronic states in the bandgap [12]. This is related to the range of stable oxidation states of Zn.

4.2 Literature Review of ZnO for Gas Sensing

ZnO as a promising gas sensing candidate have been studied by many researchers. The utilization of ZnO as a gas sensor has a long history because of its chemical sensitivity to different adsorbed gases, high chemical stability, amenability to doping, non-toxicity and low cost. In 1959, Heiland reported on the gas sensitive behavior of ZnO's electrical conductivity [13]. The conductivity of thin layers of ZnO, increased by orders of magnitude in vacuum and decreased in an atmosphere even at 500K. From then, the detection of H_2, oxygen and hydrocarbon by means of surface conductivity changes on ZnO crystals and thin films has been proposed and demonstrated [13]. ZnO for flammable gas sensing applications was demonstrated in 1962 by T. Seiyama et al. [14].

A short review of the gas sensing characteristics of ZnO towards different gases and the effect of doping on the gas sensing properties is discussed in the following section. Table 4.1 to 4.5 gives a short summary of ZnO gas sensors used for the detection of H_2, CO, NO_2, NH_3, and H_2S gases respectively.

Table 4.1: Summary of published results on H_2 gas sensing characteristics of ZnO

Material	Concentration (ppm)	Temperature (^{0}C)	*Sensitivity	Year (reference)	Method of preparation
H_2					
ZnO	100	400	100	1984	Thick film [15]
ZnO	5000	300	1000	1993	Ion beam sputtering [16]
ZnO	100	350	2	2003	Sputtering [17]
ZnO nanowire	200	250	9	2006	Thick paste [18]
ZnO nanopillar	500	350	20	2007	Thick film [19]
Zno nanobelt	10000	400	14	2007	Sputtering [20]
ZnO-µcarbon fiber	500	280	11	2010	Chemical electro deposition [21]
ZnO : Pd	500	Room temperature	4.2	2005	Sputtering [22]
ZnO: Li	10000	650	3.5	1989	Thick film paste [23]
ZnO: MoO_3	1000	450	350	1998	Screen printing [24]
ZnO : Sb	1000	350	150	1998	Screen printing [25]
ZnO: Mg	5000	300	50	2011	Pulsed laser deposition [26]
ZnO: Cd	100	Room temperature	30	2012	Electro chemical deposition [27]

* The sensitivity values presented in this table are taken directly from the respective literature. Their magnitude cannot be compared as different authors have used different formula to calculate sensitivity. The main intent of this table is to highlight the published results on ZnO based gas sensors.

Table 4.2: Summary of published results on CO gas sensing characteristics of ZnO

Material	Concentration (ppm)	Temperature (^{o}C)	*Sensitivity	Year (reference)	Method of preparation
CO					
ZnO	100	400	40	1984	Thick film [15]
ZnO	100	375	50	1984	Compressed disc [28]
ZnO	200	250	40	1997	Pellets [29]
ZnO	250	350	7.6	2003	Spin coating [30]
ZnO : CuO	1000	Room temperature	1.28	2011	Thick film paste [31]
ZnO: CuO : Pt	1000	Room temperature	2.64	2011	Thick film paste [31]
ZnO nanowire	200	250	2	2006	Thick paste [18]
ZnO flower	500	300	20	2011	Drop casting [32]
ZnO nanorods	40	400	20	2011	Thick film paste [33]
ZnO: Al	1000	400	60	2002	Sputtering [34]
ZnO: Sb	1000	350	50	1998	Screen printing [25]
ZnO : Au	20	250	7.5	2010	Rf sputtering [35]
ZnO: Au	1000	150	12	2012	Thick film paste [36]
ZnO	1000	150	6	2012	Thick film paste [13]

Table 4.3: Summary of published results on NO_2 gas sensing characteristics of ZnO

Material	Concentration (ppm)	Temperature (^{0}C)	*Sensitivity	Year (reference)	Method of preparation
NO_2					
ZnO	100	300	18	2012	Thick film paste [37]
ZnO: Ga	44.8	400	130	1993	Magnetron sputtering [38]
ZnO nanofiber	0.1	100	3	2004	Evaporation/ condensation [39]
ZnO	5	300	6	2003	Sputtering [40]
ZnO nanorods	1	300	1.8	2006	Thick film paste [41]
Zno nanobelt	8.5	250	4	2007	Sputtering [20]
ZnO nanorods	0.01	250	37	2009	R.F sputtering [42]
ZnO tetrapods	20	300	20	2010	Screen printing [43]
ZnO nanotube	0.463	190	120	2011	Thick film paste [44]
ZnO nanorods	40	400	206	2011	Thick film paste [33]
ZnO : Al	20	300	740	2007	Pellets [45]
ZnO:Sn	1.5	150	6	2005	Successive ionic layer adsorption and reaction [46]
ZnO: Er	5	250	10	2000	Sputtering [47]
ZnO	50	300	10	2012	Thick film paste [48]
ZnO : Au	50	300	4	2012	Thick film paste [48]
ZnO: Nb	4	300	1640	2011	Spin coating [49]

Table 4.4: Summary of published results on NH_3 gas sensing characteristics of ZnO

Material	Concentration (ppm)	Temperature (^{0}C)	*Sensitivity	Year (reference)	Method of preparation
NH_3					
ZnO nanowire	200	250	10	2006	Thick paste [18]
ZnO :Al	2	350	5	1986	R.F magnetron sputtering [50]
ZnO : Pd	30	Room temperature	60	1999	Thick film paste [51]
ZnO : Pd	50	210	45.7	2011	Thick film paste [52]
ZnO: Cr_2O_3	300	Room temperature	13.7	2007	Screen printing [53]

Table 4.5: Summary of published results on H_2S gas sensing characteristics of ZnO

Material	Concentration (ppm)	Temperature (^{0}C)	*Sensitivity	Year (reference)	Method of preparation
H_2S					
ZnO : Pd	15	150	57	1999	Dip coating [54]
ZnO nanostructure	500	Room temperature	26.4	2008	Vapour condensation [55]
ZnO : In	1000	250	13000	2009	Spray pyrolysis [56]
ZnO tetrapods	1	300	25	2010	Screen printing [43]
ZnO nanowire	30	350	4	2011	Spin coating [57]
ZnO nanoparticle	10	350	1.52	2011	Spin coating [57]
ZnO: Al	1000	200	3000	2011	Spray pyrolysis [56]

Thin films of ZnO were deposited on various substrates by spray-chemical vapour deposition method and found to be very sensitive for H_2 sensing at room temperature by Basu and Dutta [58]. The results showed that the films were able to detect H_2 efficiently and reproducibly between 2000 and 20000 ppm in air at room temperature.

In addition to the above discussed gases pure and doped ZnO based gas sensors were studied for the detection of various gases like liquid petroleum gas (LPG) [59-65], methanol[66, 67], propanol [68], butane[69], methane [70], acetaldehyde [37], formaldehyde [71, 72], ethanol [73-83].

The chlorine (Cl_2) gas sensing properties of pure ZnO and calcium oxide (CaO) added ZnO ceramics were studied in the temperature range 25–380°C from 0.9 ppm to 20 ppm using air or N_2 as a carrier gas by Inoue and Miyayama [84]. 3 mol% CaO added ZnO showed Cl_2 sensitivity of 10 for 0.9 ppm Cl_2 in air at 300°C, suggesting its usefulness for sensing of a low-concentration Cl_2 gas below 1 ppm. Thick films of pure and copper oxide (CuO) modified ZnO were prepared by Patil and Patil [85] and studied for their response to Cl_2 gas. Pure ZnO was almost insensitive to Cl_2 gas at room temperature. The CuO-modified ZnO sensor with 0.51 mass% of CuO in ZnO has good selectivity for 300 ppm Cl_2 against LPG, NH_3, CO_2, H_2 and C_2H_5OH gases at room temperature.

The acetylene (C_2H_2) sensing characteristics of unloaded ZnO and Pt-loaded ZnO nanoparticles have been studied by Tamaekong et al. [86]. The 2 at.% Pt loaded ZnO sensing film showed an optimum acetylene response of ~ 836 at 1% acetylene concentration and 300^0C operating temperature. A low detection limit of 50 ppm was obtained at 300^0C operating temperature.

In addition, Pt loaded ZnO sensing films exhibited good selectivity towards H_2, methane and carbon monoxide.

Pure and Co-doped (0.3wt%, 0.5wt% and 1wt %) ZnO nanofibers were synthesized by an electrospinning method and studied for acetone sensing by Liu et al. [87]. Co-doped ZnO nanofibers was able to successfully distinguish acetone and ethanol/methanol, even in a complicated ambience. The response of 0.5 wt% Co-doped ZnO nanofibers to 100 ppm acetone is about 16, which is 3.5 times larger than that of pure nanofibers (about 4.4). The response and recovery times of 0.5 wt% Co-doped ZnO nanofibers to 100 ppm acetone are about 6 and 4 s, respectively. ZnO flower functionalized with various percent of Au nanoparticles has been successfully synthesized and used as a sensitive device for detecting acetone by Wang et al. [88]. The 10 wt% Au had a high response of 74.41 for 100 ppm acetone at 270^0C

Nanto et al. [89, 90] reported that an Al doped ZnO gas sensor could be applied to the fish processing industry. Doping a sputtered ZnO thin film with Al was effective in improving the sensitivity and selectivity of the sensor for exposure to odor from seafood as well as TMA and DMA gases. TMA and DMA gases are known to be created during the deterioration of fish. Thus, Al doped ZnO sensors were suggested to monitor the freshness of seafood in an inexpensive and a rapid non-destructive manner. Tang et al. studied gas sensors based on Fe_2O_3 – ZnO nanocomposites prepared with different compositions (Fe:Zn = 1, 2, 3 and 4%) by a sol–gel and spin-coating method [91]. The results of electrical and sensing measurement indicated that the sensor with Fe:Zn = 2% exhibited fairly excellent sensitivity and selectivity to NH_3 at room temperature. The response and recovery time of the sensor were both less than 20 s. Manganese (Mn) doped

ZnO thin films with various Mn^{2+} concentration prepared via spray pyrolysis technique were studied for TMA and ethanol sensing by Sivalingam et al. [92]. The vapour sensing behaviour of the films was observed for various concentrations of TMA and ethanol at an optimized operating temperature of 373 K. The sensor response for TMA was found to be more appreciable incomparison with the response towards ethanol. The response of TMA at 75 ppm was calculated to be 300, with a response and recovery time of 11s and 20s respectively. ZnO architectures composed of nanorods and nanosheet assembled microspheres were synthesized by Zhang et al. [93].The gas sensing property of the ZnO architectures displayed high response, fast response, recovery, good selectivity and long-term stability to 1–1000 ppm DMA at 370^0C. Especially, even 1 ppm DMA could be well detected with a high response value of 16.8. More interestingly, DMA could be easily distinguished from a TMA, methylamine or NH_3 atmosphere with high selectivity.

4.3 Motivation of the Work

From the preceding literature it is clear that thin films of ZnO have been fabricated in many forms and its sensing properties to different gases were studied by many researchers. Connection between sensitive film, microstructure, crystalline structure and sensor response has been established. Besides, some metals have been identified as suitable dopants to increase sensor response. Among the various thin film fabrication techniques spray pyrolysis is a simple and inexpensive technique having ease to incorporate various materials, reproducibility, high growth rate and mass production capability of uniform coatings. This chapter deals with the preparation, structural characterization and gas sensing studies of ZnO films prepared via spray pyrolysis. The effect of dopant on the gas sensing

performance of ZnO is studied by incorporating group III element indium (In). Generally, to obtain low resistive films, group III elements such as In, Al, Ga are mostly used as dopants which substitute Zn atom thereby release free electrons and increase the carrier concentration [94, 95]. The optimum operating temperature, response and recovery time and concentration related studies of pure and indium doped ZnO thin film sensor is described in this chapter.

4.4 Gas Sensor Fabrication.

ZnO thin film gas sensors were prepared on soda lime glass substrate using chemical spray pyrolysis (CSP) technique, which is an effective method for the large area deposition of thin films of metallic oxides. Physical characteristics of the samples can be controlled through appropriate variation of deposition parameters. Zinc acetate solution (0.3 M) was prepared in a mixture of propanol and water, taken in the volume ratio 1:1. This precursor was selected due to its high vapour pressure at low temperature. Addition of few drops of acetic acid prohibits the precipitation of zinc hydroxide, thereby making the spray solution clear and producing films of better optical transmittance. Quantity of acetic acid added to the solution is also a key parameter in the film deposition process. Compressed air was used as the carrier gas (pressure ~ 0.34bar) and temperature of substrate was kept at 450 ± 5^0C. Now keeping the molarity of Zinc Acetate ($Zn(CH_3CO_2)\cdot 2H_2O$) at 0.3M and spray rate at 7 ml/min, deposition was done using automated spray machine in which the spray rate, deposition time and movement of the spray head were controlled by a microprocessor. After the deposition, samples were quickly removed from the substrate heater using mechanical holder and placed on a flat surface kept at room temperature [96]. Sprayed ZnO thin film samples were of thickness 550

nm. Indium doped ZnO sensors were prepared by adding the required quantity of indium nitrate in the spray solution itself. This is the advantage of CSP technique that doping can be easily performed by adding the required quantity of soluble salt of the dopant in the spray solution. Doping percentage of indium was varied from 0.5, 1, 3 volume %. The as prepared pure and indium doped ZnO thin film sensors were annealed at an approximate temperature of 600^0C overnight before conducting the gas sensing measurements.

4.5 Structural and Spectroscopic Characterization

4.5.1 XRD Characterization

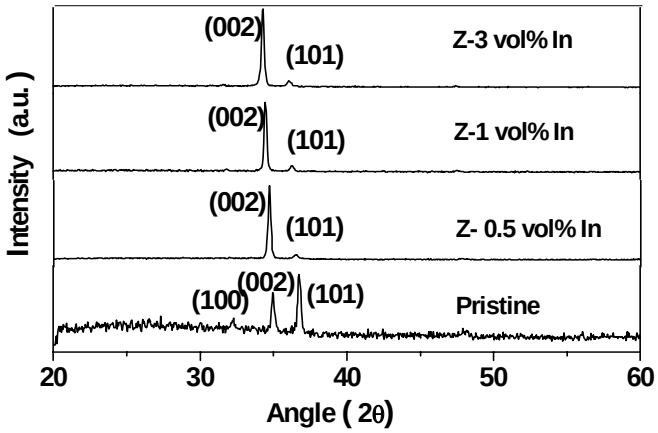

Fig. 4.2 XRD pattern of 600^0C annealed pure and indium doped ZnO thin film sensor

XRD pattern of 600^0C annealed pure and indium doped ZnO thin film sensor is shown in fig. 4.2. The 0.5, 1 and 3vol% indium doped sensors were denoted as Z - 0.5 vol% In, Z - 1vol% In and Z - 3vol% In respectively. The crystalline nature of films with hexagonal wruzite structure is revealed [JCPDS card of ZnO (36-1451)]. In the pure ZnO film main reflections were obtained in the (30^0- 40^0) 2θ range corresponding to (100), (002) and (101)

planes, the (101) plane being prominent. With the indium doping the intensity of (002) plane increased and (101) plane decreased indicating (002) as the preferred orientation. Strong orientation of the doped films along (002) plane indicates the growth of grains along the c-axis. It was also clear that the peak position corresponding to the plane (002) was shifted to lower value of 2θ, when indium was incorporated. The crystallite size (D) was calculated from peak broadening using the Scherrer approximation, which is defined as

$$D = \frac{0.9\lambda}{B\cos\theta} \tag{4.1}$$

Where λ is the wavelength of the X-ray (1.5418 A^0), B is the full width at half maximum (FWHM, radian) and θ is the Bragg angle (degree). The average crystallite size of the pure ZnO, 0.5, 1and 3vol % indium doped thin films were 38.32nm, 37.31nm, 39.14nm, 35.34nm. Particle size was estimated individually from the FWHM of each plane and the average of all the planes was taken to obtain the average particle size. Due to the low concentration of indium doping no characteristics peaks related to indium were observed in the XRD pattern.

4.5.2 Scanning Electron Microscopy

Fig. 4.3 shows the SEM images of pure and indium doped ZnO films. From the microstructural analysis, we can conclude that the dopant modifies the film growth process and by consequence the microstructure and surface morphology. The undoped ZnO film shows particle with no definite shape. The indium doped film shows a much uniform particles with round shape and the surface appears to be more porous. The particle size was found to be not much varying with the indium concentration.

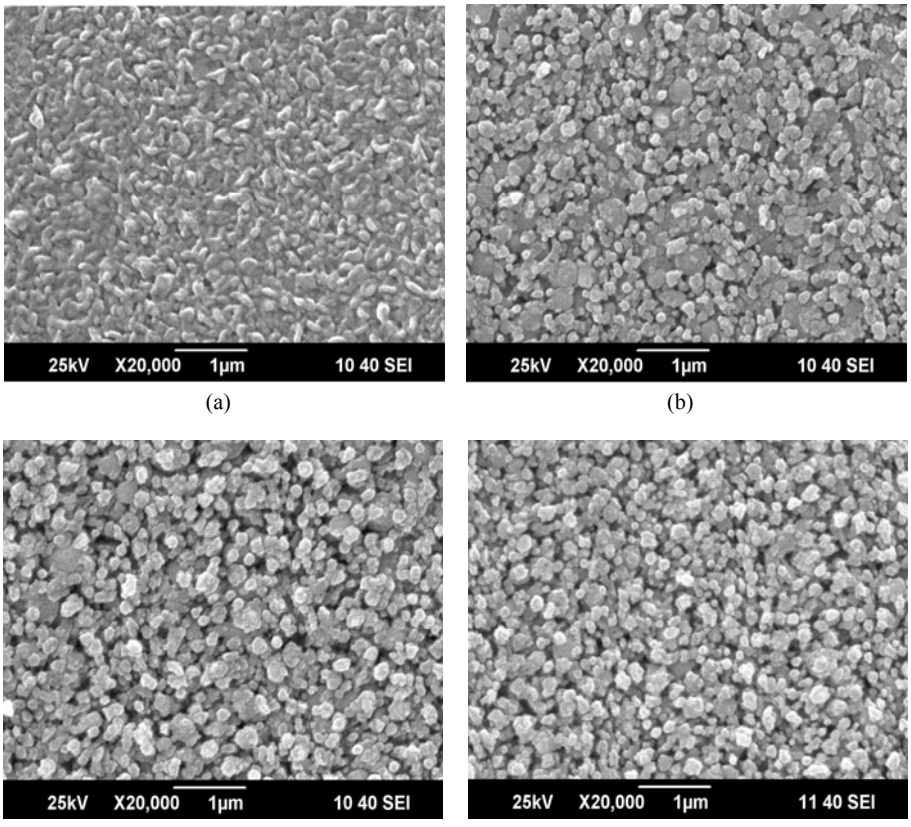

Fig. 4.3 SEM images of 600^0C annealed (a) ZnO pure (b) ZnO - 0.5vol% In (c) ZnO – 1vol% In (d) ZnO – 3vol% In

4.5.3 EDS

The composition of ZnO and indium doped thin film calcined at 600^0C was analysed by energy dispersive X-ray (EDS) measurement as shown in fig.4.4 and fig. 4.5 respectively. EDS analysis of 600^0C annealed pure ZnO film shows that zinc and oxygen are the only detected elements. In indium doped thin films the presence of indium was confirmed by the EDS analysis of 3vol% indium doped ZnO film.

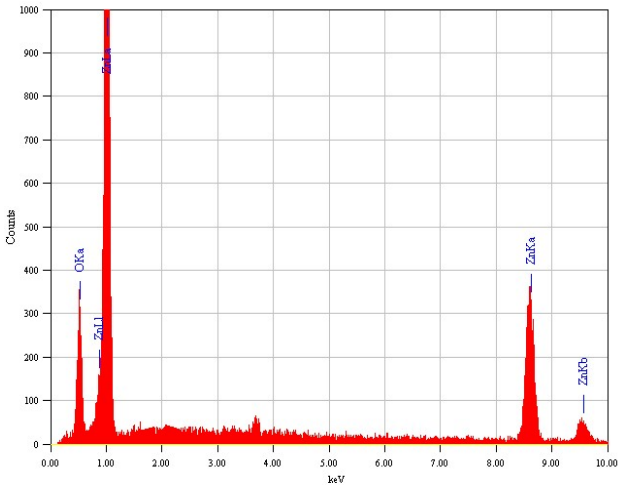

Fig. 4.4 EDS spectrum of 600^{0}C annealed pure ZnO.

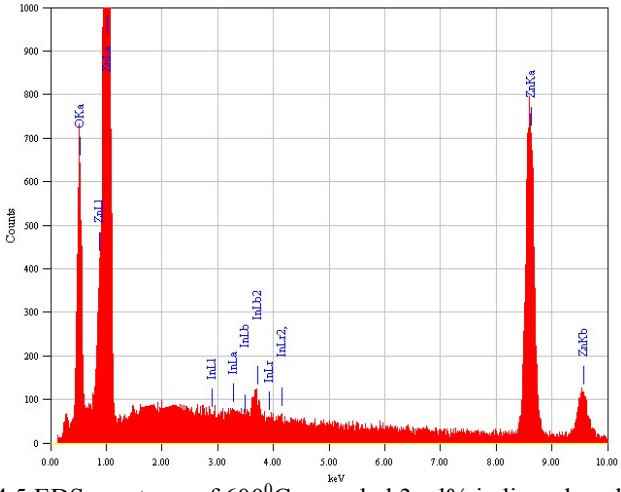

Fig. 4.5 EDS spectrum of 600^{0}C annealed 3vol% indium doped ZnO.

4.5.4 Raman Spectroscopy

Fig. 4.6 show the 600^{0}C overnight annealed Raman spectra of pure and indium doped ZnO thin film sensor. The 0.5, 1 and 3vol% indium doped sensors were denoted as Z - 0.5 vol% In, Z - 1vol% In and Z - 3vol% In

respectively. Raman spectroscopy gives information on vibrational properties of ZnO [97]. It is known for wurtzite-type ZnO (space group $p6_3mc$) that optical phonons at the Γ point of the Brillouin zone belong to the following irreducible representation: $\Gamma = A_1 + E_1 + 2E_2 + 2B_1$, where A_1 and E_1 modes are both Raman and infrared active, E_2 modes are Raman active only and B_1 modes are both Raman and infrared inactive (silent modes) [10, 11, 98, 99].

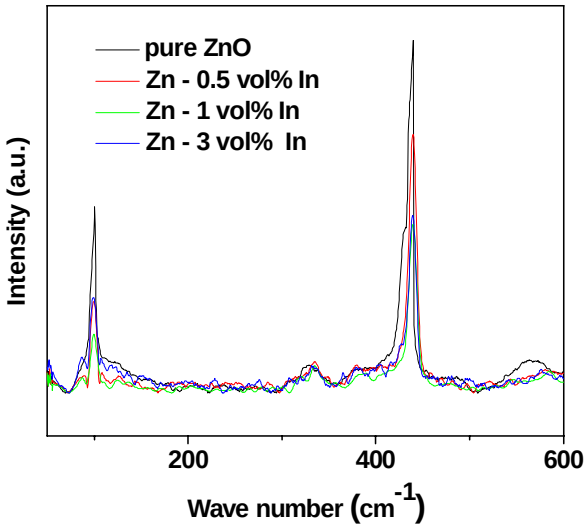

Fig. 4.6 Raman spectra of 600^0C overnight annealed pure and indium doped ZnO thin film sensor

Nonpolar E_2 phonon modes have two frequencies. The low frequency E_2 mode (E_2^{low}) and high-frequency E_2 mode (E_2^{high}). The E_2 modes at low and high frequency are at 101cm^{-1} and 437cm^{-1} respectively. The low frequency E_2 mode (E_2^{low}) is associated with vibration of the Zn sublattice, while the high-frequency E_2 mode (E_2^{high}) is related to the vibration of oxygen atoms [100, 101]. E_2^{high} of ZnO is the strongest mode in the wurtzite crystal structure. The strong E_2 (high) mode indicates a good crystallinity [102].

Peak at 556 cm^{-1} is a contribution of the E_1 (LO) mode of ZnO in the case of oxygen deficiency [103,104]. Such a strong intensity of 556 cm^{-1} E_1 mode demonstrates that ZnO thin film sensor is oxygen deficient. An additional peak is obtained at 330cm^{-1}. Peak at the same position was reported earlier in literature by various researchers [105- 107]. This peak is assigned to possible multiple-phonon-scattering. The intensity of the two prominent peaks at 101 cm^{-1} and 437cm^{-1} decreases with indium doping. No new peaks were determined due to indium doping.

4.6 Gas Sensors Based on Pure ZnO

4.6.1 Nitrogen Dioxide Detection

Response of pure ZnO thin film sensor towards a relatively low concentration of 7 ppm was studied in the temperature range of 100^0C to 225^0C. The sensor response was measured as the ratio of resistance R_{gas}/R_{air}, R_{gas} being the resistance of the sensor in presence of gas and R_{air} is the resistance of the sensor before the introduction of gas. Fig. 4.7 (a) to (f) shows the response of the sensor at different temperatures towards this concentration. The response time is taken as the time taken by the sensor to reach 90% of maximum value and recovery time is taken as the time taken by the sensor to reach 10% of base value (value before the introduction of gas) in all the NO_2 measurements.

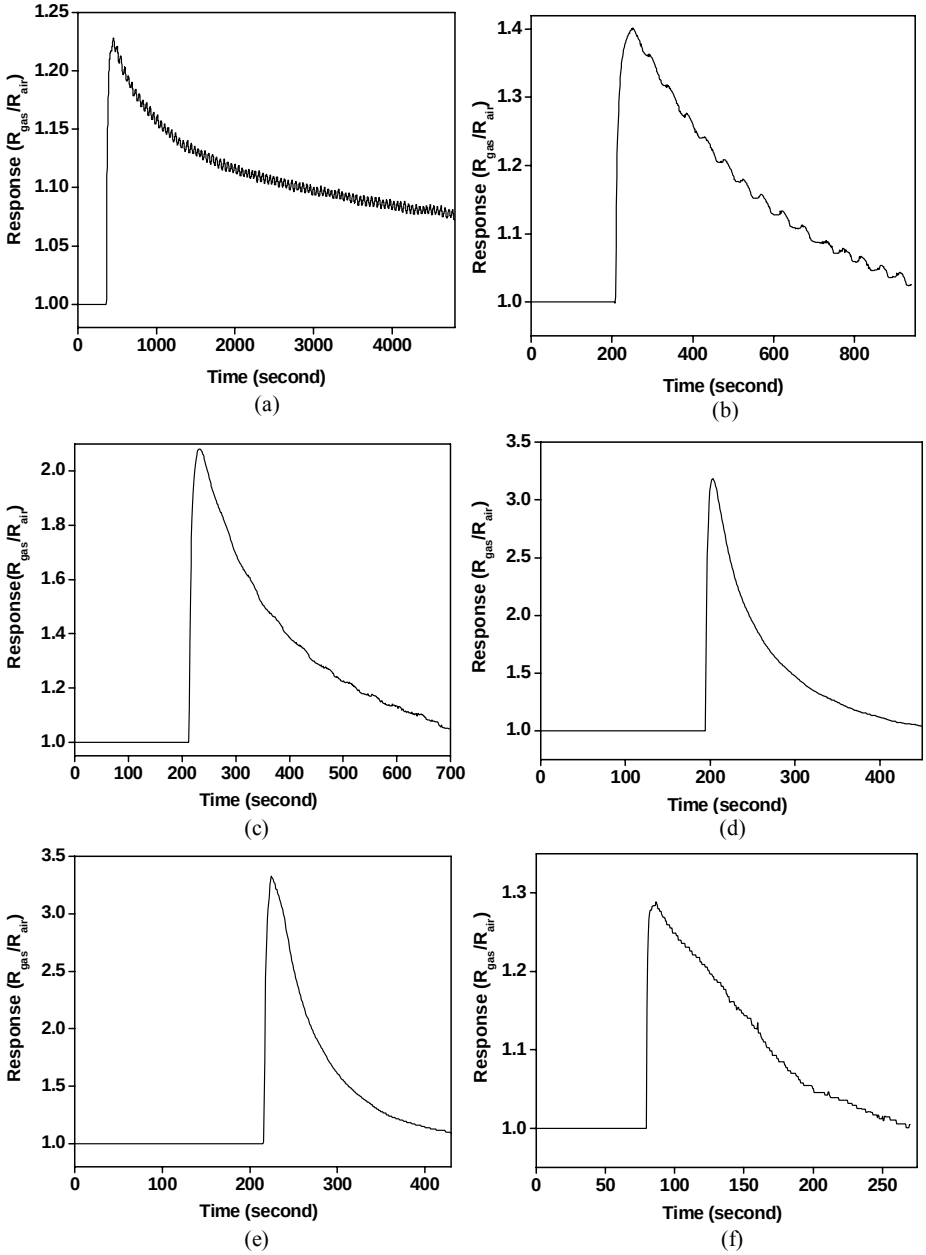

Fig. 4.7 Response of pure ZnO sensor towards 7 ppm of NO_2 gas at (a) 100 ^{0}C (b) 125^{0}C (c) 150 ^{0}C (d) 175^{0}C (e) 200^{0}C (f) 225 ^{0}C

Due to large recovery time at 100^0C the measurement was discontinued. Temperature dependent sensitivity of the sensor to 7 ppm concentration is shown in fig. 4.8 (a). Here the sensitivity value is taken as the maximum response value corresponding to respective temperature in fig. 4.7 (a) to (f). It is observed that sensitivity of the sensor increases as temperature increases and attains a maximum at 200^0C, beyond which the sensitivity decreases. The response and recovery characteristic curve of the ZnO film at different temperatures is shown in fig. 4.8 (b) and (c).

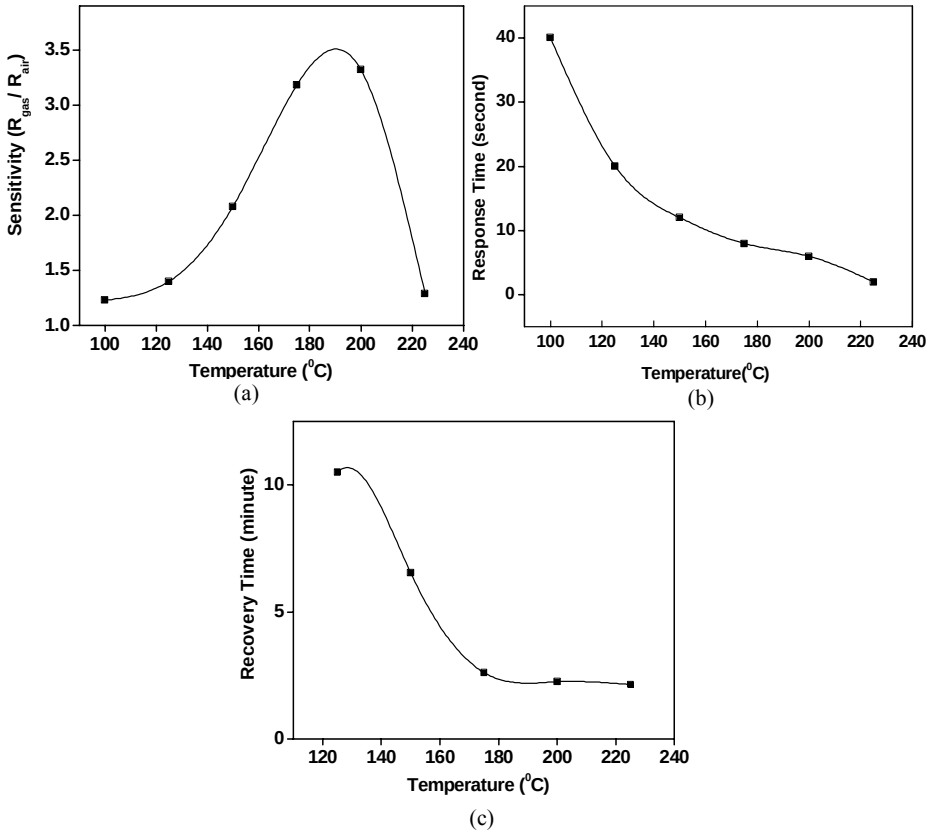

Fig. 4.8 (a) Sensitivity (b) Response time (c) Recovery time of the ZnO thin film sensor towards 7 ppm of NO_2 gas at different temperatures

An operating temperature of 200^0C is considered as the optimum operating temperature since the best compromise between the sensor response and sensor dynamics is obtained at this temperature. At this optimum temperature the sensitivity was 3.32 with a response and recovery time of 6 seconds and 2.26 minutes respectively.

Concentration dependent studies were performed at this optimum temperature. The lowest measured concentration with this method was 1.79 ppm with a sensitivity of 1.01 and the highest measured concentration is 28.58 ppm with a sensitivity of 5.05. When the concentration exceeded this concentration it was observed that the sensitivity of the sensor decreased. Hence it was generalized that the sensor could be employed for low concentration detection purpose only. Fig. 4.9 (a) and (b) shows the response of the sensor towards different concentrations and fig. 4.10 shows sensitivity to different concentrations.

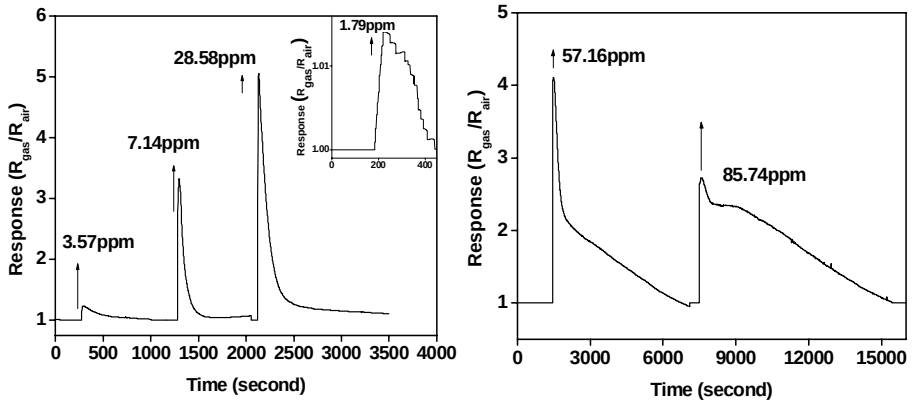

(a) (b)

Fig. 4.9 Response of the ZnO thin film sensor towards different concentrations of NO_2 at 200^0C

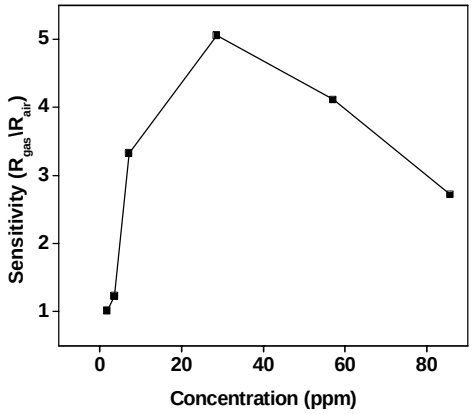

Fig. 4.10 Sensitivity of the ZnO thin film sensor towards different concentrations of NO_2 at 200^0C

4.6.2 Hydrogen Sulphide Detection

Sensor response towards 17.85 ppm of H_2S gas concentration was measured in the temperature range 100 to 225^0C. The sensor response for H_2S gas was calculated as the ratio of resistance, R_{air}/R_{gas}, here R_{air} is the resistance of the thin film sensor before the introduction of gas and R_{gas} is the resistance of the sensor in the presence of gas. Fig. 4.11 (a) to (f) shows the response of the sensor at different temperatures towards this concentration. The response time is taken as the time taken by the sensor to reach 90% of maximum value and recovery time is taken as the time taken by the sensor to reach 10% of base value (value before the introduction of gas) in all the H_2S measurements.

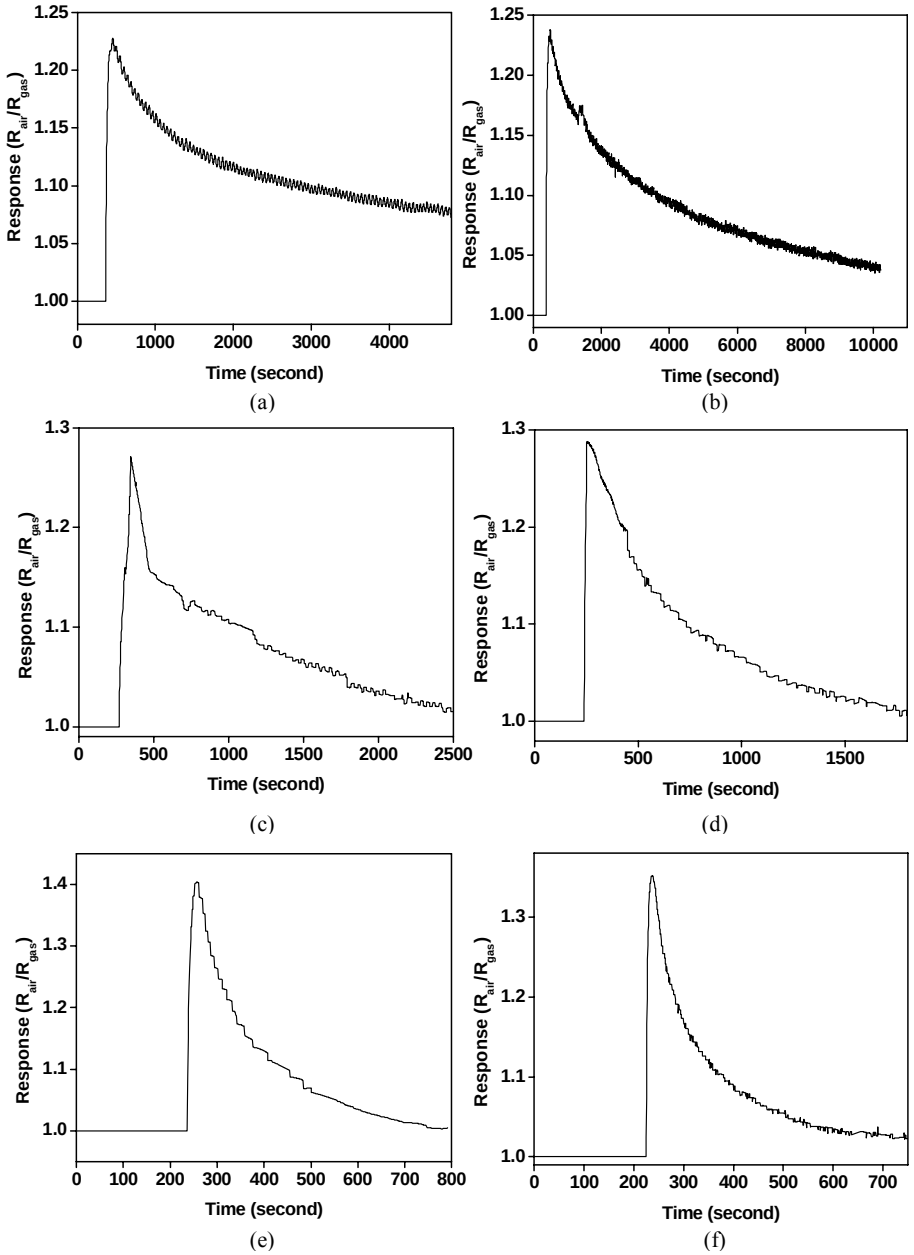

Fig. 4.11 Response of pure ZnO sensor towards 17.85 ppm of H_2S gas at (a) 100 ^{0}C (b) 125^{0}C (c) 150 ^{0}C (d) 175^{0}C (e) 200^{0}C (f) 225 ^{0}C

Due to very large recovery time the measurements at 100^0C and 125^0C were discontinued. Sensitivity of the sensor to 17.85 ppm H_2S gas at various temperatures is shown in fig. 4.12 (a). Here the sensitivity value is taken as the maximum response value corresponding to respective temperature in fig. 4.11 (a) to (f). The response and recovery characteristics of thin film sensor to concentration studied are shown in fig. 4.12 (b) and (c) respectively. Considering maximum sensitivity, response time and recovery time the optimum temperature is selected as 200^0C.

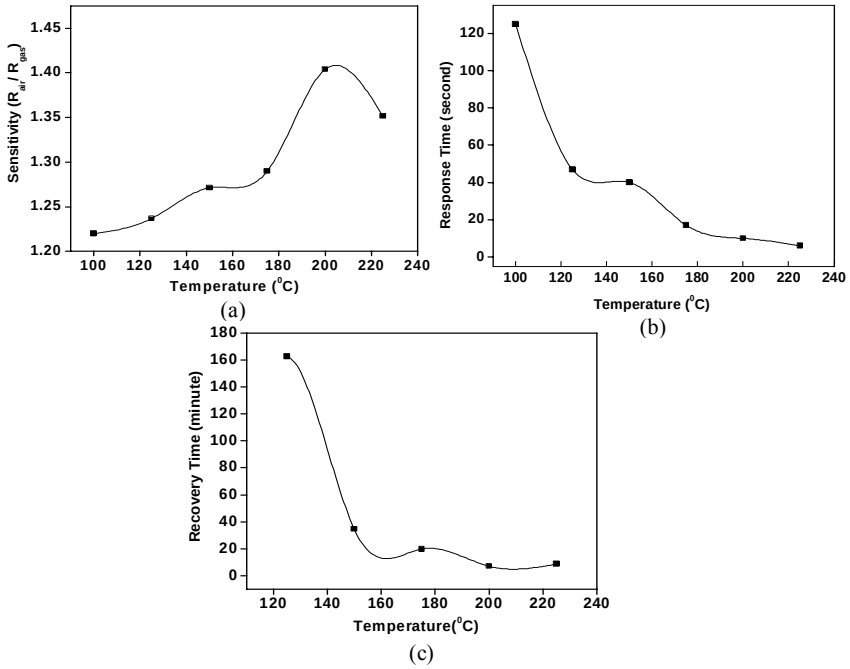

Fig. 4.12 a) Sensitivity (b) Response time (c) Recovery time of the ZnO thin film sensor towards 17.85 ppm of H_2S gas at different temperatures

At this optimum temperature the sensitivity for 17.85 ppm H_2S concentration was 1.4 with a response and recovery time of 10 seconds and 7.11 minutes respectively. Concentration dependent studies performed at this optimum temperature are shown in fig. 4.13 (a) and (b).

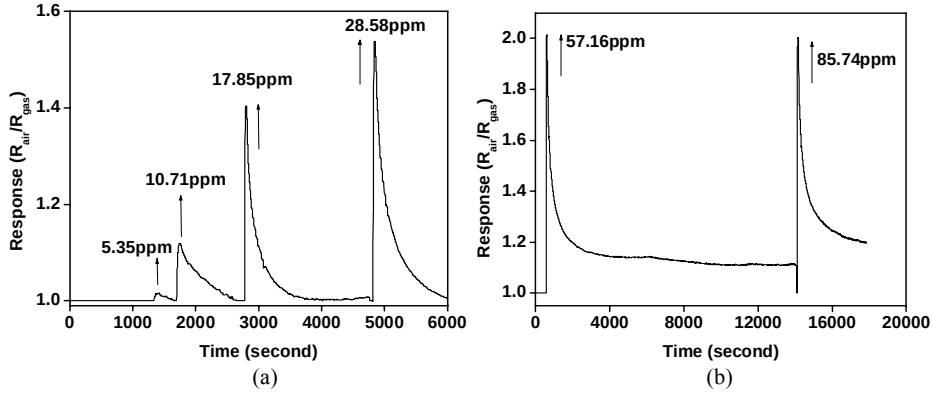

Fig. 4.13 Response of the ZnO thin film sensor towards different concentrations of H_2S at 200^0C

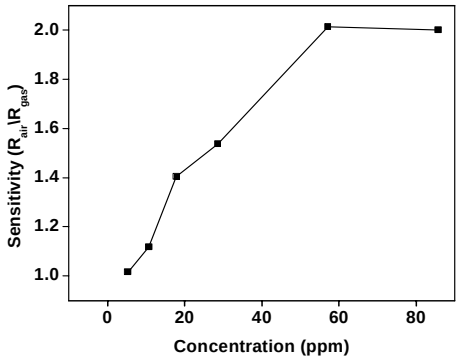

Fig. 4.14 Sensitivity of the ZnO thin film sensor towards different concentrations of H_2S at 200^0C

The lowest measured concentration with this method is 5.35 ppm with a sensitivity of 1.02 and the highest measured concentration is 57.16 ppm with a sensitivity of 2.01. After that the sensitivity does not show an increase. As shown in fig. 4.13 (b) for the 57.16 ppm concentration studied the recovery time is very large. This indicates the sensor is useful for lower concentration studies. Fig. 4.14 shows sensitivity to different concentration corresponding to the optimum temperature of 200^0C.

4.7 Gas Sensors Based on 0.5 vol% Indium Doped ZnO

4.7.1 Nitrogen Dioxide Detection

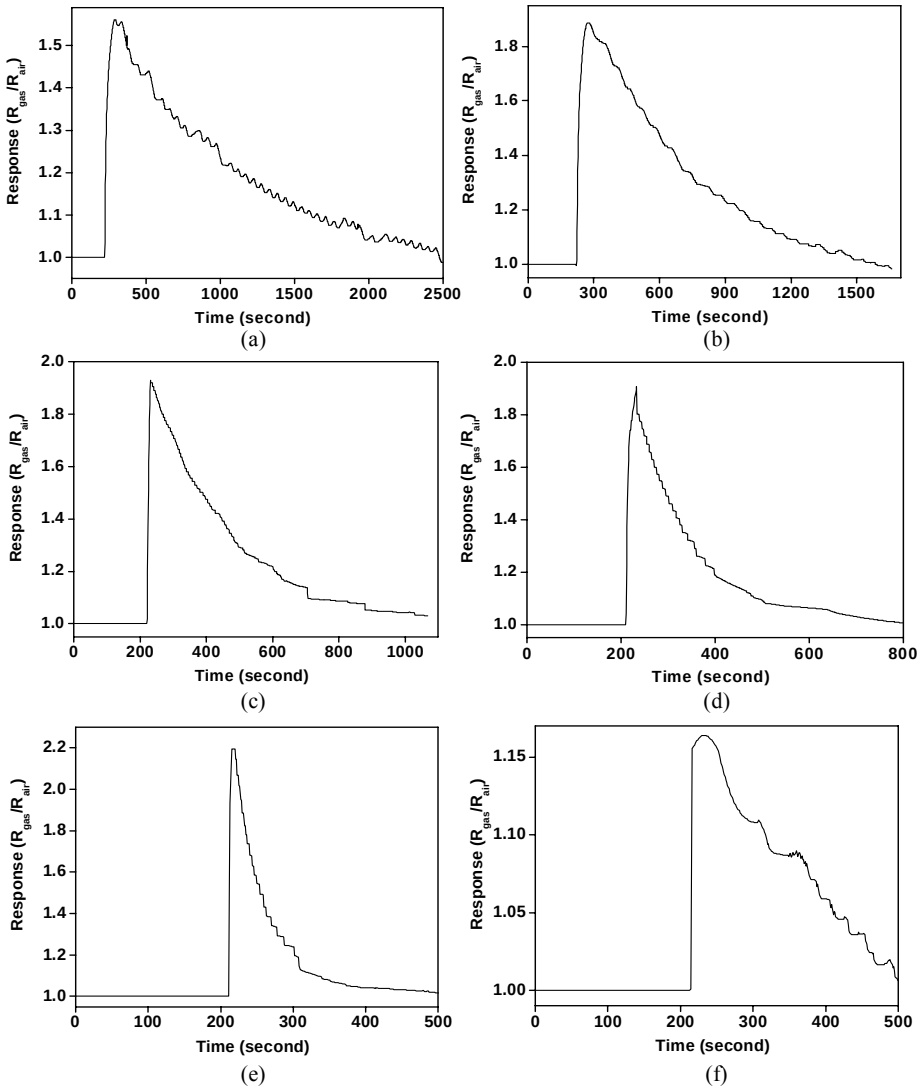

Fig. 4.15 Response of 0.5vol% Indium doped ZnO sensor towards 7 ppm of NO_2 gas at (a) 100 ^{0}C (b) 125^{0}C (c) 150 ^{0}C (d) 175^{0}C (e) 200^{0}C (f) 225 ^{0}C

Response of the 0.5 vol% indium doped ZnO thin film sensor towards a low concentration of 7 ppm was studied in the temperature range of 100^0C to 225^0C. Fig. 4.15 (a) to (f) shows the response of the sensor at different temperatures towards this concentration. Temperature dependent sensitivity, response and recovery times are shown in fig. 4.16 (a), (b) and (c) respectively. The optimum operating temperature was considered as 200^0C with a response of 2.2. The response and recovery times at this optimum temperature was 3seconds and 2.3 minutes respectively.

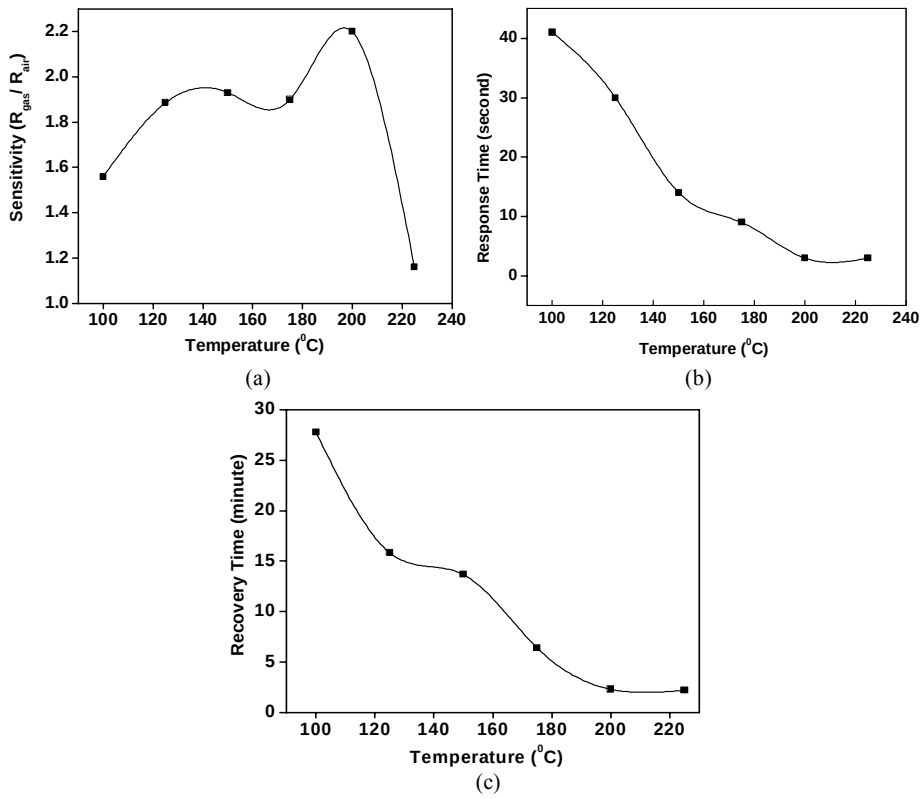

Fig. 4.16 (a) Sensitivity (b) Response time (c) Recovery time of 0.5 vol% indium doped ZnO thin film sensor towards 7 ppm of NO_2 gas at different temperatures

The concentration dependent studies shown in fig. 4.17 (a) and (b) presents that the lowest measured concentration is 1.79 ppm with a response of 1.21 and the maximum measured concentration is 57.16 ppm with a response of 6.27 at the optimum temperature of 200^0C. Beyond this concentration the sensor response decreased. The sensitivity of the sensor at different concentrations is shown in fig. 4.18

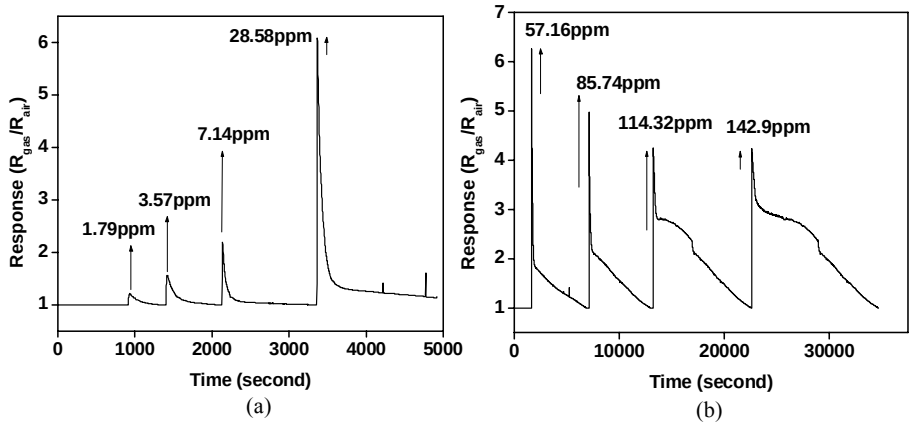

Fig. 4.17 Response of 0.5vol% indium doped ZnO thin film sensor towards different concentrations of NO_2 at 200^0C

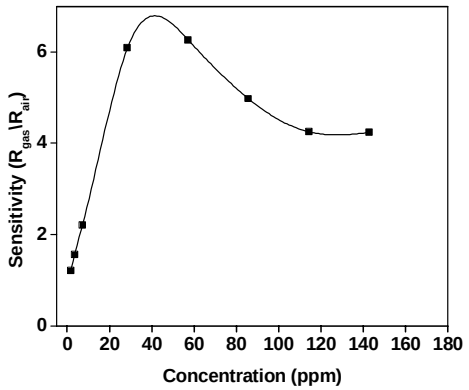

Fig. 4.18 Sensitivity of 0.5vol% indium doped ZnO thin film sensor towards different concentrations of NO_2 at 200^0C

4.7.2 Hydrogen Sulphide Detection

Sensor response towards 17.85 ppm of H_2S gas concentration was measured in the temperature range 100 to 225^{0}C. Fig. 4.19 (a) to (f) shows the sensor response at different temperatures.

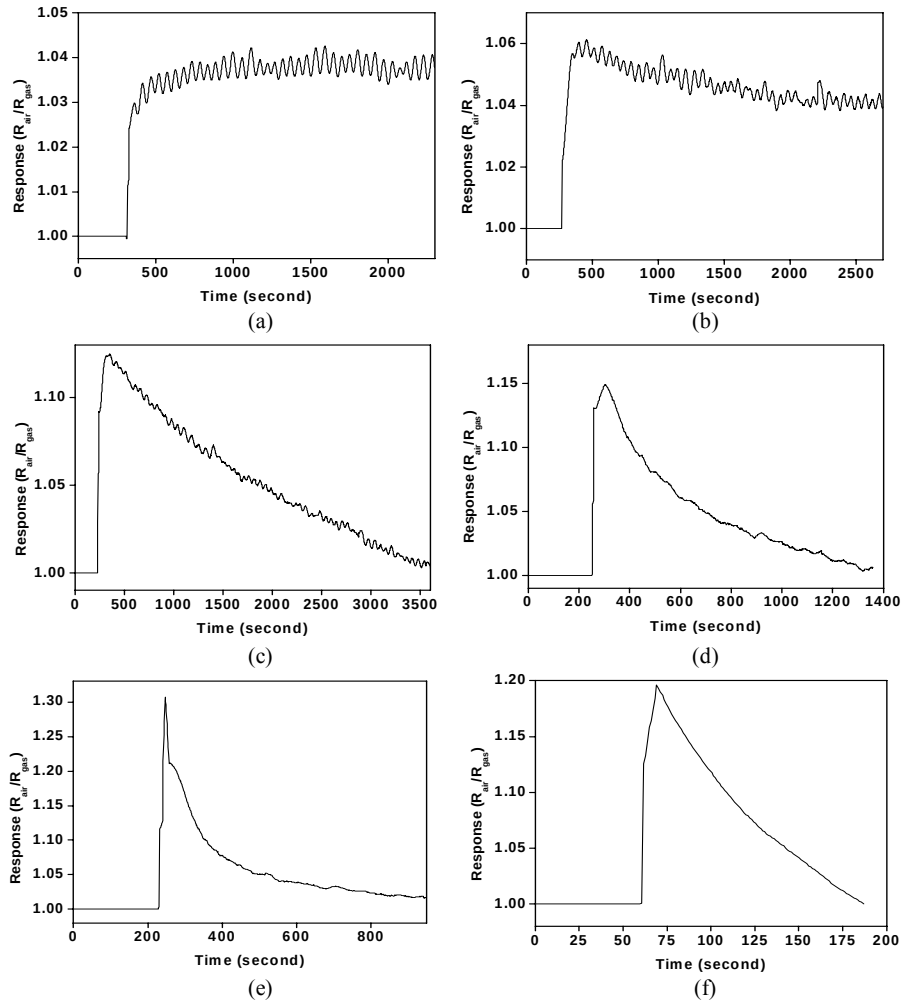

Fig. 4.19 Response of 0.5vol% indium doped ZnO sensor towards 7 ppm of H_2S gas at (a) 100 ^{0}C (b) 125^{0}C (c) 150 ^{0}C (d) 175^{0}C (e) 200^{0}C (f) 225 ^{0}C

Due to very large recovery time at 100 and 125^{0}C the response measurements were discontinued. Temperature dependent gas sensing response at 100 and 125^{0}C show a fluctuation which is due to 0.5^{0}C accuracy of the temperature controller. Since the variation of resistance upon induction of H_2S gas is small at these temperatures the accuracy of controller affects the measurements. Optimum sensor response was obtained at 200^{0}C with a response of 1.3. The response and recovery times at this optimum temperature were 8 seconds and 10.73 minutes respectively. Temperature dependent sensitivity, response and recovery times is shown in fig. 4.20 (a), (b) and (c) respectively.

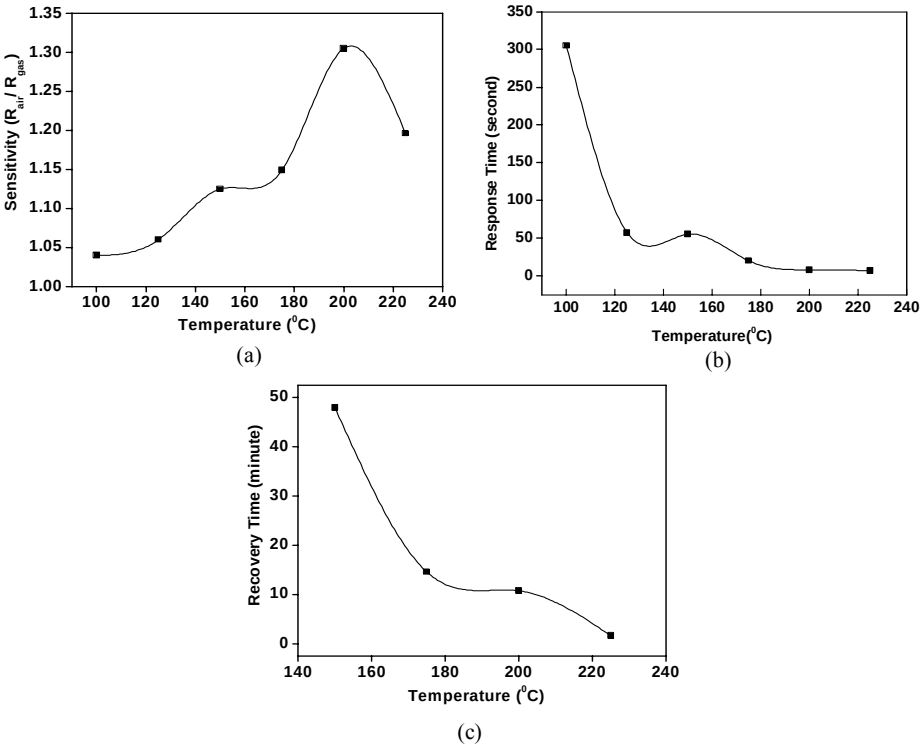

Fig. 4.20 (a) Sensitivity (b) Response time (c) Recovery time of 0.5 vol% indium doped ZnO thin film sensor towards 17.85 ppm of H_2S gas at different temperatures

The concentration dependent studies at optimum temperature of 200^0C show that the lowest measured concentration is 1.79 ppm with a sensitivity of 1.04 and highest measured concentration is 171.48 ppm with a sensitivity of 1.81. The response of sensor to different concentration and the sensitivity is shown in fig. 4.21 (a), (b) and fig. 4.22 respectively.

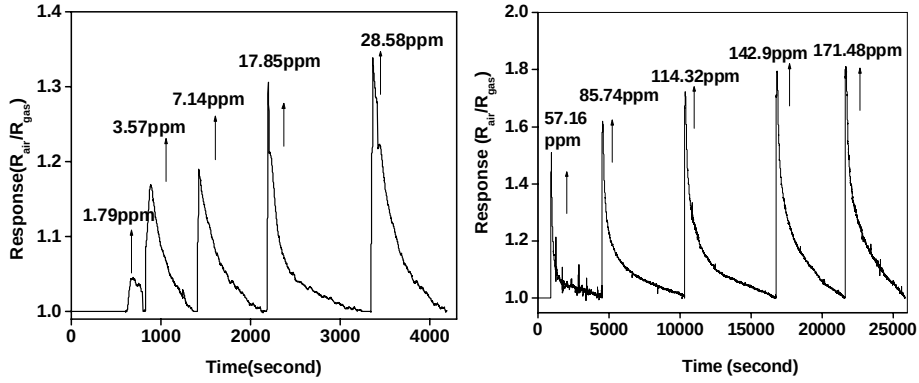

Fig. 4.21 Response of 0.5vol% indium doped ZnO thin film sensor towards different concentrations of H_2S at 200^0C

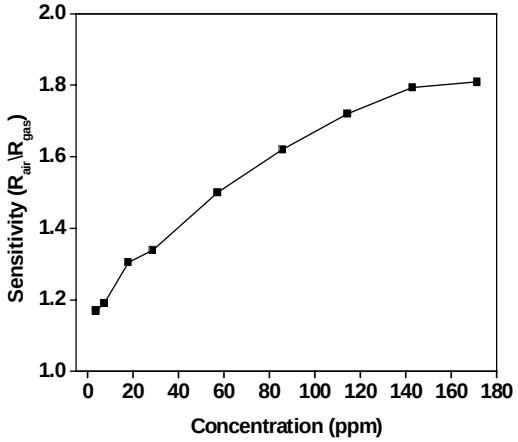

Fig. 4.22 Sensitivity of 0.5vol% indium doped ZnO thin film sensor towards different concentrations of H_2S at 200^0C

4.8 Gas Sensors Based on 1 vol% Indium Doped ZnO:

4.8.1 Nitrogen Dioxide Detection

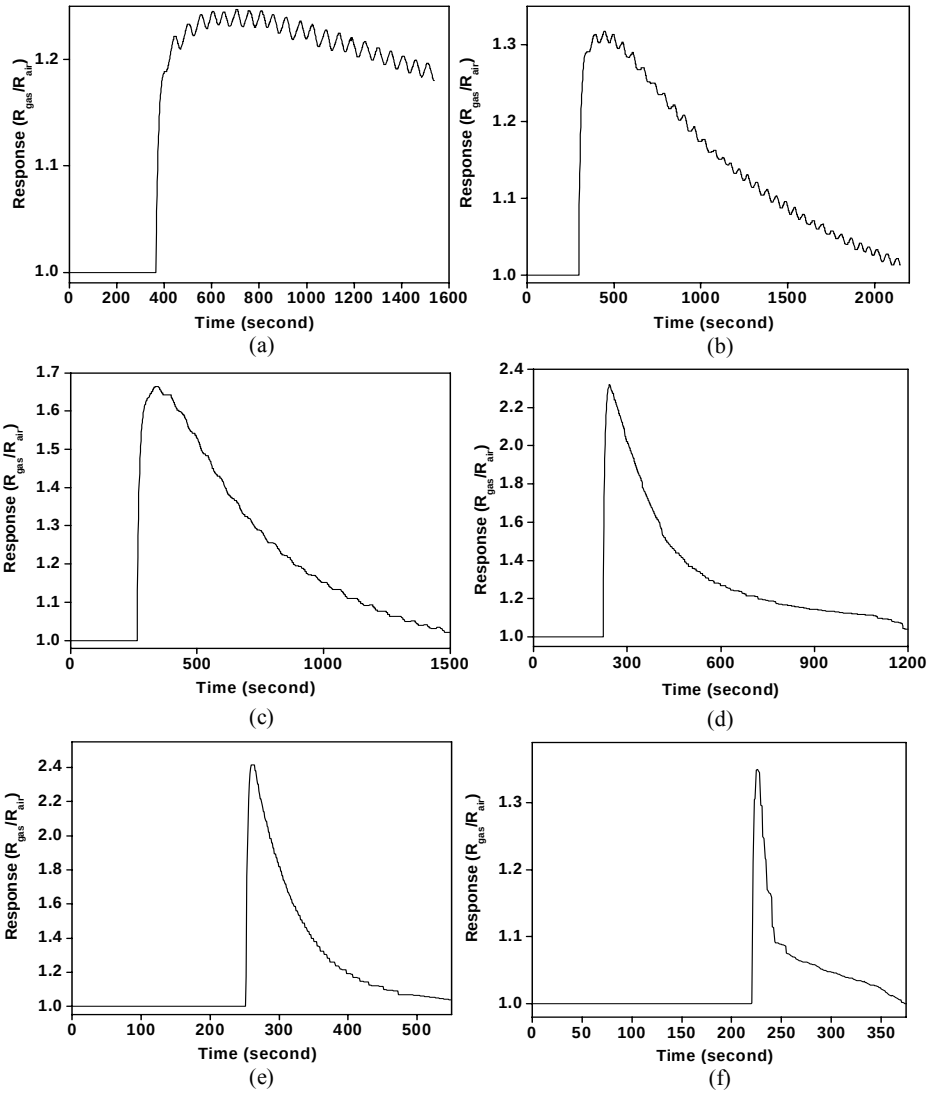

Fig. 4.23 Response of 1vol% indium doped ZnO sensor towards 7 ppm of NO_2 gas at (a) 100 ^{0}C (b) 125^{0}C (c) 150 ^{0}C (d) 175^{0}C (e) 200^{0}C (f) 225 ^{0}C

Temperature dependent gas sensing behaviour of 1vol% indium doped ZnO thin film sensors were performed in the range of 100^0C to 225^0C to a concentration of 7ppm. Fig. 4.23 (a) to (f) shows the response of the sensor to this concentration. The optimum operating temperature was obtained at 200^0C with a response and recovery time of 5 seconds and 2.8 minutes respectively. The maximum sensitivity at the optimum temperature of 200^0C was 2.4. The response and recovery characteristics curves are shown in fig. 4.24 (b) and (c) respectively. The response and recovery times attain low values at the optimum temperature.

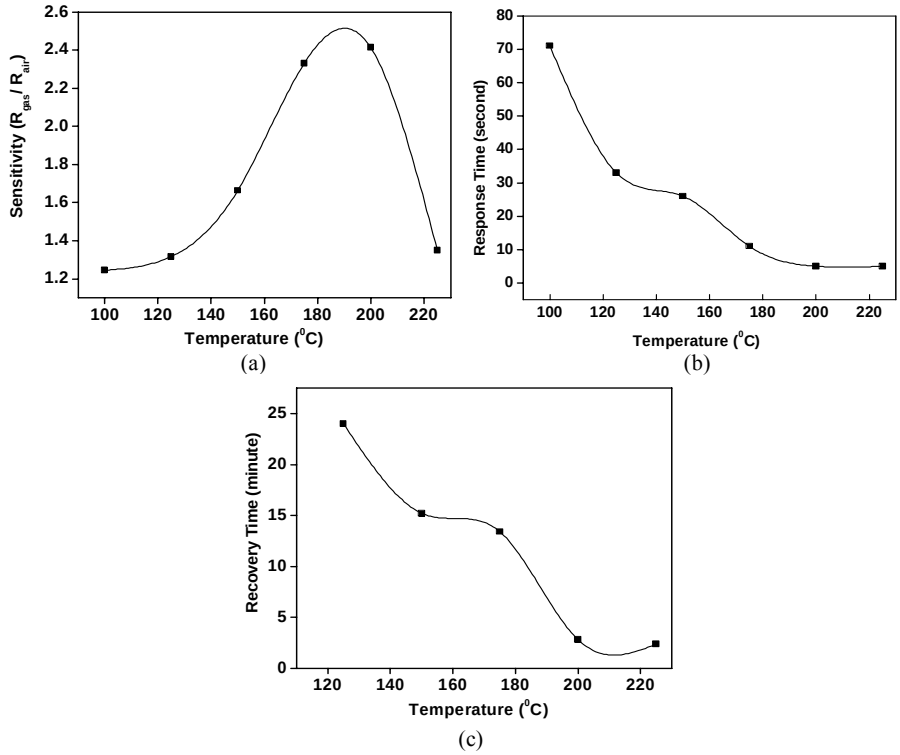

Fig. 4.24 (a) Sensitivity (b) Response time (c) Recovery time of 1 vol% indium doped ZnO thin film sensor towards 7 ppm of NO_2 gas at different temperatures

Due to very large recovery time at 100^0C the measurement was discontinued. Fig. 4.24 (a) shows the sensitivity of the sensor towards different temperature. Concentration dependence of the sensor response was studied at the optimum temperature of 200^0C. The lowest measured concentration is 1.79 ppm with a response of 1.11 and highest measured concentration is 114 ppm with a response of 4.05. Fig. 4.25 (a) and (b) shows the response of sensor to different concentrations. The sensitivity graph is shown in Fig. 4.26 and it shows that sensitivity does not increase beyond certain limit.

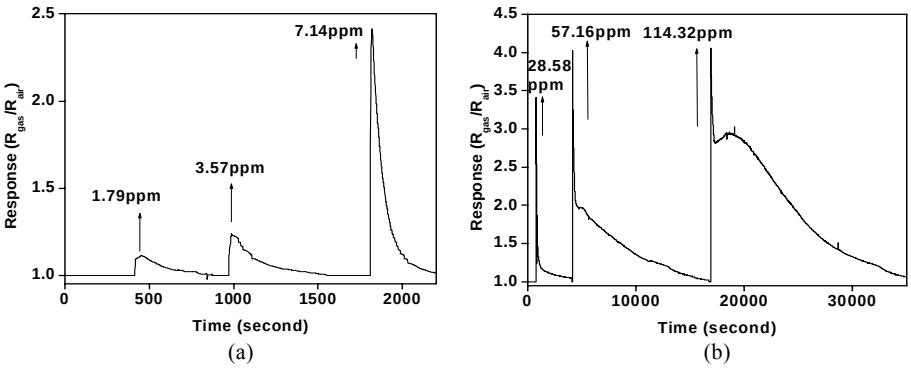

Fig. 4.25 Response of 1vol% indium doped ZnO thin film sensor towards different concentrations of NO_2 at 200^0C

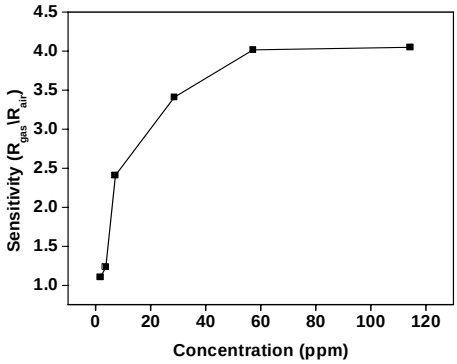

Fig. 4.26 Sensitivity of 1vol% indium doped ZnO thin film sensor towards different concentrations of NO_2 at 200^0C

4.8.2 Hydrogen Sulphide Detection

Sensor response towards 17.85 ppm of H_2S gas concentration was measured in the temperature range 100 to 225^{0}C. Fig. 4.27 (a) to (f) shows the sensor response at different temperatures.

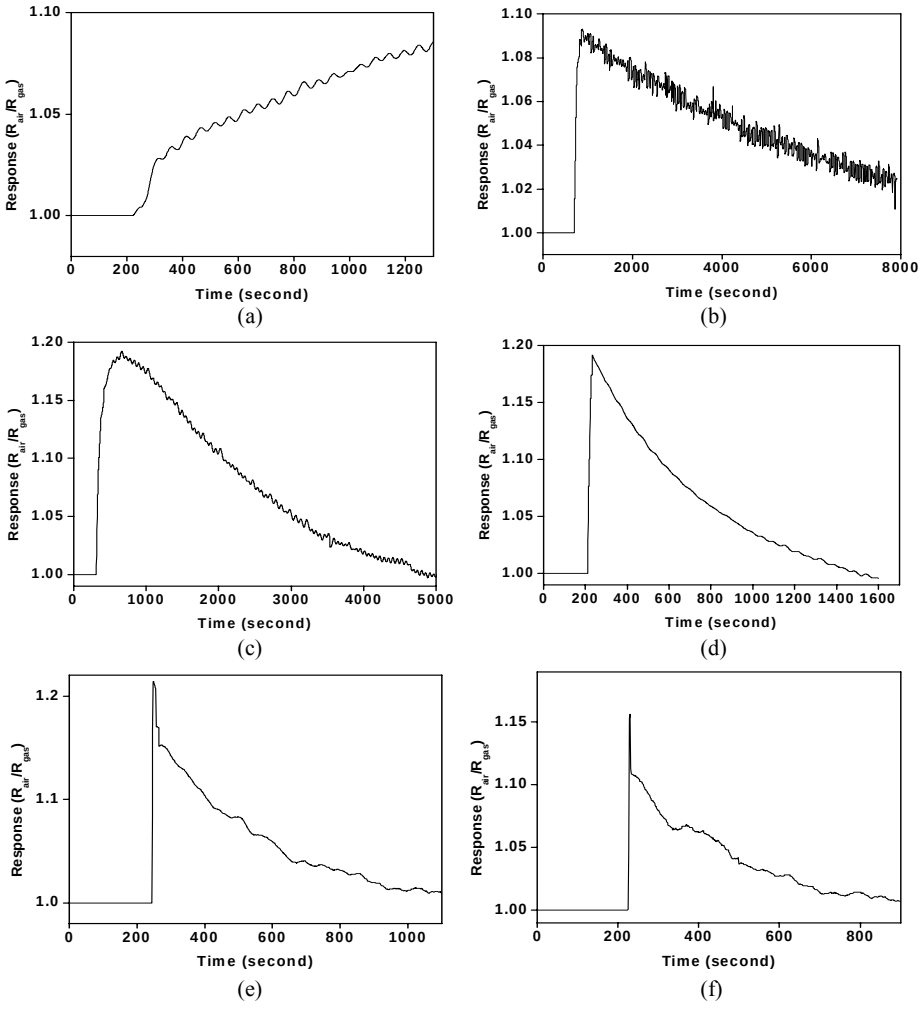

Fig. 4.27 Response of 1vol% indium doped ZnO sensor towards 17.85 ppm of H_2S gas at (a) 100 ^{0}C (b) 125^{0}C (c) 150 ^{0}C (d) 175^{0}C (e) 200^{0}C (f) 225 ^{0}C

At low temperature 100 and 125^{0}C the recovery time was very high. The measurement at 100^{0}C was discontinued due to this large recovery time. The measurements at these temperatures show a fluctuation which is due to 0.5^{0}C accuracy of the temperature controller. Temperature dependent sensitivity, response and recovery times are shown in fig. 4.28 (a), (b) and (c) respectively. The optimum operating temperature was found to be 200^{0}C with a response and recovery time of 11 seconds and 12 minutes respectively. A response of 1.2 was achieved at this temperature.

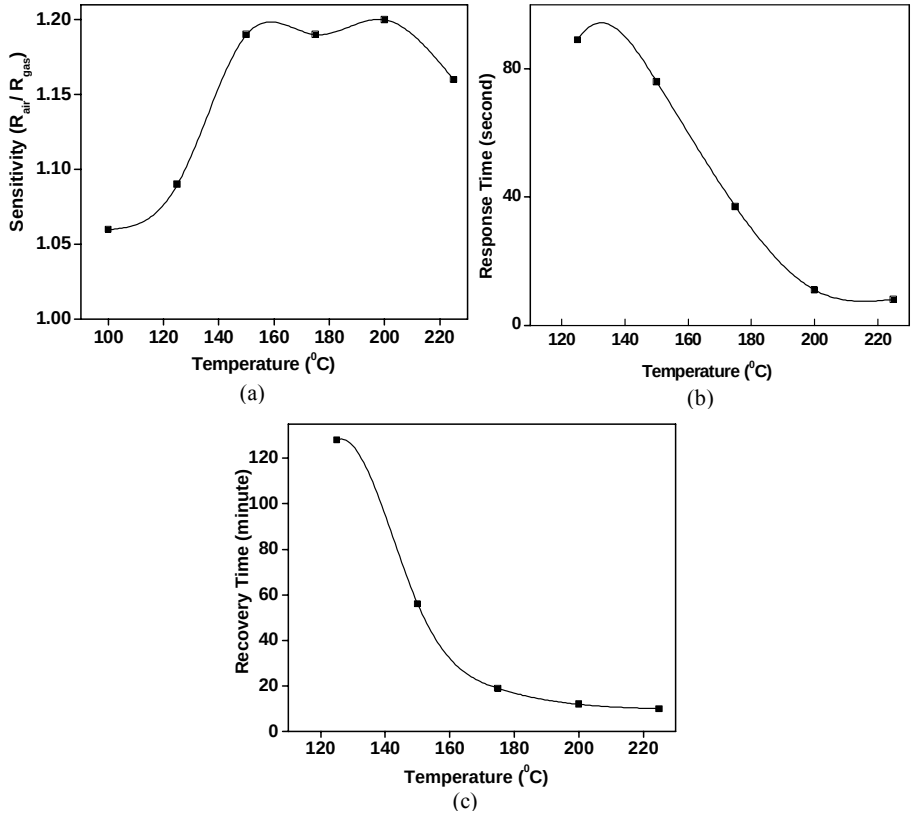

Fig. 4.28 (a) Sensitivity (b) Response time (c) Recovery time of 1 vol% indium doped ZnO thin film sensor towards 17.85 ppm of H_2S gas at different temperatures

The concentration dependent study at this optimum temperature of 200^0C is shown in fig. 4.29 (a) and (b). The lowest measured concentration is 3.57 ppm with a response of 1.01 and highest measured concentration is 257.22 ppm with a response of 2.74. The sensitivity of the sensor to different concentrations is shown in fig. 4.30.

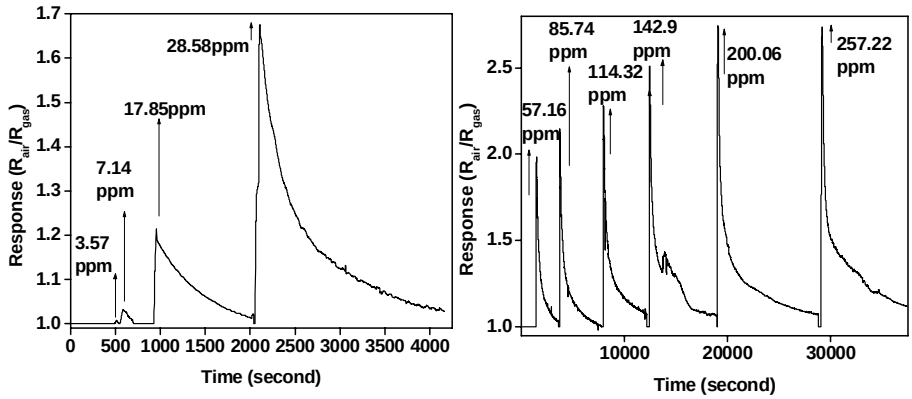

(a) (b)

Fig. 4.29 Response of 1vol% indium doped ZnO thin film sensor towards different concentrations of H_2S at 200^0C

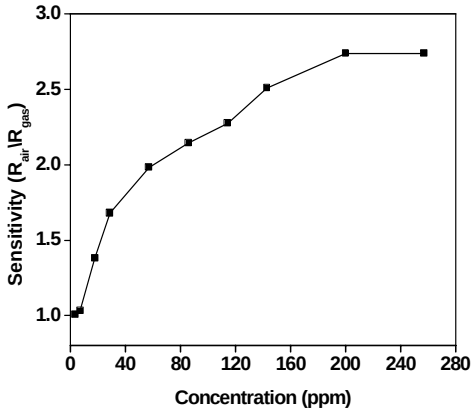

Fig. 4.30 Sensitivity of 1vol% indium doped ZnO thin film sensor towards different concentrations of H_2S at 200^0C

4.9 Gas Sensors Based on 3vol% Indium Doped ZnO

4.9.1 Nitrogen Dioxide Detection

Temperature dependent gas sensing behaviour of 3vol% indium doped ZnO to 7 ppm gas was performed in the range of 100^0C to 225^0C. Fig. 4.31 (a) to (f) shows the response of the sensor to this concentration studied.

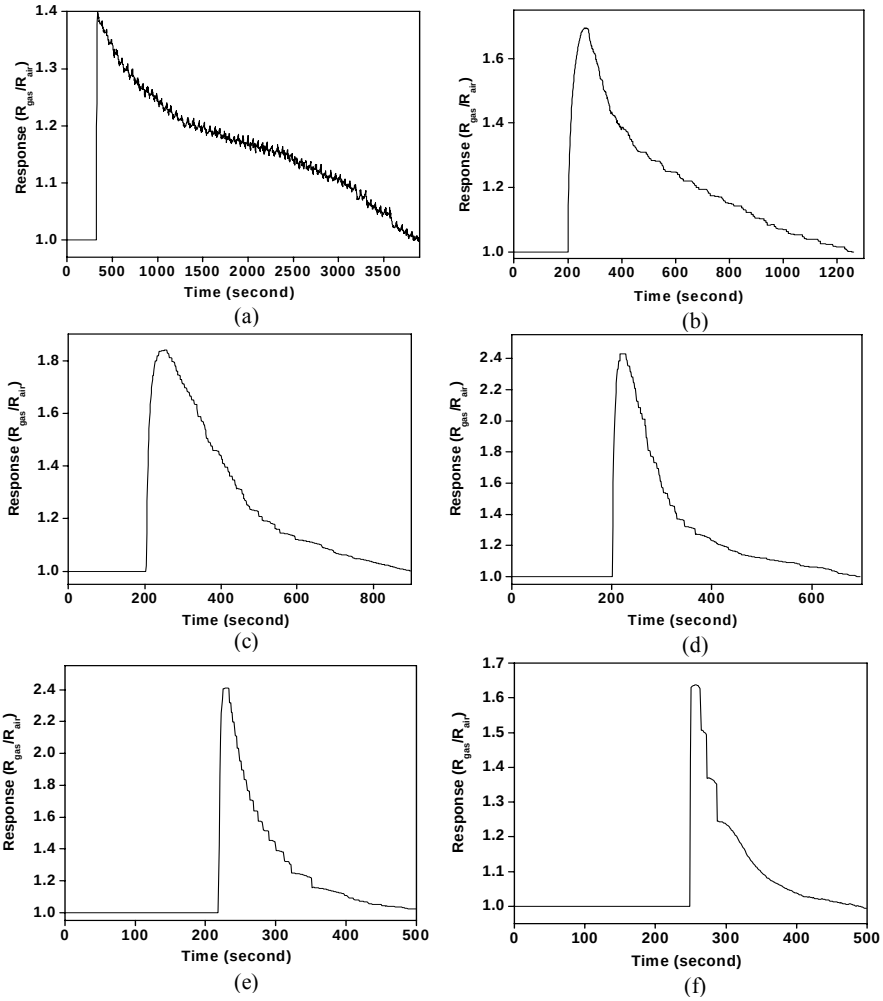

Fig. 4.31 Response of 3vol% indium doped ZnO sensor towards 7 ppm of NO_2 gas at (a) 100 ^{0}C (b) 125^{0}C (c) 150 ^{0}C (d) 175^{0}C (e) 200^{0}C (f) 225 ^{0}C

Temperature dependent sensitivity, response and recovery times are shown in fig. 4.32 (a), (b) and (c) respectively. The optimum operating temperature was found to be 200^0C with a response and recovery time of 4 seconds and 2.78 minutes respectively. Sensor response at this optimum temperature was 2.41.

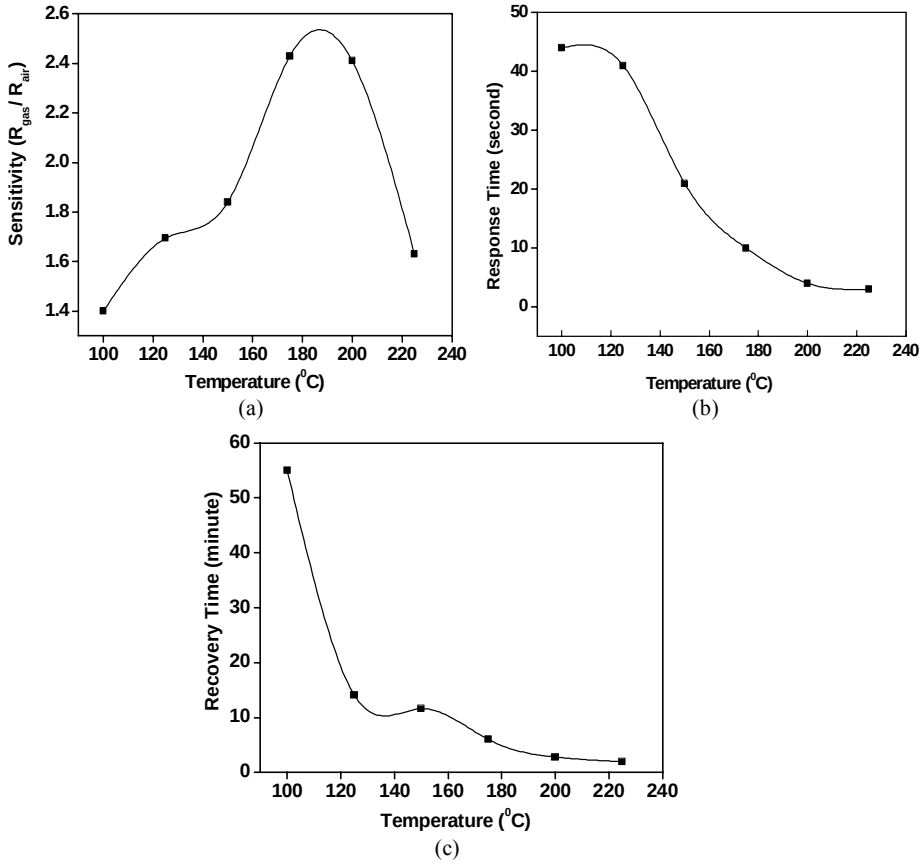

Fig. 4.32 (a) Sensitivity (b) Response time (c) Recovery time of 3vol% indium doped ZnO thin film sensor towards 7 ppm of NO_2 gas at different temperatures

The concentration dependent study at optimum temperature of 200^0C is shown in fig. 4.33 (a) and (b). The lowest measured concentration is 1.79 ppm with a response of 1.11 and highest measured concentration is 114 ppm with a response of 2.63. The sensitivity of the sensor to different concentration is shown in fig. 4.34. The sensitivity graph in fig. 4.34 shows saturation.

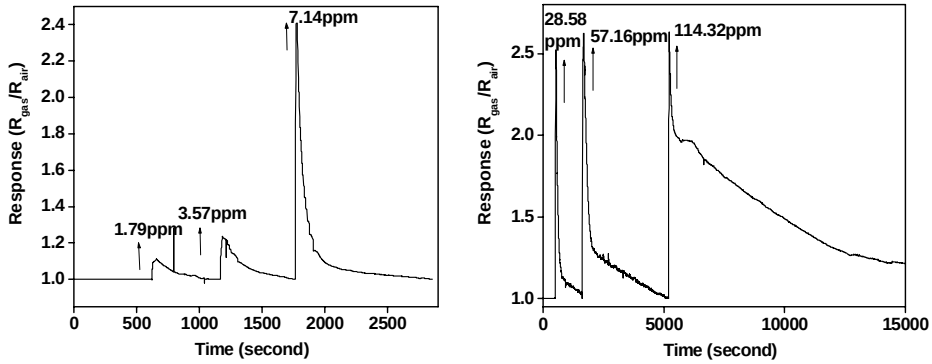

(a) (b)

Fig. 4.33 Response of 3vol% indium doped ZnO thin film sensor towards different concentrations of NO_2 at 200^0C

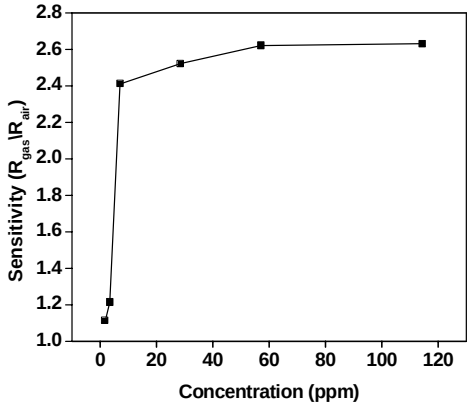

Fig.4.34 Sensitivity of 3vol% indium doped ZnO thin film sensor towards different concentrations of NO_2 at 200^0C

4.9.2 Hydrogen Sulphide Detection

Sensor response towards 17.85 ppm of H_2S gas concentration was measured in the temperature range 100 to 225^{0}C. Fig. 4.35 (a) to (f) shows the representative response profiles to different temperatures.

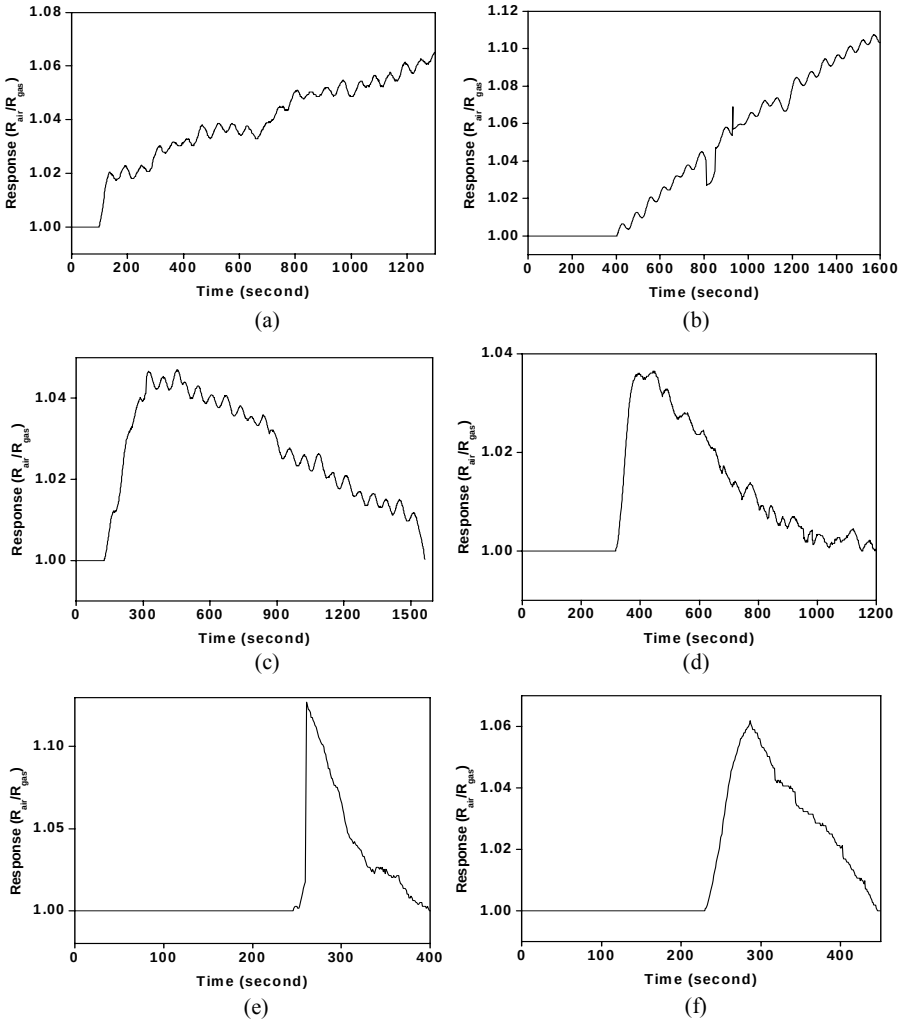

Fig. 4.35 Response of 3vol% indium doped ZnO sensor towards 17.85 ppm of H_2S gas at (a) 100 ^{0}C (b) 125^{0}C (c) 150 ^{0}C (d) 175^{0}C (e) 200^{0}C (f) 225 ^{0}C

Temperature dependent sensitivity, response and recovery time is shown in fig. 4.36 (a), (b) and (c). The optimum operating temperature was found to be 200^0C with a response and recovery time of 13 seconds and 2.0 minutes respectively. Sensor response at this optimum temperature was 1.13.

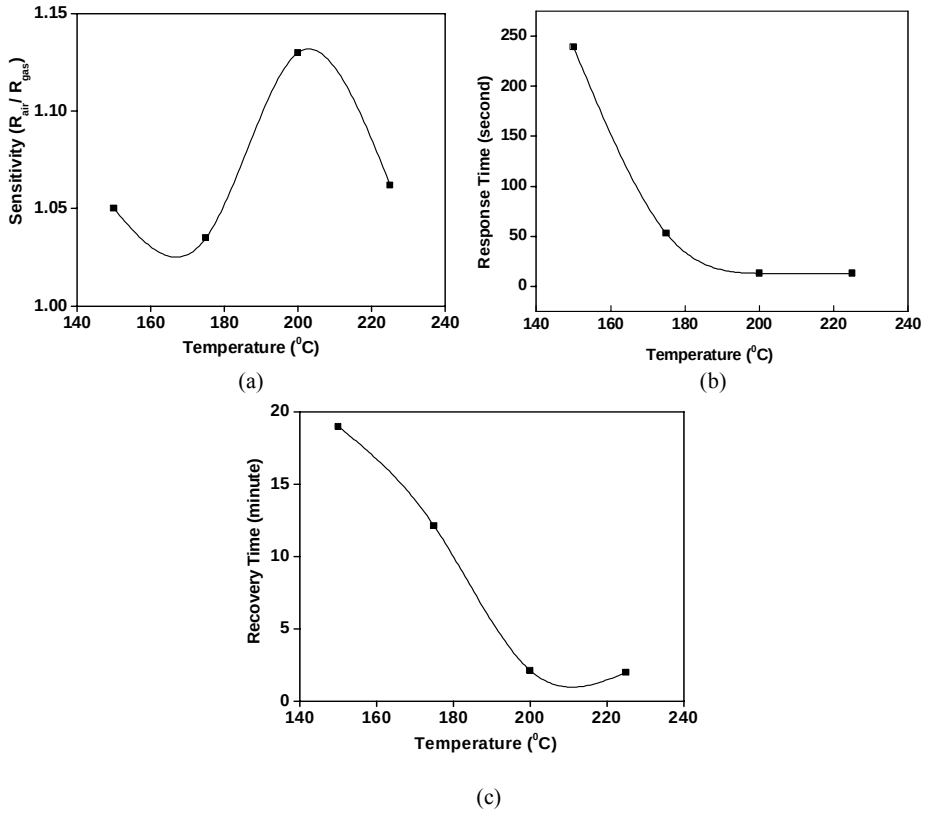

Fig. 4.36 (a) Sensitivity (b) Response time (c) Recovery time of 3 vol% indium doped ZnO thin film sensor towards 17.85 ppm of H_2S gas at different temperatures

The concentration dependent study at the optimum temperature of 200^0C is shown in fig. 4.37(a) and (b). The lowest measured concentration is

3.57 ppm with a response of 1.02 and highest measured concentration is 286 ppm with a response of 3.32. The sensitivity of the sensor to different concentration is shown in fig. 4.38.

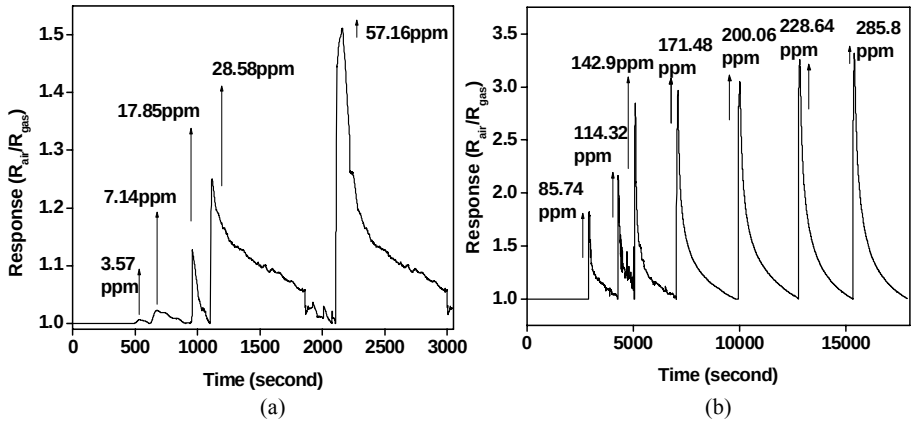

Fig. 4.37 Response of 3vol% indium doped ZnO thin film sensor towards different concentrations of H_2S at 200^0C

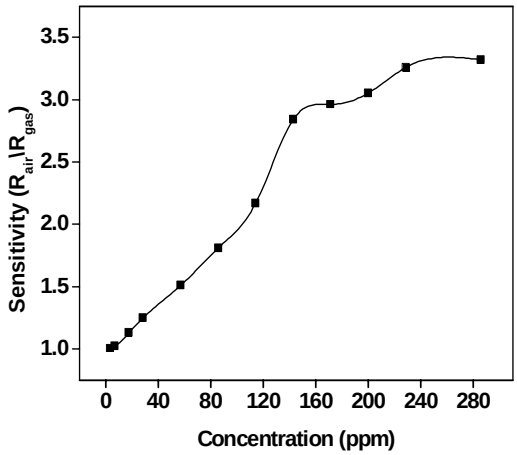

Fig. 4.38 Sensitivity of 3vol% indium doped ZnO thin film sensor towards different concentrations of H_2S at 200^0C

4.10 Discussion of the Results

n-type semiconductors are characterized by the presence of free electrons in the conduction band mainly due to lattice defects, such as oxygen vacancies, introduced during synthesis of the material. The XRD study of pure and doped sensor show that the sensors are nanocrystalline in nature. In this kind of material the mechanism of conduction is controlled by electron flow through a huge series of intergranular point contacts. At these contacts a surface barrier originates in the presence of surface states, whose amount depends both on the chemical reactions with detecting gases and on the physical intrinsic characteristics of the material. Conductivity therefore is an activated process, since only those electrons with sufficient energy to cross the barrier take part in electrical conductance. Chemoresistivity is the basis of sensing mechanism for metal oxides, which consists, of a variation of the intergranular barrier with subsequent conductivity modification as a response to surface chemical reactions with environmental gases. As the barrier modulation occurs at the surface, the bulk does not take part in the whole process of sensing, there by high surface to volume ratio is needed to amplify gas response.

It is well known that the sensing mechanism of ZnO belongs to the surface-controlled type. Its gas sensitivity is related to thickness of active layer grain size, surface state, oxygen adsorption quantity, active energy of oxygen adsorption and lattice defects [108, 109]. Similar to other semiconductor gas sensors, the ZnO based gas sensor detects the variation in electrical resistivity resulting from the adsorption on surface.

It is known that annealing at higher temperatures and in air increases resistivity of ZnO due to the chemisorption of oxygen at the grain boundaries, which in turn leads to the formation of extrinsic trap states

localized at the grain boundaries. Major et al. [110] have reported correlation of crystal orientation, grain boundaries and film thickness on the density of trap states formed due to chemisorbed oxygen in the indium doped ZnO films deposited by the spray pyrolysis. Such states trap free electrons from the bulk of the grain to create potential barrier by causing depletion in the region adjacent to the grain boundaries. Such potential barriers decrease the mobility of carriers thereby increasing the resistivity.

Atmospheric oxygen molecules are adsorbed on surface sites and get ionized by taking an electron from the conduction band and are thus ionosorbed on the surface as O_{ads} [112]. Electron transfer between adsorbed oxygen molecules and the semiconductor surface results in the formation of depletion layer also known as space charge layer. The space-charge layer is a region that has deficient carriers due to electron trapping by the chemisorbed oxygen. This electron transfer and subsequent creation of electron depleted region causes decrease in conductance of sensor material. Thus, the electrical conductivity of ZnO depends strongly on the surface states produced by molecular adsorption that results in space–charge layer changes and band modulation. The effect of adsorbed oxygen, various forms of adsorbed oxygen, the band bending associated with oxygen and gas adsorption, the temperature dependent adsorption and desorption process are discussed in detail in third chapter. In ZnO films, electrons are also extracted from the interstitial zinc atoms Zn_i^{2+}, which act as an electron donor [25, 113]. The interstitial zinc atoms in such cases are ionized via the following reversible reaction,

$$Zn_i^{2+} \leftrightarrow Zn_i^{+} + e^{-} \qquad (4.2)$$

Ma et al. studied the effect of grain size on gas sensitivity on ZnO [114]. They studied the particle size in the range of 30-40nm, beyond 34 nm the

sensitivity was found to decrease. The conduction mechanism they proposed for particle size beyond 34nm was mainly grain boundary controlled and for lower particle size the conduction mechanism was neck controlled. Considering the crystallite size, D (38.32nm, 37.31nm, 39.14nm, 35.34nm) of our samples the electrical conduction is assumed to be under grain boundary control regime.

In the presence of test gases, the electrical conductivity of porous semiconductor film sensor changes due to reactions occurring on the surface [25, 115]. The change of electrical resistance leads to the different sensitivity of the ZnO film to different target gases. The effect of temperature on device sensitivity was studied and the sensing reactions were carried out with two different analyte gases at several sensing temperatures. The gas sensitivity tests performed at room temperature show no variation on the film conductivity, even with increase of the gas concentration. The increase in the operation temperature leads to an enhancement of the films sensitivity.

4.10.1 NO_2 detection mechanism

NO_2 is an oxidizing gas. NO_2 gets chemisorbed at the surface of ZnO grains and trap electrons at the surface. The electrons are taken from ionized donors through conduction band and the density of majority charge carriers at the gas–solid interface is reduced. This leads to the formation of a surface barrier for electrons. With increase of the oxygen ions density on the surface the further oxygen adsorption is inhibited. Thus at the junctions between ZnO grains, the depletion layer and potential barrier leads to increase of electrical resistivity value. This value is strongly dependent on the concentration of adsorbed oxygen ions of the surface. Adsorption of atmospheric oxygen will lead to a band bending. Introducing the n-type pure and indium doped ZnO films in an NO_2 ambient will change the

concentration of these adsorbed oxygen ions and increase the resistance. The reaction in presence of NO_2 oxidizing gas will lead to the consumption of electrons and further increase the surface barrier height and hence resistance of the sensor. The adsorption of NO_2 gas will further increase the band bending.

The reactions that can take place on surface of ZnO on NO_2 adsorption as discussed in third chapter are given below.

$$NO_2(g) + e^- \leftrightarrow NO_2^-{}_{(ads)} \quad (4.3)$$

$$NO_2(g) + O^-{}_{2(ads)} + 2e^- \leftrightarrow NO_2^-{}_{(ads)} + 2O^-{}_{(ads)} \quad (4.4)$$

$$NO_2^-{}_{(ads)} + O^-{}_{2(ads)} \leftrightarrow 2O^-{}_{(ads)} + NO_2 \quad (4.5)$$

As in the eq. (4.3) NO_2 can react directly with surface Zn ion and remove an electron as well as it can react with adsorbed oxygen as in eq. (4.4) and (4.5). The electrons consumed in these reactions are extracted from the conduction band thus raising the resistivity of oxide film.

The sensor operating temperature also affects the properties of the materials, leading to a difference in the sensitivity of the sensor. It is obvious from the sensitivity vs temperature figures 4.8 (a), 4.16 (a), 4.24 (a) and 4.32 (a) that operating temperature plays a vital role in determining the sensitivity of the film. As operating temperature increases the sensitivity of pure and indium doped ZnO sensors also increases reaching a maximum and then decreases. In general there exists an optimum operating temperature for a sensor to achieve the maximum sensitivity to a gas of interest, the temperature being dependent upon the kind of gases i.e. the mechanism of desorption and dissociation of a gas on the particular sensor surface. At lower temperature the sensitivity was low, also the recovery time kept on

increasing, which indicates a longer time taken by the sensor to revert back to its base-line properties for the next operation. The optimum operating temperature for pure and doped sensors was found to be 200^0C. At low operating temperature response of the films to NO_2 is restricted by the speed of the chemical reaction because the electrons do not have enough thermal energy to react with the surface adsorbed oxygen species. In fact, during adsorption of atmospheric oxygen on the film surface, a potential barrier to charge transport is developed. As operating temperature increases the thermal energy obtained is high enough to overcome the potential barrier and thus the electron concentration increases significantly, which in turn leads to an increase in sensitivity of the films. At optimum operating temperature the sensitivity is maximum. This is attributed to the availability of sufficient adsorbed ionic species of oxygen on the film surface which react most effectively with NO_2 molecules at this particular temperature.

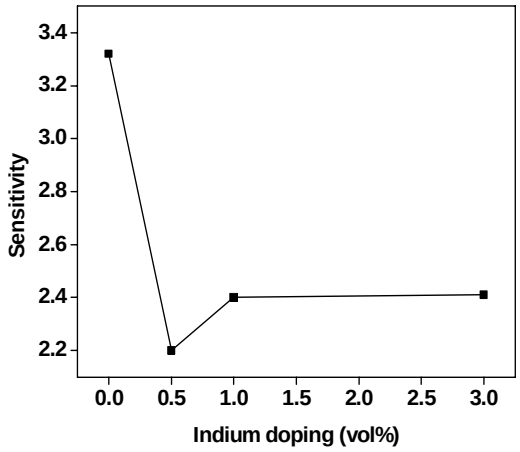

Fig. 4.39 Sensitivity at different indium doping % to 7 ppm NO_2 gas at respective optimum temperature

Dopants in metal oxide materials usually affect the physical and electrical properties. Dopant elements commonly segregate to grain boundaries in crystalline metal oxide and prohibit grain growth in subsequent annealing. Electrically, dopants generate ionic and electronic defects. These defects impact the position of the Fermi energy level which in turn is expected to influence the gas sensitivity of the semiconducting oxides. To study the catalytic effect in ZnO based sensor, indium is used as the dopant. Contrary to enhancement effect in sensitivity by the presence of additives, it was found that incorporation of indium decreases NO_2 gas sensing ability of the sensor (fig. 4.39). The poor sensor performance due to addition of indium had reported earlier also [116]. It was reported that an increase in film thickness beyond 220 nm can have an adverse effect on sensor performance. This has attributed to the predominance of bulk conductance over the surface one. As a result of indium doping there is an increase in free electron concentration and a consequent decrease in resistivity occurs due to replacement of Zn^{2+} cation by the In^{3+} cation, which acts as a donor. Due to the increased electron concentration the sensor response to oxidizing gas NO_2 is less. The fractional change in resistance is very small when compared with the free electron concentration and hence doped sensor response to NO_2 will decrease with the indium doping [117]. Eventhough the number of active adsorption sites (indium atoms and oxygen vacancies) which favor the adsorption of oxygen species increases by the additive incorporation sensor sensitivity was found to decrease in all the doped concentrations studied due to this increased electron concentration. Hence our results indicate that pure ZnO sensor itself acted as a very good NO_2 sensor. Moreover, In-doping does not decrease the temperature, at which the maximum of sensor response occur, which means that indium additive do not act as a effective catalytic site [116].

Studies conducted by Rodriguez et al. [118] on ZnO shows that at room temperature the NO_2 molecule mainly dissociates into O adatoms and gaseous NO, whereas at low temperatures (<250 K) chemisorbed NO_2 and NO_3 dominate on the surface. The photo emission and XANES results presented in the above study indicate that at 300K the result of reaction of NO_2 with polycrystalline ZnO is adsorbed NO_3 with little NO_2 or NO present on the surface of the oxide. The nitrate species were found to be stable up to temperatures near 700 K. The Zn↔NO_2 interactions on ZnO are strong and Zn sites probably get oxidized and nitrated. It is expected that in general NO_2 molecule is very efficient for fully oxidizing metal centers that are missing O neighbors in oxide surfaces (i.e., elimination of O vacancies). This oxidation process will be followed by reaction of NO_2 with O centers and subsequent formation of NO_3. At the end, nitrate will be the main product of the interaction between NO_2 and the oxide. The concentration dependent studies at optimum temperatures performed on pure and indium doped ZnO films (fig. 4.10, 4.18, 4.26, 4.34) indicates that both the sensors can only be used for detecting NO_2 gas at lower concentration range beyond which the sensitivity was found to decrease. The decrease in sensitivity at higher concentration studied may be due to the formation of NO_3 species adsorbed on the metal oxide which will prevent further adsorption of NO_2. This may be the reason for decreased sensitivity at higher concentration.

4.10.2 H_2S detection mechanism

It is well known that the gas sensing mechanism in the oxide based materials is surface controlled, where in; the grain size, surface states and oxygen adsorption play a significant role. The larger surface area usually offers more adsorption–desorption sites and thus the enhanced sensitivity [108, 109]. The atmospheric oxygen gets adsorbed on the sensor surface, and

depending upon the temperature of operation; different oxygen species are formed on the surface as discussed in chapter 3.

When the pure and indium doped ZnO sensor is exposed to a reducing gas, H_2S the test gas reacts with oxygen species chemisorbed on the semiconductor surface and release electrons to the conduction band. This will result in a decrease in the amount of surface O_2^-, O^- and O^{2-} ions, leading to an increase in concentration of electrons in the conduction band. This eventually increases the conductivity of pure and indium doped ZnO. Hence, the more the effective surface area, the more the oxygen-adsorption quantities and higher the sensitivity of these metal oxide sensors [69]. The gas response by metal oxide semiconductor, in general, can be described as

$$O_2\,(gas) + e \leftrightarrow O^-_{2(ads)} \tag{4.6}$$

$$H_2S_{\,(gas)} + O^-_{2(ads)} \leftrightarrow H_2S_{(ads)} + O_{2(gas)} + e^- \tag{4.7}$$

Initially, (Eq. (4.6)) the atmospheric oxygen acquires electron from the conduction band of ZnO and forms $O^-_{2(ads)}$ species on the surface thus decreasing the conductance of ZnO. It is known that the gas response depends directly on the number of $O^-_{2(ads)}$ species. The reducing gas H_2S, reacts with $O^-_{2(ads)}$ and releases electron back to the conduction band. In the process the conductance again increases. Therefore, gas response in general, depends on the reaction (Eq. (4.7)) that is, availability of reducing gas and $O^-_{2(ads)}$ species. The rejuvenation of the conductance takes place on removal of H_2S and the presence of ambient oxygen (Eq. (4.6)).

Xu et al. [119] described a more complex mechanism of H_2S detection in which water and sulphur dioxide is formed besides electrons creation. In the presence of H_2S gas, the reaction according to Eq. (4.8) takes place and

thereby forms H_2O and SO_2 gas by releasing electrons back to the conduction band, thus increasing the conductance of the sensor. Again on removal of H_2S the reaction (Eq. (6)) takes place leading to a decrease in the conductance. J. Kim and K. Yong [120] also reported the formation of SO_2 at temperature lower than 300^0C. The formation of SO_2 on the surface of ZnO was confirmed by the XPS studies performed.

$$2H_2S + 3O^-_{2(ads)} \leftrightarrow 2SO_2 + 2H_2O + 3e^- \quad (4.8)$$

For this reaction (eq. 4.8) to proceed to the right hand side, some amount of activation energy has to be provided thermally. An increase in operating temperature surely increases the thermal energy so as to stimulate the oxidation of H_2S. The reducing gas (H_2S) donates electrons to ZnO. Therefore the resistance of the film sensor decreases, or the conductance increases. At low temperature, the low sensitivity can be expected because the gas molecules do not have enough thermal energy to react with the surface adsorbed oxygen species. The point at which the gas sensitivity reaches maximum is the actual thermal energy needed for the reaction to proceed. This is the reason why the gas sensitivity increases with operating temperature. However, the response decreases at higher operating temperatures, as the oxygen adsorbates are desorbed from the surface of the sensor [115]. Also, at high temperatures the carrier concentration increases due to intrinsic thermal excitation and the Debye length decreases. This may be the reasons for the decreased gas response at high temperatures [121].

In addition to surface reaction with adsorbed oxygen species, chemical conversion of ZnO with H_2S is another possible reaction mechanism affecting conductivity of ZnO sensor. The chemical conversion of gas sensing materials through the direct reaction with target gas is known to be

an important mechanism that changes the conductivity and produces a high sensitivity in several sensing materials of metal oxides. For example, the chemical conversion of CuO nanoparticle to metallic copper sulphide (CuS) has been reported in H_2S sensing by Xue et al. [122] and formation of AuS by reaction of H_2S on the gold nanoparticles was also reported by Mahendra et al.[123]. Moreover, various types of complex reactions between ZnO and sulfur compounds (SO_x, H_2S, $(NH_4)_2S$, and so on.) have been reported from surface chemistry studies on ZnO [124-127]. Kim and Yong [120] reported the formation of ZnS on the surface of ZnO on exposure to H_2S gas at a temperature above 300^0C. The XPS studies revealed that at temperature above 300^0C, beside surface reaction with oxygen, H_2S also decomposes to form Zn-S bonds in ZnO; this change causes the formation of a shallow donor level and causes a drastic increase in conductivity.

Wang et al. [128] studied the sensitivity of ZnO to H_2S gas in the temperature range of 100 to 450^0C and reported the sulfuration of ZnO surface on exposure to H_2S gas. When the sensor was exposed to H_2S gas, the transformation of highly resistive ZnO into well-conducting ZnS led to the decrease of electrical resistance. The reactions in the response and recovery process can be represented as follows:

$$ZnO\ (s) + H_2S\ (g) \rightarrow ZnS\ (s) + H_2O\ (g) \qquad (4.9)$$

$$2\ ZnS\ (s) + 3O_2\ (g) \rightarrow 2\ ZnO\ (s) + 2\ SO_2\ (g) \qquad (4.10)$$

The Gibbs free energy, enthalpy and entropy for both sulfuration and desulfuration were calculated by the group and the results showed that both reactions are spontaneous. The recovery time for the gas sensors were found to be very high by this group. This was due to the slow desulfuration

process. As the temperature increased the rate of desulfuration process also increased and resulted in lower recovery time.

In our temperature dependent gas sensitivity measurements for pure and indium doped ZnO sensor (fig. 4.12 (a), 4.20 (a), 4.28 (a), 4.36 (a)) response decreases with the increase in temperature beyond 200^0C. In the response process, the sulfuration and desulfuration reactions take place at the same time. At 200^0C, the rate of sulfuration may be maximum. With increasing temperature, the desulfuration rate becomes greater while the sulfuration rate changes little, which results in a decrease of the amount of the ZnS formation and hence decreased sensitivity beyond 200^0C. When the sensor is operated at 200^0C, sulfuration can take place quickly while the desulfuration rate is still small. Hence the recovery time is large at this temperature compared to 225^0C. The recovery time vs temperature graphs in fig. 4.12 (c), 4.20 (c), 4.28 (c) and 4.36 (c) represents the larger recovery time at 200^0C compared to 225^0C. The recovery time of the sensor decreases with the increase in temperature which is attributed to the increase in the desulfuration rate as the temperature increases. The desulfuration process along with desorption of oxygen adsorbates at higher temperature contributes to the decrease in sensitivity beyond 200^0C.

In the presently studied indium doped ZnO films, the doping of In^{3+} increases the conductivity of ZnO due to enhancement in the electron density. Thus, in indium doped ZnO films, the In^{3+} facilitates formation of more number of O_{ads}^- species. But our gas sensing studies indicate a decrease in sensitivity due to indium doping (fig. 4.40). This decrease in sensitivity is attributed to the increase in free electron concentration and hence the change in resistance occurring due to the gas adsorption is very small compared to the increased carrier concentration.

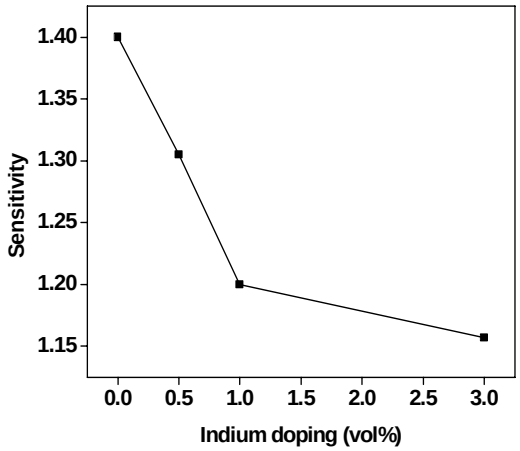

Fig. 4.40 Sensitivity at different indium doping % to 17.85ppm H_2S gas at respective optimum temperature

4.11 Conclusion

Pure and indium doped ZnO thin films of 500nm thickness were prepared by chemical spray pyrolysis method. Indium doping was done in the range of 0.5, 1 and 3vol%. The obtained films were annealed at 600^0C overnight prior to sensing characterization. The main conclusions drawn from the experimental results on pure and indium doped ZnO films are:

Crystalline structure of pure and indium doped ZnO sensor was mainly hexagonal wruzite structure. The average crystallite size for pure ZnO, 0.5vol%, 1vol%, and 3vol% indium doped thin film was found to be 38nm, 37nm, 39nm and 35nm respectively.

No separate peaks were found in the XRD peaks due to indium doping. Main reflections were obtained in the (30^0- 40^0) 2θ range corresponding to (100), (002) and (101) planes, the (101) plane being prominent. With the indium doping the intensity of (002) plane increased and (101) plane decreased indicating (002) as the preferred orientation.

Strong orientation of the doped films along (002) plane indicates the growth of grains along the c-axis.

The surface morphology and elemental composition were characterized by scanning electron microscopy and energy dispersive X-ray analysis. The undoped ZnO sensor shows particle with no definite shape. The indium doped sensor shows a much uniform particles with round shape and the surface appears to be more porous. The presence of indium was confirmed by EDS analysis.

The Raman studies indicate a decrease in intensity for the main peaks due to indium doping, which indicates an effective doping.

The temperature dependent gas sensing property of pure and indium doped ZnO sensor was investigated in order to find the optimal sensor operating temperature and sensor response to NO_2 test gas. Contrary to enhancement effect in sensitivity by the presence of additives, it was found that incorporation of indium decreases NO_2 gas sensing ability of the sensor. This decrease in sensitivity is attributed to the increase in free electron concentration and a consequent decrease in resistivity occurs due to replacement of Zn^{2+} cation by the In^{3+} cation, which acts as a donor. Hence the fractional change in resistance and thus sensor response as well, due to variation of the electron concentration when interacting with an oxidizing gas, like NO_2 will decrease with the indium doping.

The optimum operating temperature for pure and indium doped ZnO thin film sensor is 200^0C for NO_2 test gas.

The table 4.6 below presents the sensitivity of the sensors obtained, along with their optimal operating temperature, response and recovery time for the studied concentration of 7ppm NO_2 gas.

Table 4.6 Summary of 7 ppm NO_2 gas sensing results of pure and indium doped ZnO thin film sensor

Sensor	Sensitivity	Optimum temperature	Response time (sec)	Recovery time (min)
Pure ZnO	3.32	200^0C	6	2.26
ZnO+ 0.5 vol% Indium	2.20	200^0C	3	2.30
ZnO+ 1 vol% Indium	2.40	200^0C	5	2.80
ZnO+3 vol% Indium	2.41	200^0C	4	2.78

Temperature dependent H_2Sgas sensing behaviour of pure and indium doped ZnO is studied. Optimum operating temperature for pure and doped sensors for H_2S gas was found to be 200^0C. Indium doping was found to decrease the sensitivity of the sensor due to the increased free electron concentration.

Gas sensing behaviour of pure and indium doped ZnO to 17.85ppm of H_2S gas is tabulated in the table 4.7 below.

Table 4.7: Summary of H_2S gas sensing results of pure and indium doped ZnO

Sensor	Sensitivity	Optimum temperature	Response time (sec)	Recovery time (min)
Pure ZnO	1.40	200^0C	10	7.11
ZnO+ 0.5 vol% Indium	1.31	200^0C	8	10.73
ZnO+ 1 vol% Indium	1.20	200^0C	11	12.00
ZnO+3 vol% Indium	1.13	200^0C	13	2.13

Concentration dependent studies for both test gases were done at optimum operating temperature.

The results obtained from the gas sensing behaviour indicate that pure ZnO act as promising gas sensing candidate. The indium doping was found to decrease the gas sensor response.

References

[1] Z. L. Wang Journal of Physics: Condensed Matter (2004) 16, R829.

[2] Z. Fan and J. G. Lu Journal of Nanoscience and Nanotechnology (2005) 5, 1561.

[3] S. Baruah and J. Dutta Sci. Technol. Adv. Mater. (2009) 10, 013001.

[4] M. H. Huang, S. Mao, H. Feick, H. Yan, Y. Wu, H. Kind, E. Weber, R. Russo and P. Yang Science (2001) 292, 1897.

[5] R. P. Ried, E. Kim, D. M. Hong and R. S. Muller Journal of Microelectromechanical Systems (1993) 2,111.

[6] Y. Ito, K. Kushida, K. Sugawara and H. Takeuchi IEEE Transaction on Ultrasonics, Ferroelectrics, and Frequency Control (1995) 42, 316.

[7] W. Göpel and K. D. Schierbaum Sensors and Actuators B (1995) 26, 1.

[8] S. Tuzemen, G. Xiong, J. Wilkinson, B. Mischuck, K. B. Ucer and R. T. Williams Physica B (2001) 308, 1197.

[9] Y. R. Ryu, W. J. Kim and H. W. White Journal of Crystal growth (2000) 219,419.

[10] U. O¨ zgu¨r, Y. I. Alivov, C. Liu, A. Teke, M. A. Reshchikov, S. Dogan, V. Avrutin, S. J. Cho and H. Morkoc Journal of Applied Physics (2005) 98, 041301.

[11] T. Minami, H. Sato, H. Nanto and S. Takata Japanese Journal of Applied Physics (1984) 24, L781.

[12] V. E. Henrich and P. A. Cox The Surface Science of Metal Oxides Cambridge University Press U.K. (1994).

[13] G. Heiland Sensors and Actuators (1982) 2, 343.

[14] T. Seiyama, A. Kato, K. Fujiishi and M. Nagatani Anal. Chem. (1962) 34, 102.

[15] B. Bott, T. A. Jones and B. Mann Sensors and Actuators (1984) 5, 65.

[16] T. Yamazaki, S. Wada, T. Noma and T. Suzuki Sensors and Actuators B (1993) 13, 594.

[17] Y. Min, H. L. Tuller, S. Palzer, J. Wo¨llenstein and H. Bo¨ttner Sensors and Actuators B (2003) 93, 435.

[18] J. X. Wang, X. W. Sun, Y. Yang, H. Huang, Y. C. Lee, O. K. Tan and L. Vayssieres, Nanotechnology (2006) 17, 4995.

[19] L. J. Bie, X. N. Yan, J. Yin, Y. Q. Duan and Z. H. Yuan Sensors and Actuators B (2007) 126, 604.

[20] Z. Sadek, S. Choopun, W. Wlodarski, S. J. Ippolito and K. K. Zadeh Journal of IEEE Sensors (2007) 7, 919.

[21] M. Tonezzer and R. G. Lacerda Sensors and Actuators B (2010) 150,517.

[22] H. T. Wang, B. S. Kang, F. Ren, L. C. Tien, P. W. Sadik, D. P. Nortan, S. P. Pearton and J. Lin Appl. Phys. Lett. (2005) 86, 243503.

[23] M. Egashira, N. Kanehara, Y. Shimizu and H .Iwanaga Sensors and Actuators (1989) 18, 349.

[24] N. J. Dayany, S. R .Sainkarz, R. N. Karekary and R. C. Aiyery Meas. Sci. Technol. (1998) 9,360.

[25] N. J. Dayan, S. R. Sainkar, R. N. Karekar and R. C. Aiyer Thin Solid Films (1998) 325,254.

[26] Y. Liu, T. Hang, Y. Xie, Z. Bao, J. Song, H. Zhang and E. Xie Sensors and Actuators B (2011) 160, 266.

[27] O. Lupan, L. Chow, Th. Pauport´e, L. K. Ono ,B. R. Cuenya and G. Chai Sensors and Actuators B (2012) 173, 772.

[28] A. Jones, T. A. Jones, B. Mann and J. G. Firth Sensor and Actuators (1984) 5, 75.

[29] D. H. Yoon and G. M. Choi Sensors and Actuators B (1997) 45, 251.

[30] H. W. Ryu, B. S. Park, S. A. Akbar, W. S. Lee, K. J. Hong, Y. J. Seo, D. C. Shin, J. S. Park and G. P. Choi Sensors and Actuators B (2003) 96, 717.

[31] M. R. Yu, R. J. Wu and M. Chavali Sensors and Actuators B (2011) 153, 321.

[32] N. F. Hamedani, A. R. Mahjou, A. A. Khodadadi and Y. Mortazavi Sensors and Actuators B (2011) 156, 737.

[33] B. Shouli, L. Xin, L. Dianqing, C. Song, L. Ruixian and C. Aifan Sensors and Actuators B (2011) 153, 110.

[34] J. F. Chang, H. H. Kuo, I. C. Leu and M. H. Hon Sensors and Actuators B (2002) 84, 258.

[35] N. L. Hung, H. Kim, S. K. Hong and D. Kim Sensors and Actuators B (2010) 151,127.

[36] P. Rai, Y. S. Kim, H. M. Song, M. K. Song and Y. T. Yu Sensors and Actuators B (2012) 165,133.

[37] P. Rai and Y. T. Yu Sensors and Actuators B (2012) 173, 58.

[38] S. Matsushima, D. Ikeda, K. Kobayashi and G. Okada Sensors and Actuators B (1993) 14, 621.

[39] C. Baratto, G. Sberveglieri, A. Onischuk, B. Caruso and S. di Stasio Sensors and Actuators B (2004) 100, 261.

[40] Y. Min, H. L. Tuller, S. Palzer, J. Wo¨llenstein and H. Bo¨ttner Sensors and Actuators B (2003) 93, 435

[41] P. S. Cho K. W. Kim and J.H. Lee J. Electroceramics (2006) 17, 975.

[42] E. Oh, H. Y. Choi, S. H. Jung, S. Cho, J. C Kim, K. H. Lee, S. W. Kang, J. Kim, J. Y. Yun and S. H. Jeong Sensors and Actuators B (2009) 141, 239.

[43] D. Calestani, M. Zha, R. Mosca, A. Zappettini, M. C. Carotta, V. Di Natale and L. Zanotti Sensors and Actuators B (2010) 144, 472.

[44] M. Chen, Z. Wang, D. Han, F. Gu and G. Guo Sensors and Actuators B (2011) 157, 565.

[45] S. C. Navale, V. Ravia, I. S. Mulla, S. W. Gosavi and S. K. Kulkarni Sensors and Actuators B (2007) 126, 382.

[46] S. T. Shishiyanu, T. S. Shishiyanu and O. I. Lupan Sensors and Actuators B (2005) 107, 379.

[47] N. Koshizaki and T. Oyama Sensors and Actuators B (2000) 66, 119.

[48] P. Rai, Y. S. Kim, H. M. Song, M. K. Song and Y. T. Yu Sensors and Actuators B (2012) 165, 133.

[49] V. Kruefu, C. Liewhiran, A. Wisitsoraat and S. Phanichphant Sensors and Actuators B (2011) 156, 360.

[50] H. Nanto, T. Minami and S. Takata Journal of Applied Physics (1986) 60, 482.

[51] G. S. T. Rao and D. T. Rao Sensors and Actuators B (1999) 55, 166.

[52] Y. Zeng, Z. Lou, L. Wang, B. Zou, T. Zhang, W. Zheng and G. Zou Sensors and Actuators B (2011) 156,395.

[53] D. R. Patil, L. A. Patil and P. P. Patil Sensors and Actuators B (2007) 126, 368.

[54] P. Chatterjee, P. Mitra and A. K. Mukhopadhyay Journal of Material Science. (1999) 34, 4225.

[55] N. Zhang, K. Yu, Q. Li, Z. Q. Zhu and Q. Wan Journal of Applied Physics (2008) 103, 104305.

[56] S. S. Badadhe and I. S. Mulla Sensors and Actuators B (2009) 143, 164.

[57] N. S. Ramgir, M. Ghosh, P. Veerender, N. Datta, M. Kaur, D. K. Aswal and S. K. Gupta Sensors and Actuators B (2011) 156, 875.

[58] S. Basu and A. Dutta Materials Chemistry and Physics (1997) 47, 93.

[59] P. Mitra, A. P. Chatterjee and H. S. Maiti Materials Letters (1998) 35, 33.

[60] V. R. Shinde, T. P. Gujar and C. D. Lokhande Sensors and Actuators B (2007) 120, 551.

[61] V. R. Shinde, T. P. Gujar, C. D. Lokhande, R. S. Mane and S. H. Han Sensors and Actuators B (2007) 123, 882.

[62] V. R. Shinde, T. P. Gujar and C. D. Lokhande Sensors and Actuators B (2007) 123, 701.

[63] P. P. Sahay and R. K. Nath Sensors and Actuators B (2008) 133, 222.

[64] D. S. Dhawale, D. P. Dubal, A. M. More, T. P. Gujar and C. D. Lokhande Sensors and Actuators B (2010) 147, 488.

[65] K. V. Gurav, P. R. Deshmukh and C. D. Lokhande Sensors and Actuators B (2011) 151, 365.

[66] X. L. Cheng, H. Zhao, L. H. Huo, S. Gao and J. G. Zhao Sensors and Actuators B (2004) 102, 248.

[67] P. P. Sahay and R. K. Nath Sensors and Actuators B (2008) 134, 654.

[68] C. S. Prajapati and P. P. Sahay Sensors and Actuators B (2011) 160, 1043.

[69] J. Xu, Q. Pan, Y. Shun and Z. Tian Sensors and Actuators B (2000) 66, 277.

[70] P. Bhattacharyya, P. K. Basu, H. Saha and S. Basu Sensors and Actuators B (2007) 1124, 62.

[71] X. Chu, T. Chen, W. Zhang, B. Zheng and H. Shuia Sensors and Actuators B (2009) 142, 49.

[72] N. Han, L.Chai, Q. Wang, Y.Tian, P. Deng and Y. Chen Sensors and Actuators B (2010) 147, 525.

[73] R. Raju and C. N. R. Rao Sensors and Actuators B (1991) 3, 305.

[74] I. Stambolov, K. konstantinov, S. Vassilev, P. Peshev and T. Tsachev Materials Chemistry and Physics (2000) 63,104.

[75] P. Feng, Q. Wan and T. H. Wang Appl. Phys. Lett. (2005) 87, 213111.

[76] L. J. Bie, X. N. Yan, J. Yin, Y. Q. Duan, and Z. H. Yuan Sensors and Actuators B (2007) 126, 604.

[77] Z. Yang, Y. Huang, G. Chen, Z.Guoc, S. Cheng and S. Huang Sensors and Actuators B (2009) 140, 549.

[78] M. Kim, H. R. Kim, K.-Il Choi, H. J. Kim and J. H. Lee Sensors and Actuators B (2011) 155 745.

[79] T. T. Trinh, N. H. Tu, H. H. Le, K. Y. Ryu, K. B. Le, K. Pillai and J. Yi Sensors and Actuators B (2011) 152, 73.

[80] L. Zhang, J. Zhao, H. Lu, L. Li, J. Zheng, H. Li and Z. Zhu Sensors and Actuators B (2012) 161, 209.

[81] J. Chen, X. Yan, W. Liu and Q. Xue Sensors and Actuators B (2011) 160, 1499.

[82] N. F. Hamedani, A. R. Mahjoub, A. A. Khodadadi, Y. Mortazavi Sensors and Actuators B (2012) 169, 67.

[83] P. Singh, V. N. Singh, K. Jain and T. D. Senguttuvan Sensors and Actuators B (2012) 166, 678.

[84] K. Inoue and M. Miyayama Journal of Electroceramics (1998) 2, 41.

[85] D. R. Patil and L. A. Patil Sensors and Actuators B (2007) 123, 546.

[86] N. Tamaekong, C. Liewhiran, A. Wisitsoraat and S. Phanichphant Sensors and Actuators B (2011) 152, 155.

[87] L. Liu, S. Li , J. Zhuang, L. Wang, J. Zhang, H. Li , Z. Liu, Y. Hana, X. Jiang and P. Zhang Sensors and Actuators B (2011) 155, 782.

[88] X. Wang, W. Wang and Y. L. Liu Sensors and Actuators B (2012) 168, 39.

[89] H. Nanto, H. Sokooshi and T. Kawai Sensors and Actuators B (1993) 13, 715.

[90] H. Nanto, H. Sokooshi, and T. Usuda Sensors and Actuators B (1993) 10, 79.

[91] H. Tang, M. Yan, H. Zhang, S. Li, X. Ma, M. Wang and D. Yang Sensors and Actuators B (2006) 114, 910.

[92] D. Sivalingam, J. B. Gopalakrishnan and J. B. B. Rayappan Sensors and Actuators B (2012) 166, 624.

[93] L. Zhang, J. Zhao, H. Lu, L. Li, J. Zheng, J. Zhang, H. Li and Z. Zhu Sensors and Actuators B (2012) 171,1101.

[94] M. Olvera, H. Gomez and A. Maldonado Sol. Energy Mater. Sol. Cells (2007) 91, 1449.

[95] S. Major, A. Banerjee and K. L. Chopra Thin Solid Films (1985) 125, 179.

[96] T. V. Vimalkumar, N. Poornima, C. Sudha Kartha, K. P. Vijayakumar, T. Abe and Y. Kashiwab, Physica B (2010) 405, 4957.

[97] C. Charpentier, P. Prod'homme, I. Maurin, M. Chaigneau, and P. R. Cabarrocas EPJ Photovoltaics (2011) 2, 25002.

[98] H. Zhou, L. Chen, V. Malik, C. Knies, D. M. Hofmann, K. P. Bhatti, S. Chaudhary, P. J. Klar, W. Heimbrod, C. Klingshirn and H. Kalt Phys. Status Solidi a (2007) 204, 112.

[99] J. Z. Wang, M. Peres, J. Soares, O. Gorochov, N. P. Barradas, E. Alves, J. E. Lewis, E. Fortunato, A. Neves and T. Monteiro Journal of Phys. Condens. Matter (2005) 17, 1719.

[100] K. F. Lin, H. M. Cheng, H. C. Hsu and W. F. Hsieh Appl. Phys. Lett. (2006) 88, 263117.

[101] K. A. Alim, V. A. Fonoberov, M. Shamsa and A. A. Balandin Journal of Appl. Phys. (2005) 97,124313

[102] S. S. Lo, D. Huang, C. H. Tu, C. H. Hou and C.C. Chen Journal of Phys. D: Appl. Phys. (2009) 42, 095420.

[103] X. L. Xu, S. P. Lau and B. K. Tay Thin Solid Films (2001) 398, 244.

[104] X. L. Xu, S. P. Lau, J. S. Chen, G. Y. Chen and B. K. Tay Journal of Crystal Growth (2001) 223, 201.

[105] M. Rajalakshmi, A. K. Arora, B. S. Bendre and S. Mahamuni Journal of Appl. Phys. (2000) 87, 2445.

[106] T. C. Damen, S. P. S. Porto and B. Tell Phys. Rev. (1966) 142, 570.

[107] J. M. Calleja and M. Cardona Phys. Rev. B (1977) 16, 3753.

[108] A. Rothschild and Y. Komem Journal of Appl. Phys. (2004) 95, 6374.

[109] M. E. Franke, T. J. Koplin and U. Simon Small (2006) 2, 36.

[110] S. Major, A. Banerjee and K. L. Chopra Thin Solid Films (1986) 143, 19.

[111] J. Dayan, S. R. Sainkar, R. N. Karekar and R. C. Aiyer, Thin Solid Films (1998) 325, 254.

[112] J. Marc, S. Madau and R. Morrison, Chemical sensing with Solid State Devices, Academic Press New York (1989).

[113] M. Takata, D. Tsubone and H. Yanagida, Journal of American Ceram. Soc. (1976) 59, 4.

[114] Y. Ma, W. L. Wang, K. J. Liao and C. Y. Kong Journal of Wide Bandgap Materials (2002) 10,113.

[115] H. Windichmann and P. Mark Journal of Electrochem. Soc. (1979) 126, 627.

[116] R. Ferro, J. A. Rodríguez and P. Bertrand Thin Solid Films (2008) 516, 2225

[117] S. R. Morrison, Sensors and Actuators B (1982) 2, 329.

[118] A. Rodriguez, T. Jirsak, J. Dvorak, S. Sambasivan and D. Fischer Journal of Phys. Chem. B (2000) 104, 319.

[119] J. Xu, X. Wang and J. Shen Sensors and Actuators B (2006) 115, 642.

[120] J. Kim and K.Yong Journal of physical chemistry C (2011) 115, 7218.

[121] J. Mizsel Sensors and Actuators B (1995) 23, 173.

[122] X. Xue, L. Xing, Y. Chen, S. Shi, Y.Wang and T. Wang Journal of Physical Chemistry C (2008) 112, 12157.

[123] D. Shirsat, M. A. Bangar, M. A. Deshusses, N. V. Myung and A. Mulchandani Appl. Phys. Lett. (2009) 94, 083502.

[124] S. Chaturvedi, J. A. Rodriguez, T. Jirsak and J. Hrbek Journal of. Physical Chemistry. B (1998) 102, 7033.

[125] L. Dloczik, R. Engelhardt, K. Ernst, S. Fiechter, I. Sieber and R. Konenkamp Appl. Phys. Lett. (2001) 78, 3687.

[126] J. A. Rodriguez, T. Jirsak, S. Chaturvedi and M. Kuhn Surf. Sci. (1999) 442, 400.

[127] J. J. Uhlrich, R. Franking, J. Hamers and T. F. Kuech Journal Physical Chemistry C (2009) 113, 21147.

[128] D. Wang, X. Chu and M. Gong Nanotechnology (2007) 18,185601.

Chapter 5

Gas Sensors Based on Pure and Copper Doped Indium Oxide

Thick film gas sensors based on pure and copper doped indium oxide were fabricated on glass substrates and studied for NO_2 and H_2S gas sensing properties. The copper doping concentration was varied in the range 0.5, 1.5 and 3wt%. The structural properties, surface morphology and compositional analysis of the prepared sensors were done. The optimum operating temperature, response time, recovery time and concentration dependent studies for both test gases were obtained for pure and doped sensors. The detection mechanism for both the test gases to pure and doped sensors was also discussed.

5.1 Introduction

Indium oxide (In_2O_3) is a wide band gap n-type semiconductor with an energy band gap 3.6 eV[1]. The wide band gap renders In_2O_3 with high optical transparency and makes it an important material for different applications. It has been widely used in window heaters, solar cells, and liquid crystal displays [2]. Properties as high transparency in the visible region and high electrical conductivity make In_2O_3 a suitable material for application in solar cells [3, 4], optoelectronic devices [5], liquid crystal displays [6], light emitting diodes [7, 8], photo voltaic devices etc.. Several deposition techniques have been used for the deposition of In_2O_3 films including chemical vapour deposition [9], RF and DC sputtering [10, 11], sol gel [12, 13], spray pyrolysis [14, 15] and electrostatic spray deposition technique [16].

Two crystal structures have been reported for In_2O_3, i.e., the bixbyite structure (rare-earth oxide-structure) which has a body centred cubic structure with space group Ia3 and lattice parameter a = 10.118Å (JCPDS 06-0416) and the metastable corundum (a-Al_2O_3) structure which has a rhombohedral structure with space group R-3c and lattice parameters a = 5.484 Å and c = 14.508 Å (JCPDC 22-336). The rare-earth structure can be transformed into the corundum structure at high temperatures (1000^0C) and high pressure (65Kbar) [17]. Recently, Yu et al [18] have obtained rh-In_2O_3 nanofibers templated from InOOH nanofibers under ambient pressure.

In_2O_3 cubic form is the most stable one and the most used. In the cubic form, the cations form a nearly cubic face-centered lattice in which six out of the eight tetrahedral sites are occupied by oxygen ions. The unit cell of the crystal structure consists of eight such cubes, containing 32 cations and 48 O^{-2} ions. Two nonequivalent cation sites, called ''C'' and ''D'', both with 6-fold oxygen coordination, characterize the structure. The site D is axially symmetric and can be described as a cation surrounded by six oxygen ions at the corners of a distorted cube, leaving free two corners of a diagonal body. For site C the cube is more distorted and the six oxygen ions leave free two corners of a face diagonal (Fig. 5.1) [19]. The density and melting point of bcc-In_2O_3 have been reported to be 7.18 g/cm^3 and 1912^0C, respectively [20]. A thermal expansion coefficient of *7.20* ± 0.06 1/K [21], thermal capacity of 99.01 J/Kmol at 300 K [22], permittivity (ε_∞) of 4 [23] and refraction index in the visible range of 2.0 ± 0.1 [24] was reported in the literature.

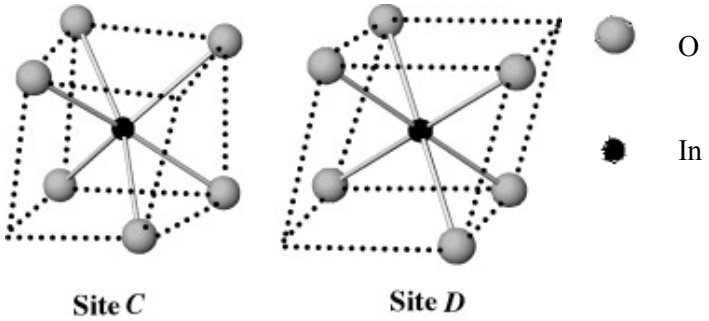

Fig. 5.1 The nearest –neighbor oxygen distribution around each cationic site C and D in the In_2O_3 bixbyite structure.

In_2O_3 in stoichiometric form is an insulator and in non-stoichometric form is an n-type semiconductor material. As the surface conductance mechanism is influenced by the semiconductor metal oxide (SMO) material's non-stoichiometric composition, the non-stoichiometry of In_2O_3 will be discussed. The chemical formulas for oxides and inorganic compounds are usually written to indicate that there is a definite ratio of cations to anions in the compound, e.g. M_aO_b, where a and b are usually small integers determined by the valency of constituents atoms. When the oxide M_aO_b does contain M and O atoms in the exact ratio a/b, it is said to have a stoichiometric composition. However numerous metal oxides exhibits marked deviation from stoichiometry. In a compound, non-stoichiometry is equivalent to the presence of point defects in the crystal lattice compared to the stoichiometric conditions and the extent of nonstoichiometry is measured by the net concentration of the corresponding defects. Non-stoichiometry in metal oxides can be of two main types with respect to stoichiometric composition [25].

1) Oxygen deficient (or excess metal) - the main defects can be either oxygen vacancies or interstitial metal ions (excess metal), both of these defects lead to the formation of complimentary free electrons.

Therefore the conductivity is due to the transport of electrons and oxygen deficient oxides are characterized by n-type conductivity.

2) Metal deficient (or excess oxygen) - the predominant defects can be either metal vacancies or interstitial oxygen atoms (excess oxygen). The formation of charged metal ion vacancies leads to the formation of complimentary positive (charge carriers, holes). Therefore the conductivity involves the transport of holes and metal deficient oxides are characterised by p-type conductivity [25].

Generally, In_2O_3 crystal structure is not ideal since oxygen vacancies are present. In an In_2O_3 film an oxygen deficiency is observed mainly in the form of oxygen vacancies [26]. These act as doubly charged donors providing electrons to the conduction band. However, it has also been reported that In_2O_3 films oxygen deficient non-stoichiometry might be due to the presence of excess indium compared to the stoichiometric composition [27]. In this case, the dominant defects are interstitial In^{3+} cations but the possible contributions of these defects to the conductivity are low**.** Therefore, it can be stated that the main contributors to the conductivity of the oxygen deficient non-stoichiometric In_2O_3 films are the oxygen vacancies. Oxygen vacancies dominate the conduction mechanism of In_2O_3. The accurate formula of In_2O_3 is In_2O_{3-x} $(V_O)_x$, where V_O is donor-like doubly-charged oxygen vacancy, and x is the oxygen vacancy portion and depends on the oxidation state. Thus, a variety of electrical properties can be obtained (metallic, semiconducting, or insulating behaviour) depending on the stoichiometry, without any further impurity doping.

The electrical properties of In_2O_3 thin films reported in the literature for semiconducting, or insulating In_2O_3 have been obtained by different methods [28]. Among them, doping, variation of growth parameter and post

annealing are frequently used. Doping In_2O_3 with Sn is used often to fabricate the ITO films used as transparent conducting electrodes. In order to alter the electrical properties, variation of growth parameters, such as the growth temperature and the content of the process gas, have frequently been used. Adurodija et al. varied substrate temperature and oxygen pressure by means of a pulsed laser deposition process [29]. By increasing the oxygen pressure, the electron density can be reduced by two orders of magnitude. By optimizing the substrate temperature, the electron density can be further reduced by one order of magnitude, while the electron mobility remains nearly constant. Similar results were obtained by Yamada et al. [30]. By varying the He/O_2 pressure in a pulsed laser ablation process, the volume resistivity can be increased from ~ 10^{-3} Ωcm up to more than 10^2 Ωcm. One of the other important methods to change the electrical properties is post annealing. Post annealing parameters, such as annealing atmosphere, gas content (normally oxygen content), and annealing temperature, can also change the electrical properties drastically [31-34]. Oxygen gas annealing can significantly increase the film resistivity as well as the internal stress of the film, which can arise at an annealing temperature as low as 100°C [31]. Alam et al. reported that by changing the annealing temperature, the film resistivity can also be altered by more than one order of magnitude [32].

In_2O_3 in non-stoichiometric form is an n-type semiconductor material suitable for gas sensing applications [35]. During recent years In_2O_3 became a very interesting material for gas sensor applications, being the best material which allows detection of ozone in the ppb range [36]. In 1993 Takada first reported an O_3 sensor using an In_2O_3 thin film [37]. Since then different deposition techniques, e.g. spray pyrolysis, spin coating, sol-gel method and magnetron sputtering have been used to enhance the sensitivity of In_2O_3 thin films [38]. The sensitivity of In_2O_3 can be attributed to the

oxygen vacancies in the films; by controlling the oxygen deficiency, the conductivity of In_2O_3 films can be altered [35]. For the application as a gas sensing material, the electrical properties of this material are very important.

5.2 Review of In_2O_3 for Gas Sensing

A short review of In_2O_3 gas sensors for the detection of Ozone (O_3), Hydrogen (H_2), Carbon monoxide (CO), Hydrogen Sulphide (H_2S), Nitrogen dioxide (NO_2), Nitric oxide(NO) is given in tables below (Table 5.1-5.6).

Table 5.1: Summary of published results on O_3 gas sensing characteristics of In_2O_3

Material	Concentration (ppm)	Temperature (^{0}C)	*Sensitivity	Year (reference)	Method of preparation
O_3(ozone)					
In_2O_3 : MoO_3	1	200	4	1998	Sol-gel [39]
In_2O_3: Au	0.03	300	40	1999	RF sputtering [40]
In_2O_3:Fe_2O_3	0.1	550	10	2000	Thick film paste [41]
In_2O_3:MoO_3	0.2	130	22	2001	Sol-gel [42]
In_2O_3:Fe_2O_3	0.1	135	450	2003	Sol-gel [43]
In_2O_3	1	270	1000	2005	Spray pyrolysis [44]
In_2O_3:Fe_2O_3	0.08	250	28.3	2006	Rheotaxial growth and thermal oxidation (RGTO) deposition [45]
In_2O_3 nanowires	0.280	400	10	2007	Evaporation [46]
In_2O_3	0.200	200	600	2008	Sol-gel [47]

* The sensitivity values presented in this table are taken directly from the respective literature. Their magnitude cannot be compared as different authors have used different formula to calculate sensitivity. The main intent of this table is to highlight the published results on In_2O_3 based gas sensors.

Table 5.2: Summary of published results on O_3 gas sensing characteristics of In_2O_3

Material	Concentration (ppm)	Temperature (^{0}C)	*Sensitivity	Year (reference)	Method of preparation
H_2(Hydrogen)					
In_2O_3 : Pd	400	220	531	1993	Vaccum evaporated [48]
In_2O_3	1000	350	88	1998	Spin coating [49]
In_2O_3 : Ho_2O_3	100	195	4.5	2006	Sol-gel [50]
In_2O_3:SnO_2	50	300	2.42	2009	Thick film paste [51]
In_2O_3:ZnO	2000	350	7	2011	Vapour deposition [52]

Table 5.3: Summary of published results on CO gas sensing characteristics of In_2O_3

Material	Concentration (ppm)	Temperature (^{0}C)	*Sensitivity	Year (reference)	Method of preparation
CO (Carbon monoxide)					
In_2O_3	1000	350	44	1998	Spin coating [49]
In_2O_3 : Ho_2O_3	100	195	47	2006	Sol-gel [50]
In_2O_3 :SnO_2	1000	300	7.5	2008	Sol-gel [53]
In_2O_3	50	250	4	2008	Sol-gel [54]
In_2O_3:SnO_2	50	300	1.56	2009	Thick film paste [51]
In_2O_3 Hollow spheres	10	400	3.81	2009	Thick film paste [55]
In_2O_3 nanofibers	100	300	5	2010	Electrospinning [56]
In_2O_3:Zn nanowires	400	300	22	2012	Vapour deposition [52]

Table 5.4: Summary of published results on H_2S gas sensing characteristics of In_2O_3

Material	Concentration (ppm)	Temperature (^{0}C)	*Sensitivity	Year (reference)	Method of preparation
H_2S					
In_2O_3 : Ho_2O_3	10	195	1061	2006	Sol-gel [50]
In_2O_3	50	269	125	2006	Thick film paste [57]
In_2O_3 whiskers	10	Room temperature	30	2008	Thin film [58]
In_2O_3:SnO_2	10	300	4.98	2009	Thick film paste [51]
In_2O_3 nanotubes	20	Room temperature	166	2010	Electrospinning [59]

Table 5.5 :Summary of published results on NO_2 gas sensing characteristics of In_2O_3

Material	Concentration (ppm)	Temperature (^{0}C)	*Sensitivity	Year (reference)	Method of preparation
NO_2					
In_2O_3 : SnO_2	250	250	7.5	1988	RF magnetron sputtering [60]
In_2O_3	1	150	60	1997	Sol-gel [61]
In_2O_3 : MoO_3	1	250	23	1998	Sol-gel [39]
In_2O_3	0.7	250	10	2000	Sol-gel [62]
In_2O_3	0.7	250	7	2000	High vacuum thermal evaporation [62]
In_2O_3-NiO	1 ppm	150	40	2000	Sol-gel [63]
In_2O_3	10 ppm	350	212	2000	R.F sputtering [64]
In_2O_3 :Au	10 ppm	350	14.26	2001	R.F sputtering [65]
In_2O_3	0.500	54	1000	2002	Laser ablation [66]
In_2O_3:Fe_2O_3	5	100	600	2003	Sol-gel [43]
In_2O_3 : SnO_2	5	250	175	2006	Sol-gel [67]
In_2O_3 : Gd_2O_3	100	195	79	2006	Sol-gel [50]
In_2O_3:Fe_2O_3	0.5	135	75	2007	Sol-gel [68]
In_2O_3 nanowires	1	250	2.57	2008	Thick film paste [69]
In_2O_3	10	250	154	2010	Thick film paste [70]
In_2O_3 nanoribbon	5	200	70	2012	Electrospinning method [71]
In_2O_3	6	200	61	2012	AC electrophoresis deposition [72]
In_2O_3	0.050	Room temperature	32	2012	Thick film paste [73]
In_2O_3 microspheres	5	250	1.5	2013	Thick film paste [74]
In_2O_3 microspheres	0.500	150	74	2013	Thick film paste [75]

Table 5.6: Summary of published results on NO gas sensing characteristics of In_2O_3

Material	Concentration (ppm)	Temperature (^{0}C)	*Sensitivity	Year (reference)	Method of preparation
NO					
In_2O_3:Se	3	150	8	1999	Thermal evaporation [76]
In_2O_3	0.500	54	100	2002	Laser ablation [66]
In_2O_3	100	150	10000	2008	Metal organic chemical vapor deposition [77]
In_2O_3	10	150	25	2010	Thick film paste [78]
In_2O_3:Au	25	500	25	2010	RF Sputtering [79]

In addition to the detection of above gases, In_2O_3 based gas sensors are used for the detection of alcohol vapour [80] , ethanol [53, 81-83], ammonia [84,85], methanol [86], humidity [87] propane [88], Acetone [89], formaldehyde [89,90] toluene [89, 91, 92], Heptanes [89] .

5.3 Motivation of the Work

Compared to other semiconducting metal oxides like ZnO, WO_3, SnO_2, In_2O_3 is a comparatively new candidate for gas sensing studies. The literature review shows that in pure form itself the material is a very good sensor for the detection of many gases and vapour. In the present work the gas sensing properties of pure and doped In_2O_3 thick film sensor to the test gases NO_2 and H_2S is studied. In our studies the dopant used for enhancing the gas sensing property of pure In_2O_3 sensor is copper. The effect of copper doping on the gas sensing properties of In_2O_3 had not studied yet. This chapter deals with the preparation of nanopowders, fabrication of gas sensor, characterization and

gas sensing properties of pure and copper doped In_2O_3 sensor. The structural properties, surface morphology and compositional analysis of obtained materials were characterized with XRD, Raman Spectroscopy, SEM and EDS. Sensors were evaluated at different working temperature under one concentration of the target gas in air to find the optimum working temperature. Sensor response to different concentration of target gas is studied at this optimum temperature. The mechanism involved in the detection of pure and copper doped tungsten oxide to both NO_2 and H_2S gas is also discussed.

5.4 Gas Sensor Fabrication

99.999% pure In_2O_3 powder was purchased from Sigma Aldrich. The powder was thoroughly powdered in mortar. For the preparation of pure In_2O_3 sensors the mortar powdered In_2O_3 powder was used. Copper doping in In_2O_3 was done by powder impregnation method. Depending upon the wt% of copper doping, known amount of copper acetate monohydrate was dissolved in water. The required ml of dissolved copper acetate solution is added drop wise into pre determined amount of In_2O_3 powder. The resultant mixture was thoroughly stirred continuously for two days. It was then dried at 100^0C overnight. The copper doping concentration was varied from 0.5, 1.5 and 3wt%. For fabrication of thick film sensor the powder was dispersed in methanol, coated on substrate and annealed at an ~ temperature of 600^0C overnight. The films thus prepared had an approximate thickness of 20µm

5.5 Structural and Spectroscopic Characterization

5.5.1 XRD Characterization

The crystalline structure and particle size of the 600^0C annealed pure and copper doped In_2O_3 thick film sensor were examined by X-ray diffraction measurement (XRD, Bruker AXS D8 Advance). Fig. 5.2 shows

the XRD spectra of pure and copper doped In_2O_3 annealed at 600^0C overnight. The 0.5, 1.5 and 3wt% copper doped In_2O_3 sensors are denoted as I + 0.5wt% Cu, I + 1.5wt% Cu and I + 3wt% Cu respectively. The XRD spectrum revealed the cubic bixbyite phase with preferred (222) orientation (JCPDS CAS No .06-0416). Therefore the thick film sensor of pure and doped In_2O_3 obtained after annealing at 600^0C was crystalline in nature. No additional peaks were observed due to copper doping. A small shift for (222) peak was observed towards lower theta side, probably due to copper doping. The intensity of all the major peaks was found to decrease with copper doping.

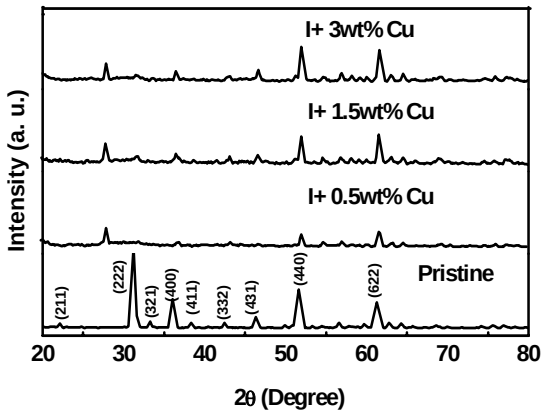

Fig. 5.2 XRD patterns of pure and copper doped In_2O_3 thick film sensor annealed at 600^0C

The crystallite size (D) was calculated from peak broadening using the Scherrer approximation, which is defined as

$$D = \frac{0.9\lambda}{B\cos\theta} \tag{5.1}$$

Where λ is the wavelength of the X-ray (1.5418 A^0), B is the full width at half maximum (FWHM, radian) and θ is the Bragg angle (degree). The particle size was estimated individually from the FWHM of each plane and the average of all the planes were taken to obtain the average particle size.

The average particle size of the pure In_2O_3 , 0.5wt%, 1.5wt%, 3wt% copper doped thick film sensor were found to be 24nm, 23nm, 24nm and 25nm respectively. Hence the pure and copper doped sensor obtained after annealing was identified by XRD as nanocrystalline in nature.

5.5.2 Scanning Electron Microscopy

Fig. 5.3 shows the SEM image of pure and copper doped In_2O_3 thick film sensor annealed at 600^0C overnight. Highly textured films were obtained after annealing at 600^0C.

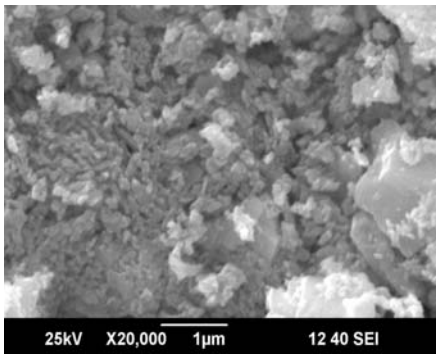

(a) SEM image of pure In_2O_3 thick film sensor

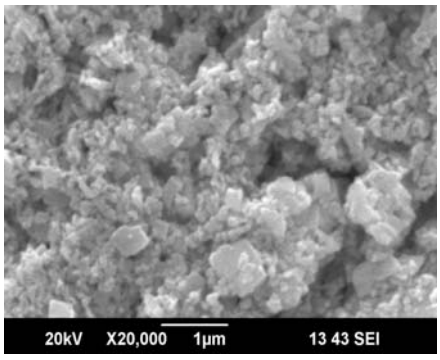

(b) SEM image of 0.5wt% copper doped In_2O_3 thick film sensor

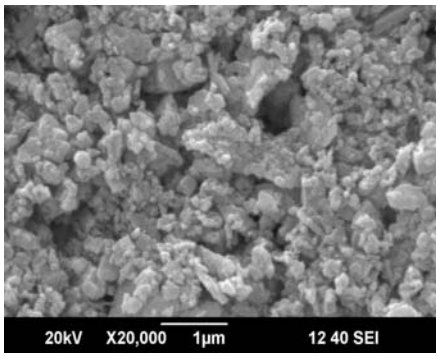

(c) SEM image of 1.5wt% copper doped In_2O_3 thick film sensor

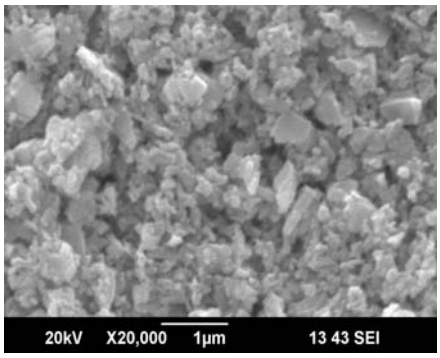

(d) SEM image of 3wt% copper doped In_2O_3 thick film sensor

Fig. 5.3 SEM images of pure and copper doped In_2O_3 thick film sensor

Separate particles are not visualized in the SEM images. Mainly particle agglomeration was found in the thick film sensors. Particles with not much definite shape are found in the SEM images for both pure and copper doped In_2O_3 sensors. Copper addition did not show any effect on the surface morphology or particle size of the sensor elements as confirmed by the XRD results.

5.5.3 EDS

The EDS spectrum of 600^{0}C annealed pure In_2O_3 thick film sensor obtained is shown in fig. 5.4. Spectrum reveals presence of indium and oxygen elements only. Fig. 5.5 shows the EDS spectrum of 3wt% copper doped In_2O_3 thick film sensor. Spectrum gives clear evidence for presence of copper in the doped samples.

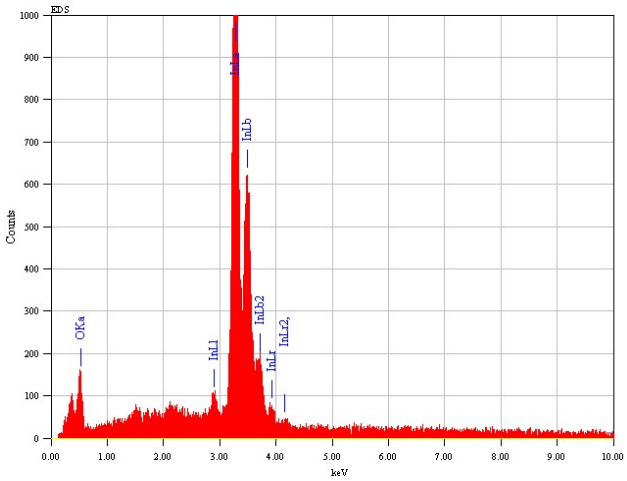

Fig. 5. 4 EDS spectrum of 600^{0}C annealed pure In_2O_3 thick film sensor.

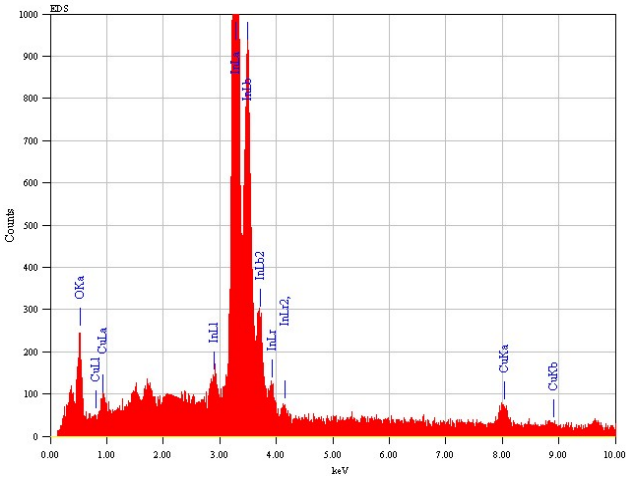

Fig. 5.5 EDS spectrum of 600^{0}C annealed 3wt% copper doped In_2O_3 thick film sensor.

5.5.4 Raman Spectroscopy

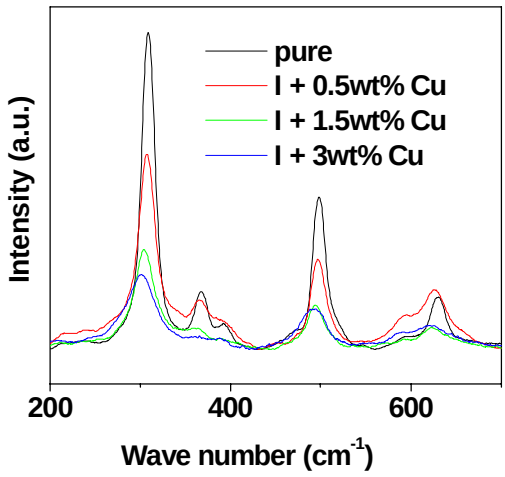

Fig. 5.6 Raman spectra of 600^{0}C annealed pure and copper doped In_2O_3 thick film sensor

Raman spectroscopy was used to further investigate the local chemical structure of the In_2O_3 based sensor films. The Raman spectrum of pure and

copper doped In_2O_3 thick film sensor is shown in fig. 5.6. The 0.5, 1.5 and 3wt% copper doped In_2O_3 sensors are denoted as I + 0.5wt% Cu, I + 1.5wt% Cu and I + 3wt% Cu respectively. Peaks are observed at 308, 367, 497, and 630 cm^{-1} and these are in general agreement with those values previously reported in the literature [92, 93]. The peak at 308 cm^{-1} corresponds to the $\delta(InO_6)$ bending vibration of InO_6 octahedra. The 367 cm^{-1} peak can be assigned to the stretching vibrations of In−O−In linkages, while peaks at 497 and 630 cm^{-1} can be attributed to octahedral stretching vibrations $\nu(InO_6)$. Significant decrease in intensity of all the main peaks was observed in the copper doped sensors.

5.6 Gas Sensors Based on Pristine In_2O_3

5.6.1 Nitrogen Dioxide Detection

Response of the thick film sensor towards a low concentration of 7 ppm was studied in the temperature range of 50 to 200^0C. The sensor response of sensor was measured as ratio of resistance R_{gas}/R_{air}, here R_{gas} is resistance of the sensor in presence of gas and R_{air} is the resistance of the sensor before the introduction of gas. Fig. 5.7 (a) to (g) shows response of In_2O_3 thick film sensor at different temperatures towards the concentration of 7 ppm. The response time is taken as the time taken by the sensor to reach 90% of maximum value and recovery time is taken as the time taken by the sensor to reach 10% of base value (value before the introduction of gas) in all the measurements.

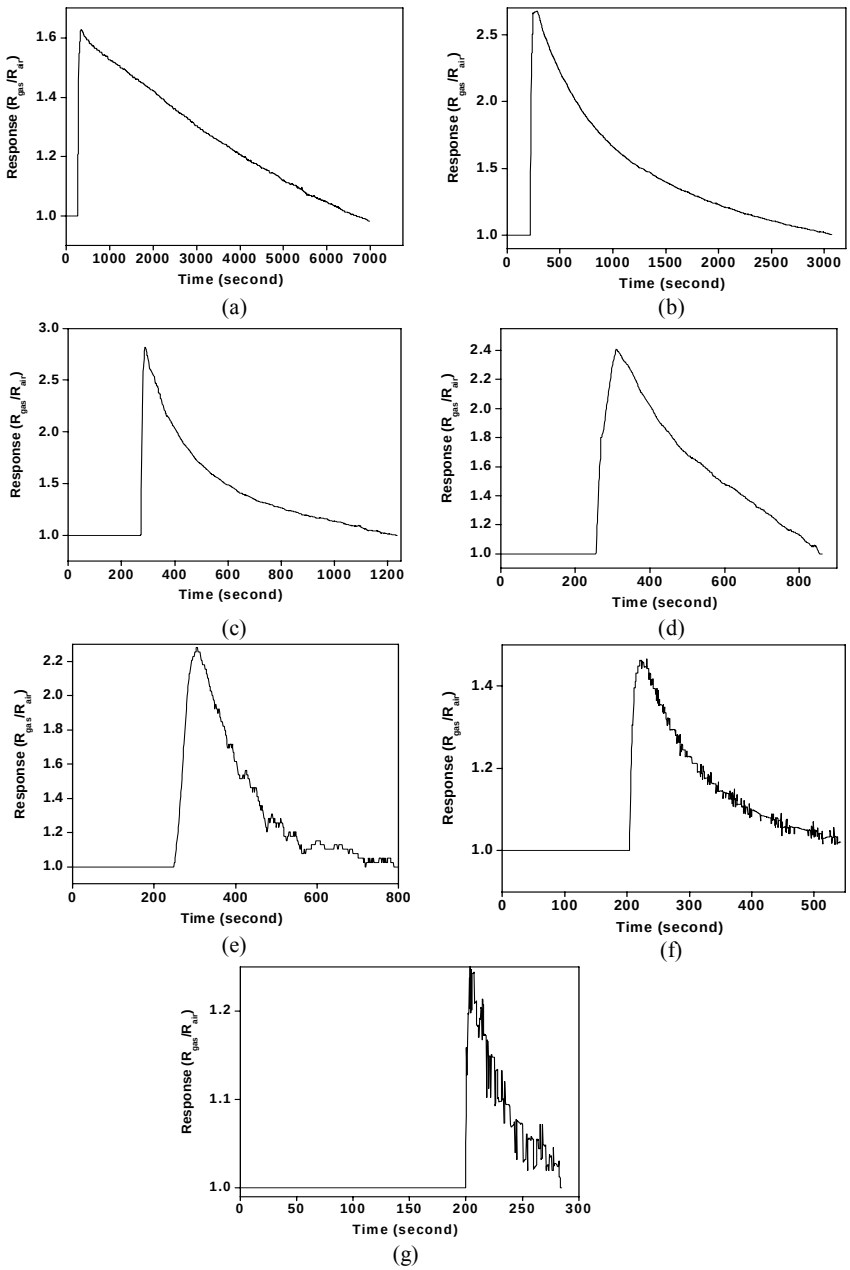

Fig. 5.7 Response of In_2O_3 thick film sensor towards 7 ppm of NO_2 gas at (a) 50^0C, (b) 75^0C (c) 100^0C (d) 125^0C (e) 150^0C (f) 175^0C (g) 200^0C

Fig. 5.8 (a) shows the sensitivity of thick film In_2O_3 sensor to 7 ppm NO_2 gas at various temperatures. Here the sensitivity value is taken as the maximum response value corresponding to respective temperature in fig. 5.7 (a) to (g). The sensor showed maximum sensitivity of 2.82 at 100^0C. The sensitivity decreases beyond this temperature. As the temperature increases beyond 150^0C the sensor resistance is not stable and this causes increased disturbance in the measurement. Fig. 5.7 (g) shows that at working temperature of 200^0C the disturbance is very high indicating that thick film sensor cannot operate satisfactorily at this temperature.

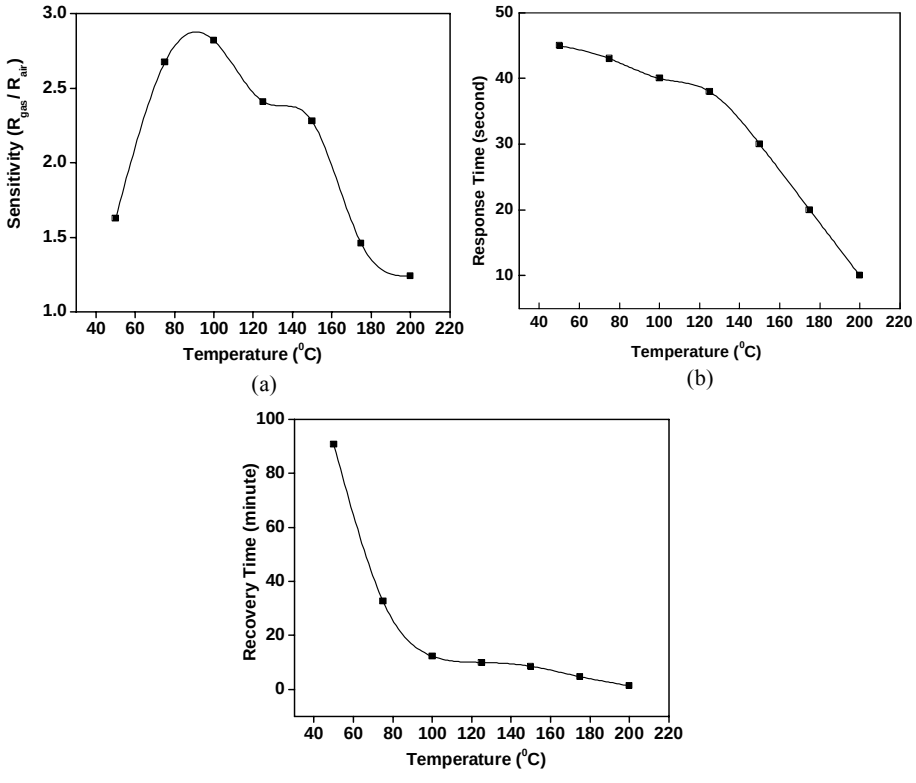

Fig. 5.8 (a) Sensitivity (b) Response time (c) Recovery time of In_2O_3 thick film sensor towards 7 ppm of NO_2 gas at different temperatures

Considering the maximum sensitivity, response and recovery time, 100^0C is considered as the optimum temperature for the gas sensing measurement. Fig. 5.8 (b) and (c) shows the response and recovery time of the In_2O_3 thick film sensor at different temperature. At the optimum temperature of 100^0C the response and recovery time was found to be 40 seconds and 12.27 minutes respectively. The response time at this temperature is found to be relatively high and the recovery time is found to be relatively low.

Concentration dependent studies were performed at this optimum temperature. Fig. 5.9 (a) & (b) shows the concentration dependent studies performed. Fig. 5.10 shows the sensitivity of the sensor to different concentration. The maximum concentration studied with the set up was 57 ppm with a sensitivity of 43.5 and minimum concentration was 1.79 ppm with a sensitivity of 1.1.

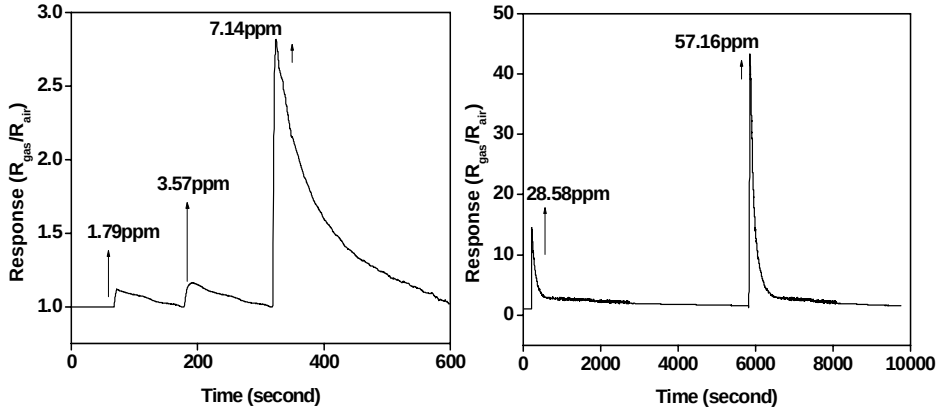

Fig. 5.9 (a) & (b) Response of In_2O_3 thick film sensor towards different concentrations of NO_2 at 100^0C

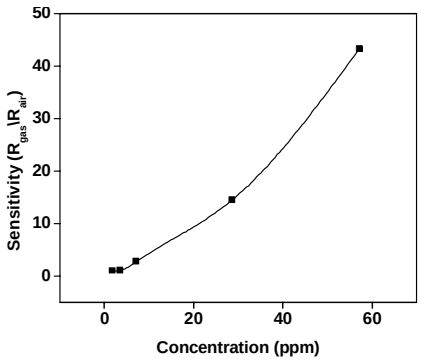

Fig. 5.10 Sensitivity of In_2O_3 thick film sensor towards different concentrations of NO_2 at 100^0C

6.2 Hydrogen Sulphide Detection

The sensor response in case of reducing H_2S gas was calculated as ratio of R_{air}/R_{gas}, here R_{air} is resistance of thick film sensor before introduction of gas and R_{gas} is resistance of sensor in presence of gas. The temperature dependent measurements were found to be not satisfactory in terms of response and recovery times and hence only room temperature measurements were done. Fig. 5.11 (a) and (b) shows the concentration dependent measurements performed at room temperature.

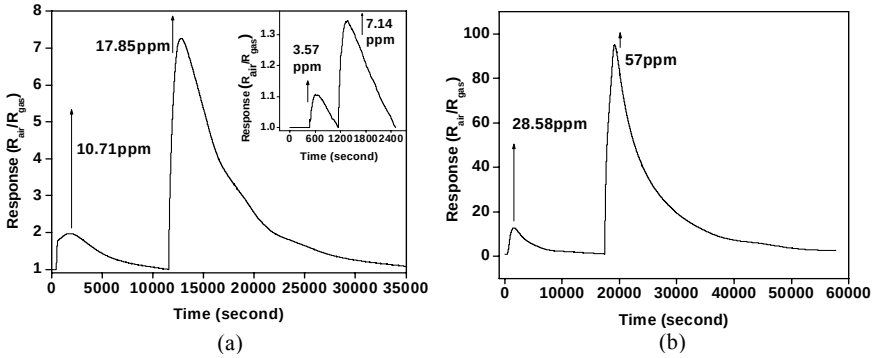

(a) (b)

Fig. 5.11 (a) & (b) Response of In_2O_3 thick film sensor towards different concentrations of H_2S at room temperature.

Since the recovery time for H_2S sensing was very high for the pure In_2O_3 thick film sensors the maximum concentration studied was limited to 57 ppm.

The lowest measured concentration was 3.57 ppm with a sensitivity of 1.1. For 57 ppm concentration the sensor measured a sensitivity of 95. The sensitivity of the sensor to different concentrations studied is shown in fig. 5.12 (a). The response and recovery time of the pure In_2O_3 thick film sensor to different concentrations studied is shown in fig. 5.12 (b) and (c).

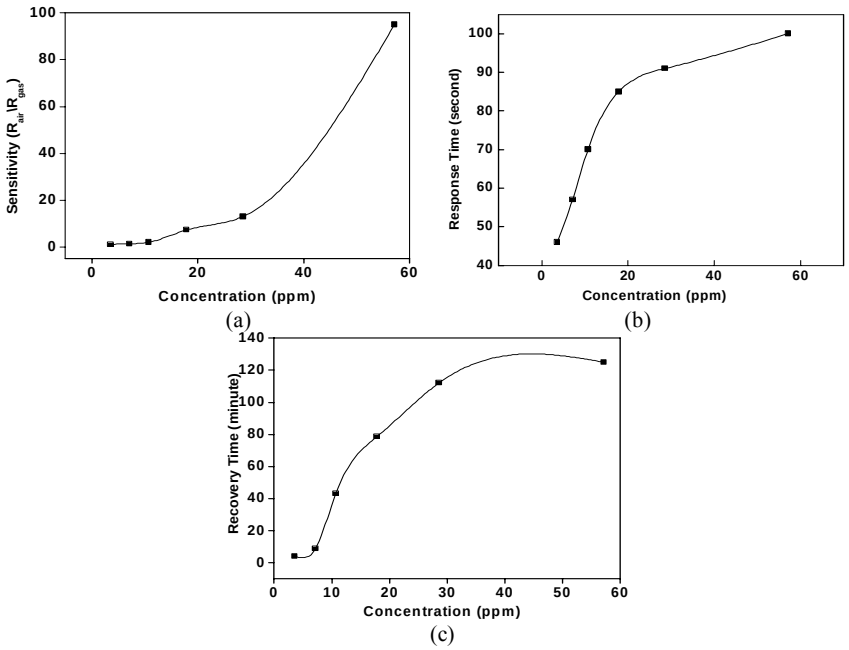

Fig. 5.12 (a) Sensitivity (b) Response time (c) Recovery time of In_2O_3 thick film sensor towards different concentrations of H_2S gas at room temperature

5.7 Gas Sensors Based on 0.5wt% Copper Doped In_2O_3

5.7.1 Nitrogen Dioxide Detection

Response of the sensor towards a concentration of 7 ppm of NO_2 gas was studied in the temperature range of 50 to 200^{0}C. Fig. 5.13 (a) to (g) shows response of sensor at different temperatures towards this concentration.

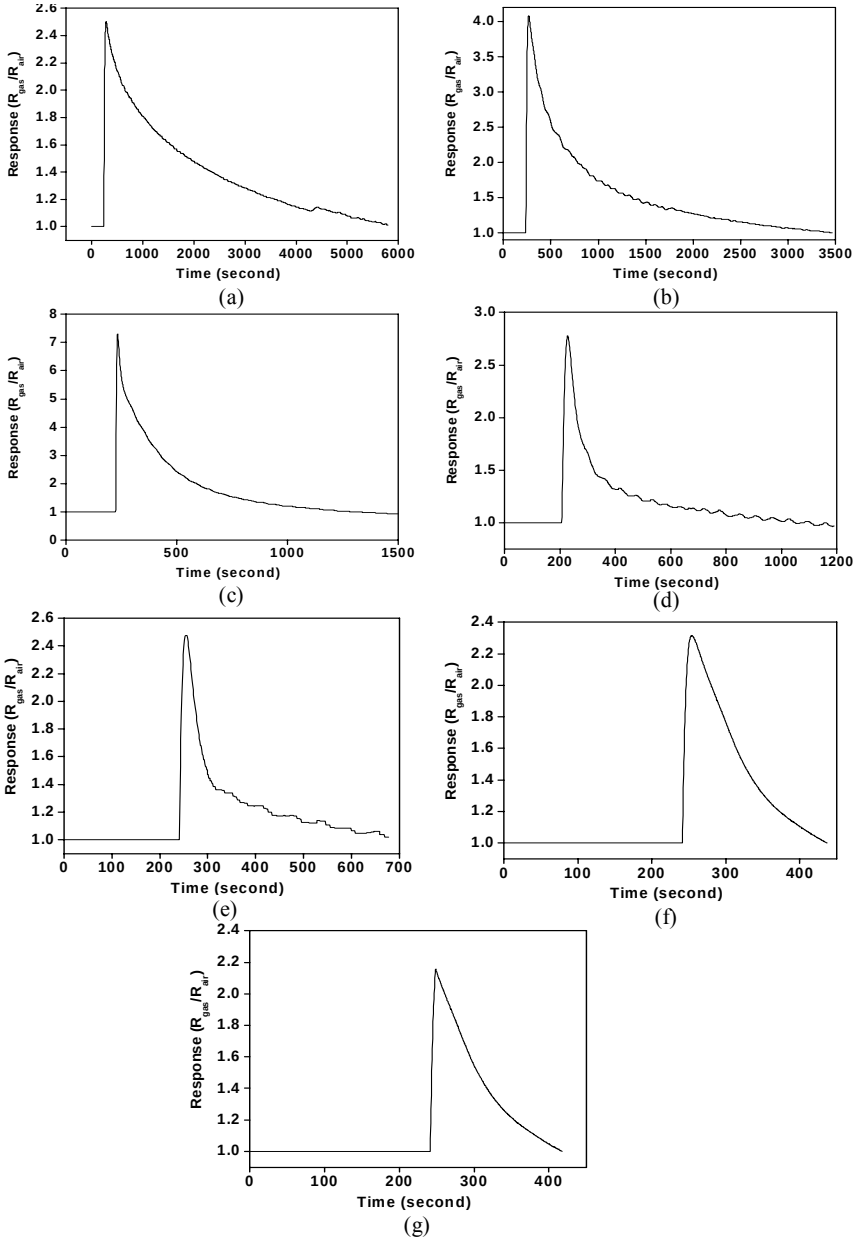

Fig. 5.13 Response of 0.5 wt% copper doped In_2O_3 thick film sensor towards 7 ppm of NO_2 gas at (a) 50^0C , (b) 75^0C (c) 100^0C (d) 125^0C (e) 150^0C (f) 175^0C (g) 200^0C

The sensitivity of sensor at different temperatures towards the concentration of 7 ppm is shown in fig. 5.14 (a). Temperature dependent gas sensing measurements shows that 100^0C is the optimum operating temperature of the 0.5wt% copper doped In_2O_3 sensor. Beyond this temperature the sensitivity decreases. The response of the sensor at this temperature is 7.29. The response and recovery time of the sensor to different temperatures are shown in fig. 5.14 (b) and (c) respectively. At optimum temperature of 100^0C the 0.5wt% copper doped sensor had a response time of 9 seconds and recovery time of 8.03 minutes. Response and recovery time recorded at this temperature are relatively small.

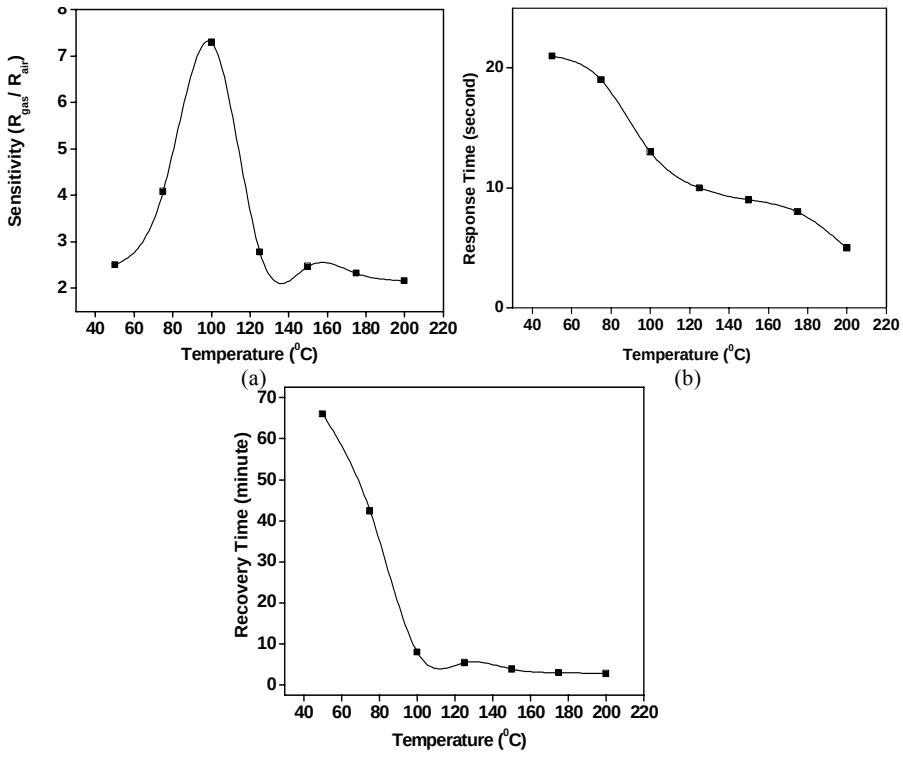

Fig. 5.14 (a) Sensitivity (b) Response time (c) Recovery time of 0.5 wt% copper doped In_2O_3 thick film sensor towards 7 ppm of NO_2 gas at different temperatures

Concentration dependent studies performed at optimum temperature of 100^0C are shown in fig. 5.15. The lowest measurable concentration was found to be 1.79 ppm with a sensitivity of 1.16. The highest measured concentration with the set up was 28.58 ppm with a sensitivity of 35.4. The sensitivity of the sensor to different concentrations of the NO_2 gas studied is shown in fig. 5.16.

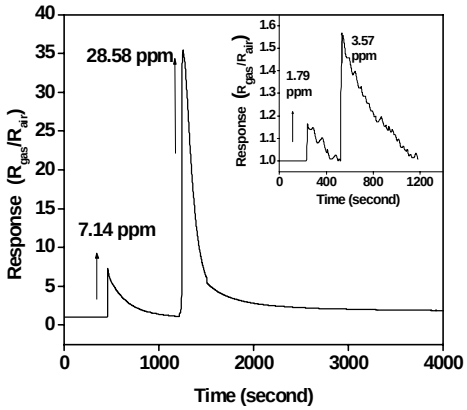

Fig. 5.15 Response of 0.5wt% copper doped In_2O_3 thick film sensor towards different concentrations of NO_2 at 100^0C.

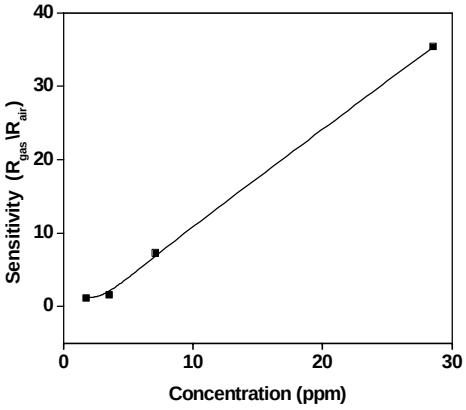

Fig. 5.16 Sensitivity of 0.5wt% copper doped In_2O_3 thick film sensor towards different concentrations of NO_2 at 100^0C

5.7.2 Hydrogen Sulphide Detection

Sensor response towards different concentrations of H_2S gas measured at room temperature is shown in fig. 5.17 (a) and (b). Only room temperature measurements were performed. The temperature dependent gas sensing measurements were found to be unsatisfactory in this case also.

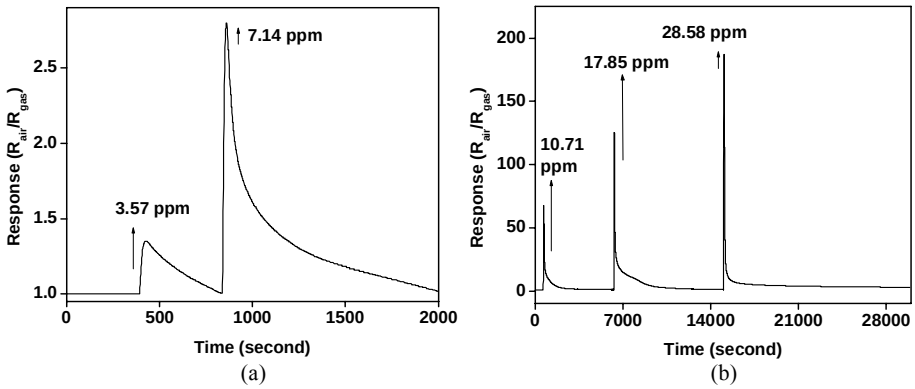

Fig. 5.17 (a) & (b) Response of 0.5wt% copper doped In_2O_3 thick film sensor towards different concentrations of H_2S at room temperature.

The sensitivity of 0.5wt% copper doped In_2O_3 thick film sensor to the concentration studied is shown in fig. 5.18 (a). Due to the large recovery time of the sensor the concentration dependent studies were limited to 28.58 ppm. The response and recovery times of the sensor to the concentration studied are shown in fig. 5.18 (b) and (c).

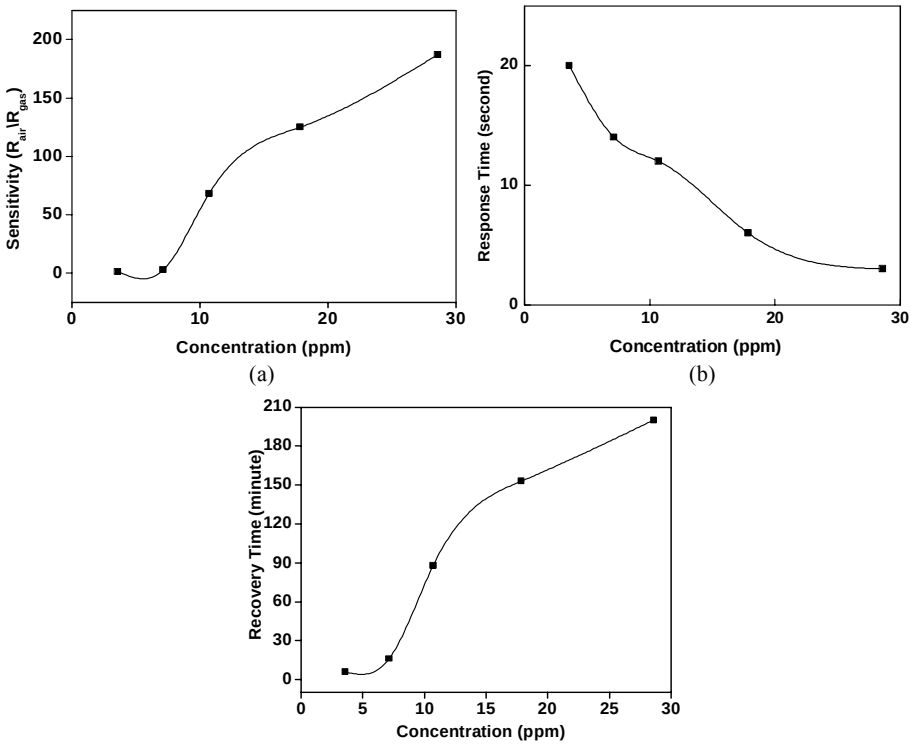

Fig. 5.18 (a) Sensitivity (b) Response time (c) Recovery time of 0.5wt% copper doped In_2O_3 thick film sensor towards different concentrations of H_2S gas at room temperature

5.8 Gas Sensors Based on 1.5wt% Copper Doped In_2O_3

5.8.1 Nitrogen Dioxide Detection

Response of sensor towards a concentration of 7 ppm of NO_2 gas studied in the temperature range of 50 to 200^0C is presented in the figures 5.19 (a) to (g).

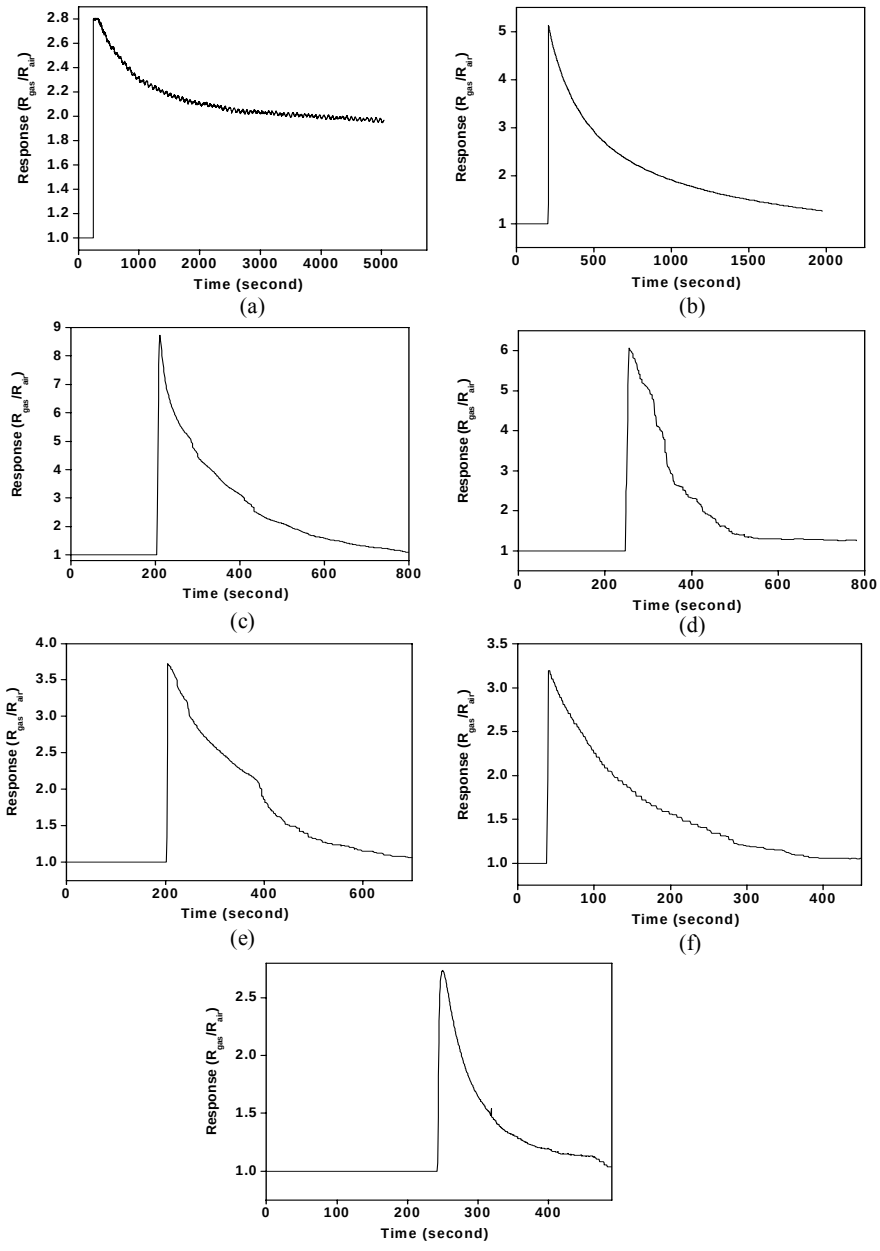

Fig. 5.19 Response of 1.5 wt% copper doped In_2O_3 thick film sensor towards 7 ppm of NO_2 gas at (a) 50^0C (b) 75^0C (c) 100^0C (d) 125^0C (e) 150^0C (f) 175^0C (g) 200^0C

Sensitivity of sensor at different temperatures towards this concentration of 7 ppm is shown in fig. 5.20 (a). At 50 and 75^{0}C the recovery time is very large and hence the measurement was discontinued. Temperature dependent gas sensing behaviour shows that optimum operating temperature for 1.5wt% copper doped In_2O_3 sensor is 100^{0}C with a response of 8.72. The response and recovery times at this temperature were 9 seconds and 6 minutes respectively. Response and recovery times of sensor at different temperatures for the 7 ppm concentration are shown in fig. 5.20 (b) and (c). Response and recovery times of the sensor at this temperature show a relatively small value.

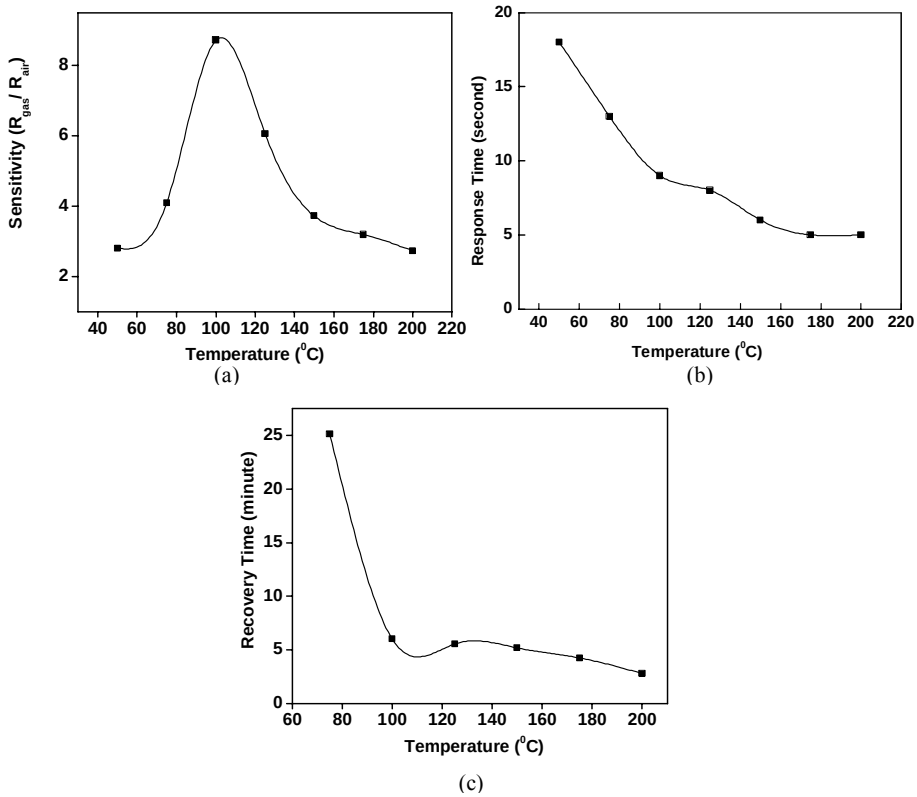

Fig. 5.20 (a) Sensitivity (b) Response time (c) Recovery time of 1.5 wt% copper doped In_2O_3 thick film sensor towards 7 ppm of NO_2 gas at different temperatures

The concentration dependent studies conducted at his optimum temperature of 100^0C show that lowest measured concentration is 1.79 ppm with a sensitivity of 1.21. The highest measured concentration with the set up was 28.58 ppm with a sensitivity of 38.74. Fig. 5.21 (a) and (b) shows response of sensor towards different concentration at the optimal temperature of 100^0C. Fig. 5.22 shows sensitivity towards different concentrations at 100^0C.

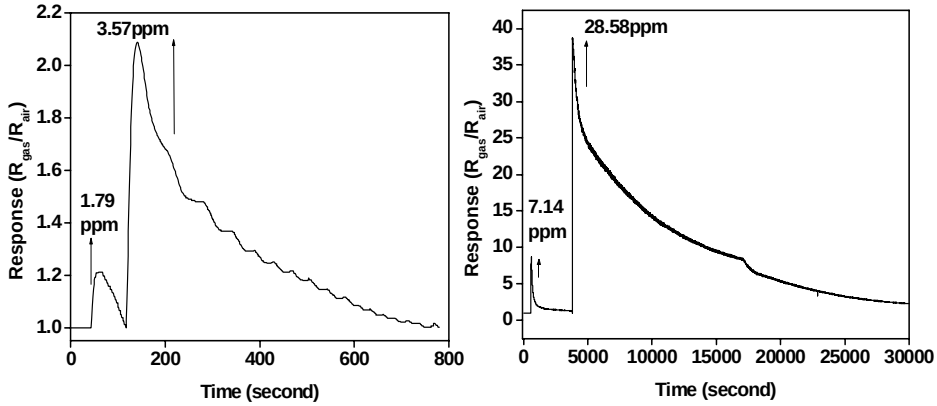

(a) (b)

Fig. 5.21 (a) and (b) Response of 1.5wt% copper doped In_2O_3 thick film sensor towards different concentrations of NO_2 at 100^0C.

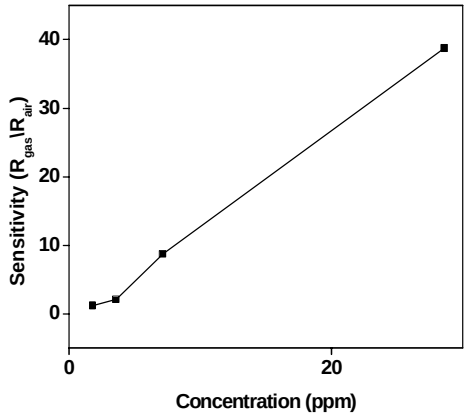

Fig. 5.22 Sensitivity of 1.5wt% copper doped In_2O_3 thick film sensor towards different concentrations of NO_2 at 100^0C

5.8.2 Hydrogen Sulphide Detection

Response of 1.5wt% copper doped In_2O_3 sensor towards different concentration of H_2S gas measured at room temperature is shown in fig.5.23 (a), (b), (c) and (d).

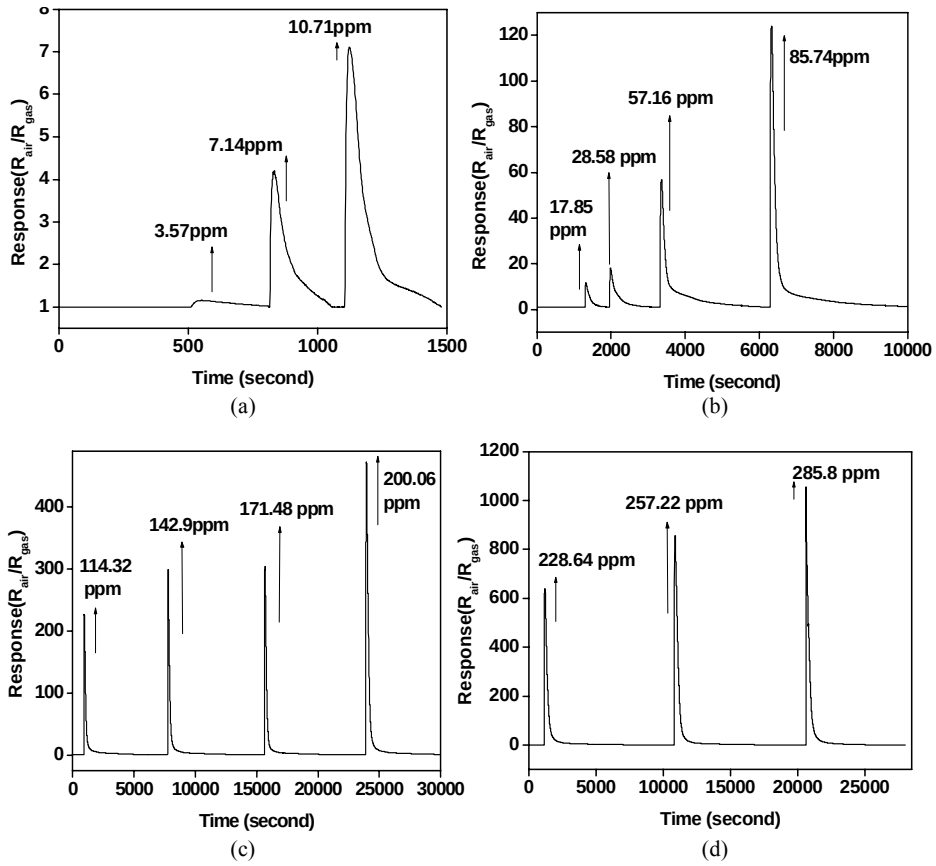

Fig. 5.23 (a) (b) (c) and (d) Response of 1.5wt% copper doped In_2O_3 thick film sensor towards different concentrations of H_2S at room temperature.

Sensitivity of sensor to different concentrations of H_2S gas at room temperature is shown in fig. 5.24 (a). The minimum measured concentration was found to be 3.57 ppm with a sensitivity of 1.15. The maximum

concentration studied with the set up was 286 ppm with a sensitivity of 1055. The response and recovery time of the sensor to different concentrations at room temperature is shown in fig. 5.24 (b) and (c).

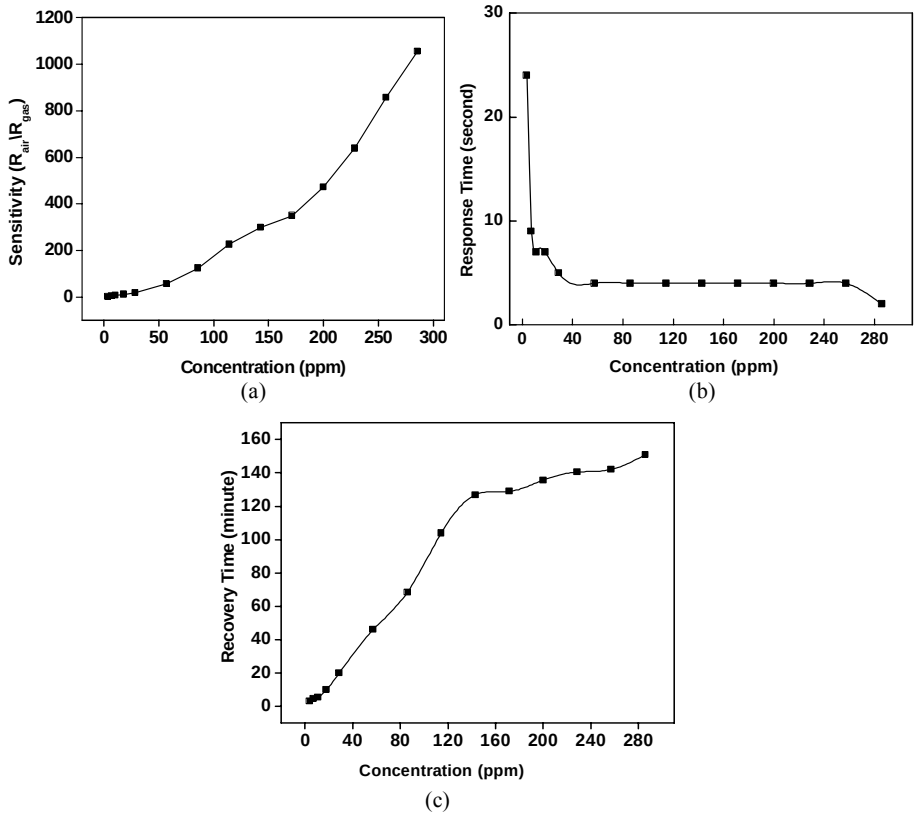

Fig. 5.24 (a) Sensitivity (b) Response time (c) Recovery time of 1.5 wt% copper doped In_2O_3 thick film sensor towards different concentrations of H_2S gas at room temperature

5.9 Gas Sensors Based on 3wt% Copper Doped In_2O_3

5.9.1 Nitrogen Dioxide Detection

Response of sensor towards a concentration of 7ppm of NO_2 gas was studied in temperature range of 50 to 200^0C. Fig. 5.25 (a) to (g) shows response of sensor at different temperatures towards this concentration.

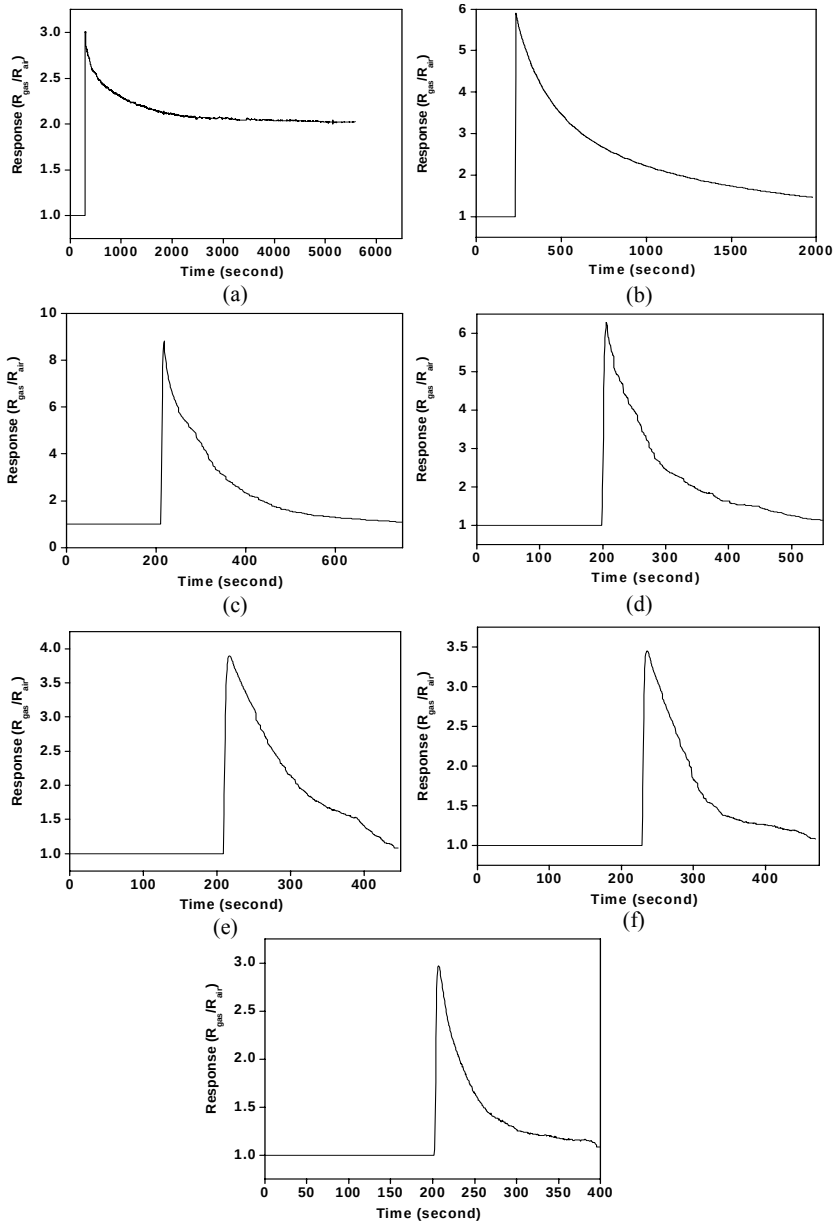

Fig. 5.25 Response of 3wt% copper doped In_2O_3 thick film sensor towards 7 ppm of NO_2 gas at (a) 50^0C (b) 75^0C (c) 100^0C (d) 125^0C (e) 150^0C (f) 175^0C (g) 200^0C

Sensitivity of sensor at different temperatures towards a concentration of 7 ppm is shown in fig. 5.26 (a). The corresponding response and recovery time of 3wt% copper doped In_2O_3 sensor at different operating temperatures is shown in fig. 5.26 (b) and (c) respectively. Due to very large recovery time the measurement was discontinued at 50^0C. Maximum sensitivity was achieved at an operating temperature of 100^0C with a response of 8.83 .The response and recovery times at this optimum temperature was found to be 6 seconds and 4 minutes respectively. Marked improvement in sensitivity, response and recovery time were obtained at this temperature.

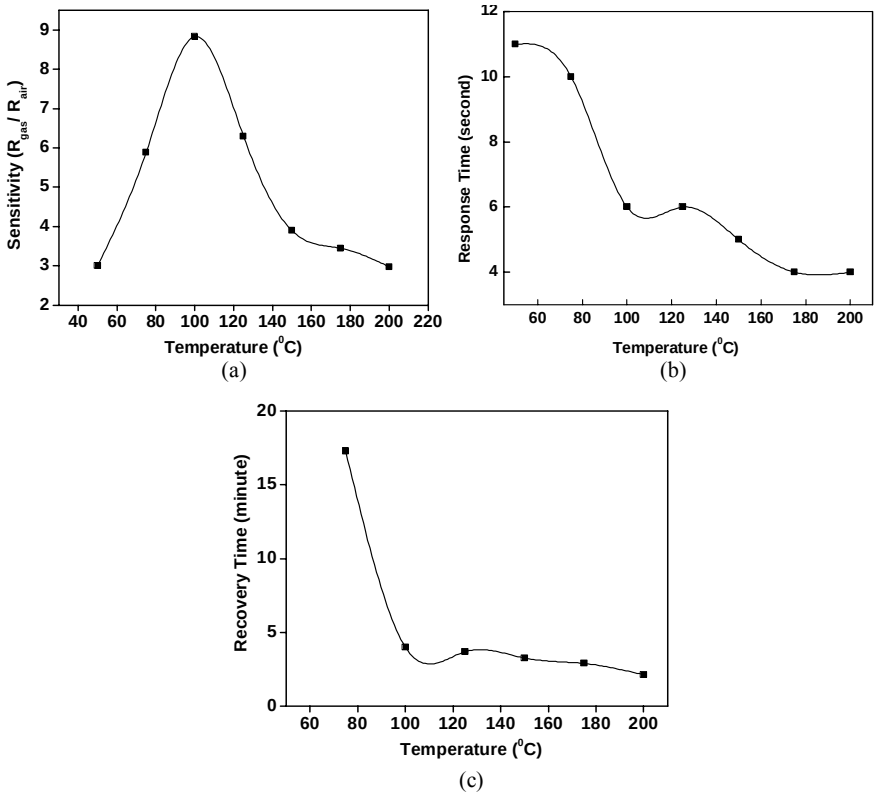

Fig. 5.26 (a) Sensitivity (b) Response time (c) Recovery time of 3wt% copper doped In_2O_3 thick film sensor towards 7 ppm of NO_2 gas at different temperatures

The concentration dependent studies at this temperature are shown in fig. 5. 27 (a) and (b). The lowest measured concentration was 1.79 ppm with a response of 1.32 and maximum measured concentration with the set up was 28.58 ppm with a response of 41.32. Fig. 5.28 shows the sensitivity towards different concentration at 100^0C.

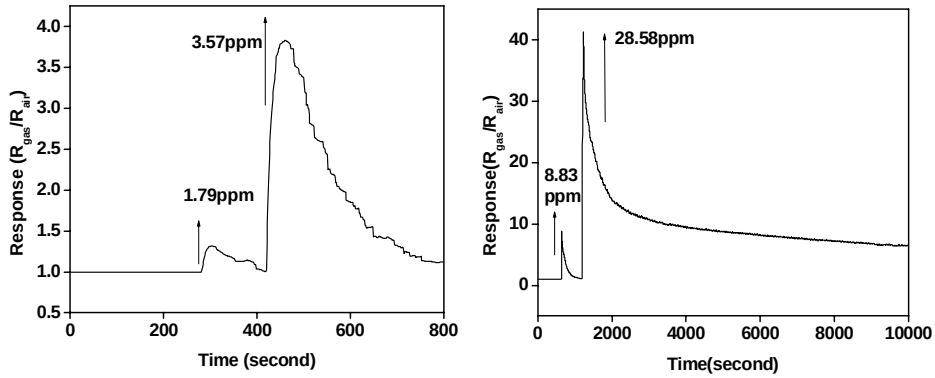

(a) (b)

Fig. 5.27 (a) & (b) Response of 3wt% copper doped In_2O_3 thick film sensor towards different concentrations of NO_2 at 100^0C.

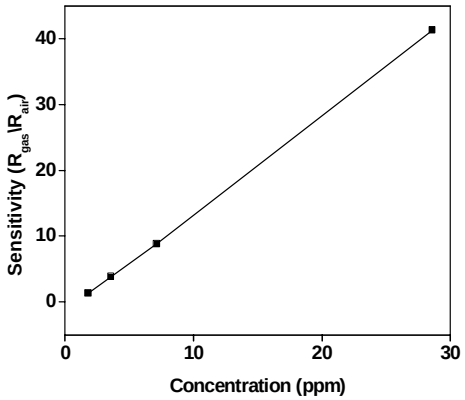

Fig. 5.28 Sensitivity of 3wt% copper doped In_2O_3 thick film sensor towards different concentrations of NO_2 at 100^0C

5.9.2 Hydrogen Sulphide Detection

Response of 3wt% copper doped In_2O_3 sensor towards different concentrations of H_2S gas measured at room temperature is shown in fig. 5.29 (a), (b), (c) and (d).

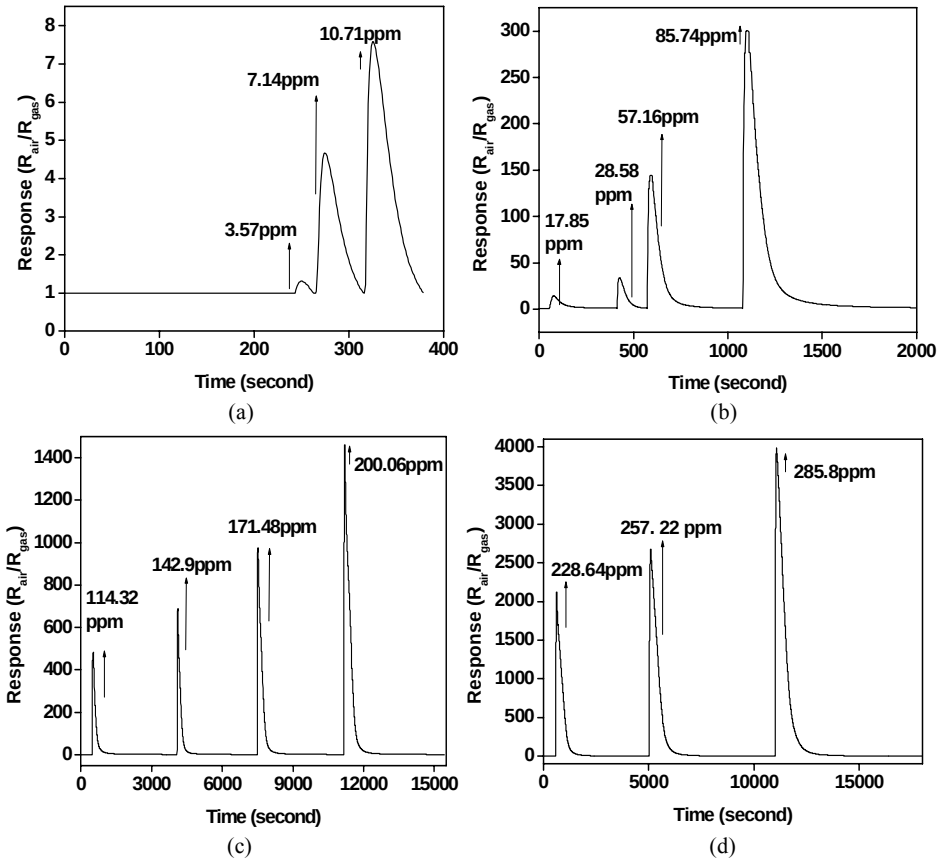

Fig. 5.29 (a), (b), (c) & (d) Response of 3wt% copper doped In_2O_3 thick film sensor towards different concentrations of H_2S at room temperature.

Sensitivity of sensor to different concentrations of H_2S gas at room temperature is shown in fig. 5.30 (a). The minimum measured concentration was 3.57 ppm with a sensitivity of 1.32. The maximum concentration

studied with the set up was 286 ppm with a sensitivity of 3986. The response and recovery time of the sensor to different concentration at room temperature is shown in fig. 5.30 (b) and (c).

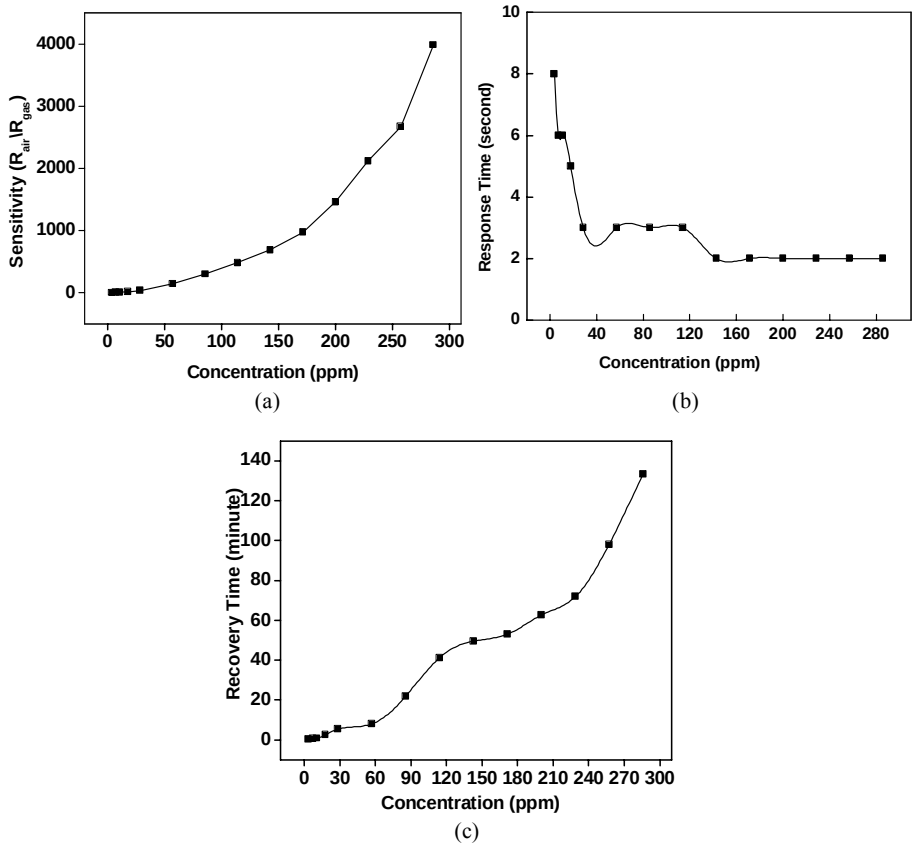

Fig. 5.30 (a) Sensitivity (b) Response time (c) Recovery time of 3wt% copper doped In_2O_3 thick film sensor towards different concentrations of H_2S gas at room temperature

5.10 Discussion of the Results

It is well known that when an n-type semiconductor metal oxide is exposed to air, oxygen molecules can adsorb on the surface of the particles and form O_2^-, O^-, O^{2-} ions by capturing electrons from the conduction band,

which in turn produces an electron-depleted space-charge layer in the surface region. As the dimensions of nanoparticles are sufficiently reduced, they can be completely depleted and the response to gases increases [94, 95].

5.10.1 NO_2 Detection Mechanism

The detection of NO_2 in air at low temperatures can be explained by the high chemical activity of NO_2. It has been proven by means of different characterization techniques that NO_2 oxidizes nonstoichiometric oxides like SnO_2 and TiO_2 [96]. Generally, changes in sensor resistances can be associated with surface chemisorption processes and explained in terms of an electron-transfer between the semiconductor and adsorbed gases [97]. The resistance of In_2O_3 films increases after exposure to the oxidizing gas NO_2 and it returns to the initial value when the NO_2 gas is removed. It is well known that n-type semiconductors have higher resistance in an NO_2 enviornment as compared to that in vacuum [98]. This is because if an electronegative molecule [98, 99] such as oxygen or NO_x, (NO and NO_2) is approaching the semiconductor surface and its electron affinity χ is larger than the semiconductor work function Φ, the molecule will tend to pick up an electron from the semiconductor conduction band and become chemisorbed at the surface. With further adsorption the surface becomes more negatively charged while a positive space-charge layer forms behind it. In this process, the energy band at the surface bends upwards, and the work function increases. The net result of the chemisorption of the acceptor-type gas such as NO_2 on the n-type semiconductor surface is an increase in electron depletion region and hence a decrease in electron concentration in the conduction band near the semiconductor surface, and hence a decrease in the conductance close to the surface.

Adsorption of electron acceptor gaseous species like O_2, NO_2 will lead to band bending ($q\Delta V_S$) due to the formation of surface depletion layer (surface charge region) with a thickness d, because of the free charge carrier capture at the surface as discussed in section 3.10 of chapter 3. So, due to the chemisorption of acceptor gases, the influence of the following factors should be discussed: (1) nature and density of active surface states S, sites for the gas adsorption. (2) possibility of electron transfer from semiconductor to the adsorbates resulting the formation of chemisorbed surface species.

In solid-state chemistry the association of active surface states with the surface defects—reducing states, such as metal cations in low oxidation states, or oxygen vacancies, or F-centers—is postulated. Earlier works done by Gurlo et al [100,101], Ivanovskaya et al.[102], Sasaki et al. [103] and De Wit [104] with the help of the combined ESR and XPS investigation established the forming of non-stoichiometric, In_2O_{3-x} upon annealing with a high concentration electronic (F-centers) and 'hole' centers (In^{2+}) in the sensitive layers. These earlier works concluded that F centers and hole centers can appear as active surface states for the adsorption of oxidizing gases and make easier electron transfer to adsorbates leading to the formation of chemisorbed surface species or depletion layers.

According to Solovjeva et al. [105] high mobility of electrons in In_2O_3 at low temperature is provided by easy electron exchange process between In^{2+} and In^{+} ions. The formation of In^{2+} in In_2O_3 lattice takes place in oxygen deficiency:

$$In_2O_3 \rightarrow In^{3+}_{2-x} In^{2+}_{x} O_{3-x} [F]_x + ½\ xO_2 \qquad (5.2)$$

In^{+} ions in In_2O_3 lattice may appear as a result of the process.

$$2\ In^{2+} \leftrightarrow In^{+} + In^{3+} \quad (5.3)$$

Additional electrons which have to be introduced into the oxide lattice by oxygen vacancies formation or interstitial metal atoms ionization in order to maintain the overall neutrality of the crystal, should be associated with neighboring lattice metal ions [106] reducing them, In^{3+} to In^{2+}. So, basically three types of defects have to be considered, i.e., In^{2+} lattice ions, interstitial In, most likely In $^{3+}$, and oxygen vacancies (V_o). Partially reduced cations (i.e In^{2+} and In^{+} in In_2O_3) play the role of NO_2 chemisorption centers at comparatively low temperature [63]. The general scheme for NO_2 detection at In_2O_3 surface is given by

$$NO_{2gas} + (Z)_s \leftrightarrow (ZO)_s + NO_{gas} \quad (5.4)$$

Here Z is the chemisorptions sites, sites being In^{2+} and F–centers. The surface species denoted as $(ZO)_s$ are $(In^{3+}\text{-}O^{-})_s$ and $(V_o\text{-}O^{-})_s$ [42]. From the above equations it can be understood that the highest activity regarding NO_2 is observed for systems with the most pronounced deviation from stoichiometry. The increase of non stoichiometry is also expected to increase the surface concentration of adsorbed oxygen since more adsorption sites are available for the atmospheric oxygen to adsorb on the surface of In_2O_3.

The properties of electron transfer in polycrystalline layers strongly depend on the grain boundaries [107], which contain a high density of surface states. These states can trap or scatter free carriers, generate potential barriers or severely deplete the grains of free carriers and determine the material conductivity. The smallest particles have the highest density of surface defects, which could negatively influence the transport properties [108]. So we can say that the transport of electrons, which is determined by the microstructure of the sensing element such as the grain size of

semiconductor particles, also determine the In_2O_3 resistance in air and NO_2. Hence we can conclude that the material's structure also play fundamental role in its NO_2 response.

Gurlo et al. [61] studied the effect of grain sizes on the NO_2 gas sensing behavior of In_2O_3. They studied the particle size in the range of 5-100nm. The highest sensitivity was obtained for sensors with small grain size in the range of 5-20nm. Another grain size related sensitivity work on indium oxide for NO_2 gas sensing by the same group reported that the sensitivity increased very much for grain sizes below 30nm. They related the results with that of grain size dependent sensitivity shown by tungsten oxide reported by Tamaki et al. [109]. Singh et al. [81] studied the size dependent gas sensing properties of In_2O_3 nanoparticle layers in the range of 8- 30nm. They reported as the size becomes larger than 15nm, electrical conduction is controlled by the interface between particles and is not dependent upon particle size. In our pure and copper doped sensor the particle size is in the range of 23-25nm. Considering the above grain size related works and results we assume that in our sensors the conduction is in the grain boundary control.

Enhanced NO_2 gas sensing properties of copper doped In_2O_3 gas sensors is discussed below. Studies on SnO_2 have shown that the copper atoms in Cu-doped tin oxide can form donor-like sites (Cu^+ centers), which possess much better stability than the intrinsic donors (oxygen vacancies) in pure tin oxides [110]. In other studies [111,112] the Cu impurity was considered as an acceptor like one which is attributed to the CuO doping [113]. CuO is a p-type semiconductor and can form heterojunctions with n-SnO_2 which results in acceptor like behaviour of the compounds. The copper impurity in the SnO_2 film can create both interstitial point defects and

film inhomogeneity on account of CuO formation. We consider the similar effects in In_2O_3 due to copper doping.

The resistance in air of the pure In_2O_3 sensor increased considerably by copper doping. Similar increase in resistance in air was obtained for pure tin oxide sensors when doped with copper [114-117]. This increase in resistance of tin oxide in pure air is atrributed due to formation of p-n heterojunctions (p-CuO and n-SnO_2), which induces an electron-depleted space charge layer at the surface of tin oxide [118-121]. In our copper doped gas sensors CuO and In_2O_3 are p and n-type semiconductors, respectively, having a strong electronic interaction due to which the CuO–In_2O_3 surface consists of numerous p–n junctions causing very high resistance of films in air. From the measured resistance value for pure (100kΩ) and copper doped In_2O_3 (0.5wt% copper doped- 2.4MΩ) at room temperature, it can be seen that copper doped sensors show very high resistance. Hence we consider that doping with Cu leads to the formation of CuO which acts as acceptor type impurity.

Two possible mechanisms can be assumed for the enhancement effect in gas sensing. The first mechanism proposed for improvement in sensor performance due to copper doping is due to cuprous ions Cu^+, which coexist with cupric ions Cu^{2+} [122]. A similar effect is reported for copper doped tin oxide sensor by Ghimbeu et al [116]. The local oxygen deficiency, when annealing, may trigger the occurrence of the following reaction:

$$2CuO \rightarrow Cu_2O + ½\ O_2\uparrow \qquad (5.5)$$

which reduces some Cu^{2+} to Cu^+ and thus, Cu^{2+} and Cu^+ coexist. When NO_2 gas molecules are brought in contact with the sensing element, NO_2 is adsorbed on active centers, Cu^+. Hence NO_2 gets reduced to NO_2^- radicals

meanwhile Cu^{+} gets oxidized to Cu^{2+}. The highly active NO_2^- combines with preadsorbed O^- or O_2^- removing electrons further from the conduction band of In_2O_3 further increasing the resistance of the In_2O_3. The reaction proceeds as follows.

$$NO_2(g) + e^- \rightarrow NO_2^-{}_{(ads)} \quad (5.6)$$

$$NO_2(g) + O_2^-{}_{(ads)} + 2e^- \rightarrow NO_2^-{}_{(ads)} + 2O^-{}_{(ads)} \quad (5.7)$$

$$NO_2^-{}_{(ads)} + O_2^-{}_{(ads)} \rightarrow 2O^-{}_{(ads)} + NO_2 \quad (5.8)$$

Another possibility for the enhanced sensitivity is increase in In^{2+} centers due to copper doping. Earlier Ivanovskaya et al. [63] and Bogdanov et al. [123] proved with the help of ESR measurements that the number of In^{2+} centers increased with nickel (Ni) doping and this resulted in enhanced sensitivity. Thus we assume that the presence of Cu^{+} ions along with 'hole' center (In^{2+}) and oxygen vacancies act as additional adsorption site for the gas which increases the sensitivity.

In our gas sensing measurement results we found that the sensitivity of 0.5wt% copper doped In_2O_3 increased to 7.29 (fig. 5.31). On increasing the doping level to 1.5wt% and 3wt% we found that the sensitivity achieves saturation level (S = 8.72 for 1.5wt% , S = 8.83 for 3wt%). With copper addition the copper forms copper oxide on the surface of In_2O_3. As the concentration of doping increases more CuO–In_2O_3 heterojunctions are formed that does not enchance the sensitivity of the sensor to NO_2 much. If the doping concentration is increased (more than 3wt%) further high covering of In_2O_3 surface by CuO occurs resulting in very little change in sensitivity. Or else it can also be explained that when the doping concentration increases the number of In^{2+} ions produced will also attain a

saturation level and hence the sensitivity also attain saturation. It is also found that the response time as well as the recovery time of the copper doped In_2O_3 sensor decreases with copper doping. The improved response as well as recovery time performance of doped In_2O_3 over pure In_2O_3 is due to the catalytic interaction of copper ion with the gas species to be detected.

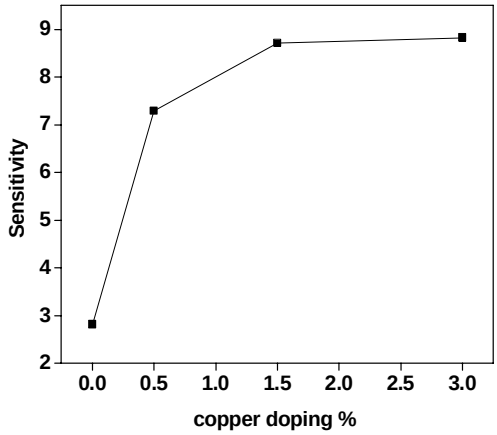

Fig. 5.31 Sensitivity at different copper doping % to 7 ppm NO_2 gas at respective optimum temperature

5.10.2 H_2S Detection Mechanism

H_2S gas detection studies were performed only at room temperature, since the temperature dependent studies were not satisfactory. The sensors were not able to recover its base resistance value or it took long recovery time especially hours for the recovery, hence only room temperature measurements were performed. On exposure to H_2S gas the resistance of pure as well as copper doped sensors was found to decrease and hence the conductivity was found to increase. The different mechanism associated with the gas sensing process is discussed below.

For most of the In_2O_3 gas sensors, the sensing mechanism was proposed as the adsorption and desorption of the gas molecules on the surface of the sensing materials, which can cause the change in resistance [57, 58, 124 - 126]. Oxygen vacancy created at high temperature annealing can induce non-stoichiometry on the surface of In_2O_3. Atmospheric oxygen can get adsorbed on to this surface site. The oxygen adsorbed on the surface directly influences the conductance of the In_2O_3 based sensors as shown in figure 5.32. When the In_2O_3 thick film sensor was exposed to H_2S gas, the strong reducing gas might react with adsorbed oxygen ions on the surface and put back the electrons into In_2O_3 semiconductor, resulting in the increase of conductance of In_2O_3. The reaction may proceed as follows (ad) represents adsorbed species and (g) represents gas.

$$O_2\,(g) + e^- \leftrightarrow O_2 - (ad) \tag{5.9}$$

$$O_2^-\,(ad) + e^- \leftrightarrow O_2^{2-}\,(ad) \tag{5.10}$$

$$H_2S\,(g) + O_2^{x-}\,(ad) \leftrightarrow H_2S\,(ad) + O_2\,(g) + xe^- \tag{5.11}$$

$$2H_2S\,(ad) + 3O_2^{\,x-}\,(ad) \leftrightarrow 2SO_2\,(g) + 2H_2O\,(g) + 3xe^- \tag{5.12}$$

The net reaction is

$$2H_2S\,(g) + 3O_2^{\,x-}\,(ad) \leftrightarrow 2H_2O\,(g) + 2SO_2\,(g) + 3xe- \tag{5.13}$$

According to this mechanism a high concentration of surface adsorbed oxygen ions would favour the forward reaction.

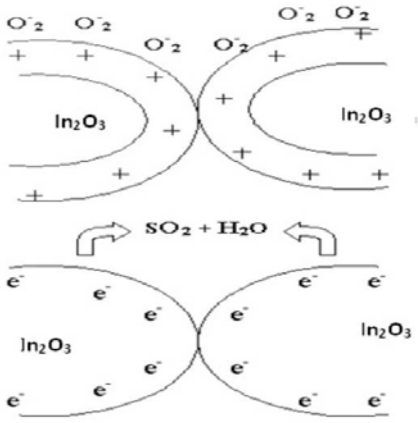

Fig. 5.32 H_2S gas sensing mechanism.

Another mechanism involves the sulfuration of the sensing materials as shown in previous studies for zinc oxide and tin oxide [127,128]. Xu et al. [129] proposed that at relatively low temperature range (25–160 ^{0}C) the dominant mechanism is the sulfuration of In_2O_3 and at relatively high temperature range (160–300^{0}C) the surface adsorption and the sulfuration both contribute to the responses of the sensors. According to their studies at room temperature, In_2O_3 might undergo partial sulfuration when exposed to H_2S and In_2O_3 transformed into well-conducting In_2S_3 [130] as follows:

$$In_2O_3(s) + 3H_2S\,(g) \rightarrow In_2S_3(s) + 3H_2O\,(g) \qquad (5.14)$$

$$In_2S_3(s) + 9/2\ O_2\,(g) \rightarrow In_2O_3(s) + 3SO_2\,(g) \qquad (5.15)$$

The above two are the possible gas sensing mechanism in pure In_2O_3 sensor. The recovery kinetics was significantly slow. In pure In_2O_3, the following reactions are necessary in series for the recovery: (1) desorption of SO_2 and H_2O (2) diffusion of oxygen to the sensing surface (3) adsorption of ambient oxygen gas (4) ionization to negative charge of surface oxygen ($O_2^-{}_{ads}$). When reducing gases are detected using n-type oxide semiconductor gas

sensors, the recovery values are usually longer than the response values [49, 53, 131, 132, 133]. This can be explained by the markedly slower serial surface reactions to form $O_2^-{}_{ads}$ during the recovery, compared to the oxidation reaction of reducing gas by $O_2^-{}_{ads}$.

Enhanced sensitivity as well as improved response and recovery characteristics was observed when indium was doped with copper. This can be explained in term of similar sensitivity increase when tin oxide was doped with copper [117]. Morrison [134] proposed two mechanisms of catalyst control on gas sensors: the spillover mechanism and the Fermi level energy control mechanism. In the spillover mechanism the surface catalyst dissociates the gas molecule, and reactive atoms formed are spilled over on the semiconductor surface and influence the conductivity. The Fermi level mechanism assumes that the H_2S converts the Cu or CuO into CuS which has a relatively high conductivity and the response is greatly improved.

It is assumed that in copper doped In_2O_3 sensors copper doping results in the formation of p-n junctions causing very high resistance of films in air. The p-n junction is formed at the interface between CuO and In_2O_3. While oxygen-deficient In_2O_3 shows n-type conductivity by electrons, oxygen-excess CuO shows p-type conductivity by holes. The CuO grains residing between In_2O grains, forms a network of p-n junctions as shown in fig. 5.33(a). Since CuO and In_2O_3 are p- and n-type semiconductors, respectively, a p-n junction forms at each interface between CuO and In_2O_3 grains, which induces an electron depleted space charge layer at the surface of In_2O_3. The schematic band diagram of the typical n-p-n-p, In_2O_3-CuO-In_2O_3-CuO and band structure in the vicinity of the In_2O-CuO interface can be drawn as shown in fig. 5.33 (b) & (c). The formation of depletion region due to *p*-type CuO and *n*-type In_2O_3 tends to reduce the effective thickness of the

underlying In_2O_3 layer through where the charge carriers can flow. Moreover diffusion of some amount of copper into In_2O_3, and the formation of electronic barriers at the In_2O_3-CuO intergranular region in the bulk of the film cannot be precluded. Copper is known to diffuse extensively and can draw oxygen from In_2O_3 to create intergranular (In_2O_3- CuO) barriers. The combined effect of the depletion layer at the interface, and the inter diffusion of copper are therefore expected to yield a high value of the resistance of film in air.

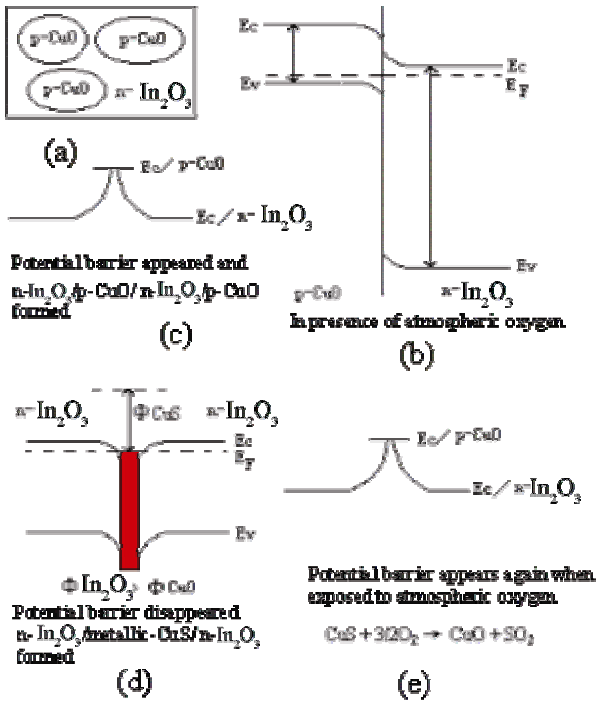

Fig. 5.33 Schematic diagram of CuO/In_2O_3 sensing mechanism.

(a). In_2O_3 particles surrounded by CuO (b). Band structure for CuO- In_2O_3 contact (c). Potential barrier diagram of n- In_2O_3/p-CuO/n- In_2O_3/p-CuO (d). Potential barrier diagram of n- In_2O_3/metallic-CuS/n-In_2O_3 (e). Potential barrier appeared again

Generally CuO layer can be formed on the surface of In_2O_3 in two ways either as a continuous layer, or dispersed in the form of dotted islands. The schematic representation for both the sensor is shown in figure 5.34

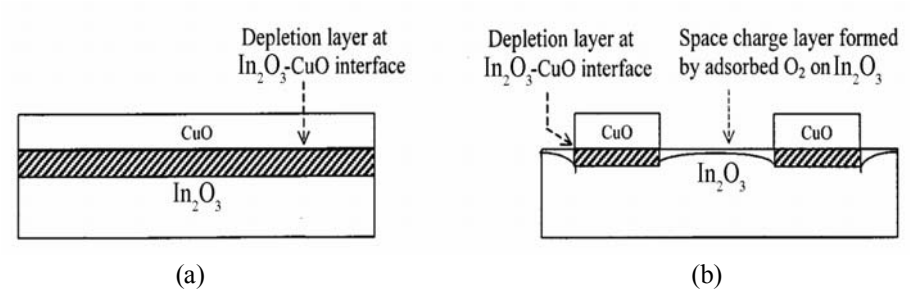

(a) (b)

Fig. 5.34 Cross-sectional views of In_2O_3- CuO sensor (a) continuous layer (b) CuO dispersed in the form of dotted islands

According to the representation fig. 5.34(b) represents a higher resistance than in fig. 5.34(a). This is because in addition to the depletion region and the inter diffusion of Cu into In_2O_3, oxygen adsorbs on the uncovered In_2O_3 surface between the CuO and captures electrons from the conduction band to remain as O_2^- ions until desorbed at high temperature or in the presence of reducing gas. The oxygen adsorption increases the extent of depletion region between the CuO dots as shown in fig 5.34 (b). Thereby the measured resistance in air for In_2O_3-CuO sensor is expected to increase further [34]. In pure In_2O_3 the resistance was found to be 100kΩ and in 0.5wt% copper doped sensors the resistance was found to be in the range of 2.4MΩ. Due to this huge variation in resistance we expect that in our copper doped sensors copper forms islands on the surface of In_2O_3. Moreover sintered gas sensors are composed of a mixture of CuO and In_2O_3 and thus CuO is dispersed here and there in a sensor

However, if the above CuO layer is exposed to H_2S the CuO is converted to copper sulphide (CuS) which is a good electronic conductor as in the following equations.

$$CuO + H_2S \rightarrow CuS + H_2O \quad (5.16)$$

The formation of CuS at room temperature is reported earlier by Kong and Li [135]. CuS is known to be highly conducting in nature and thus the n-p-n heterostructure as well as charge depletion layer will be destroyed and transformed to a metal-n-type semiconductor configuration. A typical metal-n-semiconductor band picture can be drawn in fig. 5.33(d). Since the work function of CuS is lower than that of In_2O_3 the band bending is as shown. This particular situation arises because at equilibrium there is a flow of electrons from the lower work function species, i.e., CuS, to higher work function species, i.e., In_2O_3. This results in the band bending downwards which facilitates the easy flow of electrons from CuS to In_2O_3 and vice versa, since there is no barrier between them as shown in fig. 5.33(d). This flow of electrons results in a decrease in electrical resistance. This configuration is similar to a metal-semiconductor contact for an ohmic junction where there is an unimpeded conduction of electrons in either direction. This theory explains quite convincingly the decrease in resistance on exposure of CuO/In_2O_3 sensor element to reducing gases like H_2S and the increase in resistance back to the original value once this H_2S atmosphere ceases to exist. So, the potential barrier appears again, as seen in fig. 5.33(e).The formation of CuS on the surface of tin oxide has been confirmed with the help of X-ray diffraction [136], X-ray photoelectron spectroscopy [137] and Raman spectroscopy [138] measurements in earlier works.

Besides the above described mechanism the uncovered In_2O_3 surfaces between the dispersed CuO are also exposed to H_2S simultaneously. The conversion of CuO to metallic CuS shifts the extent of depletion region towards the p-type CuO and increases the effective thickness of In_2O_3 layer. Cu present in the form of CuO is known to initiate hydrogen spillover because it chemisorbs hydrogen rather weakly [139] and the hydrogen atoms on its surface are highly mobile [140]. The hydrogen after spillover quickly interacts with the adsorbed oxygen and removes it from the uncovered In_2O_3 surface between the dispersed CuO islands. This removal of oxygen leaves behind the excess free electrons that are available for conduction. The resultant of all these reaction is increased sensitivity of copper doped In_2O_3 sensors to H_2S at room temperature.

Due to the effect of very large recovery time the concentration dependent study for pure and 0.5wt% copper doped sensors were limited in the range of 3.57 ppm to 28.58 ppm. In our copper doped sensors as shown in table 5.8 the 0.5wt% sensor was found to have a maximum sensitivity to the lower concentrations (3.57 to 17.85 ppm) studied but had very poor dynamics characteristics (response and recovery times). In our measurements we found that as the concentration of copper increased the dynamic characteristics also exhibited good values. The response and recovery time was found to be very low for the 3wt% copper doped sensors.

It is assumed that in 1.5 and 3wt% copper more CuO-In_2O_3 junctions are formed. Hence there is less uncovered In_2O_3 surface left between the dispersed CuO islands and less interaction of H_2S with In_2O_3. The presence of more CuO-In_2O_3 junctions results in the formation of more CuS. The

conversion time required for CuS to CuO is very less and results in very low recovery time for higher concentration copper doped In_2O_3 sensors. The rate of conversion of CuS to CuO is very fast. The very large recovery time for pure In_2O_3 and 0.5 wt% copper doped In_2O_3 sensors are assigned due to the formation of less CuO-In_2O_3 junction and hence more interaction between In_2O_3 and H_2S resulting in high recovery time. The similar effect also takes place with response time also.

Concentration dependent studies done on 1.5 and 3wt% copper doped sensors prove that as the gas concentration increased the 3wt% doped sensors showed increased sensitivity than 1.5wt% doped sensors. In the case of 3wt% copper doped sensors for higher concentration (286ppm) studied the sensitivity was as high as 3985, where as for the 1.5wt% the sensitivity was 1055 for the same concentration studied. This increased sensitivity is assigned due to the presence of more CuO-In_2O_3, p-n-p-n, junctions. When the concentration of H_2S increases more CuO-In_2O_3 will break resulting in the formation of more CuS and hence increased sensitivity. In 1.5 and 3wt% copper doped In_2O_3 sensors the resistance is higher than 0.5wt% in air. Hence at low H_2S concentration there is less breakage of CuO-In_2O_3 junctions in 1.5 and 3 wt% copper doped sensors than 0.5wt% doped sensor resulting in lower sensitivity at low concentration.

5.11 Conclusion

99.999% pure In_2O_3 powders were purchased and thoroughly mortar powdered to prepare the pure In_2O_3 sensor. Copper doped In_2O_3 was prepared by powder impregnation method. Required amount of copper acetate monohydrate dissolved in water was added to In_2O_3 powder, the

mixture was thoroughly stirred for two days, dried at 100^0C to obtain the copper doped In_2O_3 powder. Pure and copper doped In_2O_3 sensor was prepared by dispersing the prepared powder in methanol and drop coating on to glass substrates. The sensor was annealed at 600^0C overnight before performing the gas sensing measurements. The main conclusions drawn from the above presented experimental data on pure and copper doped In_2O_3 sensors are:

Crystalline structure of pure and copper doped In_2O_3 sensor was revealed as cubic bixbyite structure. Average crystallite size is not affected by the addition of copper. The crystallite size for pure In_2O_3, 0.5wt%, 1.5wt%, and 3wt% copper doped In_2O_3 thick film sensor was found to be 24nm, 23nm, 24nm and 25nm respectively.

The XRD spectrum revealed the cubic bixbyite phase with preferred (222) orientation. No separate peaks were obtained in XRD data due to copper doping. The intensity of all the main reflections was found to decrease with copper doping. A small shift for the (222) peak was observed towards the lower theta side due to copper doping.

The surface morphology and elemental composition were characterized by scanning electron microscopy and energy dispersive X-ray analysis. Separate particles were not visualized in the SEM images. Mainly particle agglomeration with not much definite shape was found in both pure and copper doped In_2O_3 thick film sensors. Copper addition did not show any effect on the surface morphology or particle size of the sensor elements as confirmed by the XRD results. The presence of copper in the doped sensors was confirmed by EDS analysis.

The temperature dependent gas sensing property of pure and copper doped In_2O_3 sensor was investigated in order to find the optimal sensor operating temperature and sensor response to NO_2 test gas.

Copper addition was found to enhance the gas sensing properties In_2O_3 sensor. Two possible mechanisms are suggested for enhanced gas sensing. One is the increase in In^{2+} centers that occur due to copper addition. Another mechanism is due to cuprous ions Cu^{+}, which coexists with cupric ions Cu^{2+} that can enhance the gas sensing property of doped sensors.

Optimum operating temperature for pure and copper doped In_2O_3 sensor was 100^0C. The response and recovery time was found to decrease with copper doping.

The table below presents the sensitivity of the sensors obtained, along with their optimum operating temperature, response and recovery time for the studied concentration of 7ppm NO_2 gas.

Table 5.7: Summary of NO_2 gas sensing results of pure and copper doped In_2O_3 thick film sensor

Sensor	Sensitivity	Optimum temperature	Response time (sec)	Recovery time (min)
Pure In_2O_3	2.82	100^0C	40	12.3
In_2O_3 + 0.5wt% Copper	7.29	100^0C	13	8.03
In_2O_3 + 1.5wt% copper	8.72	100^0C	9	6
In_2O_3 + 3wt% Copper	8.73	100^0C	6	4

The H_2S gas sensing property of pure and copper doped In_2O_3 sensor was performed at room temperature. The temperature dependent studies were not satisfactory. Copper addition was found to enhance the H_2S gas sensing property of In_2O_3. It is attributed to p-n heterojunction

formed by CuO-In_2O_3. In presence of H_2S gas CuO gets converted to metallic CuS which is very conducting and hence enhance the sensor performance.

Gas sensing behaviour of pure and copper doped In_2O_3 sensor to a few concentration of H_2S gas is tabulated below.

Table 5.8: Summary of H_2S gas sensing results of pure and copper doped In_2O_3 thick film sensor

Sensors	Concentration	Sensitivity	Response time(sec)	Recovery time(min)
Pure In_2O_3	3.57	1.1	46	3.98
	7.14	1.35	57	8.55
	10.71	1.98	70	42.9
	17.85	7.25	85	78.62
In_2O_3 + 0.5wt% copper	3.57	1.35	20	5.93
	7.14	2.79	14	16.13
	10.71	68	12	87.95
	17.85	125	6	153
In_2O_3 + 1.5wt% copper	3.57	1.15	24	3.28
	7.14	4.2	9	4.65
	10.71	7.11	7	5.53
	17.85	11.65	7	10.02
In_2O_3 + 3wt% copper	3.57	1.32	8	0.18
	7.14	4.67	6	0.63
	10.71	7.58	6	0.85
	17.85	14.44	5	2.57

Concentration dependent studies for NO_2 gas at optimum operating temperature for pure and copper doped In_2O_3 thick film sensors were studied. The room temperature concentration dependent studies for H_2S gas were also studied.

References

[1] L. Gupta, A. Mansingh and P. K. Srivastava *Thin Solid Films* (1989) 176, 33.

[2] K. Zakrzewakag *Thin Solid films* (2001) 391, 229.

[3] K. Hara, K. Sayama and H. Arakawa *Solar Energy Materials and Solar Cells* (2000) 62, 441.

[4] D. E. Schafer *Solar Cells* (1987) 21, 454.

[5] Y. Meng, X. L. Yang, H. X. Chen, J. Shen, Y. Jiang, Z. Zhang and Z. Hu *Thin Solid Films* (2001) 394, 218.

[6] J. F. Smith, A. J. Aronson, D. Chen and W. H. Class *Thin Solid Films* (1980) 72, 469.

[7] C. Falcony, J. R. Kirtley, D. J. D. Maria, T. P. Ma and T. C. Chen *J. Appl. Phys.* (1985) 58, 3556.

[8] C. G. Granqvist *Appl. Phys. A* (1993) 57, 19.

[9] M. Girtan and G. Folcher *Surface and Coatings Technology* (2003) 172, 242.

[10] S. Tanaka and T. Esaka *Materials Research Bulletin* (2000) 35, 2491.

[11] H. Y. Yeom, N. Popovich, E. Chason and D. C. Paine *Thin Solid Films* (2002) 411, 17.

[12] K. Daoudi, C. S. Sandu, V. S. Teodorescu, C. Ghica, B. Canut, M. G. Blanchin, J. A. Roger, M. Oueslati and B. Bessaïs *Crystal Engineering* (2002) 5, 187.

[13] S. Shukla, S. Seal, L. Ludwig and C. Parsh *Sensors and Actuators B* (2004) 97, 256.

[14] J. J. Prince, S. Ramamurthy, B. Subramanian, C. Sanjeeviraja and M. Jayachandran *Journal of Crystal Growth* (2002) 240, 142.

[15] S. M. Rozati and T. Ganj *Renewable Energy* (2004) 29, 1671.

[16] C. M. Ghimbeu, J. Schoonman and S. M. Lumbrera *Ceramics International* (2008) 34, 95.

[17] R. D. Shannon *SolidState Communications* (1966) 4, 629.

[18] D. B. Yu, S. H. Yu, S. Y. Zhang, J. Zuo, D. Wang and Y. T. Qian *Adv. Func. Mater.* (2003) 13, 497.

[19] H.O Finklea Semiconductors Electrodes. In: Elsevier, ed. Amsterdam 1988, 224.

[20] D. R. Lide Handbook of Chemistry and Physics CRC Press Boca Raton USA, 2001.

[21] K. D. Kundra and S. Z. Ali J. Appl. Crystallogr. (1970) 3, 543.

[22] E. H. P. Cordfunke and E. F. Westrum J. Phys. Chem. Sol. (1992) 53, 361.

[23] P. A. Cox, W. R. Flavell and R. G. Egdell J. Sol. Stat. Chem. (1987) 68, 340.

[24] Z. Ovadyahu, B. Ovryn, and H. W. Kraner J. Electrochem. Soc. (1983) 130, 917.

[25] P. Kofstad Nonstoichiometry diffusion and electrical conductivity in binary metal oxides Wiley (1983) New York USA,.

[26] C. X. Pedersen Growth and characterisation of indium oxide films Ph.D. Thesis, University of Crete, Greece, 1998.

[27] J. H. W. de Wit J. Sol. Stat. Chem. (1975) 13, 192.

[28] M. Bender, N. Katsarakis, E. Gagaoudakis, E. Hourdakis, E. Douloufakis, V. Cimalla, and G. Kiriakidis J. Appl. Phys. (2001) 90, 5382.

[29] F. O. Adurodija, H. Izumi, T. Ishihara H. Yoshioka, H. Matsui, and M. Motoyama Appl. Phys. Lett. (1999) 74, 3059.

[30] Y. Yamada, G. Suzuki, T. Makino and T. Yoshida J. Vac. Sci.Technol. A (2000) 18, 83.

[31] S. Takayama, A. Tanaka, T. Sugawara and T. Himuroet Jpn. J. Appl.Phys. (2002) 41, L619.

[32] M. J. Alam and D. C. Cameron Thin Solid Films (2002) 420, 76.

[33] R. X. Wang, C. D. Beling, S. Fung, A. B. Djurišić, C. C. Ling, and S. Li J. Appl. Phys. (2005) 97, 033504.

[34] M. J. Alam and D. C. Cameron Thin Solid Films (2002) 420, 76.

[35] G. Kiriakidis, H. Ouacha and N. Katsarakis Rev. Adv. Mater. Sci. (2003) 4, 32.

[36] M. Z. Atashbar, B. Gong and H. T Sun Thin Solid Films (1999) 354, 222.

[37] T. Takada, K. Suzuki and M. Nakane Sensors and Actuators B (1993) 13, 404.

[38] G. Korotcenkov, V. Brinzari., A. Cerneavschi, M. Ivanov, A. Cornet, J. Morante, A. Cabot, and J. Arbiol Sensors and Actuators B (2004) 98,122.

[39] Gurlo , N. Ba^rsan, M. Ivanovskaya, U. Weimar and W. Go pel Sensors and Actuators B (1998) 47, 92.

[40] G. Faglia, B. Allieri, E. Comini, L.E. Depero, L. Sangaletti and G. Sberveglieri Sensors and Actuators B (1999) 57, 188.

[41] S. R. Kim, H. K. Hong, C. H. Kwon, D. H. Yun, K. Lee and Y. K. Sung Sensors and Actuators B (2000) 66, 59.

[42] M. Ivanovskaya, A. Gurlo and P. Bogdanov Sensors and Actuators B (2001) 77, 264.

[43] M. Ivanovskaya, D. Kotsikau, G. Faglia, P. Nelli and S. Irkaev Sensors and Actuators B (2003) 93, 422.

[44] V. Golovanov, M. A. M. Jaskari, T. T. Rantala, G. Korotcenkov, V. Brinzari, A. Cornet and J. Morante Sensors and Actuators B (2005) 106, 563.

[45] C. Baratto, M. Ferroni, G. Faglia and G. Sberveglieri Sensors and Actuators B (2006) 118, 221.

[46] G. Sberveglieri, C. Baratto, E. Comini, G. Faglia, M. Ferroni, A. Ponzoni and A. Vomiero Sensors and Actuators B (2007) 121, 208

[47] M. Epifani, E. Comini, J. Arbiol, Ra¨ul D´ıaz, N. Sergent, T. Pagnier , P. Siciliano, G. Faglia and J. R. Morante Sensors and Actuators B (2008) 130, 483.

[48] Y. Yasukawa, T. Seki, J. Muramatsu, S. Sugie, S. Tasaka and N. Inagaki Sensors and Actuators B (1993) 13, 613.

[49] W. Y. Chung, G. Sakai, K. Shimanoe, N. Miura, D.D. Lee and N. Yamazoe Sensors and Actuators B (1998) 46, 139.

[50] X. Niu, H. Zhong, X. Wang and K. Jiang Sensors and Actuators B (2006) 115, 434.

[51] D. Chu, Y. P. Zeng, D. Jiang and Y. Masuda Sensors and Actuators B (2009) 137, 630.

[52] N. Singh, A. Ponzoni, R. K. Gupta, P. S. Lee and E. Comini Sensors and Actuators B (2011) 160, 1346.

[53] G. Neri, A. Bonavita, G. Micali, G. Rizzo, N. Pinna, M. Niederberger and J. Ba Sensors and Actuators B (2008) 130, 222.

[54] G. Neri, A. Bonavita, G. Micali, G. Rizzo, E. Callone and G. Carturan Sensors and Actuators B (2008) 132, 224.

[55] K. Il Choi, H. R. Kim and J. H. Lee Sensors and Actuators B (2009) 138, 497.

[56] S. K. Lim, S. H. Hwang, D. Chang and S. Kim Sensors and Actuators B (2010) 149, 28.

[57] J. Xu, X. H. Wang and J. N. Shen Sensors and Actuators B (2006) 115, 642.

[58] M. Kaur, N. Jain, K. Sharma, S. Bhattacharya, M. Roy, A. K. Tyagi, S. K. Gupta and J.V. Yakhmi Sensors and Actuators B (2008) 133, 456.

[59] L. Xu, B. Dong, Y. Wang, X. Bai, Q. Liu and H. Song Sensors and Actuators B (2009) 147, 531

[60] G. Sberveglieri, S. Groppelli and G. Coccoli Sensors and Actuators B (1988) 15, 235.

[61] A. Gurlo, M. Ivanovskaya, N. Baˆrsan, M. S.Berberich, U. Weimar ,W. Go pel and A. Die´guez Sensors and Actuators B (1997) 44, 327.

[62] C. Cantalini, W. Wlodarski, H.T. Sun, M. Z. Atashbar,M. Passacantando and S. Santucci Sensors and Actuators B (2000) 65, 101

[63] M .Ivanovskaya, P. Bogdanov, G. Faglia and G.Sberveglieri Sensors and Actuators B (2000) 68, 344.

[64] H. Steffes, C. Imawan, F. Solzbacher and E. Obermeier Sensors and Actuators B (2000) 68, 249

[65] H. Steffes, C. Imawan, F. Solzbacher and E. Obermeier Sensors and Actuators B (2001) 78, 106.

[66] T. K. H. Starke, G. S. V. Coles and H. Ferkel Sensors and Actuators B (2002) 85, 239.

[67] L. Francioso, A. Forleo, S. Capone, M. Epifani, A. M. Taurino and P. Siciliano Sensors and Actuators B (2006) 114, 646.

[68] M. I. Ivanovskaya, D. A. Kotsikau, A. Taurino and P. Siciliano Sensors and Actuators B (2007) 124, 133.

[69] P. Xu, Z. Cheng, Q. Pan, J. Xu, Q. Xiang, W. Yu and Y. Chu Sensors and Actuators B (2008) 130, 802.

[70] T. Hyodo, H. Inoue, H. Motomura, K. Matsuo, T. Hashishin, J. Tamaki, Y. Shimizu and M. Egashira Sensors and Actuators B (2010) 151, 265.

[71] P. S. Khiabani, A. Hosseinmardi, E. Marzbanrad, S. Ghashghaie, C. Zamani, M. Keyanpour-Rad and B. Raissi Sensors and Actuators B (2012) 162, 102.

[72] P. S. Khiabani, E. Marzbanrad, C. Zamani, R. Riahifar and B. Raissi Sensors and Actuators B (2012) 166, 128

[73] X. Xu, D. Wang, W. Wang, P. Sun, J. Ma, X. Liang,Y. Sun, Y. Ma and G. Lu Sensors and Actuators B (2012) 171, 1066

[74] Z. Cheng, L. Song, X. Ren, Q. Zheng and J. Xu Sensors and Actuators B (2012) 176, 258.

[75] X. Xu, P. Zhao, D. Wang, P. Sun, L. You, Y. Sun, X. Liang,F. Liu, H. Chen and G. Lu Sensors and Actuators B (2013) 176, 405.

[76] A. Serra, G. Micocci, M. D. Giulio, D. Manno and A. Tepore Sensors and Actuators B (1999) 58, 356.

[77] Y. Wang, M. Ali, Th. Kups, C. C. R¨ohlig, V. Cimalla, T. Stauden and O. Ambacher Sensors and Actuators B (2008) 130, 589.

[78] Y. Lin, Y. Y. Fang, C. W. Lin, J. J. Tunney and K. C. Ho Sensors and Actuators B (2010) 146, 28.

[79] S. Kannan, L. Rieth and F. Solzbacher Sensors and Actuators B (2010) 149, 8.

[80] T. Zhang, F. Gu, D. Han, Z. Wang and G. Guo Sensors and Actuators B (2010) 177, 1180.

[81] V. N. Singh, B. R. Mehta, R. K. Joshi, and F. E. Kruis Journal of Nanoscience and Nanotechnology (2007) 7, 1930.

[82] V. N. Singh, B. R. Mehta, R. K. Joshi, F. E. Kruis and S. M. Shivaprasad Sensors and Actuators B (2007) 125,482.

[83] X. Xu, H. Fan, Y. Liu, L. Wang and T. Zhang Sensors and Actuators B (2011) 160,719.

[84] C. W. Lin, H. I. Chen, T. Y. Chen, C. C. Huang, C. S. Hsu, R. C. Liu and W. C. Liu Sensors and Actuators B (2011) 160, 1484.

[85] P. Guo and H. Pan Sensors and Actuators B (2006) 114, 762.

[86] N. G. Patel, P. D. Patel and V.S. Vaishnav Sensors and Actuators B (2003) 96, 180.

[87] X. Liu, R. Wang, T. Zhang, Y. He, J. Tu and X. Li Sensors and Actuators B (2010) 150, 442.

[88] W. Y. Chung, G. Sakai, K. Shimanoe, N. Miura, D. D Lee and N. Yamazoe Sensors and Actuators B (2000) 65, 312.

[89] L. Guo, X. Shen, G. Zhua and K. Chen Sensors and Actuators B (2011) 155, 752.

[90] X. Wang, M. Zhang, J. Liu, T. Luo and Y. Qian Sensors and Actuators B (2009) 137, 103.

[91] H. Dong, Y. Liu, G. Li, X. Wang, D. Xu, Z. Chen, T. Zhang, J. Wang and L. Zhang Sensors and Actuators B (2013) 178, 302

[92] G. P. Schwartz, W. A. Sunder and J. E. Griffiths J. Electrochem. Soc. (1982) 129, 1361.

[93] C. Wang,Y. Dai, J. Pezoldt, B. Lu, T. Kups, V. Cimalla and O. Ambacher Cryst. Growth Des. (2008) 8, 1257.

[94] S. J. Ippolito, S. Kandasamy, K. Kalantarzadeh, W. Wlodarski, K. Galatsis, G. Kiriakidis, N. Katsarakis and M. Suchea Sensors and Actuators B (2005) 111, 207.

[95] S. Bianchi, E. Comini, M. Ferroni, G. Faglia, A. Vomiero and G. Sberveglieri Sensors and Actuators B Chemical (2006) 118, 204.

[96] R. D. Iuengar, M. Codell and J. Turkevich J. Catal. (1967) 9, 305.

[97] D. E. Williams Solid State Gas Sensors Adam Hilger Bristol UK 1987, 71.

[98] S. C. Chang IEEE Trans. Elec. Dev. (1979) 26, 1875.

[99] M. Ali, Ch.Y. Wang, C.C. R¨ohlig, V. Cimalla, Th. Stauden and O. Ambacher Sensors and Actuators B (2008) 129, 467.

[100] A. Gurlo, M. Ivanovskaya, A. Pfau, U. Weimar and W. Go¨pel Thin Solid Films (1997) 307, 288.

[101] A. Gurlo, M. Ivanovskaya, A. Pfau, U. Weimar and W. Go¨ pel Tech. Digest E-MRS Spring Meeting Strasbourg France (1996) BP-18.

[102] M. Ivanovskaya, P. Bogdanov, A. Gurlo and L. Ivashkevich Inorg. Mater. (1998) 34, 329.

[103] K. Sasaki, H. P. Seifert and L. J. Gauker J. Electrochem. Soc. (1994) 141, 2759.

[104] J. H. W. De Wit J. Solid State Chem. (1977) 20, 143.

[105] E. Solovjeva, V. A. Zhdanov, V. Markov and R. R. Shvangeradze Inorg. Mater. (1982) 18, 825.

[106] L. Smart and E. Mogre Solid State Chemistry: An Introduction, Chapman & Hail, London, 1995.

[107] V. Demarne, R. Sanjines and S. Sberveglieri Gas Sensors — Principles, Operation and Developments, Kluver, Dordrecht, (1992) 89.

[108] A. Die´guez, A. Romano-Rodriquez, J. R. Morante, U. Weimar, M. S. Berberich and W. Go¨ pel Sensors and Actuators B (1996) 31, 1.

[109] J. Tamaki, Z. Zhang, K. Fujimori, M. Akiyama, T. Harada, N. Miura and N. Yamazoe Journal of the electrochemical society, (1994) 141, 8.

[110] V. V. Kissine, S. A. Voroshilov, and V. V. Sysoev Thin Solid films (1999) 348, 304.

[111] Galdikas, A. Mironas and A. Setkus Sensors and Actuators B (1995) 26, 29.

[112] M. N. Rumyantseva, M. Labeau, J. P. Senateur, G. Delabouglise, M. N. Boulova and A. M. Gaskov Mater. Sci. Eng. B (1996) 41, 228.

[113] N. Yamazoe Sensors and Actuators B (1991) 5, 7.

[114] B. Esfandyarpour, S. Mohajerzadeh, A. A. Khodadadi, and M. D. Robertson IEEE Sensors Journal (2004) 4, 449.

[115] S. Hwang, J. K Choi, S. J. Kim, K. Y. Dong, J. H. Kwon, B. K. Ju and J. H. Lee Sensors and Actuators B (2009) 142, 105.

[116] M. Ghimbeu, M. Lumbrerasa, M. Siadata,R. C. van Landschoot and J. Schoonman Sensors and Actuators B (2008) 133, 694.

[117] J. Liu, X. Huang, G.Ye, W. Liu, Z. Jiao, W. Chao, Z. Zhou and Z. Yu Sensors (2003) 3, 110.

[118] Y. Choe Sens. Actuators B (2001) 77, 200.

[119] T. Maekawa, J. Tamaki, N. Miura, and N. Yamazoe J. Mater. Chem. (1994) 4, 1259.

[120] X. Zhou, Q. Cao, H. Huang, P. Yang, and Y. Hu Mater. Sci. Eng. B (2003) 99, 44.

[121] V. R. Katti, A. K. Debnath, K. P. Muthe, M. Kaur, A. K. Dua, S. C. Gadkari, S. K. Gupta, and V. C. Sahni Sensors and Actuators B (2003) 96, 245.

[122] G. Zhang and M. Liu Sensors and Actuators B (2000) 69, 144.

[123] P. Bogdanov, M. Ivanovskaya , E. Comini, G. Faglia and G. Sberveglieri Sensors and Actuators B (1999) 57, 153.

[124] Z. M. Zeng, K. Wang, Z. X. Zhang, J. J. Chen and W. L. Zhou Nanotechnology (2009) 20, 045503.

[125] V. D. Kapse, S. A. Ghosh, G. N. Chaudhari and F. C. Raghuwanshi Talanta (2008) 76, 610.

[126] V. D. Kapse, S. A. Ghosh, F. C. Raghuwanshi and S. D. Kapse Sensors and Actuators B (2009) 137, 681.

[127] D. Wang, X. F. Chu and M. L. Gong Nanotechnology (2007) 18, 185601.

[128] L. A. Patil and D. R. Patil Sensors and Actuators B (2006) 120, 316.

[129] L. Xu, B. Dong, Y. Wang, X. Bai, Q. Liu and H. Song Sensors and Actuators B (2010) 147, 531

[130] Y. Liu, H. Y. Xu and Y. T. Qian Cryst. Growth Des. (2006) 6, 1304.

[131] J. H. Park and J. H. Lee Sensors and Actuators B (2009) 136, 224.

[132] C. S. Moon, H. R. Kim, G. Auchterlonie, J. Drennan and J. H. Lee Sensors and Actuators B (2008) 131, 556.

[133] W. Y. Chung, G. Sakai, K. Shimanoe, N. Miura, D.-D. Lee and N. Yamazoe Sensors and Actuators B (1998) 46, 139.

[134] S. R. Morrison Sensors and Actuators B (1987) 12, 425.

[135] X. Kong and Y. Li Sensors and Actuators B (2005) 105, 449.

[136] R. B. Vasiliev, M. N. Rumyantseva, N. V. Yakovlev and A.M. Gasckov Sensors and Actuators B (1998) 50, 186.

[137] R. S. Niranjan, K. R. Patil, R. S. Sainkar and I. S. Mulla Mater. Chem. Phys. (2002) 80, 250.

[138] T. Pagnier, M. Boulova, A. Galerie, A. Gaskov and G. Lucazeau Sensors and Actuators B (2000) 71, 134.

[139] G. C. Bond Proceedings of the International Symposium, Lyon-Villeurbanne, edited by G. M. Pajonk, S. J. Teichner, and J. E. Germain Elsevier, New York, 1983.

[140] R. Kramer and M. Andre J. Catal. (1979) 58, 287.

Chapter 6

Summary and Scope for Further Study

6.1 Summary

Detecting gases and determining their composition has constantly been on the increase in recent years. The demand for better environmental control and safety has increased research activities of solid-state gas sensors. Gas sensors using metal oxide semiconductors have been the subject of extensive investigations for more than three decades, primarily focusing on SnO_2. In more recent research, the interests shifted to some other promising metal oxides, with interesting properties as gas sensing materials. Using metal oxides has several advantages, features such as simplicity in device structure, low cost for fabrication, robustness in practical applications and adaptability to a wide variety of reducing or oxidising gases. Gas sensors based on nano metal oxide materials are the focus of current research activity of sensor designers. One of the characteristics of nanometric materials is their high surface area/volume ratio. Many studies, then, have focused on reducing the size of the metal oxides in the form of nanoparticles and nanowires. Also reactions at grain boundaries and complete depletion of carriers in the grains can strongly modify the material transport properties in nanostructured oxides

In recent years the efforts of gas sensor designers were aimed at: (a) increasing of gas sensitivity and improvement of their selectivity (b) reduction of electric power consumption by resistive heater of gas sensors, and (c) decreasing of response and recovery times. One of the main

challenges to the developers of metal-oxide gas sensors is high selectivity without affecting the sensitivity of the sensor. In this present work we have made an attempt to address these problems. The aim of the present work is development of pure and doped semiconducting metal oxide for the detection of pollutant gases like NO_2 and H_2S gases.

The first part of this work is dedicated to the design and fabrication of a gas sensing measurement chamber for the purpose of sensing studies. The chamber was fabricated incorporating the facilities for both static and flow through method. In all the gas sensing measurements carried out we have used the static measurement method. To study the temperature dependent gas sensing properties of the semiconducting metal oxide gas sensors a microcontroller based PID temperature controller was designed. The temperature controller has an accuracy of 0.5^0C. A RTD was used as the temperature sensor. The temperature controller is able to vary temperature in the range of 50 to 400^0C. The resistance variation of sensor in presence of target gas was measured using a keithely 195A digital multimeter. A GPIB interface was used to interface the multimeter to the system.

The second part of this work is devoted to the preparation of active layers for the sensing application and their electrical and structural characterization. Nanocrystalline thick and thin films based on semiconducting metal oxides are prepared as active layers for the purpose of gas sensing application. Semiconducting metal oxides like tungsten oxide, zinc oxide and indium oxide are selected for the active layer materials. The effect of doping on the gas sensing properties of pure metal oxides is studied by adding dopants like copper and indium. The prepared sensors are characterized using different analytical characterisation tools like XRD, SEM, EDS and Raman spectroscopy. All sensor films were annealed at 600^0C overnight prior to gas

sensing studies to reduce the posterior material instabilities. Concentration dependent studies for all the sensors were obtained at the optimum operating temperature.

Pure and copper doped nanocrystalline tungsten oxide powders were prepared and thick films of the sensor are obtained on glass substrate. Pure and doped thick film sensors are investigated for NO_2 and H_2S gas sensing properties. The temperature dependent sensitivity studies are performed to obtain the optimum operating temperature. The addition of copper is found to enhance the NO_2 gas sensing property of the sensor. The 3wt% copper doped tungsten oxide thick film has sensitivity 4 times higher than the undoped for 7 ppm concentration. The incorporation of copper may lead to the formation of Cu-O-W bonds that creates adsorption sites of copper and tungsten due to their change in oxidation states. Hence the target gas molecules have more adsoption sites to react with the sensor thereby increasing the sensitivity of the sensor. With copper addition it is found that optimum operating temperature decreases from 200 to 175^{0}C. The H_2S gas sensing investigation reveal that with copper addition the sensitivity of the tungsten oxide was decreased. Hence the copper doped studies performed show that the copper doped tungsten oxide sensors is more selective to NO_2 gas.

Pure and indium doped ZnO thin film sensor prepared by spray pyrolysis is also studied for gas sensing application. The temperature dependent sensitivity studies are performed and optimum operating temperature for pure and doped sensors is found to be 200^{0}C. The doped film sensing studies proved that the pure ZnO itself is a promising candidate for gas sensing application for both the test gases studied. Contrary to enhancement effect in sensitivity by the presence of additives, it was found

that incorporation of indium decreases gas sensing ability of the sensor. This decrease in sensitivity is attributed to the increase in free electron concentration and a consequent decrease in resistivity occurs due to replacement of Zn^{2+} cation by the In^{3+} cation, which acts as a donor. No variation in optimum temperature is obtained due to the indium doping.

NO_2 gas sensing studies performed on pure and copper doped indium oxide thick film sensors proved that with copper doping the sensitivity of pure films can be enhanced. Maximum sensitivity for pure and doped sensors is achieved at a temperature of 100^0C. Pure sensor showed a maximum sensitivity of 2.82 to 7 ppm concentration of NO_2 at 100^0C while 3wt% copper doped sensor showed a sensitivity of 8.83 for the same concentration and temperature. Two possible mechanisms are suggested for enhanced gas sensing. One is the increase in In^{2+} centers that occur due to copper addition. Another mechanism is due to cuprous ions Cu^+, which coexists with cupric ions Cu^{2+} that can enhance the gas sensing property of doped sensors. With introduction of copper the response and recover time was also found to improve for NO_2 gas sensing. The improved response as well as recovery time performance of doped In_2O_3 over pure In_2O_3 is due to the catalytic interaction of copper ion with the gas species to be detected.

H_2S gas sensing investigation on pure and copper doped indium oxide thick film sensor also show an improved sensitivity for copper doping. It is attributed to p-n heterojunction formed by CuO-In_2O_3. In presence of H_2S gas CuO gets converted to metallic CuS which is very conducting and hence enhance the sensor performance. The room temperature studies performed presents that copper doped indium oxide sensors have a very response and recovery time. The 3wt% copper doped sensor has a recovery time of 2.57

minutes for 17.85 ppm of H_2S gas concentration studied while pure sensor has a recovery time of 78.62 minutes. The concentration dependent studies at room temperature show that as copper doping amount increased the sensitivity of the sensor also increased. The pure sensor has a sensitivity of 7.26 to 17.85 ppm at room temperature while 3wt% copper doped sensor has a sensitivity of 14.44.

6.2 Scope of Further Study

The scope of extending the current work for further research is suggested below.

Reduction in particle size can enhance the gas sensing property considerably. To improve the gas sensor response it would be interesting to reduce the grain size under 20nm and to examine how the sensitivity and selectivity of sensors changes as size of these nanoparticles approach to Debye length.

The stability of the obtained sensors should be confirmed by long term tests under real working conditions. Longer annealing temperature should also be explored in order to achieve high stability. Gas response studies depending on different annealing temperature can also be performed.

The adsorption-desorption kinetics of the gas can drastically vary depending on the nature of the surface. A deliberate creation of defects, non-stoichiometry or incorporation of various materials on the surface can enhance the sensitivity and selectivity of the sensors. Addition of other metal additives can also be performed.

Variation in surface morphology related studies can be further done for the purpose of gas sensing. Nanostructured materials like nanotubes,

nanowires, nanorods and nanofiber exhibit a greater response to gas sensing due to the larger surface area to volume ratio. These surface morphologies can enhance the detection levels to ppb range.

An integrated micro machined gas sensor array, associated with pattern recognition (PARC) techniques, such as artificial neural networks (ANNs), is also proposed to overcome problems associated with poor selectivity encountered during operation of individual gas sensor.

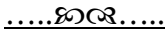

Abbreviations

APCVD	Atmospheric pressure chemical vapour deposition
CL	Cathodoluminescence
CSP	Chemical spray pyrolysis
CVD	Chemical vapour deposition
DMA	Dimethylamine
EBE	Electron Beam Evaporation
EDS	Energy dispersive X-ray
GC	Gass chromatography
GB	Grain boundary
GPIB	General purpose instrumentation bus
HCP	Hexagonal close packing
LD	Laser diodes
LED	Light emitting diodes
LPFD	Low-pressure flame deposition
LPG	Liquid petroleum gas
MFC	Mass flow controller
PECVD	Plasma-enhanced chemical vapour deposition
PID	Proportional integral differential
PLD	Pulsed laser deposition
ppb	Parts per billion
ppm	Parts per million
PVD	Physical vapour deposition
RTD	Resistance temperature detector
SAW	Surface acoustic wave
SEM	Scanning electron microscope
SGS	Semiconductor gas sensors
SILAR	Successive ionic layer adsorption and reaction
SMO	Semiconductor metal oxide
TMA	Trimethylamine
TNT	Trinitrotoluene
UV	Ultra violet
WZ	Wurtzite
XRD	X-ray diffraction
ZB	Zinc blende